The adsorption of Ni, Cu, Zn, Cd and Pb by δ-MnO_2 and its inclusion in an equilibrium model of metal partitioning in soils.

A thesis submitted to the
University of Cape Town
in fulfilment of the requirements for the degree
Doctor of Philosophy

by

Patrius Julius Pretorius

Department of Chemistry
University of Cape Town
Rondebosch, 7700
South Africa

October 1997

Matters philosophical

Destiny

"It's a book that says the same thing almost all the other books in the world say," continued the old man. "It describes people's inability to choose their own destinies. And it ends up saying that everyone believes the world's greatest lie."

"What's the world's greatest lie?" the boy asked, completely surprised.

"It's this: that at a certain point in our lives, we lose control of what's happening to us, and our lives become controlled by fate. That's the world's greatest lie."

"That's never happened to me," the boy said. "They wanted me to be a priest, but I decided to become a shepherd."

"Much better," said the old man. "Because you really like to travel."

Paulo Coelho - The Alchemist

Vrijheid/Vryheid/Freedom

Maar de vrijheid is niet gebonden door stadsgrachten en bastions; zij schuilt in de gedachten, in de daden van elk van ons.

Theun de Vries - Kenau

Kettings aan jou voorkop vas, in die tronk is daar kettings aan jou denke vas.....
Breek dit af, breek die mure om jou af, binne buite om jou af....

Johannes Kerkorrel en die Gereformeerde Blues Band - Tronk

Science

It is the mark of an instructed mind to rest easy with the degree of precision which the nature of the subject permits and not to seek an exactness where only an approximation of the truth is possible.

Aristotle

Late 20th century life

Can't you see, it all makes perfect sense, expressed in dollars and cents, pounds shillings and pence.

Roger Waters - Amused to death

Life

We can never know what to want, because, living only one life, we can neither compare it with our previous lives nor perfect it in our lives to come.... Einmal ist keinmal..... If we have only one life to live, we might as well not have lived at all.

Milan Kundera - The unbearable lightness of being

In memory of Patrius Pretorius (1936 - 1992)

Acknowledgements

This thesis would not have been possible without the support of a number of people.

My supervisor, Professor Peter Linder - Prof, thanks for your support and guidance, not only in science, but also in the more mundane things like life.

My lab mates Heather and Fran: thanks for helping change the initial lab greenness into something approaching proficiency, or is it adequacy?

Chris Woollard for many interesting discussions.

All my colleagues at RIVM, but in particular Willie Peijnenburg, Henri den Hollander, de heer Verboom, René Janssen and Marja Wouterse. *Bedankt voor de vriendschap en de leuke fietstochten!*

Some great friends: Debby, James, Lomkhosi, Winnie, Margie and Jane. Patrick, thanks for all the Backgammon, Scrabble and Squash contests.

Norbert and Barbara for taking care of my earthly possessions during my European sojourn.

Deon Fouche: *dankie vir die ondersteuning ou maat, dit word hoog op prys gestel!*

Julius (sr): thanks for being an excellent friend.

My family, in particular my parents and sister for making many sacrifices which allowed me the luxury of pursuing a tertiary education.

The staff of the Immelman Science and Engineering Library and the Inter Library Loans Section for their efficiency and helpfulness.

CSIR and RIVM for financial support.

Abstract

The adsorption of Ni, Cu, Zn, Cd and Pb by δ-$MnO_2$and its inclusion in an equilibrium model of metal partitioning in soils.

PJ Pretorius, Department of Chemistry, University of Cape Town, Rondebosch, 7700, South Africa.

Chemical equilibrium modelling provides a mechanistic tool for the prediction of metal partitioning in soils, which is important in predicting the fate and effects of metals in soil systems. In order to set up an equilibrium model of metal partitioning in soil systems, thermodynamic data for all processes influencing metal fate in soil systems are needed.

In this work, the adsorption of the metals nickel, copper, zinc, cadmium and lead by δ-MnO_2 is investigated. This was done in order to provide thermodynamic data for an important adsorption phase in soils systems. Before this work, consistent adsorption data for only one adsorption phase, hydrous ferric oxide, were available. This precluded the inclusion of manganese dioxide in equilibrium models of metal fate in soil systems.

Surface complexation properties of a synthetic manganese dioxide were investigated using glass electrode potentiometry. Experimental data were interpreted according to the surface complexation model in conjunction with the diffuse double layer model of the solid/solution interface. Adsorption constants were derived using the non-linear optimization program FITEQL. The surface complexation parameters determined in this fashion were validated against results obtained from the open literature. Following this, the surface complexation parameters were included in a chemical equilibrium model of soil systems. This model was used to predict the partitioning of nickel, copper, zinc, lead and cadmium in a number of soil

samples collected in The Netherlands.

Contrary to results presented by other workers, it was found that a non-homogeneous surface site model was needed to explain the potentiometric data obtained for proton and metal adsorption by manganese dioxide. Best fits of alkalimetric titration data were obtained with a two-site, three surface-species model of the δ-MnO_2 surface. Site concentrations of 2.231×10^{-3} mol.g^{-1} and 7.656×10^{-4} mol.g^{-1} were obtained. Corresponding equilibrium constants for the formation of the postulated surface species are -1.27 ($=XO^-$), -5.99 ($=YO^-$) and 3.52 ($=YOH_2^+$). This model was successful in a qualitative manner in describing adsorption results obtained from the open literature.

The prediction of metal partitioning in soil systems showed that although the inclusion of manganese dioxide in the model led to some improvement in the agreement between observed and predicted results, other factors are present which influence metal partitioning in soils. The discrepancy between observed and predicted results furthermore showed that the processes accounted for in the equilibrium model are incomplete.

Table of Contents

Glossary of symbols

K_p:	Partition coefficient
T_{Xi}:	Total concentration of component X_i
X_i:	Component X_i
C_j:	Species consisting of components X_i
[]:	Concentration ($mol.dm^{-3}$)
{}:	Activity
β^T:	Thermodynamic equilibrium constant
r:	Stoichiometric coefficient
γ:	Activity coefficient
≡SOH:	Surface site. Also ≡XOH and ≡YOH
σ:	Surface charge
Ψ:	Surface potential
C_1, C_2:	Capacitance
E:	EMF
E^{const}:	Electrode intercept
s:	Nernstian slope

List of illustrations

List of tables

Chapter 1 Introduction

One of the possible methods to assess the potential risk associated with the presence of toxic compounds in the environment is to derive quality criteria for individual compounds and compare actual environmental concentrations with these standards (van der Kooij *et al.*, 1991). However, for these standards to be realistic, they should take into account the complex inter-relationship between chemical behaviour and biological effects of pollutants. Allen (1996) states that environmental quality criteria should, amongst others, be predictive of (biological) effects and they should be scientifically valid. It thus follows that, in order to provide environmental quality criteria which adequately protects biota and environmental quality in the different environmental compartments (soil, sediment, water and air), cognisance should be taken of pollutant behaviour and the way it is affected by surrounding conditions.

In this thesis, the focus is on the behaviour of the metals nickel, copper, zinc, lead and cadmium in soils. In particular, the partitioning of these metals over the solid-solution phase in soils will be addressed. It is well known that the distribution, mobility and biological availability (i.e. the fate and effect) of metals in natural systems depend not simply on their total concentrations, but critically, on the chemical and physical associations they undergo in these systems (Ure and Davidson, 1995). There is a growing body of evidence which indicates that the biological effects of pollutants, including metals, in soil and sedimentary systems are better related to their concentration in the pore - or interstitial water phase, rather than to the total concentration in the solid phase (Adams *et al.*, 1992; van Stralen and Bergema, 1995). The concept of *equilibrium partitioning* (Shea, 1988) is commonly used to predict solution phase concentrations from total soil concentrations.

In the equilibrium partitioning approach, pollutant concentration in the soil solid phase is related to solution phase concentration via expression 1.1:

$$K_p = \frac{[Metal]_{solidphase}}{[Metal]_{solutionphase}} \quad \ldots\ldots\ldots\ldots\ldots\ldots \quad (1.1)$$

Quality criteria for the protection of soils and sediments may now be derived from existing water quality criteria simply by multiplying K_p with the relevant water quality criterion. This will yield a maximum concentration for the soil or sediment solid phase which will not exceed the selected water quality criteria. There are several advantages to this approach: (i) it harmonizes quality criteria for different environmental compartments, (ii) the analytical determination of solid phase metal concentrations is routinely carried out and is less time consuming than extracting pore water for analysis and (iii) water quality criteria are in many cases well established and it is therefore sensible to link soil and sediment quality criteria to these water quality criteria.

There is, however, a problem with the application of the equilibrium partitioning approach: the partition coefficient, K_p, is a function of both pollutant and soil properties. In other words, the application of the equilibrium partitioning approach to metal partitioning in soils, as described in equation 1.1, is complicated by the partition coefficient's dependency on metal speciation and the factors controlling metal speciation (van der Kooij, 1991).

Basically, there are two approaches to account for the dependency of K_p on metal speciation: the first approach is a statistical one, which aims at describing the dependency of K_p on the

soil solid phase composition. Typically, a large number of soils spanning a range of compositions and conditions are investigated. Soil solid and solution phases are separated using some mechanical technique, such as centrifugation. Metal concentrations in the solid and solution phases are determined using standard analytical techniques. From these data, partitioning coefficients are calculated. At the same time, the soil solid phase is also fully characterized in terms of important adsorption phases and pH. A statistical relationship between observed K_p's and soil parameters are then sought using multi-variate statistical techniques. Partition coefficients are then expressed in terms of regression equations consisting of soil parameters and a weighting factor to account for the importance of the specific soil parameter in describing the observed K_p. Examples of this approach may be found in van den Hoop (1995), Janssen *et al.*, 1996 and Lee *et al.*, (1996).

The second approach is a mechanistic one. Here, the interactions in the complex heterogeneous system is represented as a combination of elementary interactions, which are represented by simple chemical and electrostatic models (Westall, 1993). This approach, based on thermodynamic principles, allows the equilibrium speciation of a system to be calculated once total component concentrations are known. It includes the effect of solution speciation on the partitioning of metals over the solid/solution interface since the adsorbing phase is viewed as a ligand which competes with solution phase ligands for the metal.

The thermodynamic approach is preferable over the first, empirical approach since it has the ability to be used for predictive purposes. This is not the case of empirical methods, which are generally applicable only over their range of calibration.

In this work, an attempt is made at constructing an equilibrium model of soil solutions with the aim of predicting the partitioning of metals over the solid/solution interface in soil systems.

1.1 Factors affecting metal speciation in soils.

The factors affecting the fate (and therefore the partitioning) of metals in soil systems are represented in Figure 1.1. If biotic factors are disregarded, we are left with (a) adsorption of metals by the soil solid phase, which includes chemi-sorption of metals by the (hydr)oxides of iron, aluminium and manganese and reactive particulate organic carbon (RPOC) and physi-sorption by clay minerals, (b) formation and dissolution of precipitates and minerals and (c) complexation with solution phase ligands, such as inorganic anions and natural organic materials, such as humic and fulvic acids (see for eg. Jones and Jarvis, 1981; Bolt and van Riemsdijk, 1987; Evans, 1989; McBride, 1989, 1994; Sposito, 1989; Ritchie and Sposito, 1995). The distribution of a metal amongst the different forms is controlled by the relative concentrations of the reacting components as well as the parameters pH, redox potential pe, ionic strength I and temperature.

It thus follows that any model which aims at describing the fate of metals in soils should take the processes depicted in Figure 1.1, as well as their dependence on the system state parameters, into account. The inclusion of these processes in the general chemical equilibrium framework are discussed in the next paragraph.

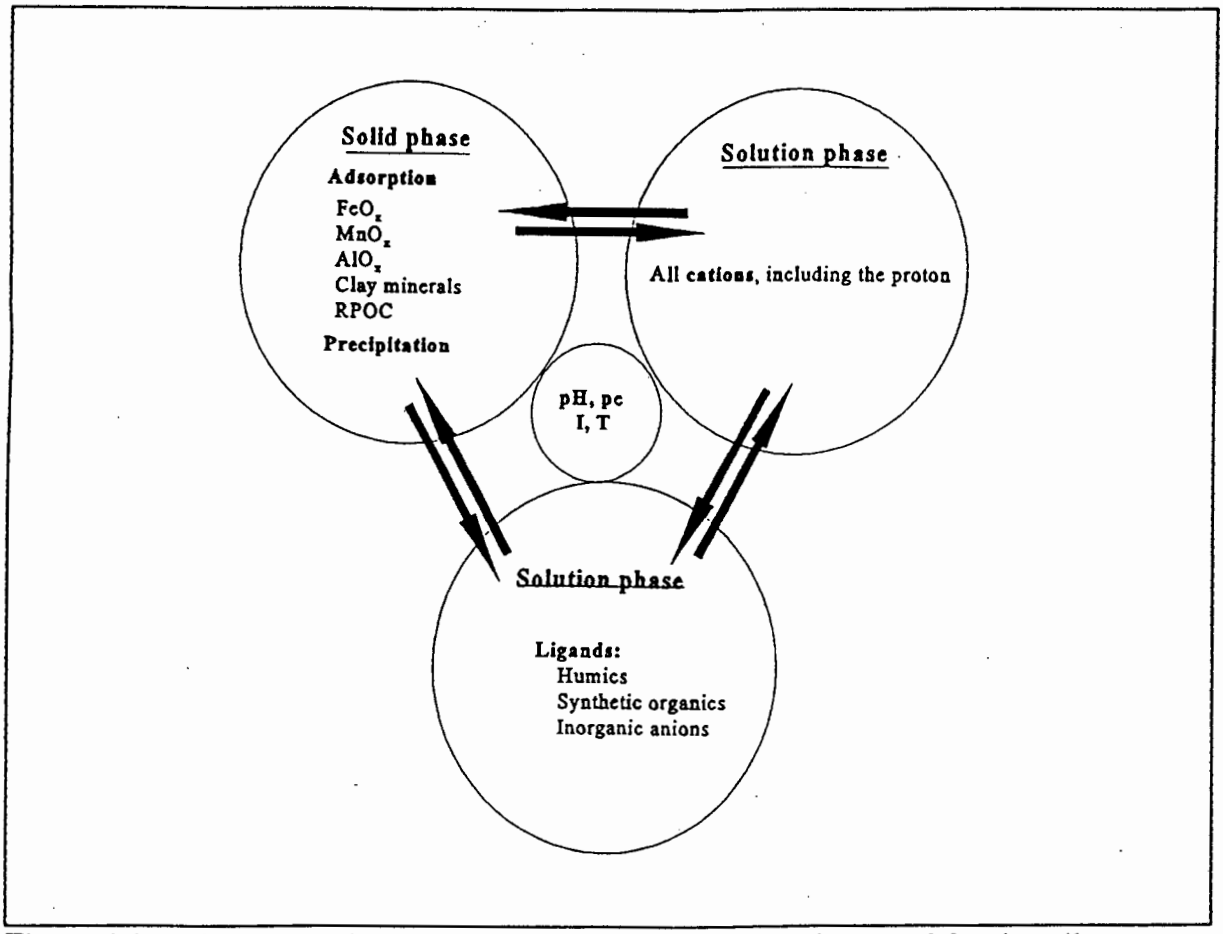

Figure 1.1 A diagrammatic representation of proceses affecting metal fate in soil systems.

1.2 The general chemical equilibrium modelling framework

The mathematical foundation of the equilibrium problem rests on the laws of mass action and mass-balance. The law of mass balance states that the total concentration of a component X_i, T_{Xi}, is equal to the sum of the concentrations of species C_j which contains component X_i.

Mathematically, this may be written as

$$T_{X_i} = [X_i] + \sum_{j=1}^{J} r_{ji}[C_j] \quad \ldots\ldots\ldots\ldots\ldots\ldots \quad (1.2)$$

where J = number of complexes formed which contains component X_i, r_{ji} = stoichiometric coefficient of X_i in species (or complex) C_j and $X_i \in \{X_1, X_2, ..., X_N\}$.

The law of mass-action relates the activity of species C_j, $\{C_j\}$, to the activities of the components, $\{X_i\}$, from which species C_j is formed through a thermodynamic formation constant β_j^T. Thus, the law of mass-action may be written as

$$\{C_j\} = \beta_j^T \prod_{n=1}^{N} \{X_n\}^{r_{jn}} \quad \ldots\ldots\ldots\ldots\ldots\ldots \quad (1.3)$$

β_j^T may be expressed in terms of concentrations and activity coefficients,

$$\beta_j^T = \frac{\gamma_{C_j}[C_j]}{\prod_{n=1}^{N} (\gamma_{X_n}[X_n])^{r_{jn}}} \quad \ldots\ldots\ldots\ldots\ldots\ldots \quad (1.4)$$

The concentration of each species C_j may now be written in terms of the concentrations of components X_n constituting the species, activity coefficients and thermodynamic equilibrium constants

$$[C_j] = \Gamma_j \beta_j^T \prod_{n=1}^{N} [X_n]^{r_{jn}} \quad \ldots\ldots\ldots\ldots\ldots\ldots \quad (1.5)$$

with

$$\Gamma_j = \frac{\prod_{n=1}^{N} \gamma_{X_n}^{r_{jn}}}{\gamma_{C_j}} \quad \ldots\ldots\ldots\ldots\ldots\ldots \quad (1.6)$$

By substituting (1.4) in (1.2), we obtain

$$T_{X_i} = [X_i] + \sum_{j=1}^{J} r_{ji}\Gamma_j\beta_j^T\prod_{n=1}^{N}[X_n]^{r_{jn}} \quad \ldots\ldots\ldots\ldots\ldots (1.7)$$

Equation 1.7 is general. That is, component X_i may refer to a component in the solution phase, including the binding sites of humic substances or, to adsorption sites on the surface of a solid.

1.3 From conceptual soil model to chemical equilibrium model

Translating the conceptual soil model presented in Figure 1.1 into the general equilibrium framework is, in principle easy. However, due to the complexity of the soil system, the number of components as well as the number of reactions each component participate in is large. This leads to a large number of complex mass balance equations describing the soil system. This may be illustrated considering a hypothetical soil system consisting of:

(i) adsorption phases ADS1, ADS2, ADS3,...., ADSx,

(ii) solution phase ligands $L^{(1)}$, $L^{(2)}$, $L^{(3)}$,...., $L^{(n)}$ and

(iii) metals $M^{(1)}$, $M^{(2)}$, $M^{(3)}$,....., $M^{(m)}$.

A mass balance equation for a metal M may be written as follows:

$$T_M^{soil} = T_M^{aqueous} + T_M^{solid} + T_M^{gaseous} \quad \ldots\ldots\ldots\ldots\ldots\ldots\ldots\ldots\ldots\ldots (1.8a)$$

Say M is not volatile. Thus, we may set $T_M^{gaseous} = 0$. Thus,

$$T_M^{soil} = T_M^{aqueous} + T_M^{solid} \quad \ldots\ldots\ldots\ldots\ldots\ldots\ldots\ldots\ldots\ldots\ldots\ldots\ldots\ldots (1.8b)$$

In the soil system (soil solid phase and pore-water), the metal may participate in numerous chemical reactions. The metal may form complexes with dissolved organic matter (DOM), inorganic ligands such as PO_4^{3-}, CO_3^{2-}, SO_4^{2-}, Cl^- etc., the metal may be oxidized or reduced, the metal may form insoluble precipitates with anions and the metal may sorb onto the adsorption surfaces present in the soil solid phase.

For each component present in the soil system (i.e. metal, ligand and adsorption phase), a Mass Balance Equation (MBE), which includes all of the processes a given component participates in, may be written. Thus, for metal M under consideration, we may write:

$$T_M^{soil} = [M \text{ complexed}] + [M \text{ adsorbed}] + [M \text{ precipitated}]$$

This may be rewritten as:

$$T_M^{soil} = [M^{n+}] + [ML^{(1)}] + [ML_2^{(1)}] + ... + [ML_n^{(1)}] + [ML^{(2)}] + [ML_2^{(2)}] + ... + [ML_p^{(2)}] + ... + [ML^{(q)}] + [ML_2^{(q)}] + ... + [ML_r^{(q)}] + [MOH] + [M(OH)_2] + ... + [M(OH)_k] + [M\text{-}ADS1] + [M\text{-}ADS2] + [M\text{-}ADS3] + ... + [M\text{-}ADSz] + [ML^{(1)}\text{-}ADS1] + [ML_2^{(1)}\text{-}ADS1] + ... + [ML_r^{(1)}\text{-}ADS1] + ... + [ML_r^{(q)}\text{-}ADSz] \quad (1.9a)$$

Through the expression for the equilibrium constant β (equation 1.4), the MBE may be written in terms of ß's, $[M^{n+}]$, $[L^{(i)}]$, [ADSx]:

$$T_M^{soil} = [M^{n+}] + \Sigma^q_{i=1}\Sigma^r_{j=1}\Sigma^K_{k=-K} {}^i\beta_{1jk}[M^{n+}][L^{(i)}]^j[H^+]^k + \Sigma^q_{i=1}\Sigma^r_{j=0}\Sigma^K_{k=-K}\Sigma^z_{x=1} {}^i\beta_{1jkx}[M^{n+}][ADSx][L^{(i)}]^j[H^+]^k \quad (1.9b)$$

An analogous MBE for each component M, $L^{(i)}$, H, ADSx may be written.

Thus, it is in principle possible to solve MBE's and determine system speciation if T_M^{soil}, T_L^{soil}, T_{ADS}, $[H^+]$ and ß's are known.

In reality, however, several confounding factors are present which necessitates several assumptions and simplifications to enable setting up an equilibrium model of soil systems. Assumptions and simplifications are necessary on two levels: first, soil chemical processes accounted for in the chemical model must be trimmed down or simplified. Second, due to experimental difficulties in characterizing soil systems, certain assumptions and operational definitions have to be employed.

The major problems encountered in modelling metal fate in soil systems are the inclusion of (i) adsorption of metals by the soil solid phase and (ii) the complexation of metals by dissolved organic matter (DOM) present in the soil matrix. These problems are a direct result of the nature of the adsorption surfaces and DOM. Both soil adsorption phases and DOM are structurally poorly characterized. The nett result of this is that very little is known about the functional group arrangements responsible for metal binding. This forces the use of secondary - or meta models to incorporate these very important aspects in a soil equilibrium model.

1.4 Models for the inclusion of metal - dissolved organic matter and metal - soil solid phase interactions.

In the previous section, the conceptual model was translated into the general equilibrium framework. In this section, we focus on filling in the terms of the mass balance equations

describing the soil system in chemical equilibrium terms. The sub-models employed to facilitate the inclusion of dissolved organic matter and adsorption processes in the equilibrium model is discussed.

1.4.1 Complexation with Dissolved Organic Matter

Several approaches have been developed to describe the metal complexation properties of Dissolved Organic Matter. In general, these may be grouped as (a) discrete ligand approaches and (b) continuous distribution approaches. Discrete ligand models describe the complexation characteristics of humic substances through a set of discrete ligands and associated equilibrium constants. Ligand concentrations and equilibrium constants are determined through the application of least squares optimization techniques on a specific data set (Evans, 1989). Continuous distribution models assumes a continuum of binding sites, with some statistical distribution in log K space. Again, model parameters are determined from a specific data set. According to Evans (1989), a problem with these approaches are that they lack generality, i.e. the model parameters a describing the complexation properties of the humic substance are generally only applicable to the conditions under which they were derived and to the specific sample for which they were derived.

Recently, Benedetti *et al.* (1995) developed a non-ideal competitive adsorption model which was able to describe the binding of H, Ca, Cu and Cd over a wide range of conditions. This model belongs to the continuous distribution family. Although the results from this approach is promising, it suffers from two draw backs. First, the model requires to be coded into a chemical equilibrium programme. Thus, the binding parameters obtained from the model is

not generally usable. Second, at present data for a number of metals are not available.

Tipping (1994) developed the WHAM model. This is a discrete ligand model which also includes the polyelectrolyte properties of humic substances. However, this model is also part of a specific modelling package which does not allow the inclusion of adsorption processes. Seen in the light of the importance of adsorption processes, this is a major shortcoming. Furthermore, this model is also not freely available.

Other examples of models for the complexation behaviour of metals are available (Marinsky *et al.*, 1995; Westall *et al.*, 1995). Although all of these approaches have merit, they suffer from the same problems as those mentioned above viz. data availability and generality. For a DOM - metal complexation model to be included in the equilibrium framework, binding site concentrations and equilibrium constants describing the acid-base and metal complexation properties of these binding sites are needed. Because of this, none of the approaches discussed above can at this stage be included in a general equilibrium model.

MINTEQA2 v. 3.11 (Allison, 1991) is released with its own cation - DOM interaction model. The model is in essence a continuous distribution model which assumes a large number of monoprotic binding sites which are normally distributed with respect to their equilibrium constants. The model uses ideas developed by Perdue *et al.* (1984) and Dobbs *et al.* (1989). The equilibrium constants included in the data base were measured by Susetyo *et al.* (1991), using Suwannee River fulvic acid. In order to use this model, the user is required to enter an estimate of total binding site concentration. However, the available database for metal interactions is limited.

A discrete ligand approach which allows for the modelling of metal complexation by DOM in a general way was developed by Murray and Linder (1983, 1984). The basis of this approach is the assumption that the differences observed in the binding properties of different humic materials are caused by different functional group arrangements on the underlying carbon backbone. To take this into account, a method was developed which generates a large number of molecules, each with a random arrangement of functional groups. Certain predetermined binding site configurations are identified and linked to simple organic ligands with similar binding site configurations. These simple organic acids are then used as models for humic substance binding sites. The major advantages of this approach are (a) it's generality and (b) thermodynamic data describing the protonation and metal complexation behaviour of the model binding sites are readily available. This method has been used by Mountney and Williams (1992) to model metal complexation by soil derived humic substances. Because of it's generality, this model was used to account for the influence of dissolved organic matter on metal speciation in soil systems.

This model, RANDOM, requires information about the elemental composition, degree of aromaticity and functional group content of humates. From this information, subject to certain chemical rules, carbon backbones are generated and functional groups are assigned to the backbones. The atomic environment of each functional group is compared to a number of simple, well defined ligands, which are used as model binding sites. For each set of elemental composition and functional group content data, a large number of molecules is generated and average binding site concentrations are calculated.

The generation of each molecule proceeds via two steps viz. (a) the generation of a carbon

backbone and (b) the assignment of functional groups to the carbon backbone. The generation of the carbon backbone is controlled by the following assumptions:

(i) Only single aromatic rings are allowed i.e. fused ring systems are not permitted.

(ii) Two aliphatic side chains are assumed per aromatic ring, ortho, meta or para to each other.

(iii) Each aromatic ring is joined to two other rings via the aliphatic chains. This results in an overall cyclic structure.

(iv) Branching of aliphatic chains is limited to methyl groups.

(v) Double and triple bonds in the aliphatic chains are neglected.

(vi) Carbonyl groups are positioned randomly on the aliphatic chains as ketones. However, α-diketone arrangements are avoided.

The positioning of functional groups on the carbon backbone is controlled by the following rules:

(i) Quinone oxygens occur only in pairs, either ortho or para to each other.

(ii) Phenolic OH, methoxyl and aromatic carboxyls are randomly assigned to aromatic carbons not occupied by aliphatic chains or quinone oxygens.

(iii) Alcoholic OH and the remaining carboxyls are assigned to random positions on aliphatic side chains. Two restrictions are, however, observed: (a) Not more than two groups may be assigned to a methyl carbon and (b) β-keto acid arrangements are avoided.

Output from the model is average binding site concentrations, expressed as $mol.g^{-1}$ organic matter. Site concentrations in $mol.dm^{-3}$ for input into a chemical equilibrium model is

determined from the average binding site concentrations and organic matter content, in $g.dm^{-3}$.

This approach allows metal complexation by DOM to be easily incorporated into the chemical equilibrium modelling framework. The incorporation of this approach into the chemical equilibrium modelling framework is a two-step process. First, RANDOM is executed to provide concentration estimates for the selected binding sites. Second, these discrete binding sites are included as input for the speciation programme. The database employed contains thermodynamic data (log K's) for reactions between the binding sites and cations. Thus, the amount of cation complexed to all the ligands used as model compounds for binding sites on humic material estimates the amount of cations complexed by humic materials.

1.4.2 Accounting for adsorption processes at the solid-solution interface

The Surface Complexation Model (SCM), pioneered by the Stumm and Schindler school (for recent reviews, see Schindler and Stumm, 1987; Schindler, 1991) provides a useful framework for the discussion of adsorption processes. In this approach, adsorption of cations is viewed as taking place at specific sites and the coordinating surface functional groups are viewed as complexant ligands. The advantage of this approach is that adsorption reactions may be easily incorporated into the thermodynamic framework, discussed in paragraph 1.3, for aqueous phase complexation.

The fundamental chemical interactions between solutes and the surface groups are given below:

Hydrolysis (Acid-base)

$$\equiv SOH_2^+ \rightleftharpoons \equiv SOH + H^+ \quad (1.10)$$

$$\equiv SOH \rightleftharpoons \equiv SO^- + H^+ \quad (1.11)$$

Complexation

$$\equiv SOH + M^{n+} \rightleftharpoons \equiv SOM^{(n-1)+} + H^+ \quad (1.12)$$

$$2\equiv SOH + M^{n+} \rightleftharpoons (\equiv SO)_2M^{(n-2)+} + 2H^+ \quad (1.13)$$

Ligand exchange

$$\equiv SOH + L \rightleftharpoons \equiv SL + OH^- \quad (1.14)$$

$$2\equiv SOH + L \rightleftharpoons (\equiv S)_2L + 2OH^- \quad (1.15)$$

Ternary complexes

Type A (metal sandwiched between surface and ligand)

$$\equiv SOH + M^{n+} + jL \rightleftharpoons \equiv SOML_j + H^+ \quad (1.16)$$

Type B (Ligand exchange at surface takes place first, metal binds to adsorbed ligand)

$$\equiv SOH + L + M^{n+} \rightleftharpoons \equiv SOLM + OH^- \quad (1.17)$$

In principle, equilibrium or adsorption constants for each of the above reactions can be obtained experimentally. These constants are conditional constants which, apart from dependence on temperature, pressure and ionic strength, also exhibits a dependence on the degree of surface coverage. Factors that could contribute to the observed dependence include (a) the existence of a surface potential, (b) lateral interactions between adsorbed species and (c) surface heterogeneity. Most efforts to account for the surface coverage dependency of adsorption constants focuses on the effect of the surface potential.

The overall change in Gibbs free energy during an adsorption reaction, ΔG_{ads}, is the sum of the change in Gibbs free energy due to specific chemical interactions and that due to electrostatic interactions. The change in free energy arising from specific chemical interactions, ΔG_{int}, is independent of surface charge. The free energy change arising from electrostatic effects, ΔG_{coul}, is dependent on surface charge. The overall change in Gibbs free energy in the system is given by

$$\Delta G_{ads} = \Delta G_{int} + \Delta G_{coul} \quad \ldots\ldots\ldots\ldots\ldots\ldots \quad (1.18)$$

It should be noted that this separation of ΔG_{ads} into its constituent parts is not experimentally possible (Westall, 1987). It is, however, theoretically convenient to perform this separation, as will be seen below.

ΔG_{coul} is related to the surface potential. By considering the work performed when transporting charges through a potential field, an expression for ΔG_{coul} may be derived. We have

$$\Delta G_{coul} = \Delta Z F \Psi \quad \ldots\ldots\ldots\ldots\ldots\ldots\ldots\ldots \quad (1.19)$$

where

F = Faraday's constant (96485 $C.mol^{-1}$)

ΔZ = change in charge of surface species due to the sorption reaction

Ψ_0 = surface potential

Thus, the expression for ΔG_{ads} becomes

$$\Delta G_{ads} = \Delta G_{int} + \Delta Z F \Psi \quad \ldots\ldots\ldots\ldots\ldots\ldots \quad (1.20)$$

Now, from

$$\Delta G = -RT \text{ Ln } K$$

where R = Gas constant, T = temperature in K, an expression for the intrinsic equilibrium constant K_{int} is obtained:

$$K_{intr} = K_{app}\, e^{\frac{\Delta Z F \Psi_0}{RT}} \quad \ldots\ldots\ldots\ldots\ldots\ldots \quad (1.21)$$

From the last equation it is clear that Ψ_0, the surface potential, is required. However, it is a general result that Ψ_0 is not experimentally accessible (Hiemenz, 1986). Therefore, Ψ_0 is calculated by employing a model which gives the relationship between surface charge and potential. This aspect is discussed in the next paragraph.

1.4.3 Models of the solid/solution interface

Several models relating surface charge to surface potential are available. Although these models differ from each other in terms of the surface species postulated or the exact location where adsorption occurs, they are all related to the Gouy-Chapman-Stern theory of the electrical double layer (see Westall and Hohl, 1980; Stumm and Schindler, 1987; Westall, 1987). A thorough discussion on the underlying Gouy-Chapman theory of the double layer can be found in Hiemenz (1986).

Models commonly used for relating surface charge to surface potential are (i) the Constant Capacitance (CC) model, (ii) the Diffuse Double Layer (DDL) model and (iii) the Triple Layer (TL) model. The way in which the models view the structure of the double layer is

illustrated in Figures 1.2 and 1.3.

For the CC model, surface charge is related to surface potential through

$$\sigma_0 = C\Psi_0 \quad \ldots\ldots\ldots\ldots\ldots\ldots \quad (1.22)$$

Surface charge σ_0 results because of specifically adsorbed ions. These ions experience a potential Ψ_0. All non-specifically adsorbed counter ions are excluded from the "0" layer. In the application of the CC model, the capacitance term, C, is treated as an adjustable parameter.

The DDL model relates surface charge to surface potential through

$$\sigma_0 = (8RT\varepsilon\varepsilon_0 c10^3)^{\frac{1}{2}}\sinh\left(\frac{Z\Psi_0 F}{2RT}\right) \quad \ldots\ldots\ldots\ldots \quad (1.23)$$

This equation simplifies to

$$\sigma_0 = (8RT\varepsilon\varepsilon_0 c10^3)^{\frac{1}{2}}\left(\frac{Z\Psi_0 F}{2RT}\right) \quad \ldots\ldots\ldots\ldots\ldots \quad (1.24)$$

for $\Psi_0 < 25$mV because the hyperbolic sine function may be approximated by ($F\Psi/2RT$) at such low values of Ψ_0. Here the assumption is also made that surface charge σ_0 results from ions specifically adsorbed on the surface. These ions are subjected to a potential Ψ_0.

The TL model (Davis *et al.*, 1978) differs from the CC and DDL models in that it assumes regions of different dielectric constants and capacitances in close proximity to the surface, as shown in Figure 1.3.

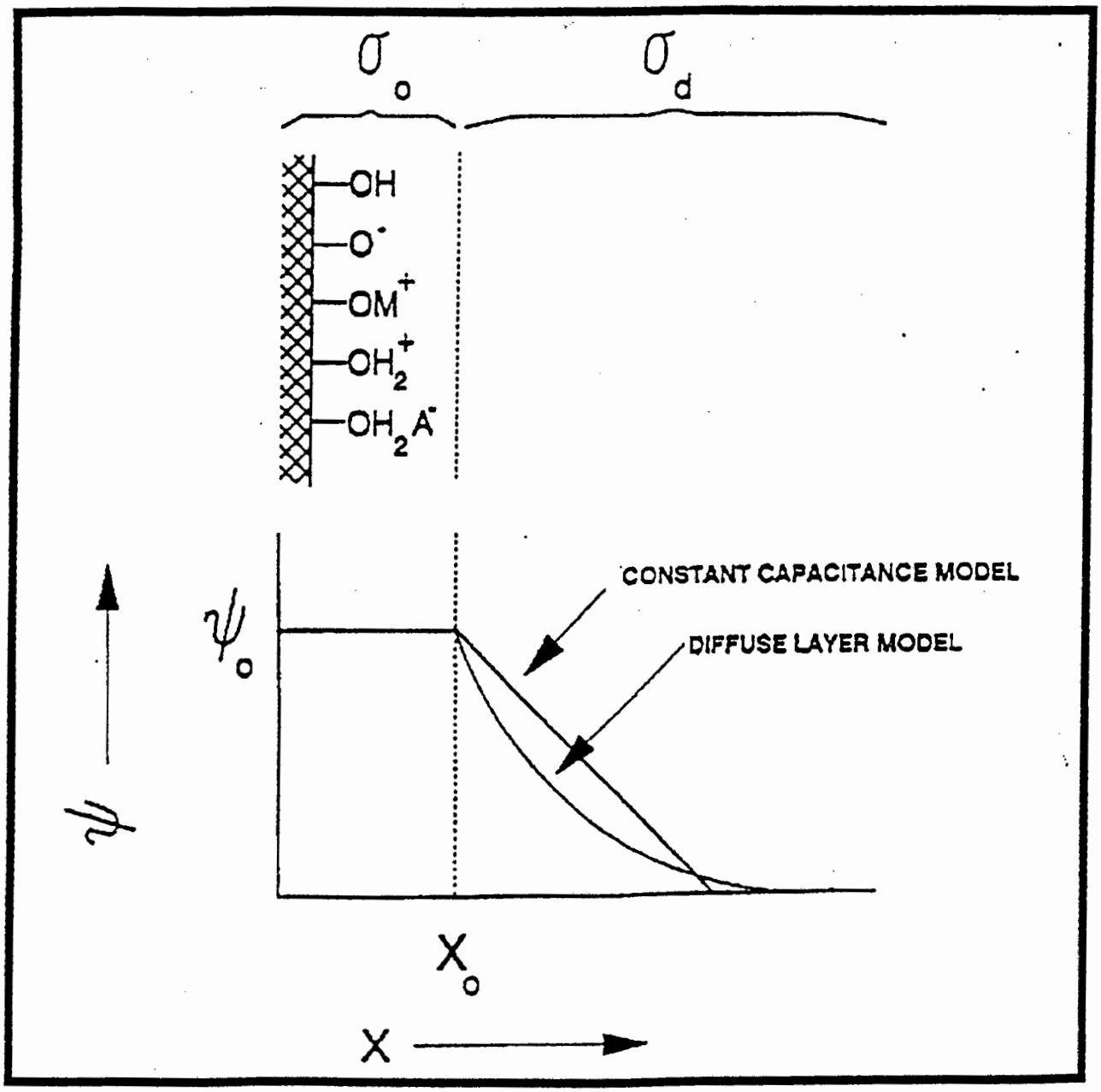

Figure 1.2 Schematic representation of the surface charge/potential relationships used in the constant capacitance and diffuse double layer models (Allison *et al.*, 1991).

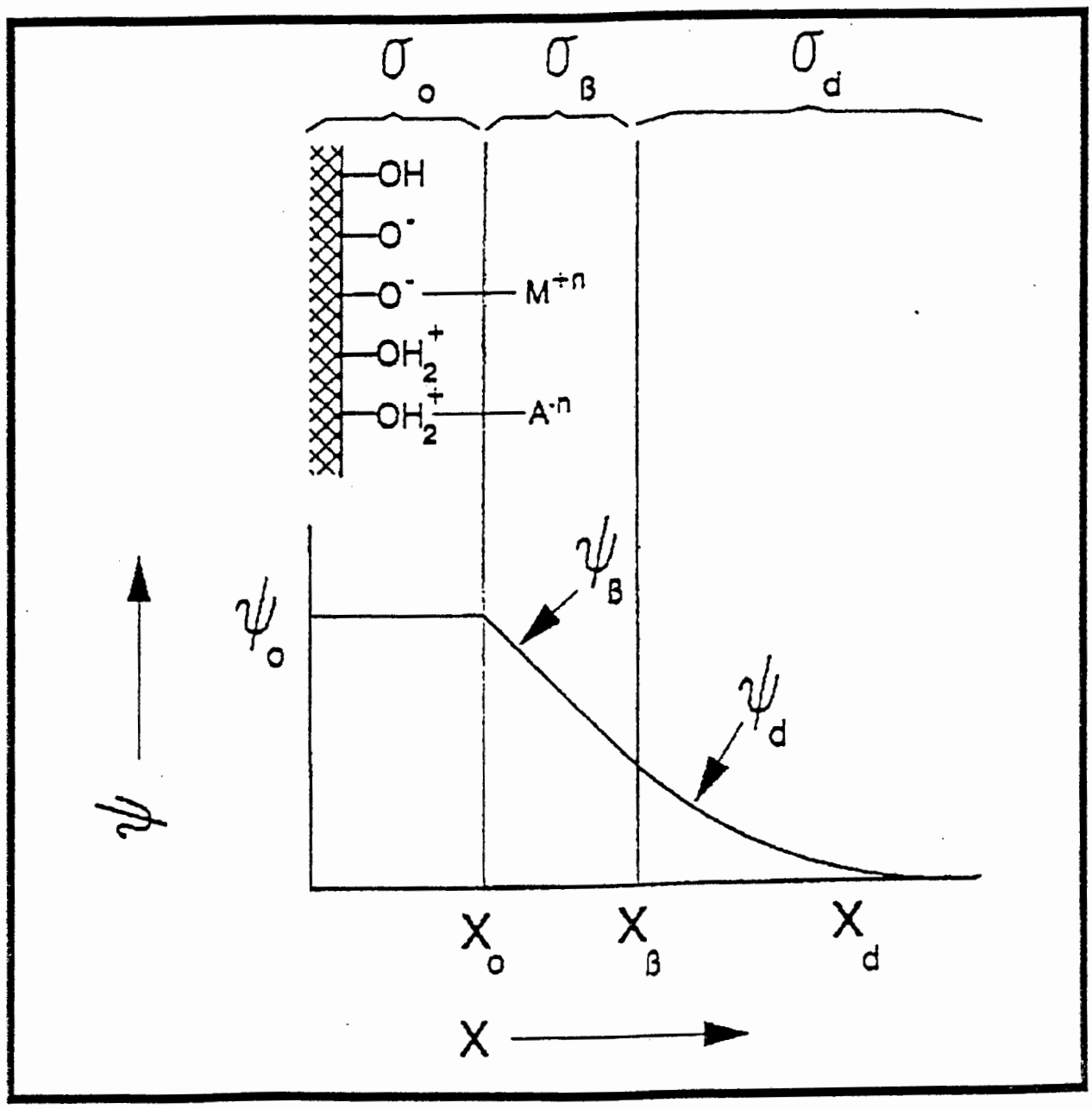

Figure 1.3 Schematic representation of surface species and charge/potential relationships in the triple layer model (Allison *et al.*, 1991).

The surface is denoted as the "0" plane, the inner layer or Inner Helmholz Plane (IHP) by "β" and the outer layer or Outer Helmholz Plane (OHP) by "d". The region between the surface and the IHP is characterized by a capacitance C_1 while the region between the IHP and OHP is characterized by a capacitance C_2. The boundaries of each of these regions or planes have a different charge distribution, σ, and potential Ψ. The surface is characterized by charge σ_0 and Ψ_0, the inner layer by σ_β and Ψ_β and the outer layer by σ_d and Ψ_d. Furthermore, the model assumes that only H^+ and OH^- ions enters the innermost layer and contribute to σ_0 and experiences Ψ_0. All other interactions between solute and surface is confined to the β - plane.

Charge - potential relationships for the TL model are given by

$$\sigma_0 = C_1 (\Psi_0 - \Psi_\beta) \quad \ldots\ldots\ldots\ldots\ldots\ldots \quad (1.25)$$

$$\sigma_\beta = C_1(\Psi_\beta - \Psi_0) + C_2(\Psi_\beta - \Psi_d) \quad \ldots\ldots\ldots\ldots \quad (1.26)$$

$$\sigma_d = C_2(\Psi_d - \Psi_\beta) \quad \ldots\ldots\ldots\ldots\ldots\ldots \quad (1.27)$$

These models of the solid/solution interface have been reviewed by Westall and Hohl (1980). They showed that each of the available models of the solid/solution interface is capable of describing material balance data well. A major difference amongst the models are the number of adjustable parameters required by each model to describe experimental data. Of the models discussed, the DDL model has the smallest number of adjustable parameters. The TL model uses capacitances for the regions between the surface and the IHP and the IHP and OHP, together with adsorption constants for electrolyte adsorption as adjustable parameters.

In the present work, the DDL model of the solid/solution interface is used in all instances where Ψ_0 is needed. That is, the adsorption data obtained for δ-MnO_2, which are reported in Chapters 2, 3 and 4, are interpreted using the surface complexation and diffuse double layer models.

The major criticism levelled against the DDL model is that it fails to describe electrokinetic data. More specifically, surface potentials calculated with the DDL model are typically higher than zeta potentials obtained from electrophoretic studies (Dzombak and Morel, 1990). However, Dzombak and Morel illustrates that the DDL model may be used to fit zeta potential data by specifying the location of the shear plane as a function of solution conditions.

The purpose of the model should also be kept in mind. In the present work, the purpose of the model is to describe material balance data in order to obtain parameters useful in the modelling of adsorption processes. There are many uncertainties involved in this. To minimize uncertainty, the simplest possible model which describes experimental data adequately should be used. In the present case, it is the DDL model. Furthermore, by employing the DDL model for the interpretation of MnO_2 adsorption data, a significant step forward in the modelling of adsorption processes can be made since the MnO_2 data set can be used in conjunction with the HFO data set of Dzombak and Morel, thereby enabling the incorporation of more than one solid phase in our models.

The preceding may be summarized as follows:

(i) A surface complexation model is used to model adsorption reactions.

(ii) Adsorption constants exhibit a surface coverage dependency.

(iii) The surface coverage dependency is ascribed solely to electrostatic effects.

(iv) Electrostatic effects are taken into account by calculating the change in Gibbs free energy due to moving charges through a potential field arising from the charged surface.

(v) Surface potential is calculated using the Diffuse Double Layer model.

(vi) By combining equations 1.23 and 1.21 an expression for adsorption constant incorporating the dependence on surface potential/charge is obtained.

(vii) the expression for the adsorption constant and the reactions depicted in equations 1.10 to 1.17 thus allows the inclusion of adsorption processes in the general equilibrium framework of equation 1.6.

1.5 Chemical equilibrium modelling data requirements

From the preceding discussion it is clear that in order to set up a chemical equilibrium model of a system, the following information is required:

(a) the total concentrations of the components constituting the system to be modelled

(b) chemical reactions that take place in the system under investigation (a chemical reaction is known once we know the identities and amounts of components participating in the reaction),

(c) parameters defining the state of the system, such as pH, temperature, ionic strength and redox potential.

(d) the equilibrium constants for each of these chemical reactions,

Data required under points (a), (b) and (c) are problem and site specific, i.e. the reactions included in the model will depend on the analytical data available (i.e. components for which total concentrations are available) and parameters such as pH and redox potential will vary from site to site. These must be determined for the specific soil sample that is to be modelled.

Data required under point (d) warrants further discussion. In the case of aqueous phase reactions, data are available from compilations of thermodynamic data, such as NIST (1989), JESS (May and Murray, 1991a,b) and MINTEQA2 (Allison *et al.*, 1991). These data are universally applicable, i.e. once a thermodynamic database has been established, it may be used for several different applications (this is not strictly true since procedures to correct constants to different sets of conditions may only be applicable over limited ranges).

In the case of adsorption processes, adsorption constants describing the sorption of metals by the phases are needed. This is problematic because, contrary to the situation for solution phase equilibria, extensive compilations of sorption data for metal sorption by important soil solid phases are not available. To compound the problem further, sorption constants are also expressed using the different models of the surface discussed in the previous paragraph. These models are based on the same concepts but they assume different physical-chemical configurations for ions sorbed at the mineral/water interface. As a result, the various models employ somewhat different parameters and the parameters that are common among the models are not directly comparable (Dzombak and Hayes, 1992). Thus, sorption constants expressed in terms of different models are not interconvertible. The net result of this is that the consideration of surface complexation in chemical equilibrium modelling of natural

systems has been impeded by the lack of sorption data. In an attempt to overcome some of these problems, Dzombak and Morel (1990) published a consistent set of Diffuse Double Layer adsorption constants for sorption by Hydrous Ferric Oxides. This compilation of data has been included in the MINTEQA2 (Allison *et al.*, 1991) speciation programme. However, for other important phases, such as MnO_2, no consistent set of adsorption constants are available.

The importance of manganese dioxide, in particular δ-MnO_2, in the scavenging of metals in natural systems has been postulated by a number of workers (Morgan and Stumm, 1964; McKenzie, 1989; Onuki, 1990). However, to date, few studies aimed at measuring surface complexation constants for this solid have been reported. Catts and Langmuir (1986) measured Triple Layer constants for Cu, Pb and Zn by δ-MnO_2 while Fu *et al.* (1991) measured Triple Layer constants for Cd and Cu by δ-MnO_2. Smith and Jenne (1991) reworked some published adsorption data and published a set of Triple Layer adsorption constants for the adsorption of a number of metals by manganese and iron oxides. However, no Diffuse Double Layer adsorption constants for metal sorption by manganese dioxide have been published to date. Because of this, it is not possible to include sorption by both Hydrous Ferric Oxide and δ-MnO_2 in an equilibrium model to predict metal partitioning in soils.

1.6 Aims and objectives

The aims of this work is thus the expansion of the available adsorption constant data base so that chemical equilibrium models of soil systems can be developed which are more complete

in terms of important soil sorption phases included.

The objectives of this work may be stated as:

(i) measurement of adsorption constants for Ni, Cu, Zn, Cd and Pb sorption by δ-MnO_2,

(ii) elucidation of the surface chemistry of δ-MnO_2,

(iii) assessment of the applicability of the surface complexation approach to describe sorption data

(iv) predicting the partitioning of Ni, Cu, Zn, Cd and Pb over the solid/solution interface in a number of soils collected in the Netherlands.

In the chapters that follow, the approach followed in this endeavour is outlined. Chapters 2, 3 and 4 describe the potentiometric determination of surface complexation parameters for δ-MnO_2. Chapter 5 discusses the construction of a chemical equilibrium model to predict metal partitioning on a number of field soils. The modelling results are presented in chapter 6 while chapter 7 contains concluding remarks.

Chapter 2 A surface protonation model for δ-MnO_2

This chapter describes the protonation study carried out to determine surface acid/base parameters for δ-MnO_2. The preparation, characterization and potentiometric procedure is discussed. Experimental results are shown and the reproducibility obtained is discussed. Consideration is then given to the determination of surface protonation constants.

2.1 Materials and methods

All reagents were used from the container without further purification. KOH (0.1 M) and HNO_3 (0.1M) were prepared from Merck Titrisol ampoules with boiled-out glass distilled water. The 0.1 M KOH and 0.5 M KNO_3 (Merck GR) background electrolyte solution were prepared using boiled-out glass distilled water in a glove box under N_2 atmosphere. KOH solutions were stored in N_2 flushed polyethylene bottles fitted with Metrohm glass transfer units and self-indicating "Carbosorb" CO_2 traps. Reagent storage bottles were attached to Metrohm Dosimat exchange units. At no point were these reagents exposed to air.

KOH and HNO_3 was standardized against potassium hydrogenphthalate and sodium tetraborate respectively (Vogel, 1981).

2.1.1 Preparation of MnO_2

Manganese dioxide was prepared according to the "redox" method suggested by Stroes-Gascoyne *et al.* (1987). Manganese dioxide forms according to the reaction

$$3Mn^{2+} + 2MnO_4^- + 2H_2O \rightharpoonup 5MnO_2 + 4H^+.$$

δ-MnO_2 was prepared by dissolving 5.2 g $Mn(NO_3)_2.4H_2O$ (SAARCHEM, AR) in 900 cm^3 deionized, glass-distilled water. To this, a 100 cm^3 premixed solution of 2.2 g $KMnO_4$ (May and Baker) and 1.6 g KOH (SAARCHEM, AR) was added from a fast dripping burette. A dark brown to black precipitate formed immediately. The solution was stirred continuously during the addition. Stirring of the covered solution was continued for one hour. Stirring was discontinued and the suspension was allowed to settle out (ca. 30 minutes). Excess supernatant was removed by suction.

The concentrated suspension was transferred to glass centrifuge tubes and centrifuged for 20 minutes. The supernatant was decanted, distilled water was added to the tube and the solid was resuspended by shaking the tube. After each decantation the conductivity of the supernatant was measured and compared with that of a $1x10^{-4}$ M KNO_3 solution. After four cycles of washing and centrifuging a conductivity of twice the $1x10^{-4}$ M KNO_3 solution was obtained. However, at this stage the background electrolyte level was so low that the suspension stayed in a dispersed state even after prolonged centrifuging. The washed suspension was transferred to a round bottom flask and the volume was made up to 1000 dm^3 with distilled water. The conductivity of the suspension was approximately a factor of four lower than that measured for the $1x10^{-4}$ M KNO_3 solution. The suspension was stored in a stoppered round bottom flask with constant stirring, using a Teflon coated magnetic stirrer bar.

The concentration of δ-MnO_2 solid was determined by transferring six 20.0 cm^3 aliquots of suspension into six pre-weighed glass vials. Supernatant was removed by drying in a vacuum

oven at 90°C for 48 hours. The vials were removed and transferred into a desiccator containing silica gel as desiccant. The vials containing the dried solid were weighed again and the difference in mass yielded the amount of solid present in a 20.0 cm^3 aliquot of suspension. A solids concentration of 1.75 ± 0.0082 $g.dm^{-3}$ was obtained.

2.1.2 Characterization of MnO_2

Brunauer-Emmet-Teller (BET) analysis of N_2 sorption data and X-Ray Diffraction analysis were employed to characterize the MnO_2 sample. The results obtained from each technique are summarized below.

2.1.2(a) Brunauer-Emmet-Teller (BET) surface area determination

BET surface area determinations were carried by the Department of Chemical Engineering of the University of Cape Town. Samples submitted for BET analysis were dried beforehand in a vacuum oven at 90°C for 48 hours and homogenized using an agate mortar and pestle. Prior to BET analysis, samples were outgassed at 120°C for 12 hours. BET analysis of N_2 adsorption data yielded a surface area of 331 $m^2.g^{-1}$. This corresponds well with values reported by other workers (Fu *et al.*, 1991; Catts and Langmuir, 1986). It is also in the range found by Stroes-Gascoyne using copper adsorption maxima data (Stroes-Gascoyne *et al.*, 1987).

The gas adsorption isotherms (c.f. Figure 2.1) obtained showed marked hysteresis and corresponded to a *Type IV* isotherm according to the IUPAC isotherm classification system

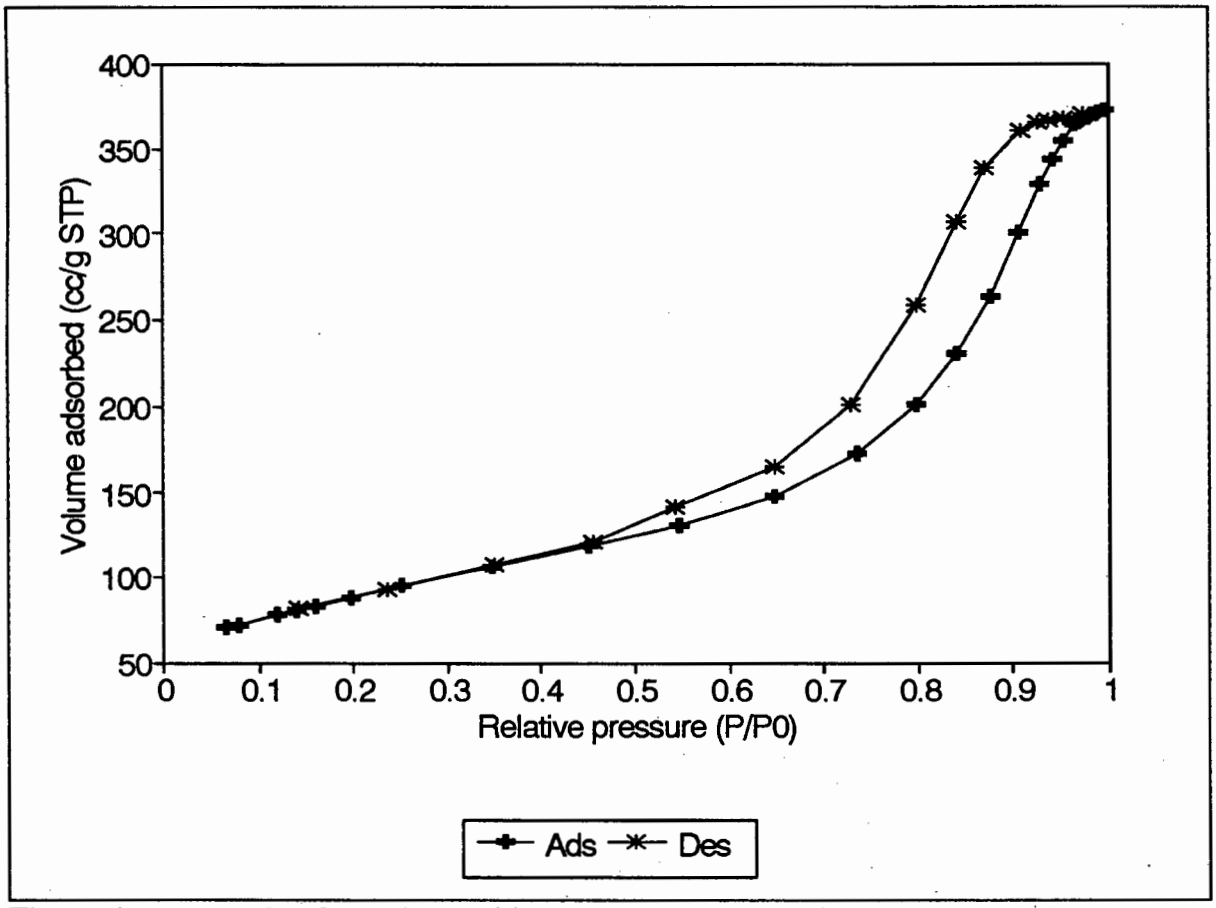

Figure 2.1 Example of a typical $N_2(g)$ adsorption isotherm obtained for δ-MnO_2.

(Sing, 1985). This type of isotherm is associated with capillary condensation taking place in mesopores, that is, pores ranging from 2 nm to 50 nm in width (Sing, 1985). The idea that δ-MnO_2 is a porous solid has been put forward by a number of workers (Manceau, 1992a,b).

2.1.2(b) X-Ray Diffraction (XRD) analysis

Manganese dioxide suspension was dried for 48 hours at 90°C in a vacuum oven. The dried solid was ground to a powder using an agate mortar and pestle. XRD analysis was carried out using CuKα radiation (λ = 1.542 Å) on a Philips diffractometer. The resulting XRD pattern is shown in Figure 2.2. The pattern is indicative of an amorphous solid. The peaks at d=2.44 Å and d=1.44 Å are indicative of δ-MnO_2 (McKenzie, 1989).

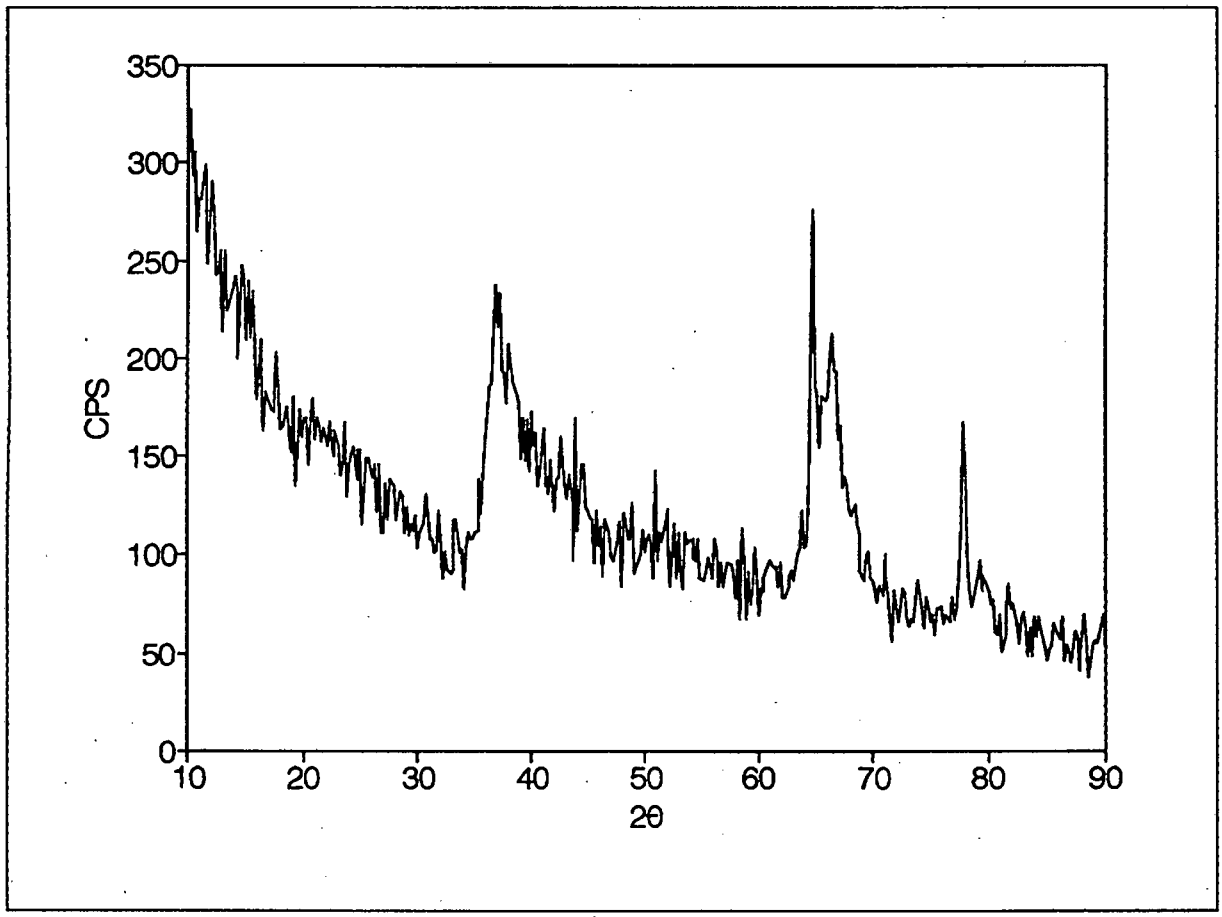

Figure 2.2 X-Ray diffraction pattern for the manganese dioxide used in this study.

2.1.3 Measuring [H^+]

Hydrogen ion concentration was measured using a glass electrode and a calomel reference electrode (Metrohm). A common deficiency in reported equilibrium constant determination studies is the improper calibration of the pH meter (May *et al.*, 1982; Martell *et al.*, 1988). This stems from a failure to appreciate that pH (or hydrogen ion activity) cannot be measured explicitly. In studies aimed at measuring equilibrium constants, the variable of interest is hydrogen ion concentration, [H^+], instead of hydrogen ion activity.

Hydrogen ion concentration is calculated from EMF readings using the Nernst equation:

$$E = E^{const} - sLog[H^+] \quad \cdots\cdots\cdots\cdots\cdots\cdots \quad (2.1)$$

where E^{const} and s are the electrode intercept and slope respectively. The parameter E^{const} incorporates electrode potentials, liquid junction potential effects and activity coefficients. In order to measure $[H^+]$ accurately, a thorough electrode calibration regime should be followed to obtain values for E^{const} and electrode slope s. Three approaches are possible. First, the EMF values measured in two or three standard buffer solutions may be plotted against buffer pH. From this curve the slope s may be calculated and E^{const} may be obtained by extrapolating the curve to pH of zero. However, this procedure is inappropriate because of the difference in buffer and test solution ionic strengths.

Second, a strong acid - strong base titration may be carried out at the ionic strength of the test solution. $Log[H^+]$ can be calculated from the proton mass-balance and the slope s can be taken as the Nernstian value of 59.16. Extrapolation of the resulting straight line to $-Log[H^+]$ zero then yields the value for E^{const}. This method suffers from the following limitations (Linder *et al.*, 1984):

(i) small errors in poorly buffered solutions become very significant,

(ii) glass electrodes do not behave well in alkaline regions because they are somewhat sensitive to alkaline metal ions, and

(iii) at low pH acid effects upon liquid junction potentials becomes significant.

Limitations (ii) and (iii) are usually included in the value of E^{const} by making the assumption that these effects stay constant. Limitation (i) is illustrated in Figure 2.3, which shows a plot of measured and calculated EMF values, in millivolt, against $-Log[H^+]$, which was obtained

by solving the proton mass-balance at each titration point of a strong acid - strong base titration. The points denoted by □ represent EMF values which were calculated by the Nernst equation with the value for E^{const} determined by extrapolating to $-Log[H^+] = 0$ and the Nernstian slope of 59.16. The points denoted by + show EMF values measured during the course of the titration. It is obvious that Nernstian behaviour is observed only in very limited ranges of $[H^+]$ ($-Log[H^+] = 2$ to 3 and $-Log[H^+] > 11$). A more appropriate calibration procedure would be one which provides usable titration points in the $Log[H^+]$ region of 3 to 11 in which most titrations are performed.

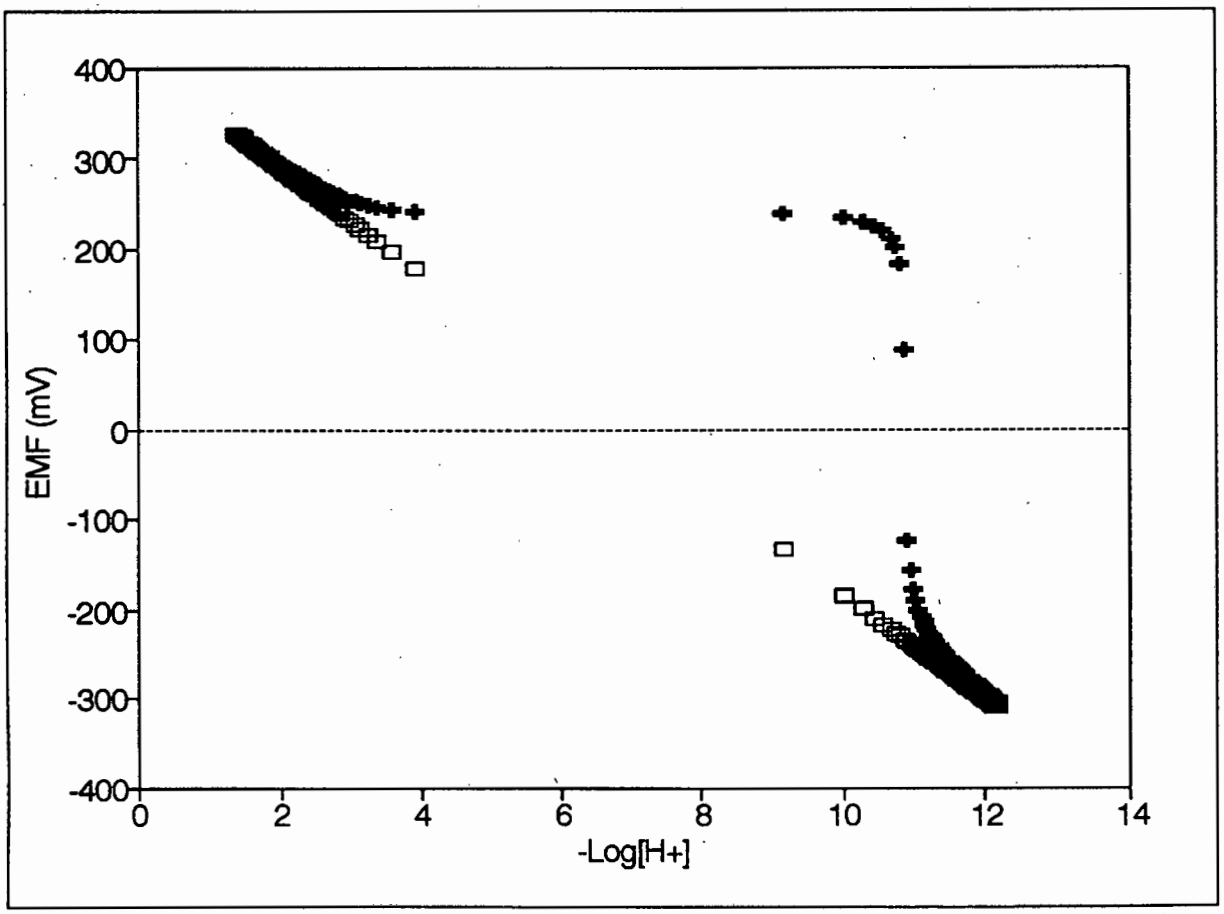

Figure 2.3 Theoretical (□) and measured (+) EMF values for a strong acid - strong base titration as a function of $-Log[H^+]$, calculated from the proton mass-balance.

This may be accomplished by titrating a known concentration of a weak acid or base at the

ionic strength of the test system. This method overcomes liquid junction effects arising from differences in ionic strength between the calibration and test solutions and it provides a wider buffered region and thus usable titration points in the -Log[H^+] range 3 to 11.

The calibration procedure followed in this work consisted of 2 steps. First, the Nernstian behaviour of the glass electrode was checked using three buffer solutions (Radiometer buffers 4.01, 7.00 and 9.18). EMF was plotted against buffer pH. A deviation of less than 5% from the theoretical Nernstian value was deemed to be acceptable. Second, a known amount of glycine was weighed out into a titration vessel and dissolved in 20.0 cm^3 0.1 **M** KNO_3. The solution was titrated with a standardized 0.1 **M** KOH solution containing 0.1 **M** KNO_3. Titration data, which consisted of volume of titrant (cm^3) and EMF readings (millivolt) were used as input into ESTA (May *et al.* 1985; 1988), a programme which allows the simultaneous determination of equilibrium constants and electrode parameters. From the titration data collected, glycine protonation constants and electrode intercept, E^{const}, were determined. The theoretical Nernstian slope of 59.16 mV/pH was used. The agreement between glycine protonation constants determined here and those published in the literature (NIST, 1989) were taken as a measure to assess the quality of the electrode parameters. For all calibration titrations, differences in the order of 0.05 log units for Log β's were obtained. Titrations were carried out in duplicate or until the difference in E^{const} calculated from the different titrations were less than 0.2 mV.

Due to the fact that this calibration procedure is time consuming, a single point calibration was also performed at the time of electrode calibration. This consisted of measuring the EMF of a 0.1 **M** HNO_3 solution at 25°C containing 0.1 **M** KNO_3. This single point calibration

point is denoted as E_{acid}^{cal}. This exercise was repeated before each subsequent titration to obtain E_{acid}^{exp} which was then used to adjust E_{cal}^{const} to yield E_{exp}^{const}. Implicitly the assumption is made here that the electrode response to change in $[H^+]$ (i.e. the slope) remains constant.

2.1.4 Assessing the influence of the suspension effect

The suspension effect refers to the difference in pH observed between a suspension and its supernatant (Jenny, 1950; Bates, 1964). This effect implies that accurate $[H^+]$ determination is not possible in a suspension. The presence of this effect was assessed using the method used by Jenny to illustrate it. EMF was measured with the electrodes in the suspension under constant stirring. Stirring was discontinued and the suspension allowed to settle out. The electrodes were lifted so that they were in contact only with the supernatant. A drop in EMF of approximately 0.4 mV was observed. However, this drop corresponds well with the 0.6 mV drop observed in an 0.1 **M** HNO_3 solution upon discontinuation of stirring. The same result was obtained after the addition of 1 cm^3 0.1 **M** KOH to the suspension, indicating that the effect is also not observable at high pH. It may thus be concluded that no evidence of the suspension effect was found.

2.1.5 Alkalimetric titration of δ-MnO_2

20.0 cm^3 aliquots of the δ-MnO_2 suspension was transferred from the stock solution to a jacketed Pyrex titration vessel using a calibrated pipette. Using a Metrohm Dosimat 665 auto burette, 5.00 cm^3 0.5 **M** KNO_3 background electrolyte was added to ensure a background electrolyte concentration of 0.1 **M**. This resulted in an initial solids concentration of

1.40 $g.dm^{-3}$. The system was allowed to reach thermal equilibrium at 25°C while being continually stirred with a magnetic stirrer and Teflon coated stirrer bar. An inert atmosphere in the titration vessel was ensured by a constant flow of pre-wetted, high purity nitrogen gas. The gas was bubbled through a 50% KOH solution to remove CO_2 and Fiesser's solution (Vogel, 1989) to remove O_2.

Once thermal equilibrium had been achieved, the suspension was titrated with standardized potassium hydroxide (approximately 0.1 **M**) containing 0.1 **M** KNO_3. KOH was added in 0.02 cm^3 increments using a computer controlled Metrohm Dosimat 665 Automatic burette. An increment of base was added once EMF drift was less than 0.2 mV per 600 seconds or after 1200 seconds (20 minutes), whichever condition was satisfied first. This condition is similar to that employed by other workers (Fu *et al.*, 1991) but slower than that employed by Catts and Langmuir (1986), who employed an equilibration criterium of $\Delta pH \leq 0.01$/minute or 2 minutes. Rönngren *et al.* (1994), in their studies of the surface reactions of sulphide systems accepted an EMF drift of 0.6 mV/hour. EMF was monitored with a Radiometer pHM 64 pH meter.

A titration of 20.0 cm^3 supernatant, collected over a 0.22 μ membrane filter (Millipore) was also performed under exactly the same conditions as for the suspension titrations.

2.2 Data Treatment

Experimental data consist of EMF readings (mV) and volume titrant (cm^3) added to the titration vessel. EMF readings were converted to pH through the Nernst equation (eq. 2.1),

which rearranges to

$$\frac{E - E^{const}}{s} = -Log[H^+] \quad \ldots\ldots\ldots\ldots\ldots\ldots \quad (2.2)$$

Total hydrogen ion concentration, T_H, at each titration point was calculated using equation 2.3:

$$T_{H_i} = \frac{(C_{acid}V_{acid}) - ((C_{base}v_i) + \frac{K_w}{10^{-pH}})}{V_0 + v_i} \quad \ldots\ldots\ldots\ldots \quad (2.3)$$

where

C_{acid} = molar concentration of acid

C_{base} = molar concentration of base

V_{acid} = volume of excess acid added at start of titration

V_0 = volume of suspension at start of titration

v_i = volume acid added at each titration point

A dilution factor D_i, which takes into account concentration changes at each titration point due to the volume change resulting from titrant addition was calculated according to

$$D_i = \frac{V_0}{V_0 + v_i} \quad \ldots\ldots\ldots\ldots\ldots\ldots\ldots\ldots \quad (2.4)$$

Serial data for T_{Hi}, $\log[H^+]$ and D_i, obtained from equations 2.2, 2.3 and 2.4 were used as input data in the programme FITEQL version 3.1 (Herbelin and Westall, 1994). A detailed

description of the application of FITEQL to the experimental data is given in paragraph 2.4.

2.3 Potentiometric results and discussion

A typical alkalimetric titration curve obtained for the δ-MnO_2 suspension is shown in Figure 2.4. On the same graph, an actual supernatant titration curve is compared with a theoretical blank titration curve.

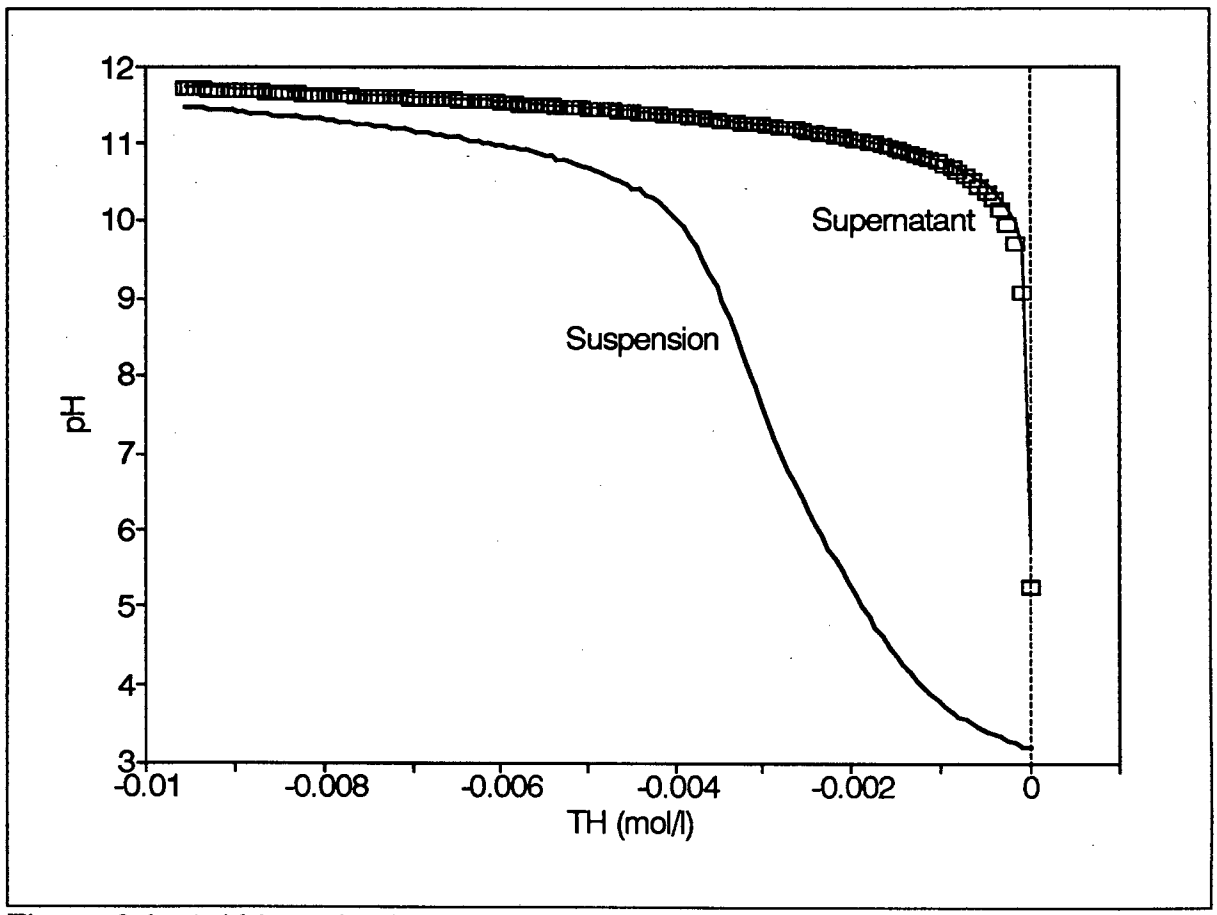

Figure 2.4 Acid-base titration curves of δ-MnO_2 suspensions and an actual supernatant titration (□) compared with a theoretical blank titration (-).

Titrations usually took in the order of 16 hours to go to completion. The equilibrium criterion

of $\Delta EMF \leq 1.2$ mV/hour was not satisfied at all points. The points concerned occurred mostly in the region $6 < pH < 8$. It was generally observed that the EMF reading drifted slowly towards the more acidic region. This immediately ruled out a leaking burette tip since titrations were carried out with alkali.

A number of possible reasons may be forwarded for the observed drift. First, it may be that the proton exchange reaction is very slow and therefore not complete within 20 minutes. This has been postulated by other workers (Murray, 1974). Onada and de Bruyn (1966) and Bérubé *et al.* (1967) provides evidence for a two-step process. According to these workers, adsorption of protons consists of a fast, nearly instantaneous adsorption reaction followed by a slow reaction. From their studies on proton and tritium exchange kinetics on α-Fe_2O_3 (goethite) precipitates, they found that the slow step could take as long as ten days to reach equilibrium. They ascribe the slow step to diffusion of the proton into or out of the solid through an ordered (or goethite like) hydrated layer which exists between the aqueous phase and the bulk goethite phase. However, in a similar study using TiO_2, tritium exchange studies did not support the diffusion mechanism postulated for goethite (Bérubé and de Bruyn, 1968).

Second, an interaction between the manganese dioxide suspension and the glass and/or reference electrode(s) may be occurring. It is known that adsorption at the electrode glass membrane or at the reference electrode liquid junction will cause sluggish electrode response (METROHM Monographs). This was examined by adding an aliquot of base to the suspension at ionic strength of 0.1<u>M</u> without the electrodes present. Electrodes were kept in a thermostatted vessel from which they were transferred to the titration vessel containing the suspension. EMF was monitored for 3 minutes and electrodes were removed and inserted in

the background electrolyte solution. The process was repeated after a few minutes and EMF was monitored for 3 minutes. This was repeated a number of times. It was observed that the EMF reading after each 3 minute monitoring event showed a drift towards the more acidic region. Thus, it may be concluded that the drift is a result of processes occurring in the system and not simply electrode effects.

Third, the observed drift may be caused by the dissolution of the δ-MnO_2 solid phase as pH is increased. This, however, may be discounted based on results reported by Murray (1974), who did not observe any Mn^{2+} release in samples with pH above 3.5. In a solution with pH 2.45, Mn^{2+} release was observed only after approximately 200 hours. In the present titrations, the starting pH was in the region of 3. However, the system remained at this low pH for a short time compared with the 200 hours needed for significant dissolution to occur and it is therefore highly unlikely that any dissolution of the solid occurred.

The effect of the observed drift would manifest itself as a systematic error in the values of calculated adsorption constants (Martell and Motekaitis, 1988). Since the drift here is towards the more acidic region, it may be expected that calculated surface acidity constants will underestimate the true values. The magnitude of this underestimation is, however, unknown.

The reproducibility achieved between the different titrations should also be discussed. Figure 2.5 shows the variability observed between the different titrations. The figure should be interpreted as follows:

the Y-axis represents ΔpH, which is defined as $pH_{Titration\ i}$ - $pH_{Titration\ j}$, with i < j, while the X-

axis represents T_H in $mol.dm^{-3}$. A value of $\Delta pH < 0$ indicates that titration i, at a corresponding T_H, had a lower pH than titration j (or put differently, consumed more base than titration j to reach a given pH). A value of $\Delta pH > 0$ indicates that titration i had a higher pH than titration j at a corresponding T_H (i.e titration i consumed less base than titration j to reach a given pH).

From Figure 2.5 it is evident that (i) ΔpH increases with amount of base added, (ii) all titrations, with the exception of titration 6, lie within 0.2 pH units of each other, (iii) titrations 5 and 6 required more base to reach a given pH than titration 4 and titration 8 required less base than the other titrations to reach a given pH. There is no apparent pattern in the observed variability. Murray (1974) noted that alkalimetric titrations of an aged sample of δ-MnO_2 needed approximately 10 - 15% less base to reach a given pH. The observation that ΔpH involving titration 8 is negative indicates that for a given T_H, titration 8 had a higher pH than any of the other titrations. This observation may be indicative of a certain degree of aging. However, the fact that ΔpH between titration 6 and titration 8 is more negative than ΔpH between titration 8 and titration 4 does not support this. Titration T8 was recorded 45 days after titration 6 and 60 days after titration 4. Thus, one would've expected the difference between titration 4 and titration 8 to be larger than the difference between titration 8 and titration 6. It may thus be concluded that the surface characteristics of the solid did not change over the period covered by this study. This result is similar to findings by Stroes-Gascoyne *et al.* (1987) who found that a δ-MnO_2 sample prepared according to the redox method did not change its surface characteristics, even after storage of four years.

Other possible reasons for the observed variability may be put forward. These include (a) non-

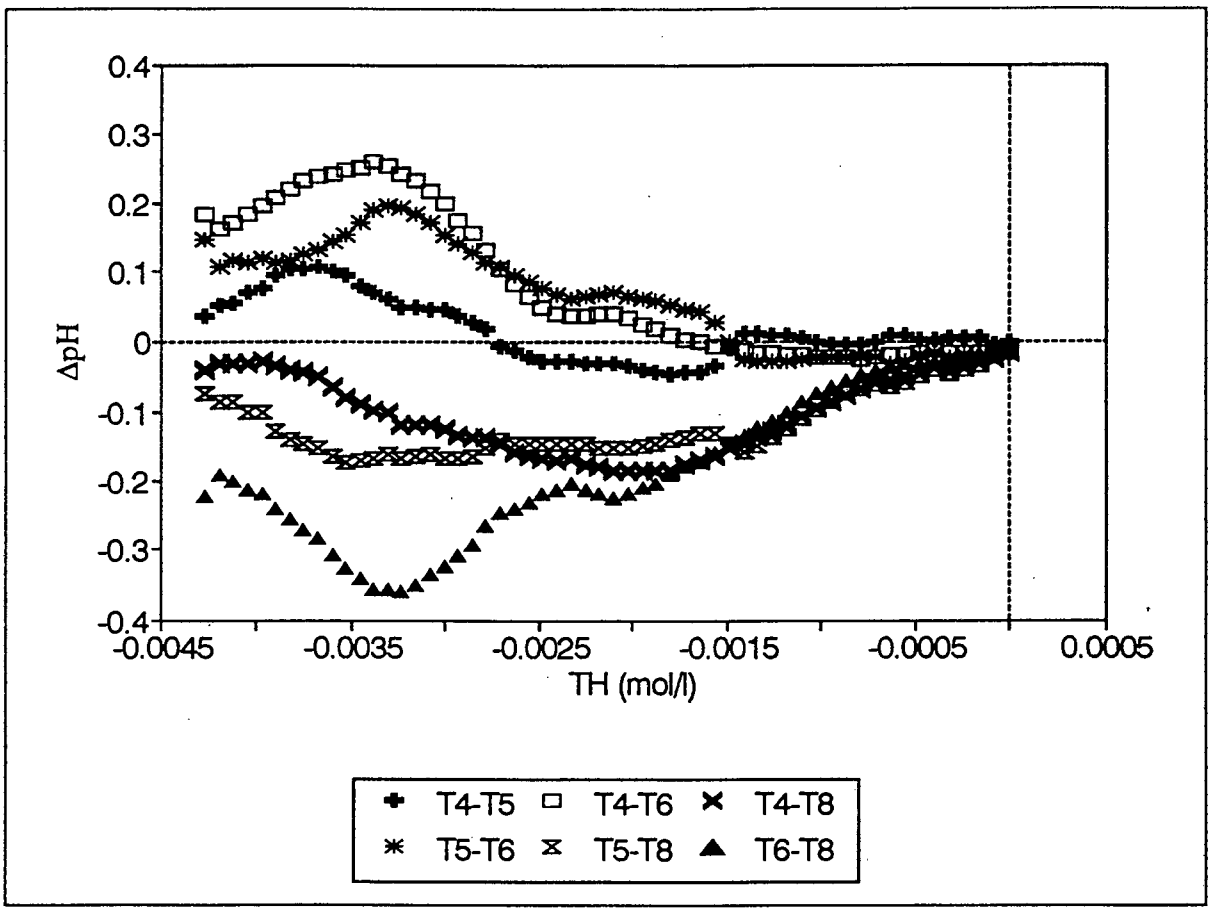

Figure 2.5 Variability observed for base titrations of δ-MnO_2.

uniform intervals between addition of successive titrant increments and (b) variability in the amount of suspension transferred to the titration vessel titration. Reason (a) may be discounted since all titrations followed the same time profile. Reason (b) is a strong candidate, although the determination of solids concentration showed that, for 6 determinations, a coefficient of variation of less than 1% was obtained.

With the data available here, it is not possible to determine the cause(s) of the observed variability amongst the alkalimetric titrations. It is also difficult to assess whether or not the observed variability is similar to that observed by other workers since it is not usually mentioned or discussed in papers. However, an estimate of reproducibility may be obtained from potentiometric determinations of the Point of Zero Charge (PZC) for δ-MnO_2. This may

be explained as follows. PZC determinations using potentiometry consists of a series of alkalimetric or acidimetric titrations being performed at different background electrolyte concentrations. Under ideal conditions, such as a fully indifferent electrolyte, no hysteresis and constant surface composition etc., a sharp common intersection point should be observed which is then identified as the PZC (Lyklema, 1991). However, workers who have used this technique to determine the PZC for manganese dioxide reported values with a 0.2 to 0.3 log unit error estimate. Morgan and Stumm (1964) found a PZC of 2.8 ± 0.3; Catts and Langmuir (1986) obtained a value of 2.3 ± 0.2 and Balistriery and Murray (1982) found the PZC to be 1.5 ± 0.2. If the reported PZC's are interpreted as being average values ± one standard deviation, they may serve as an indication that variability in the order of 0.2 to 0.3 pH units was observed.

These results are similar to results obtained by Bérubé and de Bruyn (1968), in their investigation of adsorption at the rutile/solution interface. They observed a variability of approximately 10% in measurements made under identical conditions but on different samples of rutile precipitate. Furthermore, they found a variability in the PZC determined for this solid in the order of 0.1 pH units. All these facts taken together suggest that the variability observed in the current work is similar to that which had been observed by other workers.

Surface charge density was determined by calculating the difference in $[H^+]$ between the supernatant and suspension titration curves for a given T_H. The true and theoretical blank titrations correspond closely (c.f. Figure 2.4). The discrepancies that do exist between the curves may be a result of the non-ideal behaviour of glass electrodes in poorly buffered solutions, as shown in Figure 2.3 or the presence of carbonate in the supernatant. However,

in the light of the variability observed for the suspension titrations, it was decided that the agreement between the theoretical blank and actual blank titrations was close enough to approximate the supernatant titration curve by the theoretical expression

$$T_{H_i} = [H^+]_{supn,i} - \frac{K_w}{[H^+]_{supn,i}} \quad \ldots\ldots\ldots\ldots\ldots\ldots \quad (2.5)$$

For the suspension, we can write

$$T_{H_i} = [H^+]_{susp,i} - \frac{K_w}{[H^+]_{susp,i}} + [\equiv SOH_2^+] - [\equiv SO^-] \quad \ldots\ldots\ldots \quad (2.6)$$

Equations (2.5) and (2.6) may now be combined to yield equation (2.7) and $\{[\equiv SOH_2^+] - [\equiv SO^-]\}$ may be calculated.

$$[\equiv SO^-] - [\equiv SOH_2^+] = [H^+]_{susp,i} - \frac{K_w}{[H^+]_{susp,i}} - [H^+]_{supn,i} + \frac{K_w}{[H^+]_{supn,i}} \quad \ldots \quad (2.7)$$

At high pH, it may be assumed that $[\equiv SOH_2^+] = 0$. Thus, at high pH equation (2.8) may be used to estimate the total concentration of titratable surface sites. The maximum titratable surface site concentration as determined from equation (2.7) is 4.1×10^{-3} mol.dm^{-3} at pH 11 (see Figure 2.6).

This corresponds to a site density of roughly 6 sites.nm^{-2}, which falls within the range

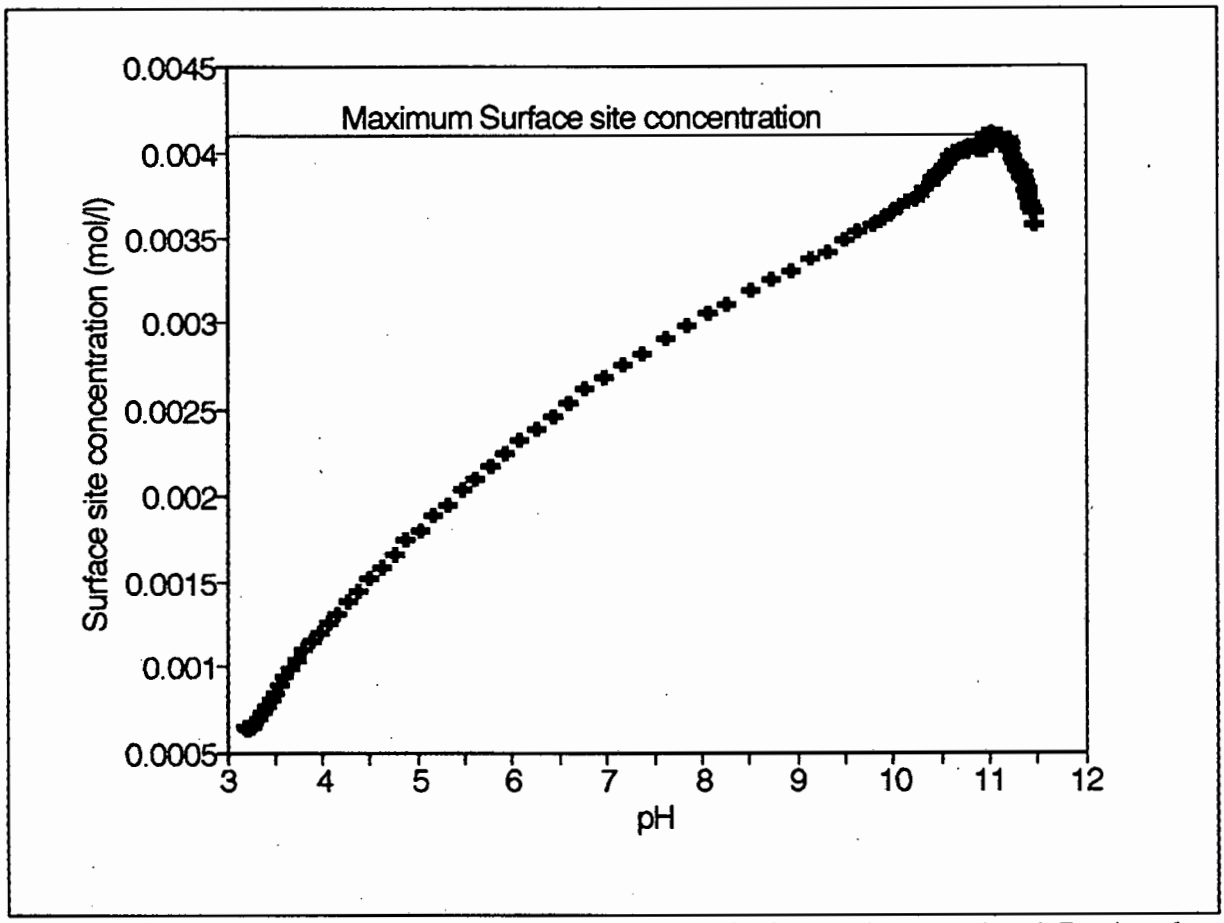

Figure 2.6 Maximum binding site concentration as calculated with equation 2.7 using data from titration 4.

commonly reported for hydroxides (Schindler and Stumm, 1987). The value is slightly lower than the 8.1 reported by Fu *et al.* (1991) and substantially lower than the values of 18 to 21 obtained from tritium exchange studies (Balistriery and Murray, 1982; Catts and Langmuir, 1986). This may be an indication that there are hydroxyl groups present which are accessible in tritium exchange experiments but which are not titratable under the conditions (i.e. pH range and equilibration times) employed in the titration experiments.

At pH = 8, a value of -66μC.cm^{-2} was obtained for surface charge density (see Figure 2.7).

This is comparable with the value of -50μC.cm^{-2} found by Catts and Langmuir at pH 8 and

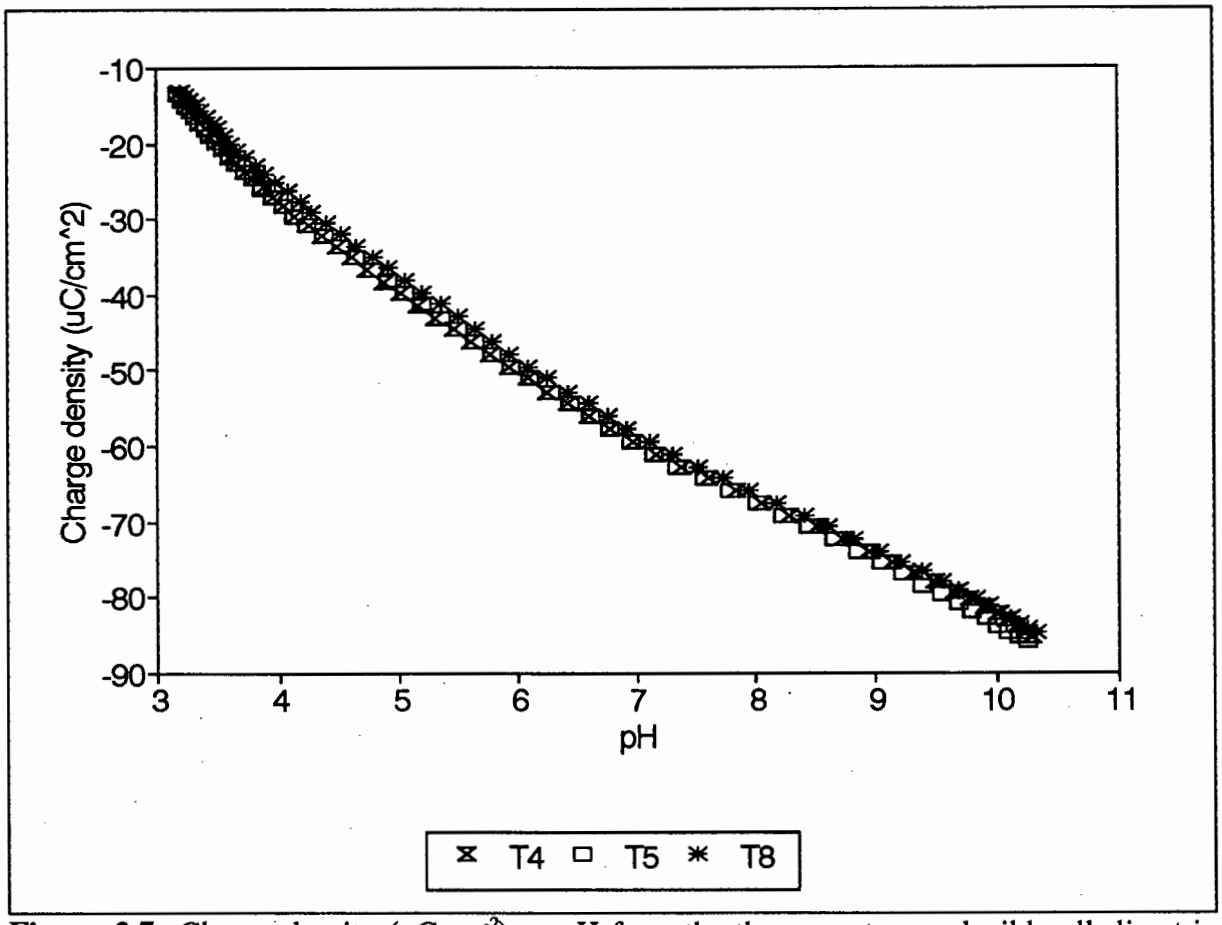

Figure 2.7 Charge density (μC.cm^{-2}) vs pH from the three most reproducible alkalimetric titrations.

I=0.1**M**. Other values available in the literature are: -35μC.cm^{-2} (pH 8, I=0.01**M**) reported by Fu *et al.* (1991) and -40μC.cm^{-2} (pH 8, I=0.01**M**) by Catts and Langmuir (1986).

2.4 Surface protonation constant determination

Protonation constants were determined using the non-linear optimization programme FITEQL version 3.1 (Herbelin and Westall, 1994). FITEQL is an iterative optimization programme which allows the optimization of a number of specified parameters. The Goodness of Fit of a given model is given by, WSOS/DF, which is the weighted sum of squares divided by the degrees of freedom of the problem. WSOS/DF values between 0.1 and 20 is indicative of

good agreement between model and experiment. Input data consisted of (a) Total hydrogen ion concentration (T_H) in mol.dm^{-3}, (b) the logarithm of free hydrogen ion concentration, log[H^+], (c) dilution factors and (d) mass of solid in g.dm^{-3}. Parameters to be optimized were adsorption constants and surface site concentration. In order to select the best model, constants and binding site concentrations were determined on a titration by titration basis. Once the best model was selected, best estimates for adsorption constants and binding site concentrations were determined by lumping all titrations in one input file.

An important input parameter for FITEQL is the error estimates assumed for Log[H^+] and T_H since the value of the Goodness of Fit parameter and standard deviations of adsorption constants depend on these estimates (Dzombak and Morel, 1990). In this study, it was decided to use FITEQL's default error estimates for T_H and Log[H^+]. For T_H, FITEQL assumes a relative error of 0.01 (i.e. 1%) and an absolute error of 10^{-6} M. For Log[H^+], a relative error of 0.023, which is equivalent to 0.01 pH unit, is assumed. The relative error assumed for Log[H^+] may be criticised as being too small, especially seen in the light of the variability observed between replicate titrations. However, it should be kept in mind that the variability between replicate titrations does not reflect the accuracy of EMF readings (and therefore [H^+]), but the precision. A better estimate or reflection of the accuracy may be obtained from the electrode calibration procedure followed. As was shown in paragraph 2.1.3, the excellent agreement (±0.05 log units) between glycine protonation constants determined during the calibration procedure with published constants indicates that electrode parameters are accurately known. There is thus little reason to doubt the accuracy of Log[H^+].

Two reaction schemes were postulated in an attempt to explain experimental data. The first

scheme assumed an ideal surface covered with chemically equivalent surface hydroxyl groups (denoted by ≡XOH) and allowing the existence of three surface species, viz. ≡XOH, ≡XO^- and ≡XOH_2^+. This is the classical single site 2 pK approach which has been applied to sorption data by a number of workers (see e.g. Dzombak and Morel, 1990). The second scheme evaluated took surface heterogeneity into account. It consisted of two types of surface sites (denoted as ≡XOH and ≡YOH) and allowing six surface species viz. ≡XOH, ≡XO^-, ≡XOH_2^+, ≡YOH, ≡YO^- and ≡YOH_2^+ to form.

Model selection was based on (i) the value of the goodness of fit parameter WSOS/DF, (ii) the standard deviations of calculated Log K's, (iii) Ockham's razor and (iv) visual comparison of plotted modelling results with experimental data. Thus, the best model was one which described experimental data best on (i) a statistical basis (as expressed by WSOS/DF) and (ii) a visual basis (based on comparison of experimental and calculated titration curves), using the smallest number of adjustable parameters to achieve the best fit.

2.5 Modelling results and discussion

2.5.1 Homogeneous surface assumption:

The first reaction scheme evaluated was

$$\equiv XOH + H^+ \rightleftharpoons \equiv XOH_2^+$$

$$\equiv XOH \rightleftharpoons \equiv XO^- + H^+$$

FITEQL failed to solve the mass balance equations for this model. Surface site concentration [≡XOH] and Log K for reaction ≡XOH ⇌ ≡XO^- + H^+ converged but Log K for the diprotonated surface species failed to converge. This failure to converge may be caused by

the concentration of $\equiv XOH_2^+$ being too small.

According to previous studies (Stumm and Morgan, 1964; Murray, 1974; Balistriery and Murray, 1982; Catts and Langmuir, 1986; Stroes-Gascoyne *et al.*, 1987; Zasoski and Burau, 1988; Fu *et al.*, 1991), δ-MnO_2 has a PZC in the region of pH 1.5 to pH 3. This is supported by Figure 2.6, which shows that the δ-MnO_2 used in this study is negatively charged at pH values of approximately 3. This points to a PZC below 3. It may thus be deduced that positively charged sites will be present at significant levels only at pH values close to or below the PZC. No data points were collected below pH 3.2. Therefore, the present data set cannot be used to calculate Log K for the species $\equiv XOH_2^+$ since this species is not expected to be present at significant levels in the pH range investigated.

Optimization was successful with the reaction $\equiv XOH + H^+ \rightharpoonup \equiv XOH_2^+$ discarded. Optimization results are listed in Table 2.1. Figure 2.8 shows a comparison of experimental and model results. The Goodness of Fit indicator, WSOS/DF and the visual comparison in Figure 2.8 shows that this model is not successful in describing experimental data. The binding site concentration of approximately 4.5 sites.nm^{-2} determined by this model is also lower than the 6 sites.nm^{-2} obtained from Figure 2.6.

A direct comparison of results listed in Table 2.1 with literature values is not possible since only two studies in which constants were determined could be identified from the open literature. In these studies (Catts and Langmuir, 1986; Fu *et al.*, 1991), the Triple Layer Model was used to derive adsorption constants. However, Pretorius *et al.* (1996) recomputed diffuse double layer constants from these publications. For the work published by Catts and

Langmuir, Log K for the reaction $\equiv XOH \rightleftharpoons \equiv XO^- + H^+$ was found to be -2.65 with a binding site concentration of 3 site.nm^{-2} (used BET surface area of 290m^2.g^{-1}). Similarly, for Fu *et al.*, values of -2.61 and 3 site.nm^{-2} (used BET surface area of 296m^2.g^{-1}) was obtained. Goodness of Fit parameters were 100 and 91 respectively, using default FITEQL error estimates. These results indicate that the Log K's and fits obtained are quite similar to that obtained in this work. The discrepancy in binding site concentrations stems from the different pH ranges employed by the different workers. The results obtained for the data of Catts and Langmuir and Fu *et al.* also indicate that the homogeneous surface model is not appropriate for the description of δ-MnO_2 alkalimetric titration data. Thus, modelling experimental data with a heterogeneous surface model was attempted.

Table 2.1 Proton sorption parameters as determined with the 1 site sorption model.

Parameter	Titration 4	Titration 5	Titration 6	Titration 8
Log K_1 ($\equiv XO^-$)	**-2.37**	**-2.38**	**-2.36**	**-2.47**
$\sigma_{Log\ K}$	0.013	0.013	0.013	0.013
[XOH](mol.g^{-1})	**2.465x10^{-3}**	**2.460x10^{-3}**	**2.452x10^{-3}**	**2.414x10^{-3}**
$\sigma_{[XOH]}$	5.695x10^{-6}	5.729x10^{-6}	6.016x10^{-6}	5.767x10^{-6}
Sites.nm^{-2}	4.5	4.5	4.5	4.4
WSOS/DF	62.8	68.0	65.3	62.9
Data points	69	61	51	59
pH range	3.19-11.48	3.19-10.47	3.20-10.08	3.20-10.43

2.5.2 Heterogeneous surface assumption:

The first reaction scheme investigated here consisted of 4 reactions:

$$\equiv XOH + H^+ \rightleftharpoons \equiv XOH_2^+$$

$$\equiv XOH \rightleftharpoons \equiv XO^- + H^+$$

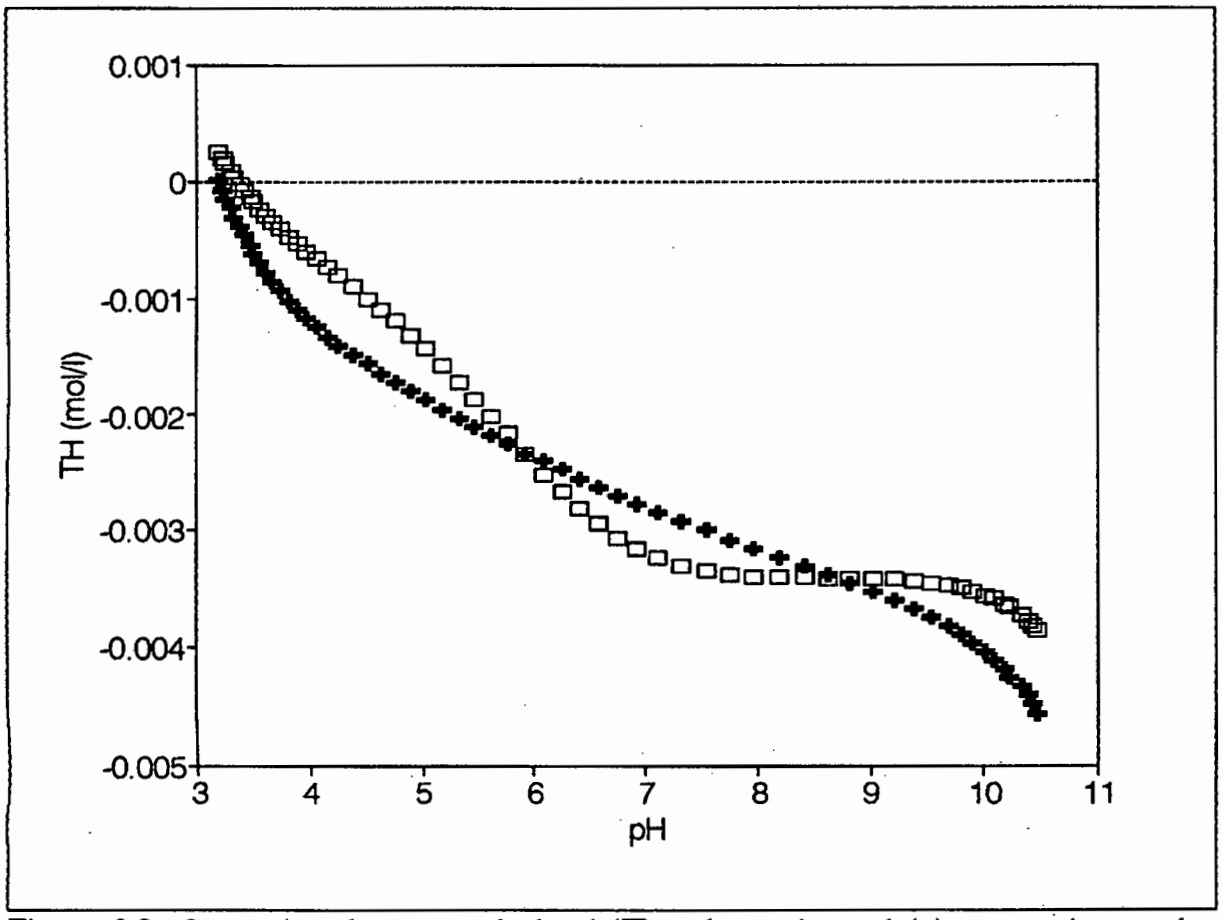

Figure 2.8 Comparison between calculated (□) and experimental (+) protonation results, using the 1 site surface model.

$$\equiv YOH + H^+ \rightleftharpoons \equiv YOH_2^+$$

$$\equiv YOH \rightleftharpoons \equiv YO^- + H^+$$

However, this model failed to converge. As in the case of the single site model with diprotonated surface species, Log K for $\equiv XOH_2^+$ failed to converge. Log K's for the other species stabilized as did the concentrations for ≡XOH and ≡YOH. The explanation for the observed failure to converge is the same as that given in the homogeneous surface model.

The most successful reaction scheme was obtained by discarding the $\equiv XOH_2^+$ species from the two site model. Optimization results for this model are summarized in Table 2.2. Figure 2.9 shows a comparison of model results with a typical experimental titration curve. The

success of the multi-site model in describing experimental results is reflected in the low WSOS/DF values obtained for all titrations. The visual comparison shown in Figure 2.9 endorses the low WSOS/DF values. This model calculates binding site densities as being between 5.3 and 5.7 sites.nm^{-2}. These values correspond closely to the site density 6 sites.nm^{-2} calculated from alkalimetric titrations.

Application of the heterogeneous model to the data of Catts and Langmuir and of Fu *et al.* was met with mixed success. The model did not converge on the data set of Fu *et al.*. However, with the constants fixed at the average values listed in Table 2.2 and optimizing site concentrations, convergence was obtained. Total binding site concentration of 4 sites.nm^{-2} was obtained with WSOS/DF = 6. Applied to the data of Catts and Langmuir, the model converged with Log K_1 = -1.36, Log K_2 = -5.10 and Log K_3 = 3.04, total binding site concentration of 4 sites.nm^{-2} and WSOS/DF = 0.4. These results indicate that the heterogeneous surface model is a significant improvement over the homogeneous surface model case.

The concept of different classes of surface hydroxyl groups has been proposed and illustrated by a number of workers for a variety of solids (see for example: Contescu *et al.*, 1993, 1994; Schindler and Stumm, 1987; Barrow, 1993; Hiemstra *et al.*, 1989; Rustad *et al.*, 1996). The explanations given are all based on the coordinative environments of metal ions and surface hydroxyl groups in hydrated surfaces. Surface hydroxyls may be present as bridging and terminal groups and metal centres may be coordinated with two or more hydroxyls. Since none of the studies mentioned were carried out on manganese dioxide, the results cannot be presented as proof for the validity of the heterogeneous surface model proposed here. They

do, however, indicate that the assumption of surface heterogeneity is justified.

Table 2.2 Proton sorption parameters as determined with the 2 site sorption model.

Two site model	Titration 4	Titration 5	Titration 6	Titration 8	Best estimates
Log K_1 (≡XO$^-$)	**-1.23**	**-1.20**	**-1.28**	**-1.34**	**-1.27**
$\sigma_{Log\ K}$	0.031	0.035	0.037	0.035	0.017
Log K_2 (≡YO$^-$)	**-6.42**	**-5.90**	**-5.75**	**-5.89**	**-5.99**
$\sigma_{Log\ K}$	0.070	0.066	0.082	0.069	0.035
Log K_3 (≡YOH$_2^+$)	**3.67**	**3.45**	**3.46**	**3.51**	**3.52**
$\sigma_{Log\ K}$	0.055	0.065	0.075	0.071	0.033
[XOH](mol.g^{-1})	**2.338x10^{-3}**	**2.231x10^{-3}**	**2.259x10^{-3}**	**2.186x10^{-3}**	**2.231x10^{-3}**
$\sigma_{[XOH]}$	1.637x10^{-5}	1.751x10^{-5}	2.142x10^{-5}	1.866x10^{-5}	9.067x10^{-6}
[YOH](mol.g^{-1})	**7.821x10^{-4}**	**7.735x10^{-4}**	**7.386x10^{-4}**	**7.464x10^{-4}**	**7.656x10^{-4}**
$\sigma_{[YOH]}$	1.937x10^{-5}	1.709x10^{-5}	2.000x10^{-5}	1.797x10^{-5}	9.102x10^{-6}
Sites.nm^{-2}	5.7	5.5	5.5	5.3	5.5
WSOS/DF	1.1	0.7	0.6	0.7	1.8
Data points	69	61	51	59	240
pH range	3.19-11.48	3.19-10.47	3.20-10.08	3.20-10.43	3.19-11.48

Binding sites belonging to different chemical classes may also be rationalized in terms of what little information on the structure of δ-MnO_2 is available. Manceau *et al.* (1992a,b), based on XANES and EXAFS studies, express the opinion that δ-MnO_2 should be pictured as a "3-D (O,OH) framework where cubic and hexagonal close-packing arrangements alternate at random and where octahedral sites are randomly filled, but where two adjacent $Mn(O,OH)_6$ octahedra cannot share faces". According to these workers, the δ-MnO_2 structure "probably consists of a mosaic of single and multiple octahedral chains having variable length and width". They provide evidence which links the δ-MnO_2 structure with the Todorokite tunnel structure. Thus, on the basis of this proposed structure, hydroxyl groups of differing

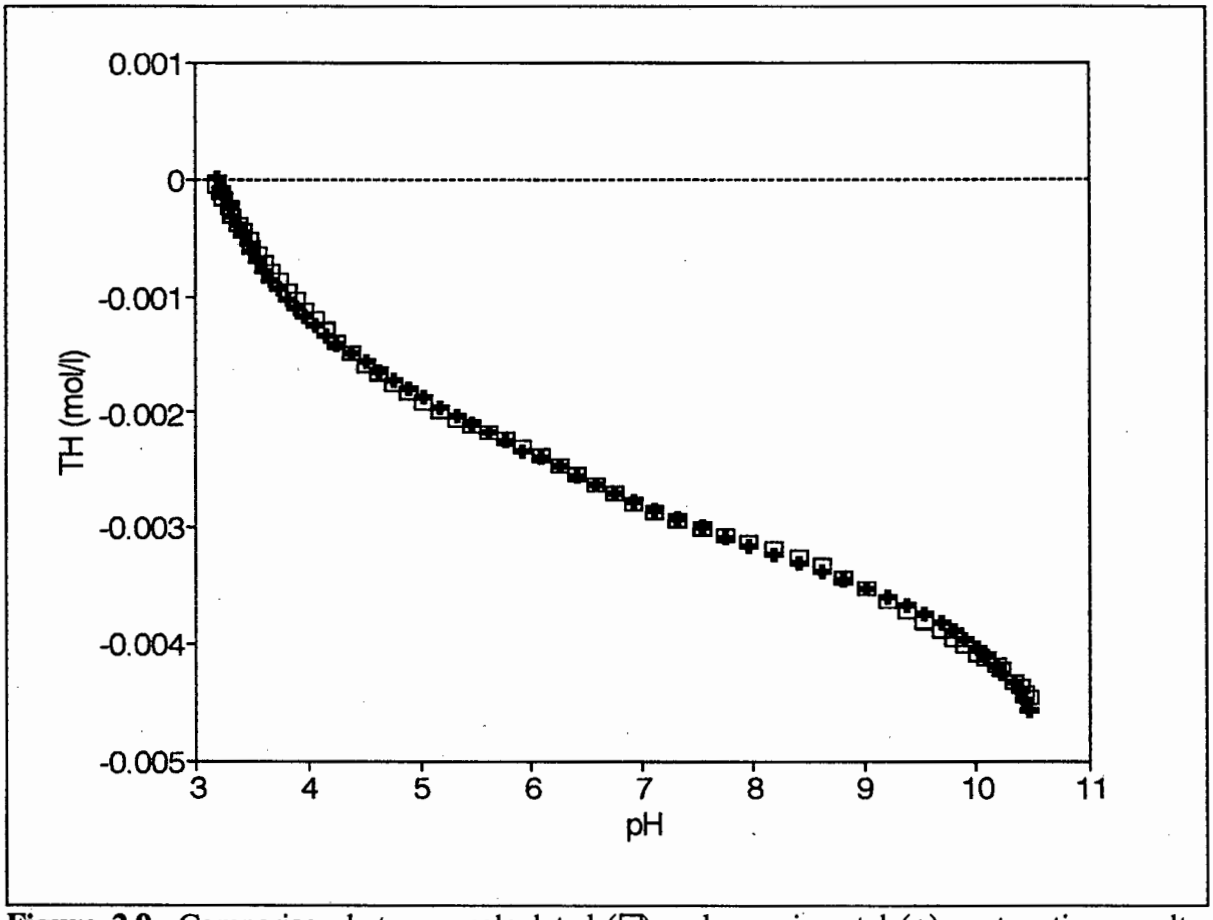

Figure 2.9 Comparison between calculated (□) and experimental (+) protonation results, using the 2-site surface model.

reactivity may be expected on the basis of cavities or tunnels, close packing of atoms and surface defects.

A point which should be discussed is the validity of optimizing site concentrations as well as adsorption constants simultaneously. From a mathematical point of view, no objection to this point can be made. However, to illustrate that the simultaneous optimization of parameters does in fact provide the correct answer, the following procedure was followed. A hypothetical surface consisting of two classes of binding sites was assumed. Surface protonation constants and site concentrations were entered in MINTEQA2 and a alkalimetric titration curve was synthesized. The alkalimetric curve was used as input in FITEQL and

adsorption constants and binding site concentrations were simultaneously determined. Results are listed in Table 2.3.

The results indicate that the optimization procedure was successful in determining the parameters which were used to synthesize the data set. A discrepancy does exist between the "known" constants and the optimized values. However, seen in the light of factors such as numerical inaccuracy and loss of significance figures in the two calculation steps which were involved, the result is satisfactory.

Table 2.3 Agreement between known and optimized values. Optimized values were obtained by applying FITEQL to a data set synthesized by MINTEQA2 using the known parameter set.

Parameter	Known values	Optimized values
Log K_1	-1.90	-1.79
Log K_2	-4.30	-4.19
Log K_3	2.50	2.41
[XOH] (g/l)	2.231×10^{-3}	2.236×10^{-3}
[YOH] (g/l)	7.656×10^{-4}	7.574×10^{-4}

Further evidence which supports the approach followed here is provided by results obtained for the protonation properties of Hydrous Ferric Oxide (HFO). Results listed in Appendix E are in excellent agreement with the surface protonation constants determined by Dzombak and Morel (1990). HFO surface site concentration is similar to values found by other workers, as summarized by Dzombak and Morel.

2.5.3 Binding site speciation

Surface speciation, as predicted by the heterogeneous surface model, is shown in Figure 2.10.

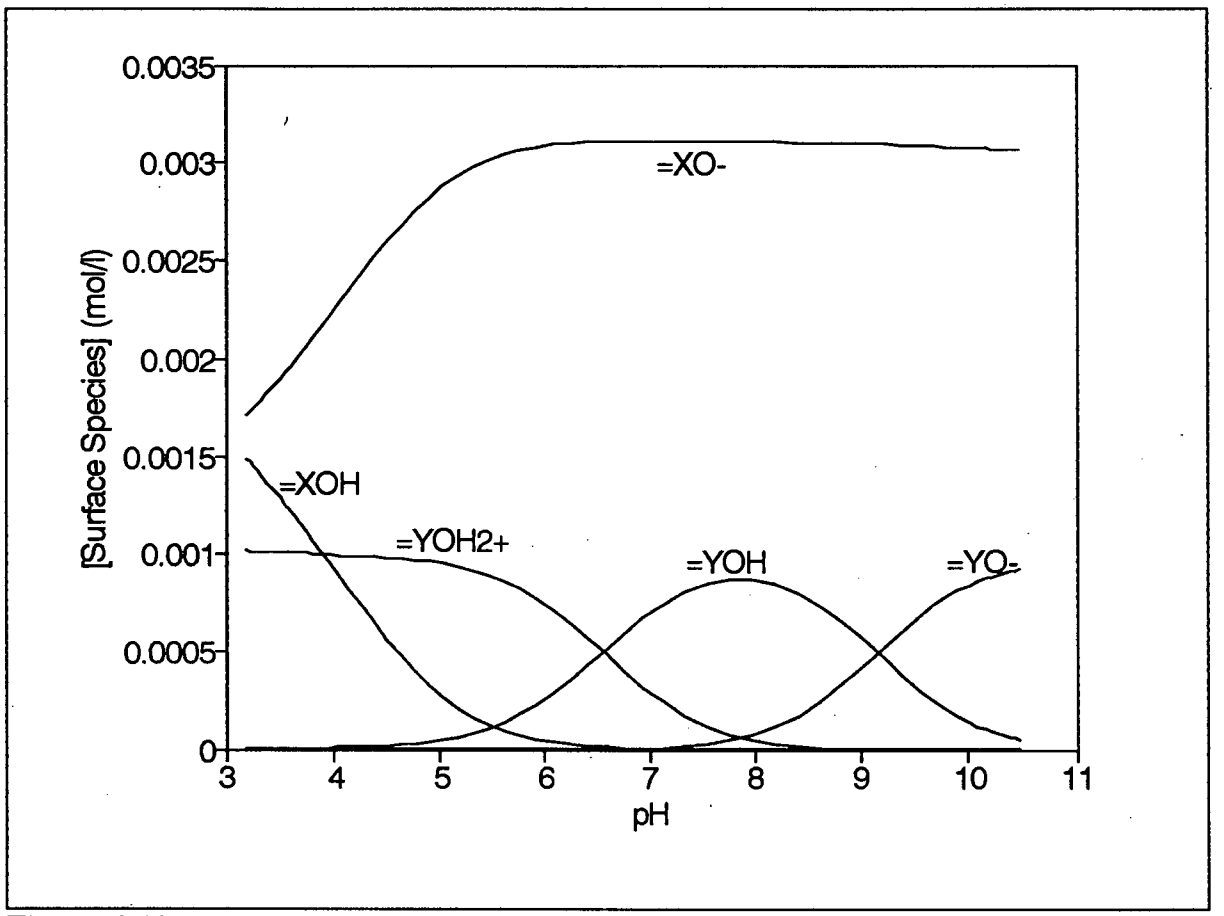

Figure 2.10 Surface speciation as a function of pH as predicted by the 2-site 3-surface species protonation model.

All species are present at levels of 25% or higher of total site concentration. This provides further confidence in the proposed model. The dominant site over the pH range investigated is $\equiv XO^-$. $\equiv YOH$ and $\equiv YOH_2^+$ are the dominant second site species in the lower pH range. $\equiv YO^-$ becomes significant from pH 6 onwards. The relative abundance of site 1 over site 2 has probably led previous workers to postulate the existence of only one type of surface site.

2.6 Conclusion

The acid/base behaviour of δ-MnO_2 was investigated using potentiometric titrations. The reproducibility achieved in these titrations is comparable to that achieved by others, based on reported errors in PZC determinations. The assumption of a surface consisting of sites of equivalent chemical reactivity (classical homogeneous surface approach) failed to reproduce the potentiometric data. Only by assuming a surface consisting of variable chemical reactivity could the potentiometric results be explained. The existence of non-equivalent surface sites is supported by data available for other solids as well as by (albeit limited) structural data for δ-MnO_2. The possibility that the heterogeneous surface model is an artefact of experimental error can be discounted since it was shown, by using a synthetic data set, that the modelling procedure is capable of reproducing the parameters used to create the synthetic data set. The successful determination of surface protonation parameters for Hydrous Ferric Oxide provides further support for the experimental and modelling procedure employed in this work.

A test of the applicability of the proposed heterogeneous surface model will be its ability to provide an interpretation of metal adsorption data consistent with the alkalimetric model. This is described in the next section.

Chapter 3 Adsorption of Ni, Cu, Zn, Cd and Pb by δ-MnO_2

In this chapter, potentiometric results obtained from alkalimetric titrations of systems consisting of δ-MnO_2 suspensions and metal ion are presented and discussed. Following this, the determination of adsorption constants from the potentiometric results is presented and discussed.

3.1 Experimental

Metal stock solutions were prepared using boiled out distilled water containing 0.5 $mol.dm^{-3}$ KNO_3 (Merck GR) background electrolyte, using the nitrate salts of nickel, copper, zinc, cadmium and lead (all Merck Pro Analysi). Stock solutions were standardized titrimetrically against EDTA (Vogel, 1981). Stock solution concentrations are listed in Appendix C. Solutions were transferred to polyethylene bottles connected to Dosimat exchange units fitted with self indicating Carbosorb soda lime CO_2 traps. The titration procedure followed consisted of adding $20.0cm^3$ suspension to the titration vessel. This was followed by the addition of $5.0cm^3$ of the metal stock solution. The mixture was allowed to reach 25°C under N_2 atmosphere and constant stirring. Addition of base was started as soon as the suspension reached 25°C.

3.2 Potentiometric results and discussion

To illustrate that adsorption did indeed take place, typical titration curves obtained in the presence and absence of each metal are shown in Figures 3.1 to 3.5.

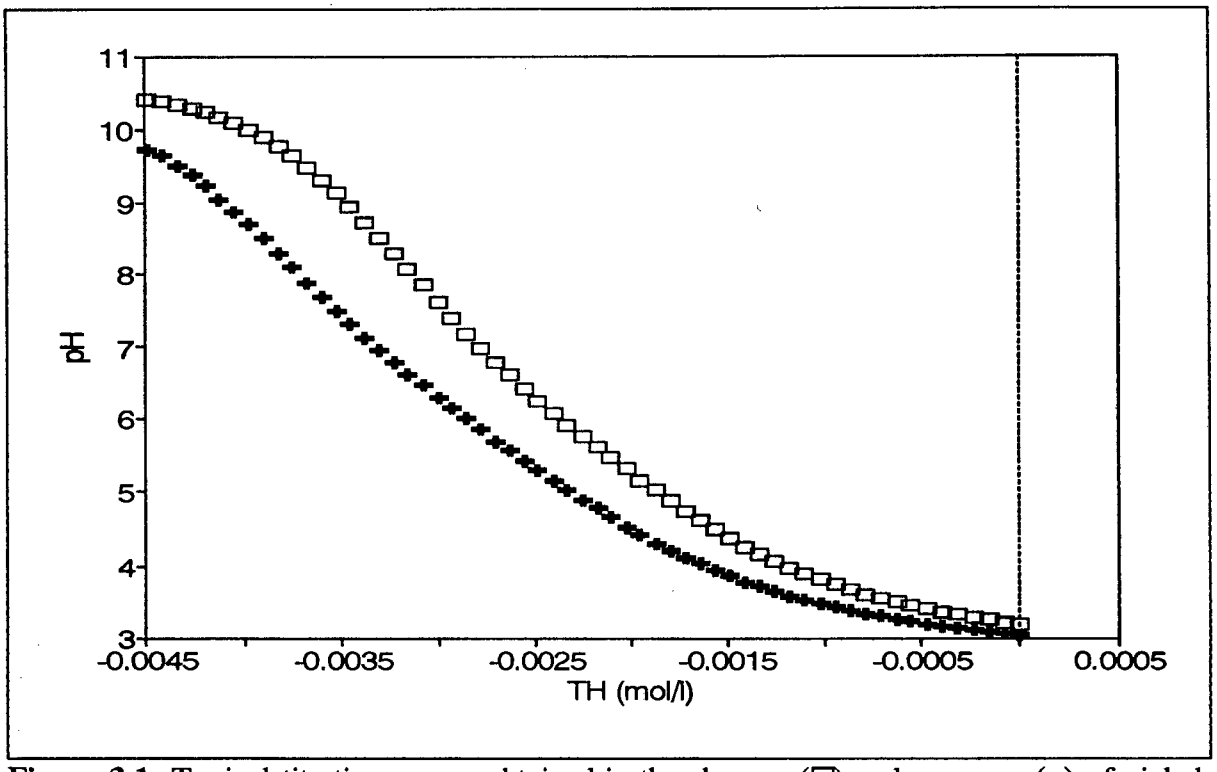

Figure 3.1 Typical titration curves obtained in the absence (□) and presence (+) of nickel.

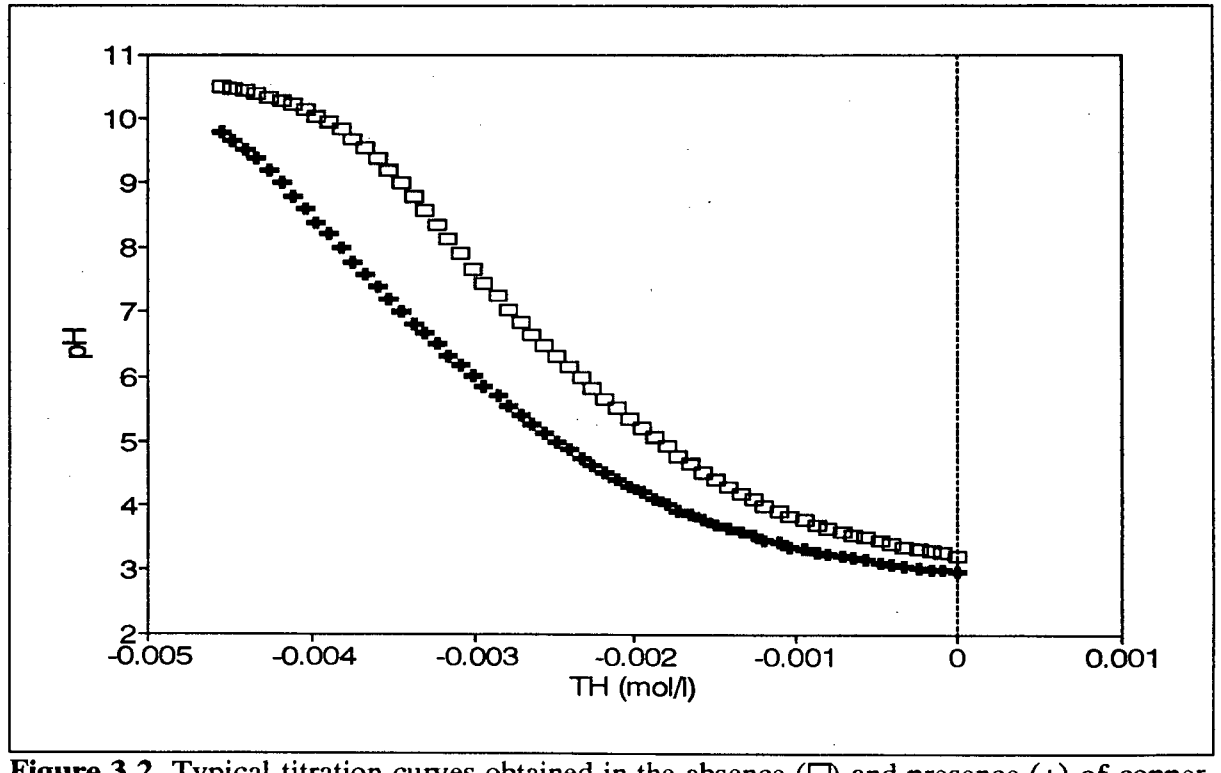

Figure 3.2 Typical titration curves obtained in the absence (□) and presence (+) of copper.

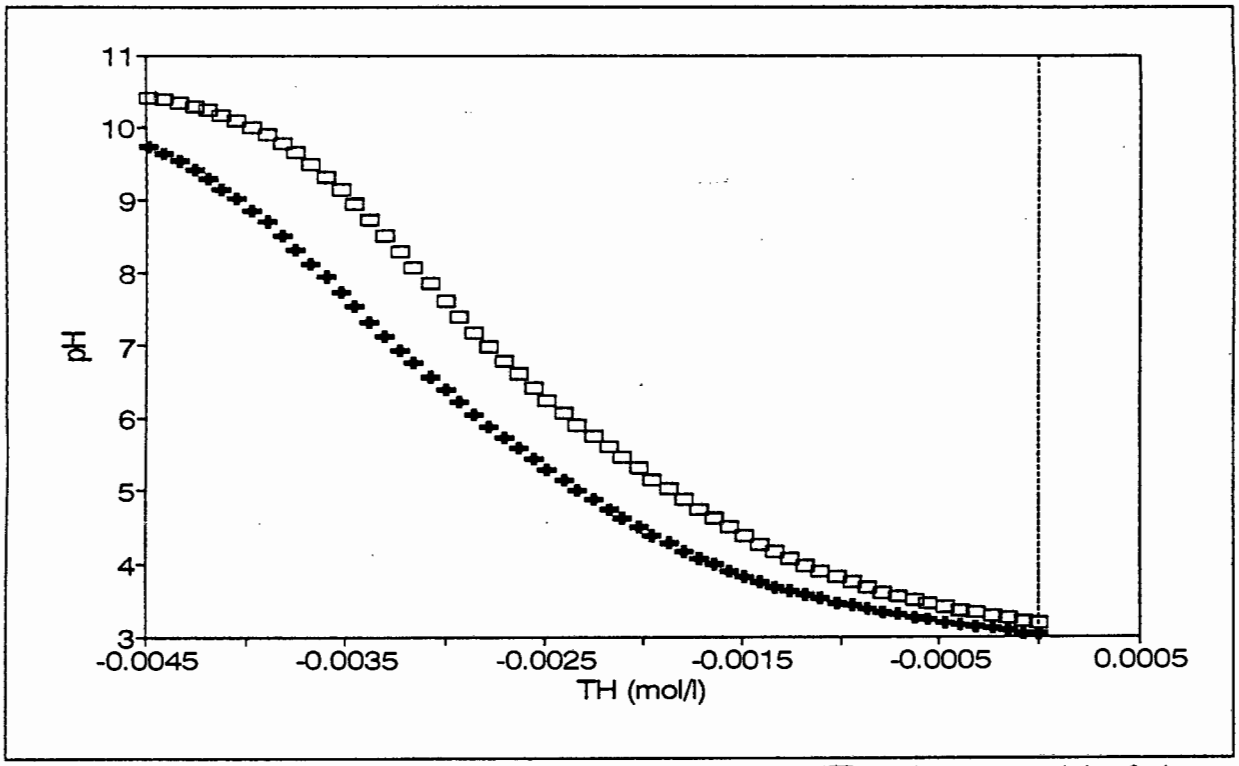

Figure 3.3 Typical titration curves obtained in the absence (□) and presence (+) of zinc.

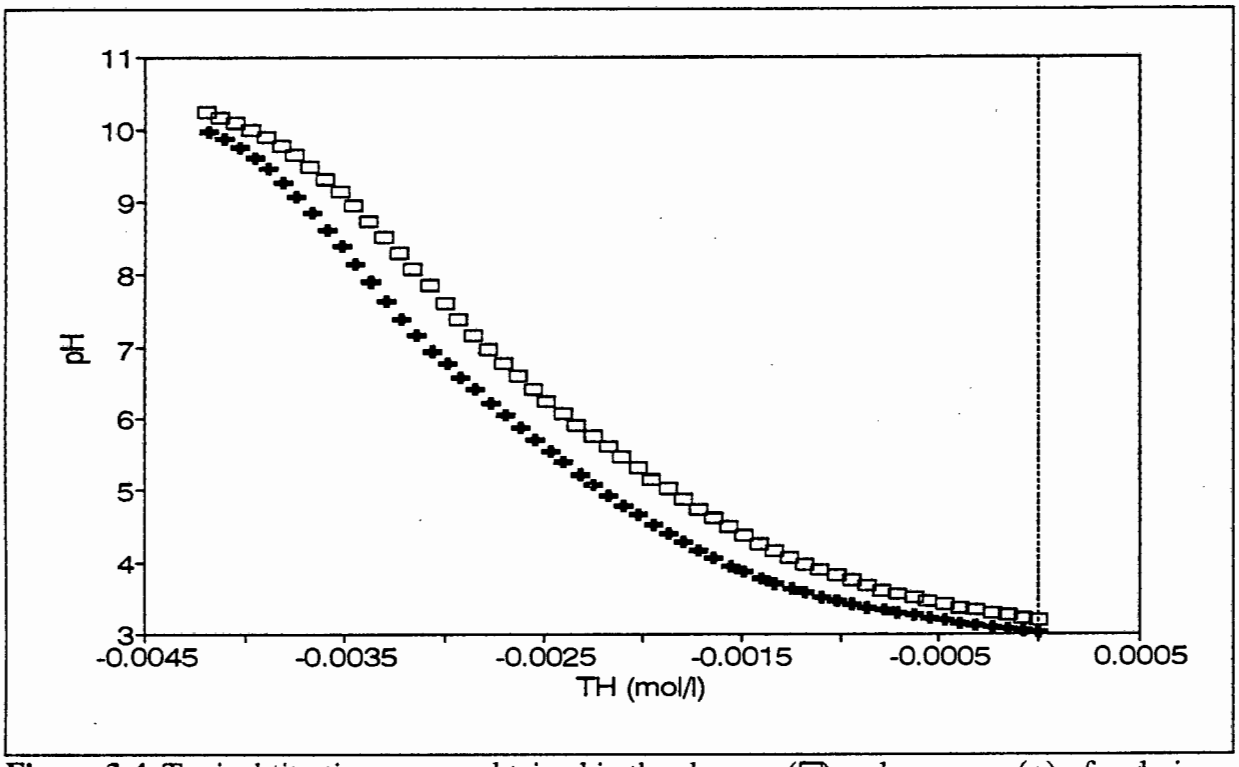

Figure 3.4 Typical titration curves obtained in the absence (□) and presence (+) of cadmium.

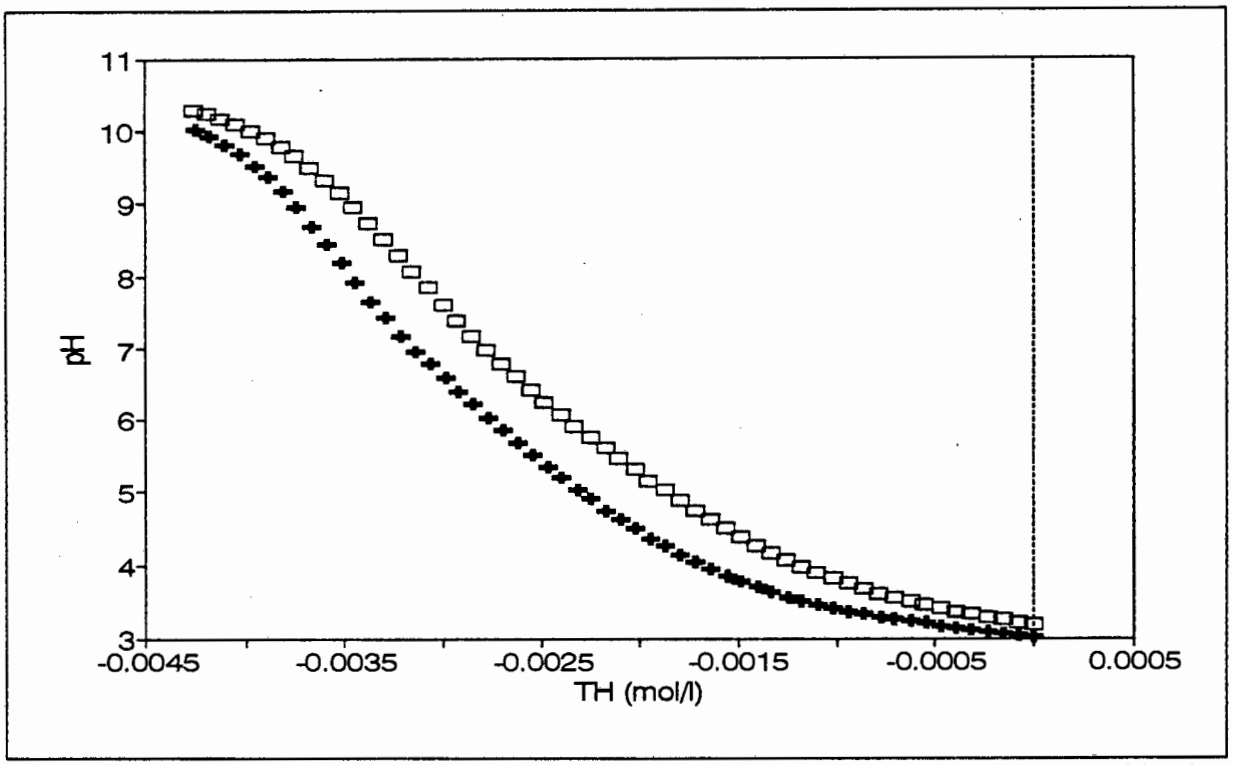

Figure 3.5 Typical titration curves obtained in the absence (□) and presence (+) of lead.

In the presence of metal, titration curves were displaced towards the more acidic region, in other words the system consumed more base to reach a corresponding pH on the base titration curve than in the absence of metal. The observed shift may be explained in terms of competition between metal ions and protons for binding sites as well as the hydrolysis of metal ions. The number of protons displaced per mole of metal added to the system, at pH 4 and pH 6, is shown in Table 3.1. The values shown are averages which were calculated using all alkalimetric titration data collected in the presence and absence of metal ions.

Protons liberated by the adsorption reaction are not only a result of the stoichiometry of the adsorption reaction. Rather, it results from competition between metals and protons for binding sites. The extent of this competition is influenced by the magnitude of the equilibrium constant, or in other words, the magnitude of ΔG for the adsorption reaction, compared with ΔG for protonation.

Table 3.1. Displacement in titration curve with metal present from titration curve without metal present.

Metal	$\Delta T_H/T_M$ @ pH 4	$\Delta T_H/T_M$ @ pH 6
Ni	1.28 ± 0.13	1.34 ± 0.14
Cu	1.43 ± 0.12	1.64 ± 0.12
Zn	1.10 ± 0.10	1.2 ± 0.1
Cd	0.85 ± 0.11	0.72 ± 0.09
Pb	1.31 ± 0.14	1.04 ± 0.14

This in turn is influenced (or determined) by reaction enthalpy ΔH and the entropy term $-T\Delta S$. Therefore, to use protons liberated per metal ion added, or protons liberated per metal ion adsorbed as an absolute measure of the stoichiometry of the adsorption process, is not strictly valid.

The shift in titration curves do have a limiting value, which is equivalent to quantitative complex formation. In this case, the number of protons released corresponds to the composition of the complexes formed in the whole range of the titration curve (Beck and Nagypál, 1990). The number of protons released upon adsorption may be used as an indication of the stoichiometry of the dominant species at a given pH, but it should be interpreted with care.

All titrations were carried out in triplicate. Figures 3.6 to 3.10 illustrate the degree of reproducibility obtained for each metal. In these figures, ΔpH, defined as $pH_{Titrn\ i}$-$pH_{Titrn\ j}$, $i < j$, is plotted as a function of volume of base added.

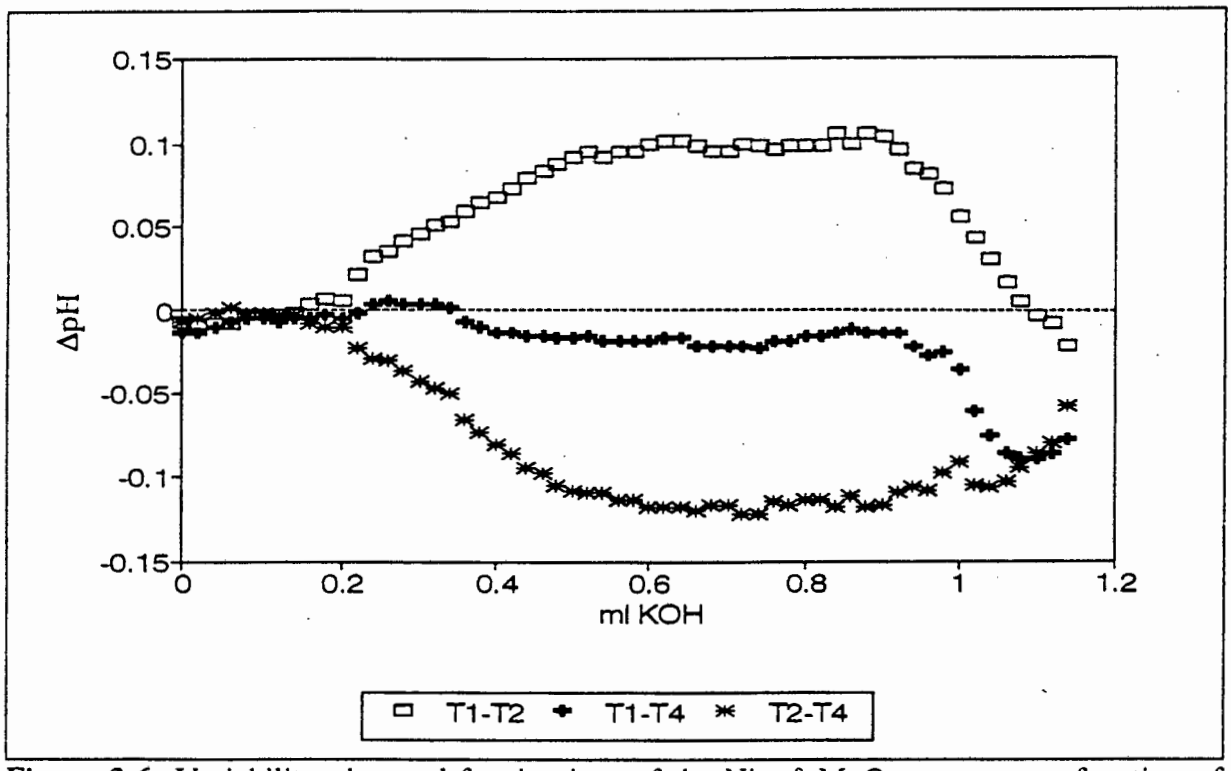

Figure 3.6 Variability observed for titrations of the Ni - δ-MnO_2 system as a function of volume base added.

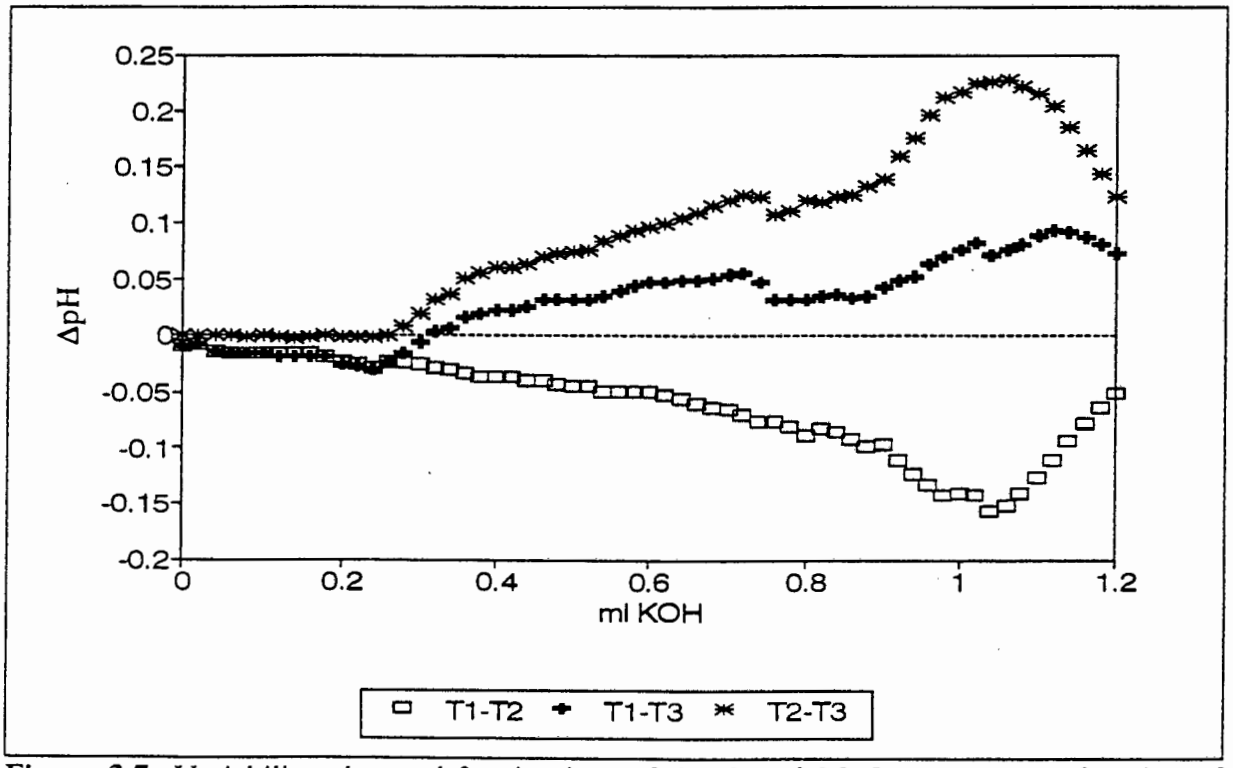

Figure 3.7 Variability observed for titrations of the Cu - δ-MnO_2 system as a function of volume of base added.

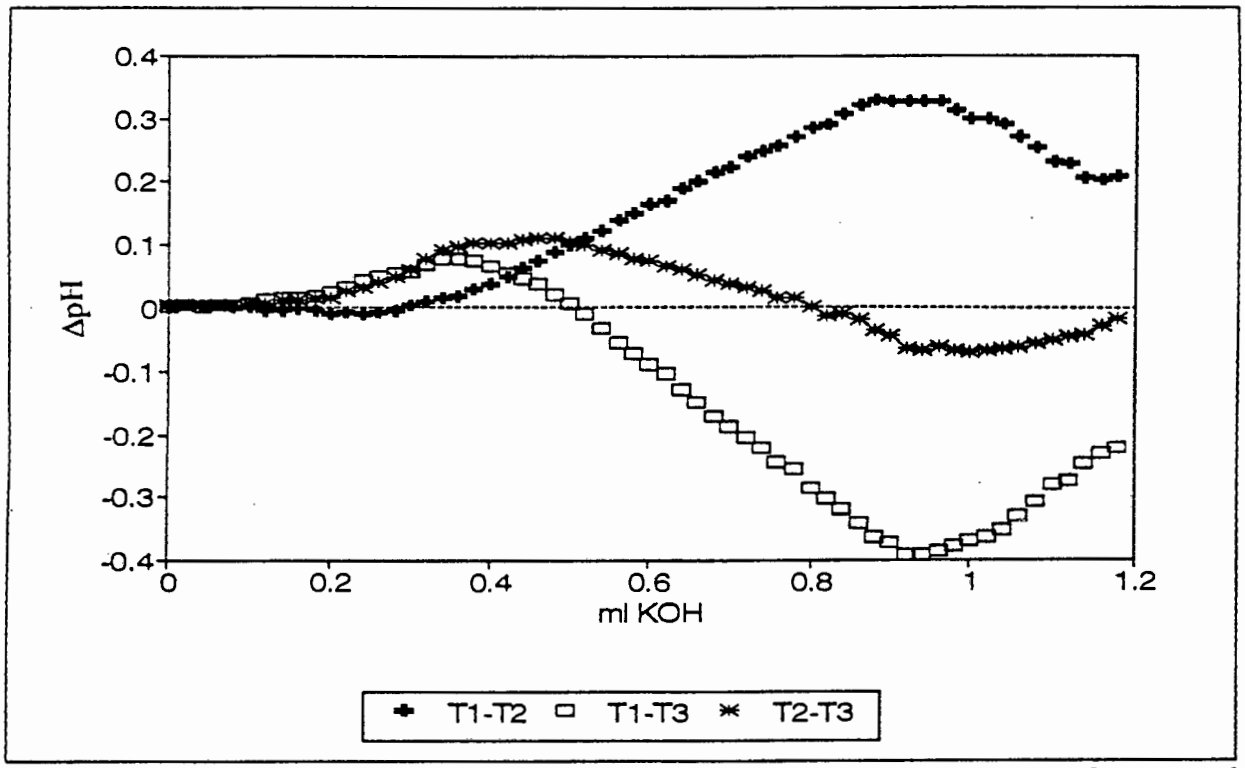

Figure 3.8 Variability observed for titrations of the Zn - δ-MnO_2 system as a function of base added.

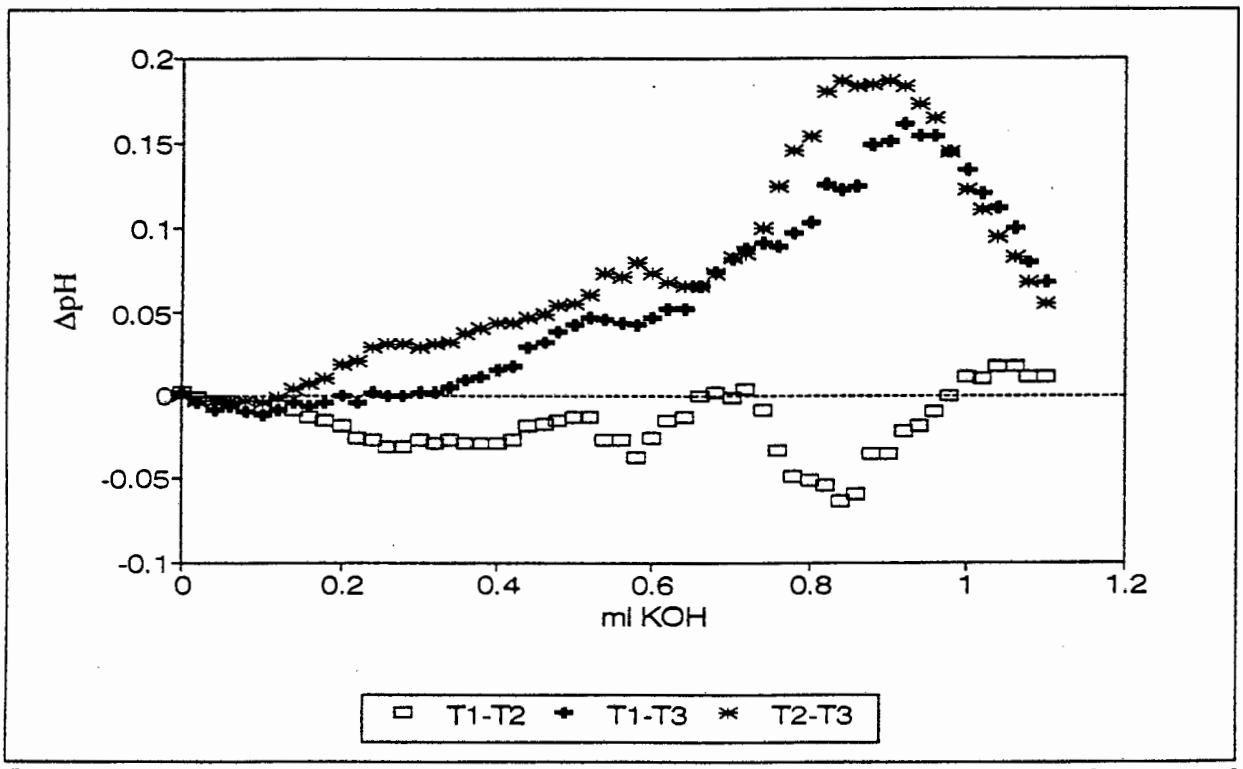

Figure 3.9 Variability observed for titrations of the Cd - δ-MnO_2 system as a function of base added.

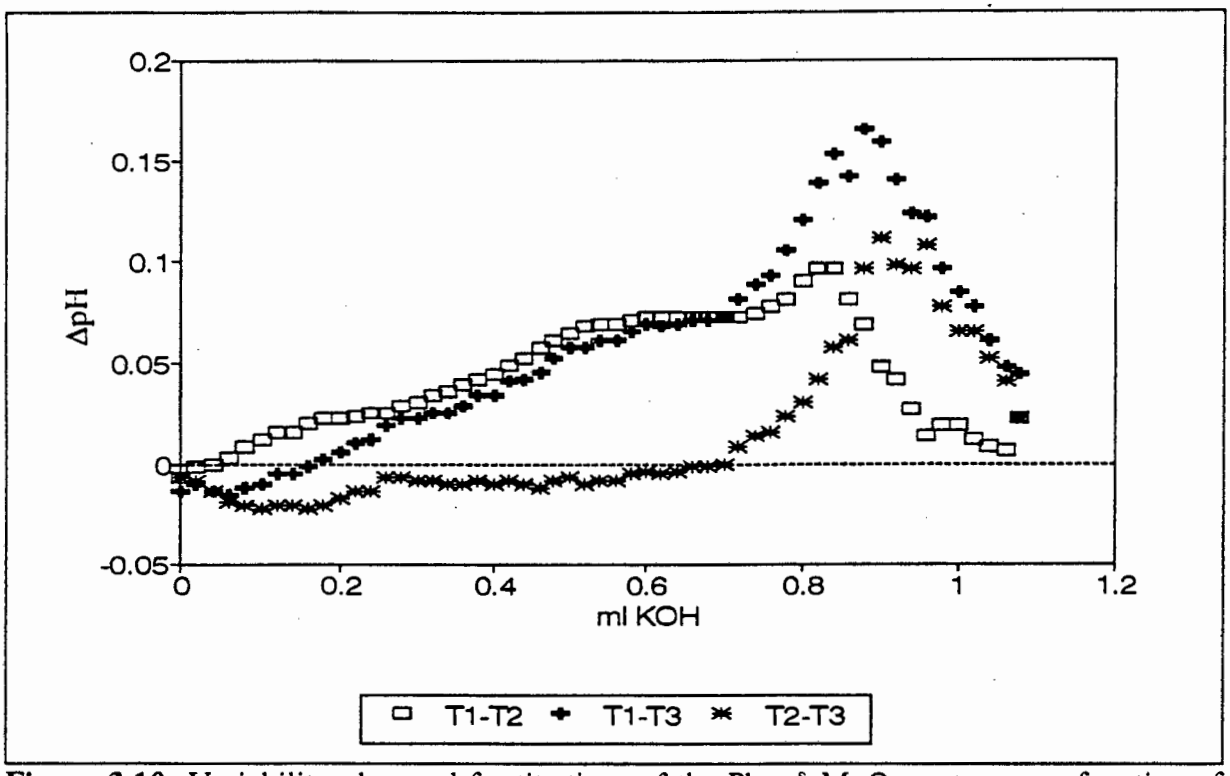

Figure 3.10 Variability observed for titrations of the Pb - δ-MnO_2 system as a function of base added.

The observed variability ranges from 0.1 to 0.2 pH units. An exception to this is zinc (Figure 3.8), where variability of up to 0.4 pH units is observed between titration 1 and the other two zinc titrations. However, ignoring titration 1, variability drops to approximately 0.1 pH units. Thus, the variability is of the same order as that observed in the protonation studies (Figure 2.5).

As was observed for titrations in Chapter 2, no underlying pattern in the variability is apparent. In the case of cadmium (Figure 3.9), the sign of ΔpH is related to the time elapsed between the start and end of the titrations. Although the same equilibrium criterion was used for all titrations, titrations did not all proceed according to the same time profile (i.e. time elapsed between the start of the titration and point i). This is due to the fact that EMF drift was not consistent in the different titrations.

Titration 2 was faster than titration 1 by twenty minutes and titration 1 was faster than titration 3 by ten minutes. The difference pH_{T2}-pH_{T3} is positive, which indicates that titration 3 consumed more base than titration 2. This is also observed for pH_{T1}-pH_{T3}. The difference pH_{T1}-pH_{T2} is negative, which indicates that titration 1 consumed more base that titration 2. This suggests a trend of slower titrations consuming more base. However, this trend was not observed for all metals.

For nickel (Figure 3.6), titration times could explain the sign of ΔpH in two instances (pH_{T1}-pH_{T2} and pH_{T2}-pH_{T4}), but not pH_{T1}-pH_{T4}. For copper (Figure 3.7), titration 3 was the slowest. This could explain the sign of ΔpH involving titration 3. However, titrations 1 and 2 took exactly the same time to complete and followed the same time intervals throughout, but ΔpH for these titrations is significant. ΔpH for titrations 1 and 3 is the smallest, which shows that completion time (and therefore equilibration time) does not play a role. A similar result is obtained for lead (Figure 3.10). The situation for zinc was not investigated since the titration time profile was not monitored for this metal.

It may thus be stated that time to completion cannot be used to explain variability between titrations. As before, it is not possible to make any statement regarding possible causes of the variability observed between titrations. The results do, however, suggest that the observed variability does not result from a systematic process but that a random or poorly reproducible process is responsible.

3.3 Adsorption constant determination

Metal adsorption constants were determined from the potentiometric titration data using FITEQL (Herbelin and Westall, 1994). Adsorption constants were the only parameters which were optimized. Total binding site concentration and protonation constants were fixed at the values which were determined in the protonation study (Chapter 2). As with the protonation study, model selection was performed on a "titration by titration" approach. Best estimates for adsorption constants were obtained by using the final model together with all titration data. Error estimates used in the FITEQL optimizations are listed in Table 3.2.

Table 3.2 Error estimates used in metal adsorption model selection.

Parameter	Relative	Absolute (M)
T_{XOH}	0.0245	$1x10^{-6}$
T_{YOH}	0.0238	$1x10^{-6}$
T_M	0.01	$1x10^{-6}$
T_H	0.01	$1x10^{-7}$
$[H^+]$	0.023	-

Estimates for errors in binding site concentrations T_{XOH} and T_{YOH} were obtained from the standard deviations calculated by FITEQL in the protonation study (Table 2.2). FITEQL defaults were used for T_H and $[H^+]$. This choice has been discussed in the paragraph on protonation constant determination (Chapter 2, paragraph 2.4). Error estimates for T_M were based on the standard deviations obtained for the standardization of metal stock solutions (Appendix C).

The possible surface species which were considered are (a) $\equiv XOM^+$, (b) $\equiv YOM^+$, (c) $\equiv XOMOH$ and (d) $\equiv YOMOH$. These species are fundamental to the surface complexation

model (Schindler and Stumm, 1987). The existence of these species has not been proven although evidence has been presented which suggests the formation of complexes similar to those postulated here (Manceau *et al.*, 1992c; Chisholm-Brause *et al.*, 1990a and 1990b). These surface species may thus be viewed as modelling constructs whose only function is to describe experimental data. Surface precipitation processes were not considered. Equilibrium simulations of the experimental systems, excluding MnO_2, indicated that, at the starting pH of each titration, no positive saturation indices, which would be indicative of supersaturation, were observed.

Surface species were then used in FITEQL to reproduce experimental data. The strategy followed was a "bottom up" strategy, i.e. models were built from the most simple to more complicated. Based on results obtained from the simple models, additional surface species were postulated to improve the agreement between model and experiment.

Each model also included solution phase reactions. These reactions consisted of metal hydrolysis reactions as well as reactions between background electrolyte ions and metals. The constants employed in the model were corrected to an ionic strength of 0.1 M, using MINTEQA2 (Allison *et al.*, 1991). Aqueous phase formation constants used are listed in Table 3.3.

Model selection was based on (i) the Goodness if Fit parameter WSOS/DF, (ii) Ockham's razor and (iii) visual comparison between plot of model and experimental data. The procedure for model selection may be described as follows: in cases where exactly the same number of surface species yielded different Goodness of Fit parameters, the model with the lowest Goodness of Fit parameter was selected.

Table 3.3. Solution phase species included in FITEQL calculations. All data are listed I=0.1**M**. Data source: MINTEQA2 database, corrected to required I using the Davies equation.

Dissociation of H_2O	
OH^-	-13.78
Potassium and Nitrate interaction	
KNO_3	-0.20
Nickel	
$NiNO_3^+$	0.51
$Ni(NO_3)_2$	-0.01
$NiOH^+$	-9.79
$Ni(OH)_2$	-19.01
$Ni(OH)_3^-$	-29.89
$Ni(OH)_4^{-2}$	-43.56
Ni_2OH^{+3}	-9.71
$Ni_4(OH)_4^{+4}$	-25.97
Copper	
$CuNO_3^+$	0.61
$Cu(NO_3)_2$	-0.44
$CuOH^+$	-7.39
$Cu(OH)_2$	-16.21
$Cu(OH)_3^-$	-26.79
$Cu(OH)_4^{-2}$	-39.16
$Cu_2(OH)_2^{+2}$	-9.92
Zinc	
$ZnNO_3^+$	0.51
$Zn(NO_3)_2$	-0.31
$ZnOH^+$	-8.89
$Zn(OH)_2$	-17.88
$Zn(OH)_3^-$	-27.99
$Zn(OH)_4^{-2}$	-40.06
Zn_2OH^{+3}	-8.01
Cadmium	
$CdNO_3^+$	0.61
$Cd(NO_3)_2$	0.19
$CdOH^+$	-9.97
$Cd(OH)_2$	-20.37
$Cd(OH)_3^-$	-33.19
$Cd(OH)_4^{-2}$	-46.91
Cd_2OH^{+3}	-8.40
$Cd_4(OH)_4^{+4}$	-31.08

Table 3.3 continued

	Lead
$PbNO_3^+$	1.28
$Pb(NO_3)_2$	1.39
$PbOH^+$	-7.49
$Pb(OH)_2$	-17.11
$Pb(OH)_3^+$	-27.99
$Pb(OH)_4^{-2}$	-39.26
Pb_2OH^{+3}	-5.37
$Pb_3(OH)_4^{+2}$	-23.44
$Pb_4(OH)_4^{+4}$	-18.23
$Pb_6(OH)_8^{+4}$	-41.83

In cases where the addition of an extra adjustable parameter resulted in a small decrease in the value of the Goodness of Fit parameter, a statistical test was used to evaluate whether the decrease in fitting parameter was significant or not. The Goodness of Fit parameter WSOS/DF calculated by FITEQL is a measure of the overall variance in the model or the residuals. According to Hamilton (1965), the F-test (or variance ratio test) may be employed to test whether the difference in Goodness of Fit observed between two models is significant or not. The F-test is defined as

$$F = \frac{s_A^2}{s_B^2} \quad \ldots\ldots\ldots\ldots\ldots\ldots\ldots\ldots \quad (3.1)$$

where s_A and s_B are standard deviations for samples A and B. The value of F calculated from equation 3.1 is now compared against values listed in F-tables (see for example CRC Handbook of Chemistry and Physics). If $F_{exp} < F_{Tables}$, the two models do not differ significantly from each other at the probability level which F_{Tables} refers to. If the situation is reversed, there is a significant difference between the models.

Other workers (Fu *et al.*, 1991; Catts and Langmuir, 1986) who have studied metal adsorption by δ-MnO_2 do not report on their model selection procedure. Herbelin and Westall

(1994) state that values of the Goodness of Fit parameter WSOS/DF between 0.1 and 20 indicate good agreement between model and experiment, whereas WSOS/DF ≈ 0 indicates a model consisting of too many adjustable parameters.

3.3.1 Results

Modelling results are discussed separately for each metal. The basic approach followed is discussed fully for copper. For the other metals, a summary of results and some pertinent remarks are presented.

3.3.1(a) Copper

The simplest model postulated is one in which all copper is adsorbed at the most acidic surface site, site ≡XOH. This model (Model 1) consists of the following reaction scheme:

Model 1:

$\equiv XOH \rightleftharpoons \equiv XO^- + H^+$ Log K_1 = -1.26

$\equiv YOH \rightleftharpoons \equiv YO^- + H^+$ Log K_2 = -5.99

$\equiv YOH + H^+ \rightleftharpoons \equiv YOH_2^+$ Log K_3 = 3.52

$\equiv XOH + Cu^{2+} \rightleftharpoons \equiv XOCu^+ + H^+$ Log K_4: determine

Results for **Model 1** are listed in Table 3.4 and the agreement between model and experiment is shown in Figure 3.11. This model is not successful in describing experimental data. The Goodness of Fit parameter is not acceptable and the visual fit indicates that the model is not capable of explaining experimental results above pH 3.2.

Table 3.4 Copper adsorption constant as determined by Model 1 for three titrations.

Parameter	Titration 1	Titration 2	Titration 3
Log $K_4 \pm \sigma_{Log\ K}$	-0.52 ± 0.077	-0.84 ± 0.056	-0.74 ± 0.063
WSOS/DF	34.3	28.3	37.7
Data points	61	61	61
pH range	2.97 - 9.80	2.97 - 9.85	2.98 - 9.72

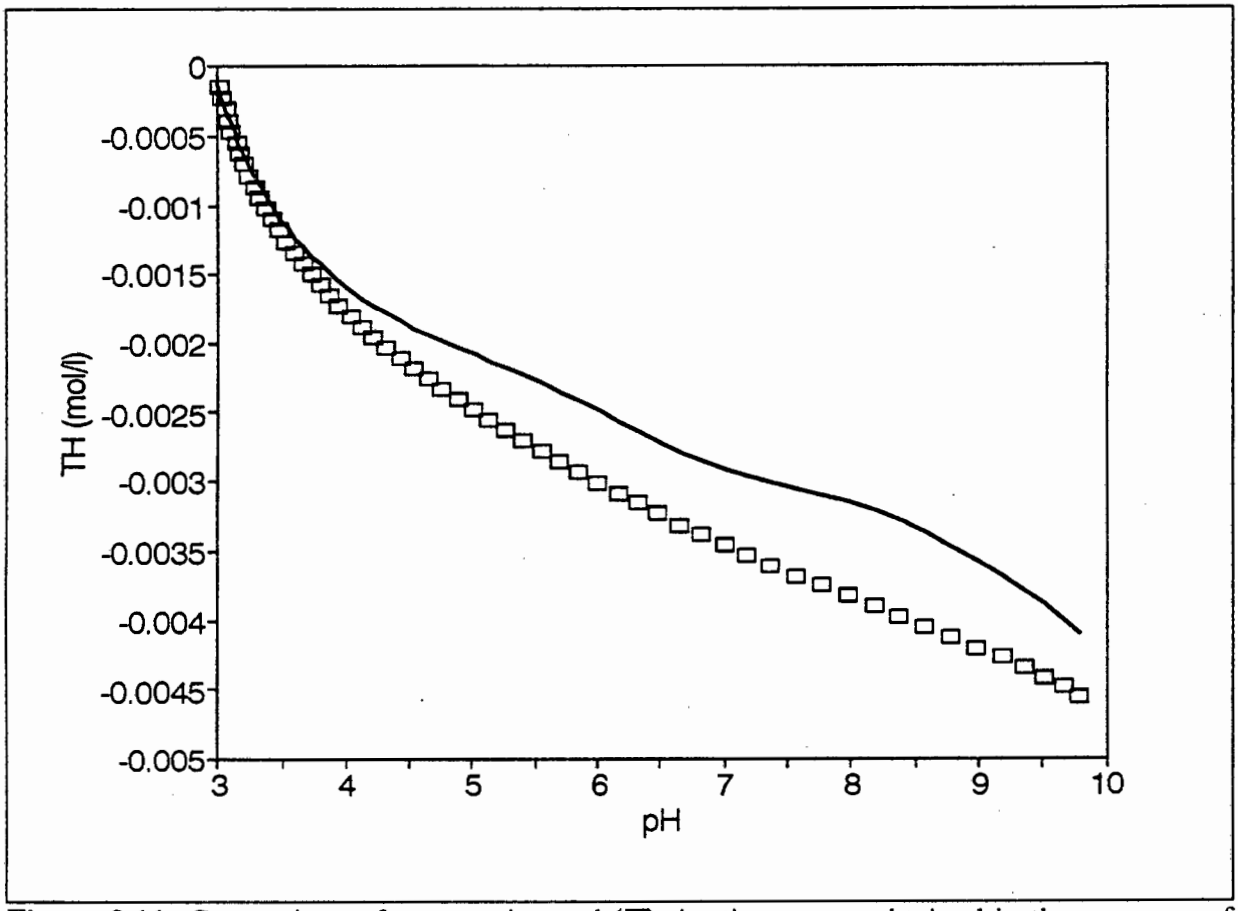

Figure 3.11 Comparison of an experimental (□) titration curve, obtained in the presence of copper, with a calculated (—) titration curve generated with Model 1.

The model underpredicts the amount of base required to attain a given pH value. In other words, the model predicts a smaller base consumption than that observed experimentally. It would therefore appear that account should be taken of other sources of protons, eg. (i) adsorption of Cu^{+2} at site ≡YOH or (ii) adsorption of $CuOH^+$ at ≡XOH. From the speciation diagram in Figure 2.10, ≡YOH and $\equiv YOH_2^+$ are the major protonated species in the pH region where the discrepancy between Model 1 and potentiometric data occurs. Thus, the second model assessed consisted of the following reactions:

Model 2:

$\equiv XOH \rightleftharpoons \equiv XO^- + H^+$	$\text{Log } K_1 = -1.26$
$\equiv YOH \rightleftharpoons \equiv YO^- + H^+$	$\text{Log } K_2 = -5.99$
$\equiv YOH + H^+ \rightleftharpoons \equiv YOH_2^+$	$\text{Log } K_3 = 3.52$
$\mathbf{\equiv XOH + Cu^{2+} \rightleftharpoons \equiv XOCu^+ + H^+}$	**Log K_4: determine**
$\mathbf{\equiv YOH + Cu^{2+} \rightleftharpoons \equiv YOCu^+ + H^+}$	**Log K_5: determine**

Results are listed in Table 3.5 and the agreement between model and experiment is shown in Figure 3.12.

The Goodness of Fit parameter calculated for **Model 2** indicates a significant improvement over **Model 1**. Figure 3.12, which shows a comparison between this model and experiment, supports this. Agreement between model and experiment extends over a wider pH range than for model 1. The model explains experimental data up to a pH of approximately 4.5. In the region $4.5 < pH < 5.8$, the modelled curve drops below the experimental curve, overestimating the amount of base needed to reach a given pH.

Table 3.5 Copper adsorption constants as determined by Model 2 for three titrations.

Parameter	Titration 1	Titration 2	Titration 3
Log $K_4 \pm \sigma_{Log\ K}$	-0.85 ± 0.067	-0.93 ± 0.057	-1.16 ± 0.058
Log $K_5 \pm \sigma_{Log\ K}$	0.46 ± 0.056	0.082 ± 0.059	0.34 ± 0.045
WSOS/DF	6.5	5.4	6.8
Data points	61	61	61
pH range	2.97 - 9.80	2.97 - 9.85	2.98 - 9.72

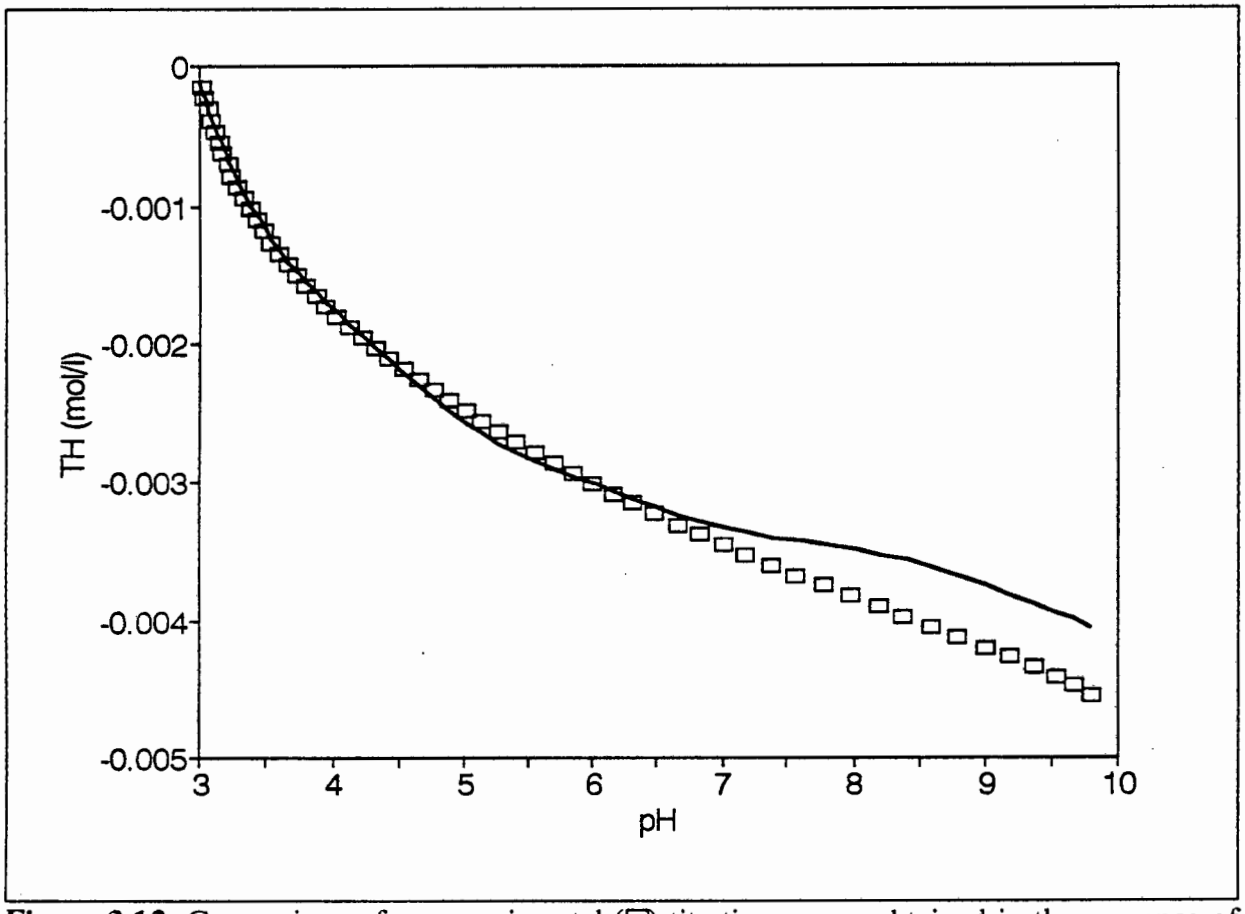

Figure 3.12 Comparison of an experimental (□) titration curve, obtained in the presence of copper, with a calculated (—) titration curve generated with Model 2.

Above pH 5.8, the model crosses over the experimental curve and from approximately pH 6 to 6.5 underestimates the amount of base needed to reach a given pH.

The fit between model and experiment suggests, as before, that an additional proton contributing surface species should be included. Species which qualify for consideration are ≡YOCuOH and ≡XOCuOH. Species ≡YOCuOH was selected since the discrepancy between model and experiment is above pH 6, a region where site ≡XOH may be expected to be fully deprotonated (see Figure 2.10) and therefore adsorption at this site will not liberate any further protons. From Figure 2.10 it is clear that ≡YOH and $\equiv YOH_2^+$ are the dominant protonated species at pH ≥ 6. Thus, the following model was postulated:

Model 3:

$\equiv XOH \rightleftharpoons \equiv XO^- + H^+$	Log K_1 = -1.26
$\equiv YOH \rightleftharpoons \equiv YO^- + H^+$	Log K_2 = -5.99
$\equiv YOH + H^+ \rightleftharpoons \equiv YOH_2^+$	Log K_3 = 3.52
$\equiv XOH + Cu^{2+} \rightleftharpoons \equiv XOCu^+ + H^+$	**Log K_4: determine**
$\equiv YOH + Cu^{2+} \rightleftharpoons \equiv YOCu^+ + H^+$	**Log K_5: determine**
$\equiv YOH + Cu^{2+} + H_2O \rightleftharpoons \equiv YOCuOH + 2H^+$	**Log K_6: determine**

Results are summarized in Table 3.6 and Figure 3.13 compares the agreement between model and experiment.

The results indicate that **Model 3** is an improvement over **Model 2.** The Goodness of Fit parameter's value has decreased significantly.

Table 3.6 Copper adsorption constants as determined by Model 3 for three titrations.

Parameter	Titration 1	Titration 2	Titration 3
Log $K_4 \pm \sigma_{Log\ K}$	-0.84 ± 0.067	-0.93 ± 0.057	-1.16 ± 0.058
Log $K_5 \pm \sigma_{Log\ K}$	0.46 ± 0.056	0.076 ± 0.059	0.33 ± 0.045
Log $K_6 \pm \sigma_{Log\ K}$	-3.84 ± 0.15	-4.47 ± 0.16	-3.85 ± 0.15
WSOS/DF	0.8	0.6	0.8
Data points	61	61	61
pH range	2.97 - 9.80	2.97 - 9.85	2.98 - 9.72

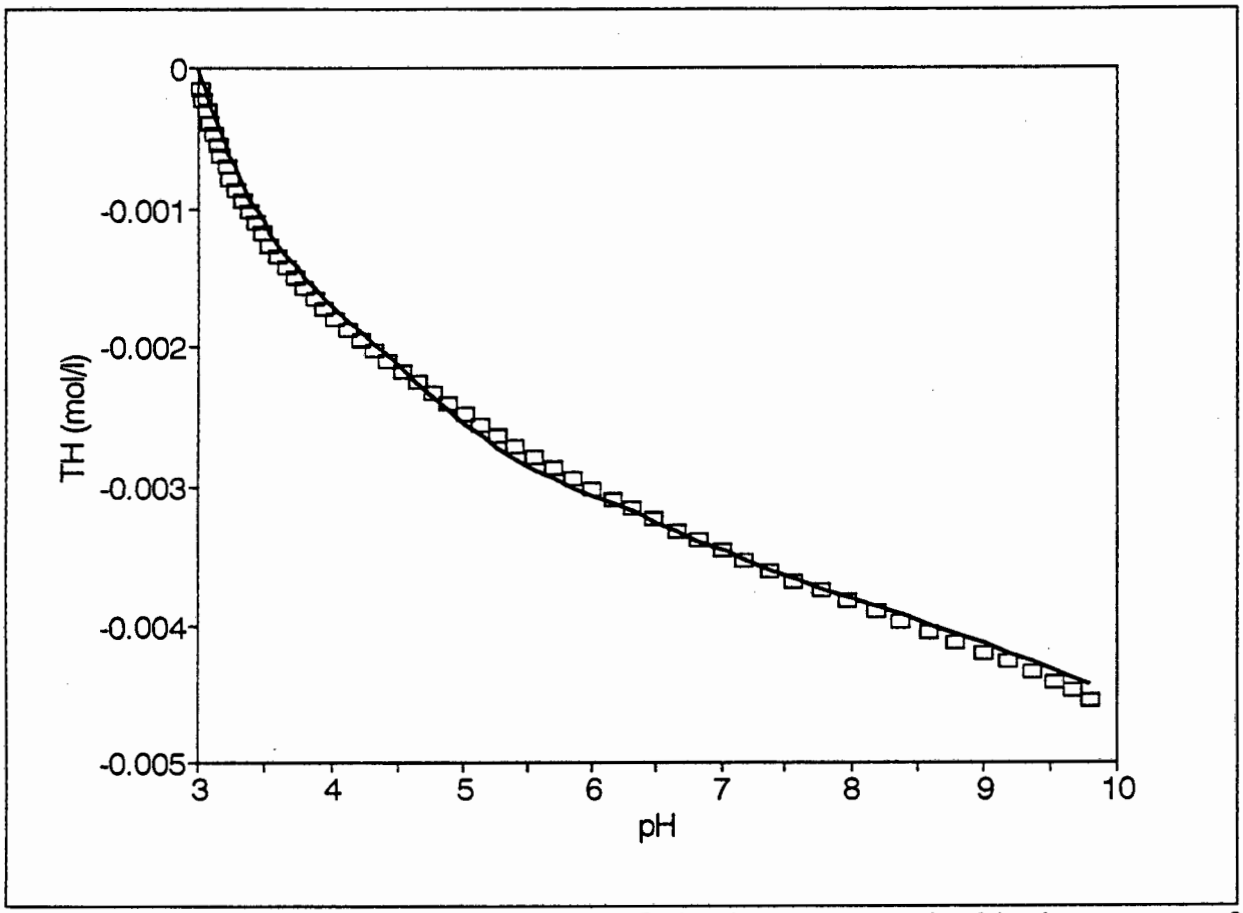

Figure 3.13 Comparison of an experimental (□) titration curve, obtained in the presence of copper, with a calculated (—) titration curve generated with Model 3.

The improved agreement between model and experiment is also evident in Figure 3.13. **Model 3** approximates experimental results well over the full pH range investigated. The fit is not perfect, however. The model overpredicts the amount of base needed to reach pH values of about 5. Some discrepancy also exists at the high pH end of the titration. In an attempt to improve the agreement between model and experiment further, the species ≡XOCuOH was included in the model. This yielded Model 4.

Model 4

$\equiv XOH \rightleftharpoons \equiv XO^- + H^+$	Log K_1 = -1.26
$\equiv YOH \rightleftharpoons \equiv YO^- + H^+$	Log K_2 = -5.99
$\equiv YOH + H^+ \rightleftharpoons \equiv YOH_2^+$	Log K_3 = 3.52
$\mathbf{\equiv XOH + Cu^{2+} \rightleftharpoons \equiv XOCu^+ + H^+}$	**Log K_4: determine**
$\mathbf{\equiv YOH + Cu^{2+} \rightleftharpoons \equiv YOCu^+ + H^+}$	**Log K_5: determine**
$\mathbf{\equiv YOH + Cu^{2+} + H_2O \rightleftharpoons \equiv YOCuOH + 2H^+}$	**Log K_6: determine**
$\mathbf{\equiv XOH + Cu^{2+} + H_2O \rightleftharpoons \equiv XOCuOH + 2H^+}$	**Log K_7: determine**

Results for this model are shown in Table 3.7. Model and experiment are compared visually in Figure 3.14. This model fits experimental results well over the whole pH range studied. The discrepancy between model 3 and experiment in the pH range 4.75 to 6.3 has been removed. Model 4 deviates from experimental results at pH > 9, where the model curve lies above the experimental data.

A question which should be answered is whether the decrease brought about in the Goodness of Fit parameter by the inclusion of ≡XOCuOH is significant or not.

Table 3.7 Copper adsorption constants as determined by Model 4 for three titrations.

Parameter	Titration 1	Titration 2	Titration 3	Best estimates
Log $K_4 \pm \sigma_{Log\,K}$	-1.24 ± 0.12	-1.22 ± 0.090	-1.50 ± 0.12	-1.31 ± 0.062
Log $K_5 \pm \sigma_{Log\,K}$	-0.087 ± 0.13	-0.42 ± 0.13	-0.096 ± 0.12	-0.20 ± 0.074
Log $K_6 \pm \sigma_{Log\,K}$	-4.20 ± 0.15	-4.80 ± 0.16	-4.13 ± 0.15	-4.37 ± 0.090
Log $K_7 \pm \sigma_{Log\,K}$	-2.86 ± 0.066	-3.10 ± 0.074	-3.07 ± 0.078	-3.01 ± 0.041
WSOS/DF	0.3	0.1	0.4	0.5
Data points	61	61	61	183
pH range	2.97 - 9.80	2.97 - 9.85	2.98 - 9.72	2.97 - 9.85

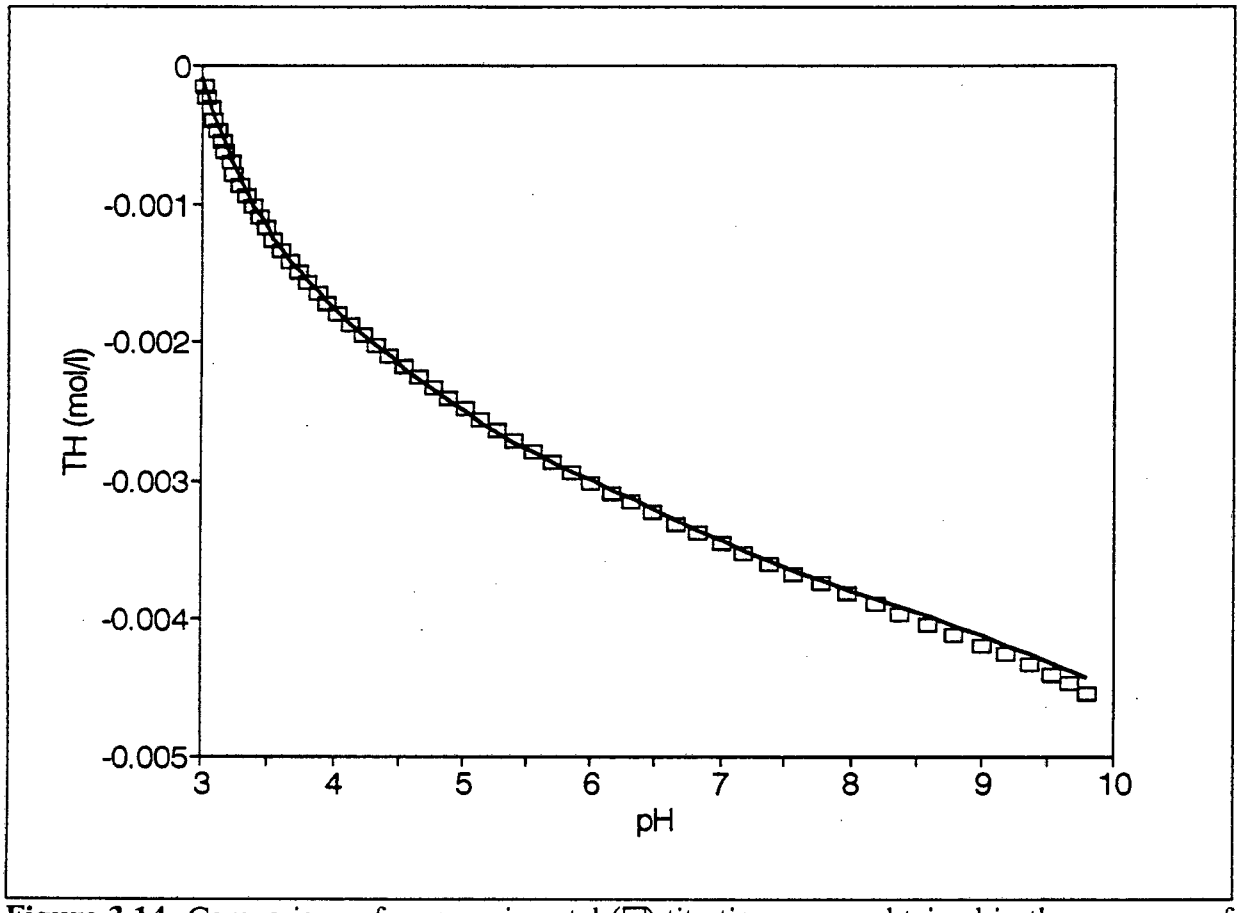

Figure 3.14 Comparison of an experimental (□) titration curve, obtained in the presence of copper, with a calculated (—) titration curve generated with Model 4.

Using the F-test (eq. 3.1), values of F for each titration are:

$$F_{\text{Titration1}} = 0.8/0.3 = 2.667;$$

$$F_{\text{Titration 2}} = 0.6/0.1 = 4.286 \text{ and}$$

$$F_{\text{Titration 3}} = 0.8/0.4 = 2.000.$$

The models have 58 and 57 degrees of freedom respectively. At the 5% probability level, $F_{0.05}(60,60) = 1.53$ is the value which corresponds closest to the number of degrees of freedom of the models. Thus, $F_{0.05} < F_{\text{Titration 1,2,3}}$ and it may be concluded that, at the 5% probability level, the two models differ significantly from each other. Taken further, a significant difference between the models exists up to the 0.5% probability level. It may thus be concluded that the four surface species model provides a significantly better explanation of the experimental data. Based on this result, the four surface species model, Model 4, was selected as the best model.

The best estimate adsorption constants for the surface species postulated in model 4 are also shown in Table 3.7. These results provide further support for Model 4. The standard deviations of all constants are within the $\sigma_{\text{Log K}} \leq 0.15$ criterion used by others (Dzombak and Morel, 1990; Baes and Mesmer, 1976) to decide whether a species is real or not.

Examination of a speciation plot of the 4 surface species model (Figure 3.15) indicates that all surface species are present at significant levels. The species ≡XOCuOH represents 65% of total copper at pH 4.5.

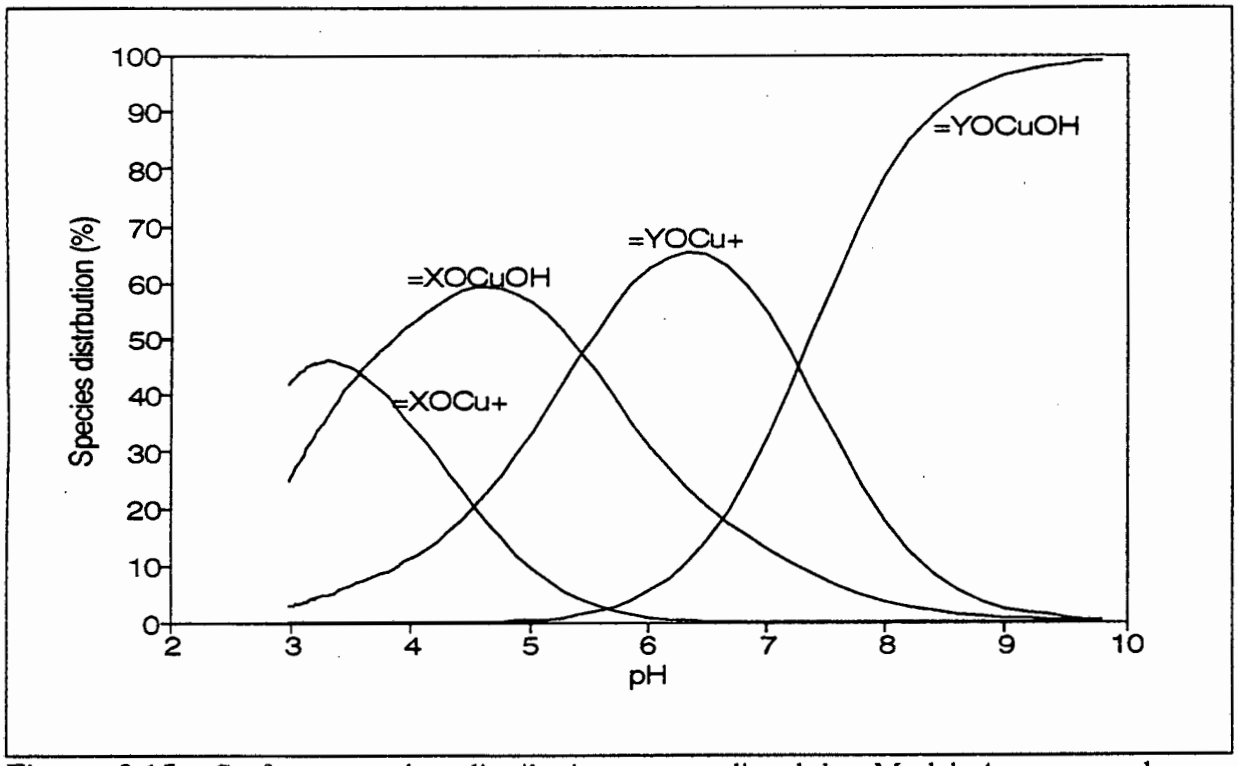

Figure 3.15 Surface complex distribution, as predicted by Model 4, expressed as a percentage of total copper vs pH.

3.3.1(b) Zinc:

Models which were assessed for their ability to explain zinc adsorption data are listed in Table 3.8.

Table 3.8 Models assessed to explain zinc adsorption data.

Species (Log K_i)	Model 1	Model 2	Model 3	Model 4
$\equiv XO^-$ (Log K_1)	-1.26	-1.26	-1.26	-1.26
$\equiv YO^-$ (Log K_2)	-5.99	-5.99	-5.99	-5.99
$\equiv YOH_2^+$ (Log K_3)	3.52	3.52	3.52	3.52
$\equiv XOZn^+$ (Log K_4)	**Determine**	**Determine**	**Determine**	**Determine**
$\equiv YOZn^+$ (Log K_5)	-	**Determine**	**Determine**	**Determine**
$\equiv YOZnOH$ (Log K_6)	-	-	**Determine**	**Determine**
$\equiv XOZnOH$ (Log K_7)	-	-	-	**Determine**

The first column of Table 3.8 shows the surface species and the Log K_i referring to that species, i.e. in the text Log K_4 refers to species $\equiv XOZn^+$ etc. It should be noted that only two titrations were used to determine zinc adsorption constants since titration 1 was discarded, based on the results shown in Figure 3.8.

Results are summarized in Tables 3.9 to 3.12 and model and experiment are compared visually in Figure 3.16 to 3.19. The results obtained are similar to those obtained for copper. The four species model led to a significant improvement over the three species model, both on a statistical and a visual basis. According to the F-test, the models were significantly different on both the 5% and 1% significance levels.

Best estimates for zinc adsorption constants together with their standard deviations are also listed in Table 3.12.

Figure 3.20 shows the relative abundance of the surface species as a function of pH. It shows that zinc speciation is dominated by species $\equiv XOZn^+$, $\equiv XOZnOH$ and $\equiv YOZnOH$. The speciation pattern is similar to that observed for copper except that species $\equiv YOZn^+$ does not become a dominant species at any pH value in the range covered by the experiments.

Table 3.9 Zinc adsorption constant as determined by Model 1 for two titrations.

Parameter	Titration 2	Titration 3
Log $K_4 \pm \sigma_{Log\ K}$	-1.37 ± 0.044	-1.53 ± 0.042
WSOS/DF	16.8	16.4
Data points	60	60
pH range	3.04 - 9.96	3.05 - 9.80

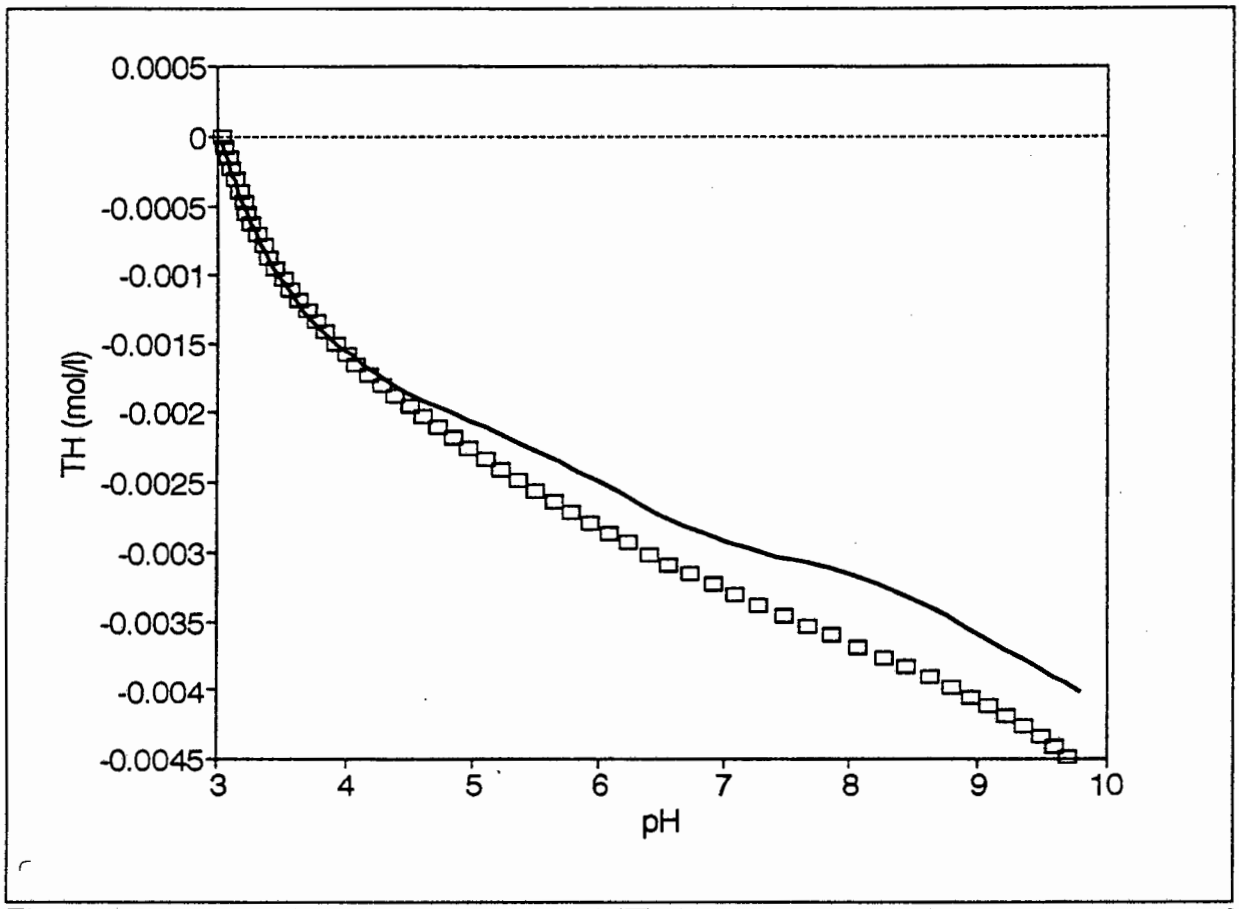

Figure 3.16 Comparison of an experimental (□) titration curve, obtained in the presence of zinc, with a calculated (—) titration curve generated with Model 1.

Table 3.10 Zinc adsorption constants as determined by Model 2 for two titrations.

Parameter	Titration 2	Titration 3
Log $K_4 \pm \sigma_{Log\,K}$	-1.39 ± 0.043	-1.54 ± 0.042
Log $K_5 \pm \sigma_{Log\,K}$	-1.22 ± 0.079	-1.83 ± 0.086
WSOS/DF	4.3	3.9
Data points	60	60
pH range	3.05 - 9.96	3.05 - 9.80

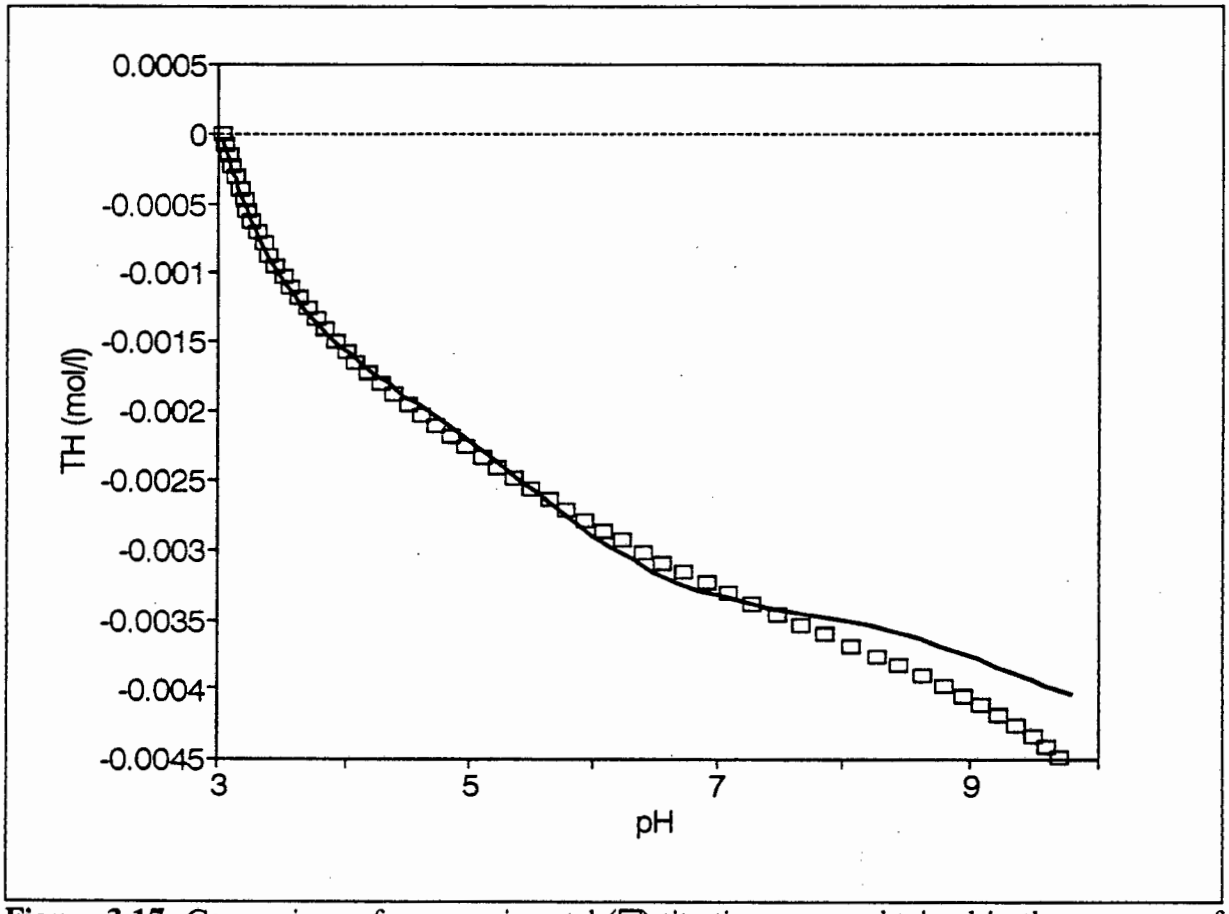

Figure 3.17 Comparison of an experimental (□) titration curve, obtained in the presence of zinc, with a calculated (—) titration curve generated with Model 2.

Table 3.11 Zinc adsorption constants as determined by Model 3 for two titrations.

Parameter	Titration 2	Titration 3
Log $K_4 \pm \sigma_{Log\,K}$	-1.39 ± 0.043	-1.54 ± 0.042
Log $K_5 \pm \sigma_{Log\,K}$	-1.23 ± 0.079	-1.84 ± 0.086
Log $K_6 \pm \sigma_{Log\,K}$	-6.55 ± 0.16	-7.03 ± 0.16
WSOS/DF	1.2	0.6
Data points	60	60
pH range	3.04 - 9.96	3.05 - 9.80

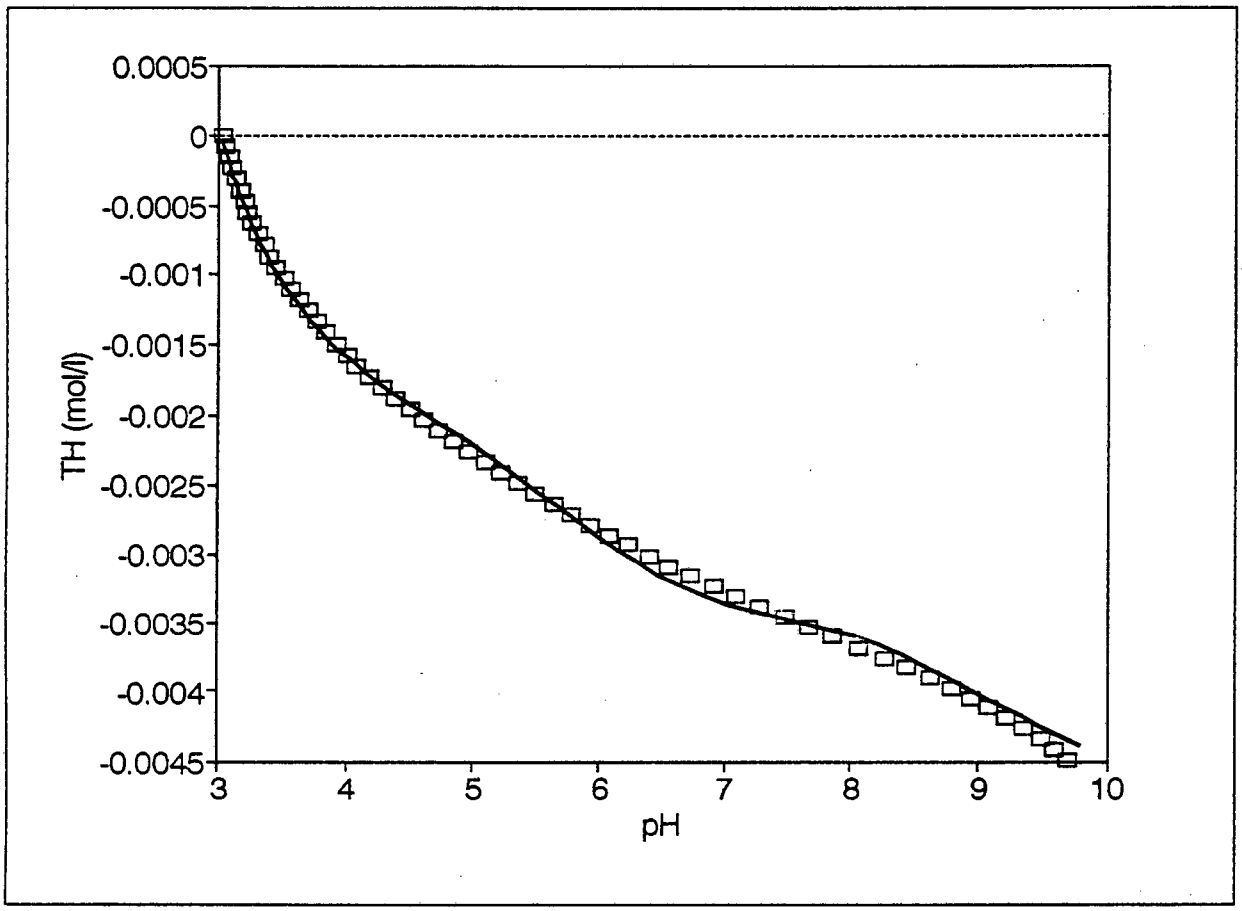

Figure 3.18 Comparison of an experimental (□) titration curve, obtained in the presence of zinc, with a calculated (—) titration curve generated with Model 3.

Table 3.12 Zinc adsorption constants as determined by Model 4 for two titrations.

Parameter	Titration 2	Titration 3	Best estimates
Log $K_4 \pm \sigma_{Log\,K}$	-1.67 ± 0.064	-1.63 ± 0.048	-1.62 ± 0.037
Log $K_5 \pm \sigma_{Log\,K}$	-2.42 ± 0.52	-2.38 ± 0.23	-2.39 ± 0.23
Log $K_6 \pm \sigma_{Log\,K}$	-7.06 ± 0.21	-7.24 ± 0.18	-7.16 ± 0.13
Log $K_7 \pm \sigma_{Log\,K}$	-3.67 ± 0.061	-4.24 ± 0.11	-3.95 ± 0.059
WSOS/DF	0.1	0.3	0.5
Data points	60	60	120
pH range	3.04 - 9.96	3.05 - 9.80	3.04 - 9.80

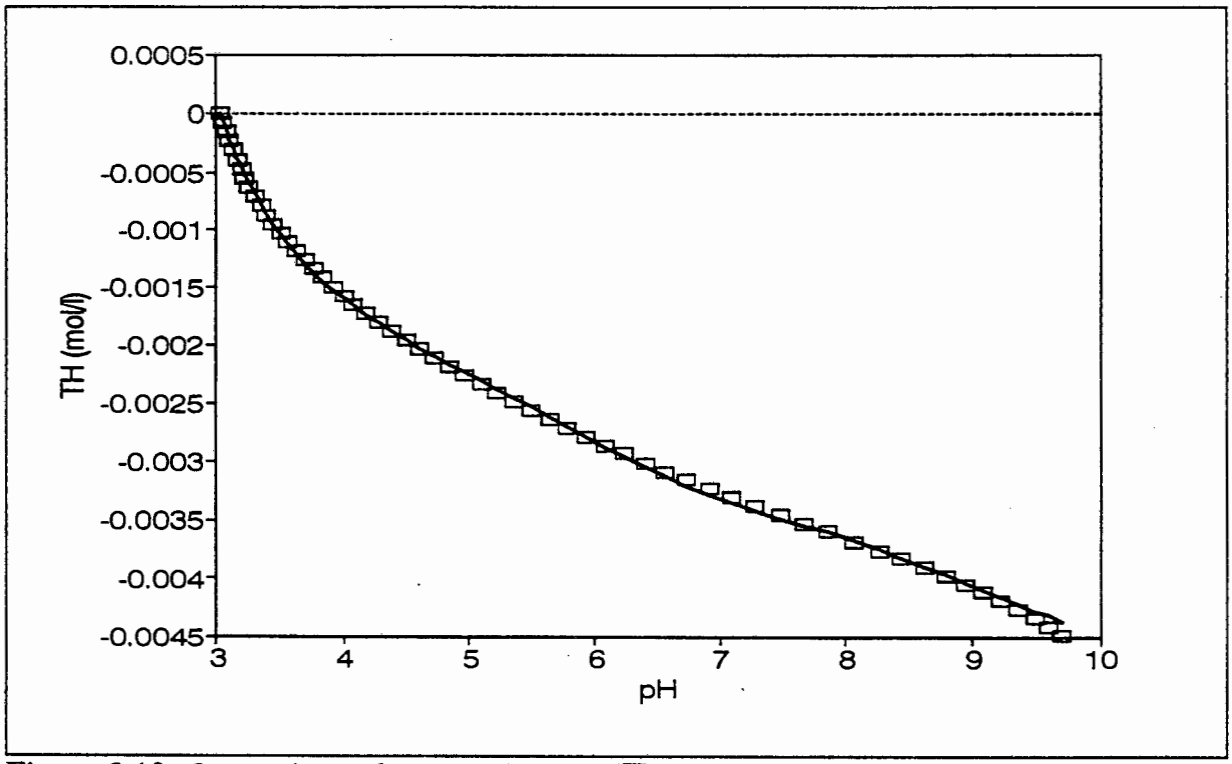

Figure 3.19 Comparison of an experimental (□) titration curve, obtained in the presence of zinc, with a calculated (—) titration curve generated with Model 4.

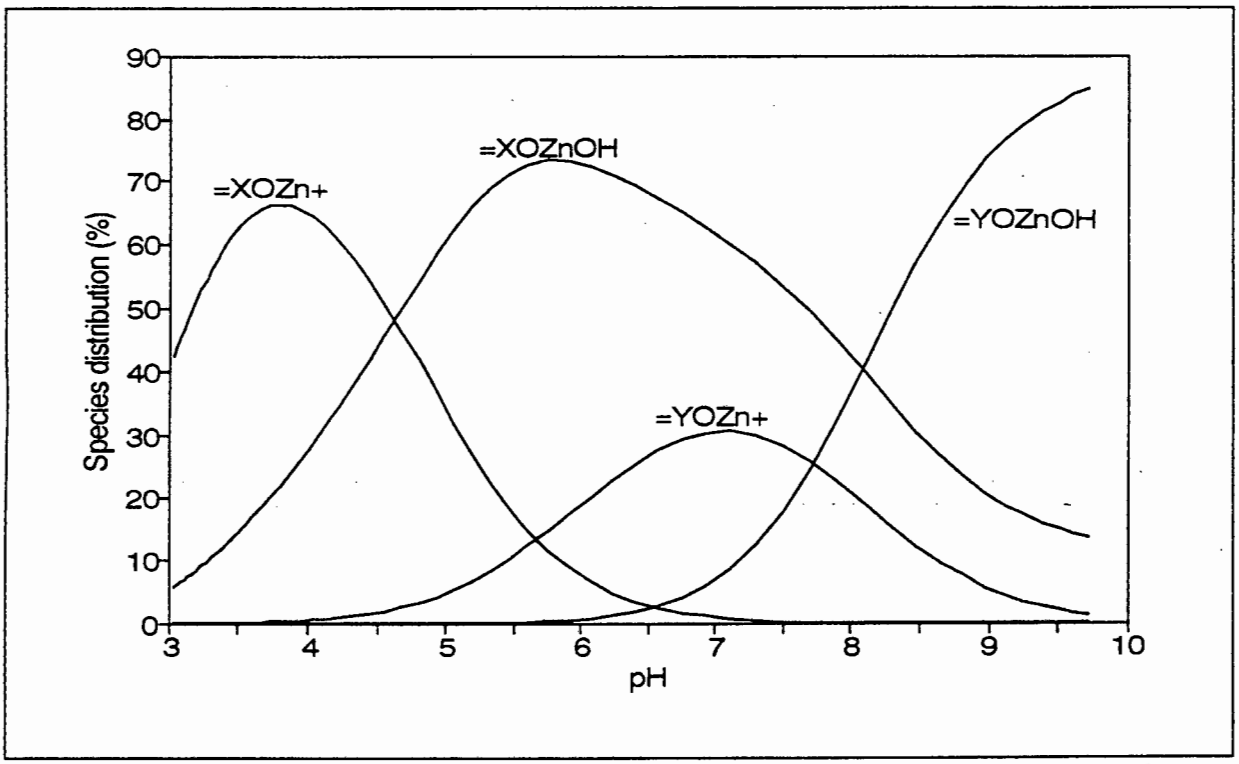

Figure 3.20 Surface complex distribution, as predicted by Model 4, expressed as a percentage of total zinc vs pH.

3.3.1(c) Nickel:

The models which were assessed for their capability to explain nickel adsorption data are listed in Table 3.13. Results for the different models are presented in Tables 3.14 to 3.17 and Figure 3.21 to 3.24.

The best explanation of nickel adsorption results is provided by the four surface species model. According to the F-test, the decrease in the Goodness of Fit parameter observed between Models 3 and 4, which was brought about by the introduction of ≡XONiOH, is significant at both the 5% and 1% significance levels.

Table 3.13 Models assessed to explain nickel adsorption data.

Species (Log K_i)	Model 1	Model 2	Model 3	Model 4
$\equiv XO^-$ (Log K_1)	-1.26	-1.26	-1.26	-1.26
$\equiv YO^-$ (Log K_2)	-5.99	-5.99	-5.99	-5.99
$\equiv YOH_2^+$ (Log K_3)	3.52	3.52	3.52	3.52
$\equiv XONi^+$ (Log K_4)	**Determine**	**Determine**	**Determine**	**Determine**
$\equiv YONi^+$ (Log K_5)	-	**Determine**	**Determine**	**Determine**
$\equiv YONiOH$ (Log K_6)	-	-	**Determine**	**Determine**
$\equiv XONiOH$ (Log K_7)	-	-	-	**Determine**

The speciation plot obtained for this model is shown in Figure 3.25. The observed speciation pattern is similar to that observed for Zn. It also differs from the copper speciation pattern in that $\equiv YONi^+$ is never a dominant species. The dominating species in the pH range 3 to 3.5 is $\equiv XONi^+$. Species $\equiv XONiOH$ dominates in the region 3.5 to 6.8. In the pH range of ca. 6.8 - 7.5, species $\equiv YONi^+$ and $\equiv XONiOH$ are present in equal concentrations. Above pH 7.5, $\equiv YONiOH$ is the dominant species.

Table 3.14 Nickel adsorption constant as determined by Model 1 for three titrations.

Parameter	Titration 1	Titration 2	Titration 3
Log $K_4 \pm \sigma_{Log\ K}$	-1.33 ± 0.047	-1.26 ± 0.047	-1.39 ± 0.044
WSOS/DF	21.5	25.2	20.1
Data points	60	58	60
pH range	3.04 - 9.69	3.05 - 9.46	3.05 - 9.74

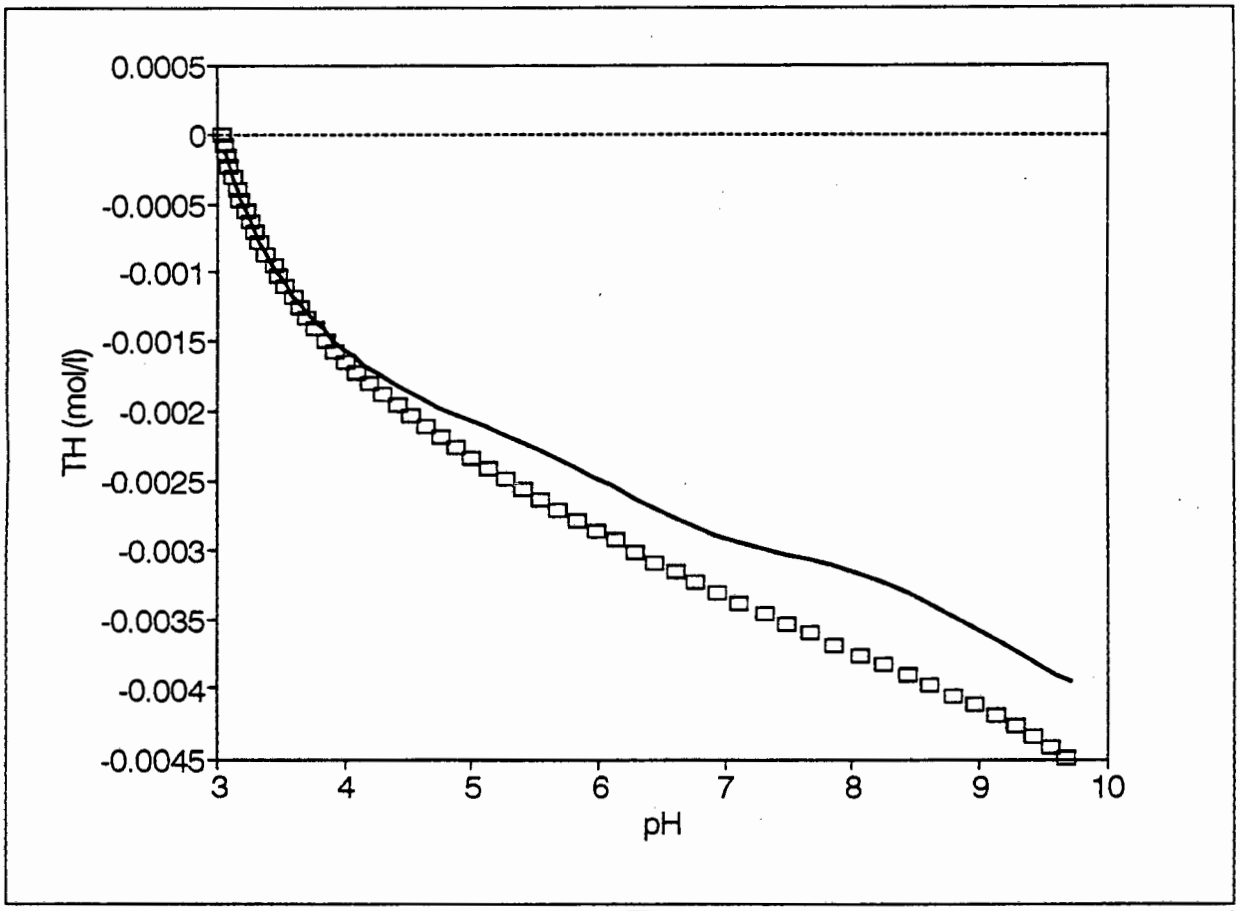

Figure 3.21 Comparison of an experimental (□) titration curve, obtained in the presence of nickel, with a calculated (—) titration curve generated with Model 1.

Table 3.15 Nickel adsorption constants as determined by Model 2 for three titrations.

Parameter	Titration 1	Titration 2	Titration 3
Log $K_4 \pm \sigma_{Log\ K}$	-1.39 ± 0.044	-1.43 ± 0.044	-1.44 ± 0.043
Log $K_5 \pm \sigma_{Log\ K}$	-1.15 ± 0.077	-0.55 ± 0.058	-1.27 ± 0.078
WSOS/DF	4.9	4.6	4.5
Data points	60	58	60
pH range	3.04 - 9.69	3.05 - 9.46	3.05 - 9.74

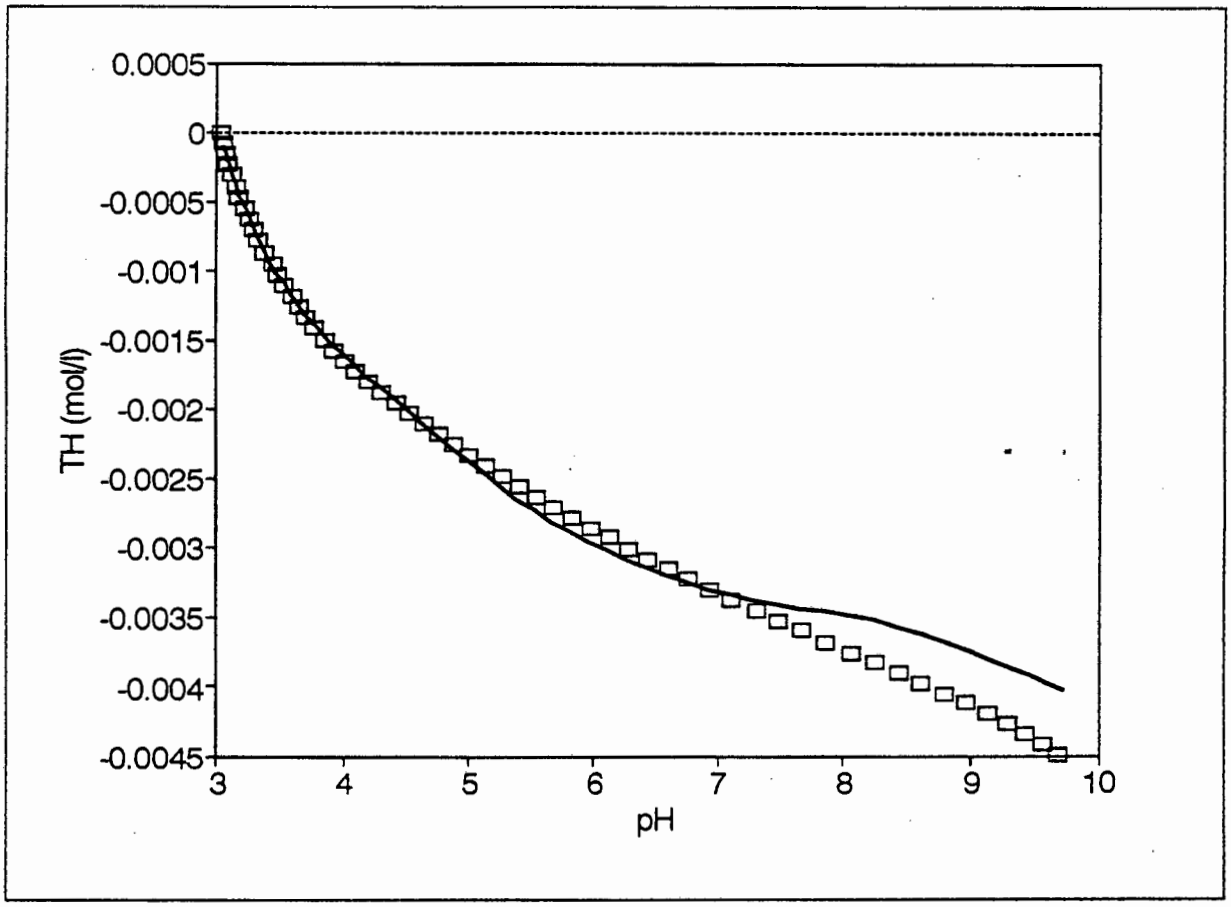

Figure 3.22 Comparison of an experimental (□) titration curve, obtained in the presence of nickel, with a calculated (—) titration curve, generated with Model 2.

Table 3.16 Nickel adsorption constants as determined by Model 3 for three titrations.

Parameter	Titration 1	Titration 2	Titration 3
Log $K_4 \pm \sigma_{Log\,K}$	-1.38 ± 0.044	-1.43 ± 0.044	-1.44 ± 0.043
Log $K_5 \pm \sigma_{Log\,K}$	-1.16 ± 0.077	-0.55 ± 0.058	-1.29 ± 0.079
Log $K_6 \pm \sigma_{Log\,K}$	-5.96 ± 0.16	-5.22 ± 0.16	-6.16 ± 0.16
WSOS/DF	0.8	1.2	0.8
Data points	60	58	60
pH range	3.04 - 9.69	3.05 - 9.46	3.05 - 9.74

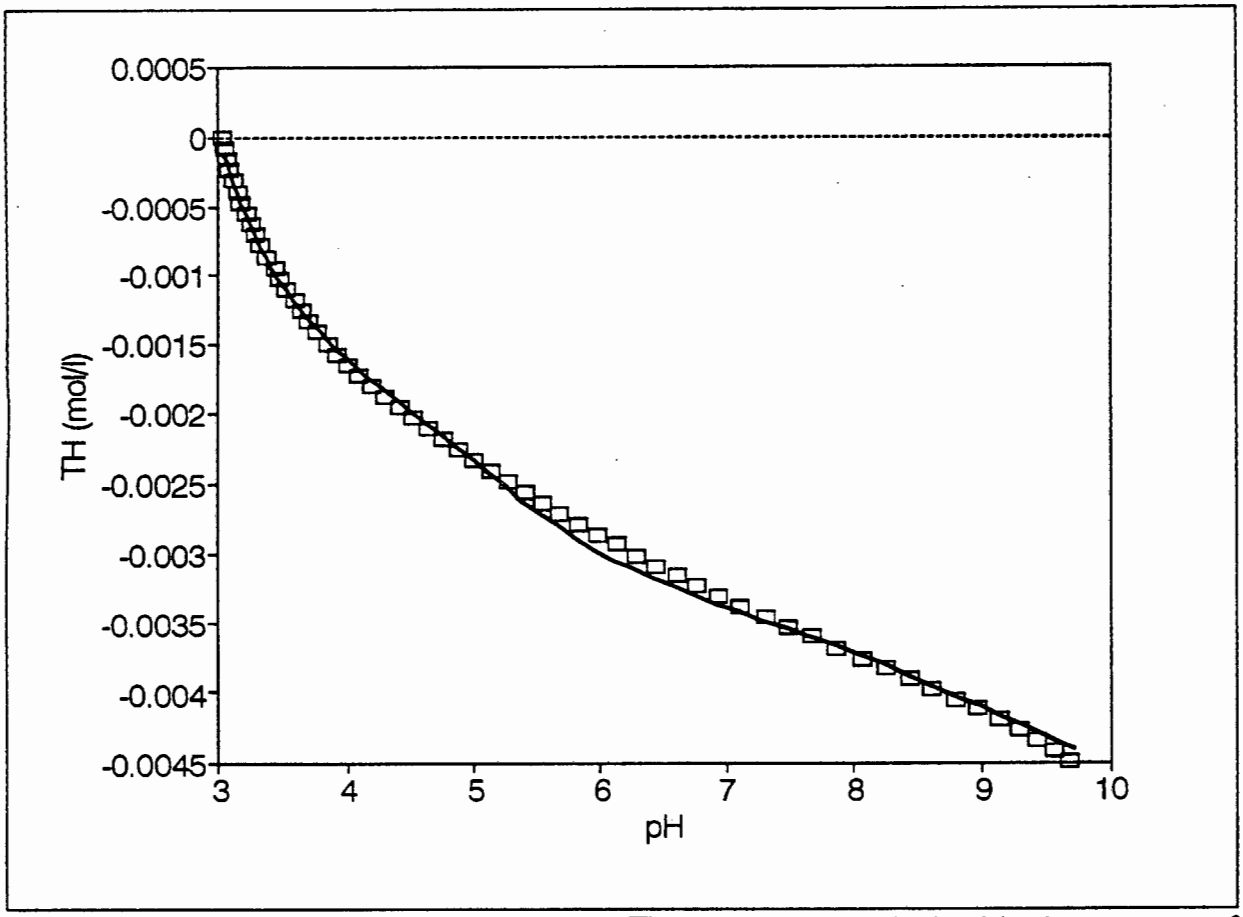

Figure 3.23 Comparison of an experimental (□) titration curve, obtained in the presence of nickel, with a calculated (—) titration curve generated with Model 3.

Table 3.17 Nickel adsorption constants as determined by Model 4 for three titrations.

Parameter	Titration 1	Titration 2	Titration 3	Best estimates
Log $K_4 \pm \sigma_{Log\,K}$	-1.57 ± 0.059	-1.84 ± 0.095	-1.63 ± 0.058	-1.65 ± 0.038
Log $K_5 \pm \sigma_{Log\,K}$	-1.71 ± 0.18	-1.28 ± 0.17	-1.90 ± 0.21	-1.63 ± 0.11
Log $K_6 \pm \sigma_{Log\,K}$	-6.21 ± 0.17	-5.63 ± 0.16	-6.40 ± 0.17	-6.08 ± 0.098
Log $K_7 \pm \sigma_{Log\,K}$	-3.81 ± 0.085	-3.49 ± 0.054	-3.85 ± 0.081	-3.70 ± 0.041
WSOS/DF	0.3	0.2	0.2	0.5
Data points	60	58	60	178
pH range	3.04 - 9.69	3.05 - 9.46	3.05 - 9.74	3.04 - 9.74

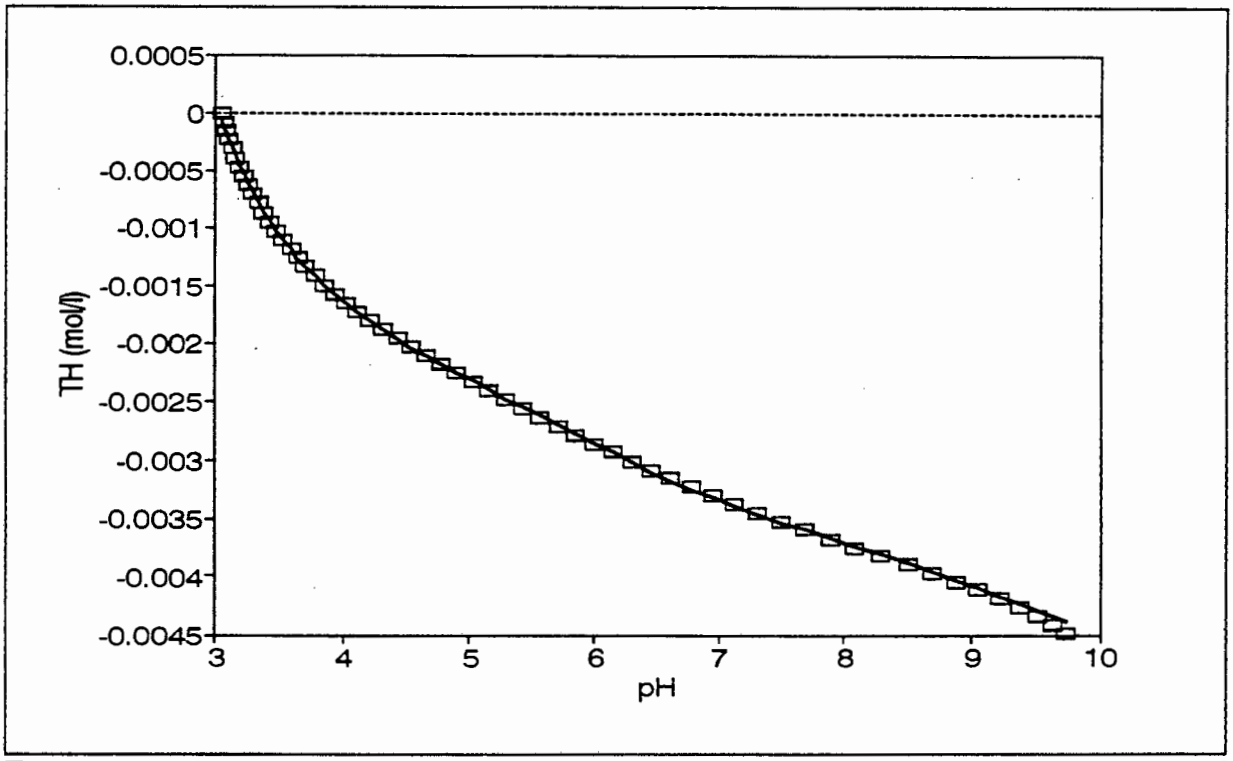

Figure 3.24 Comparison of an experimental (□) titration curve, obtained in the presence of nickel, with a calculated (—) titration curve generated with Model 4.

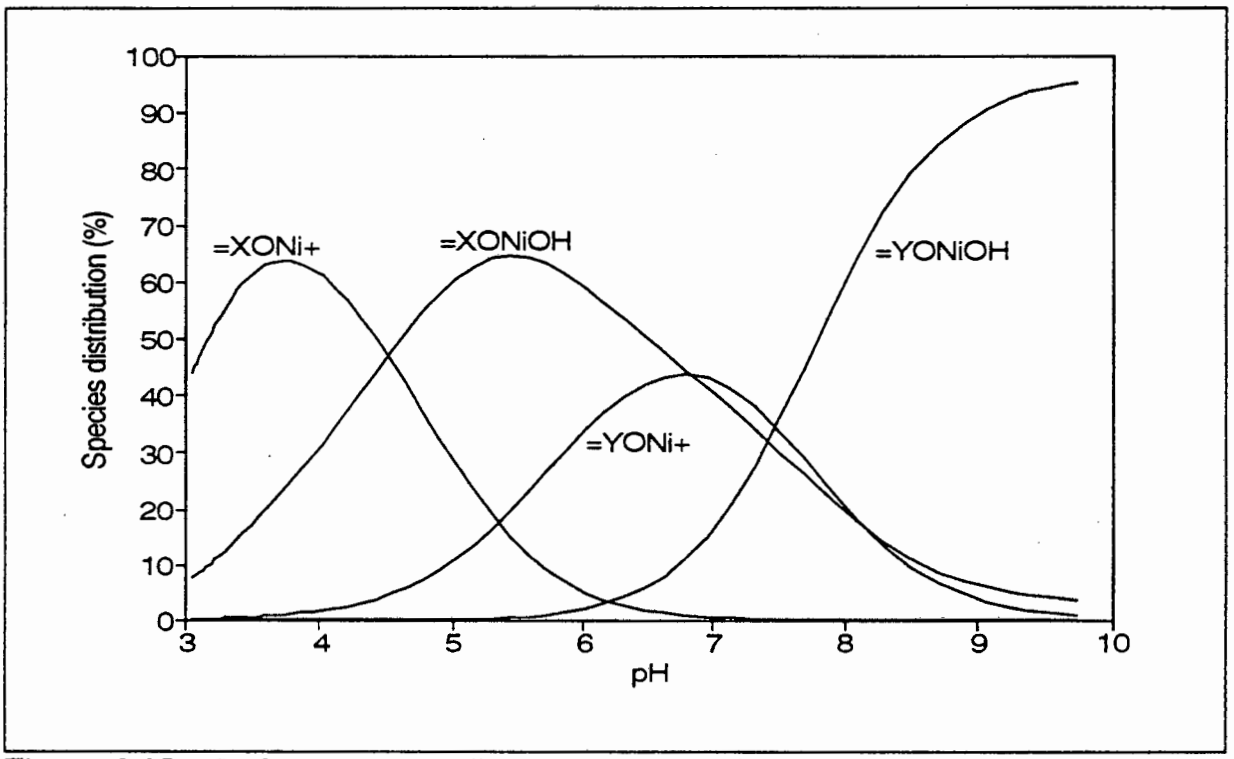

Figure 3.25 Surface complex distribution, as predicted by Model 4, expressed as a percentage of total nickel vs pH.

3.3.1(d) Cadmium:

The models assessed for their ability to describe cadmium adsorption data are listed in Table 3.18. Only two of the models listed in Table 3.18 converged for the cadmium data set. Models incorporating cadmium hydroxy species did not converge. Cadmium data were explained well up to pH 4.5 by the species $\equiv XOCd^+$ (Table 3.19 & Figure 3.26). Above this pH, the model underpredicted the amount of base needed to reach a given pH. Inclusion of $\equiv YOCd^+$ (Table 3.20 & Figure 3.27) improved the agreement between model and experiment. Application of the F-test shows that the improvement in the Goodness of Fit parameter observed between Model 1 and Model 2 is significant at the 1% probability level.

Table 3.18 Models assessed to explain cadmium adsorption data.

Species (Log K_i)	Model 1	Model 2	Model 3	Model 4
$\equiv XO^-$ (Log K_1)	-1.26	-1.26	-1.26	-1.26
$\equiv YO^-$ (Log K_2)	-5.99	-5.99	-5.99	-5.99
$\equiv YOH_2^+$ (Log K_3)	3.52	3.52	3.52	3.52
$\equiv XOCd^+$ (Log K_4)	**Determine**	**Determine**	**Determine**	**Determine**
$\equiv YOCd^+$ (Log K_5)	-	**Determine**	**Determine**	**Determine**
$\equiv YOCdOH$ (Log K_6)	-	-	**Determine**	**Determine**
$\equiv XOCdOH$ (Log K_7)	-	-	-	**Determine**

Cadmium surface speciation is shown in Figure 3.28. The species $\equiv XOCd^+$ dominates over a wide pH range. $\equiv YOCd^+$ becomes dominant at pH values greater than 7.5. The fact that $\equiv XOCdOH$ and $\equiv YOCdOH$ were not required to fit experimental data may be explained by noting that cadmium is less prone to form hydroxy species than the other elements investigated.

Table 3.19 Cadmium adsorption constant as determined by Model 1 for three titrations.

Parameter	Titration 1	Titration 2	Titration 3
Log $K_4 \pm \sigma_{Log\ K}$	-1.56 ± 0.037	-1.65 ± 0.036	-1.59 ± 0.036
WSOS/DF	1.8	1.7	3.0
Data points	56	56	56
pH range	3.02 - 9.98	3.02 - 9.97	3.02 - 9.91

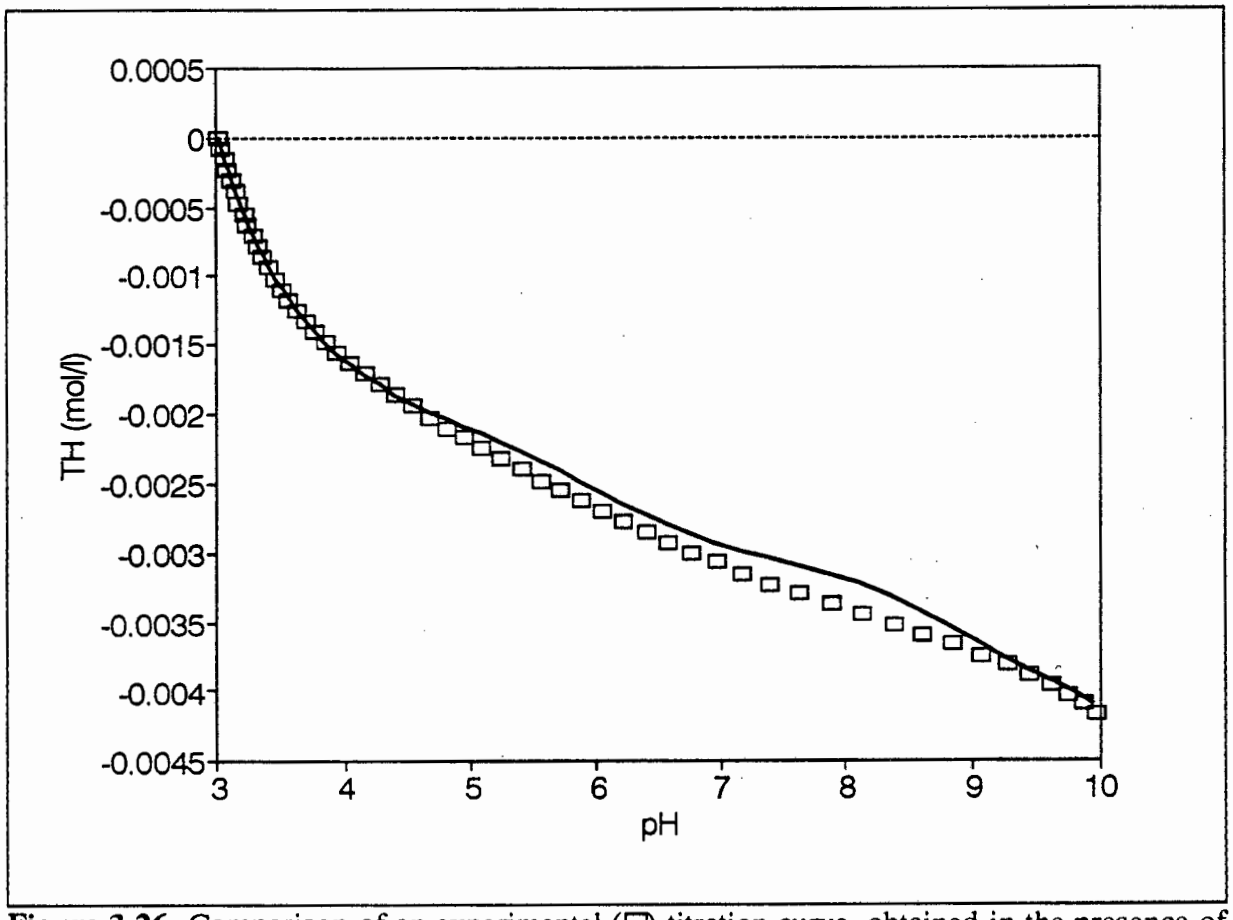

Figure 3.26 Comparison of an experimental (□) titration curve, obtained in the presence of cadmium, with a calculated (—) titration curve, generated with Model 1.

Table 3.20 Cadmium adsorption constants as determined by Model 2 for three titrations.

Parameter	Titration 1	Titration 2	Titration 3	Best estimates
Log $K_4 \pm \sigma_{Log\ K}$	-1.56 ± 0.037	-1.65 ± 0.036	-1.59 ± 0.036	-1.60 ± 0.021
Log $K_5 \pm \sigma_{Log\ K}$	-4.41 ± 0.14	-4.66 ± 0.14	-3.90 ± 0.11	-4.32 ± 0.073
WSOS/DF	0.7	0.7	1.0	0.9
Data points	56	56	56	168
pH range	3.02 - 9.98	3.02 - 9.97	3.02 - 9.91	3.02 - 9.98

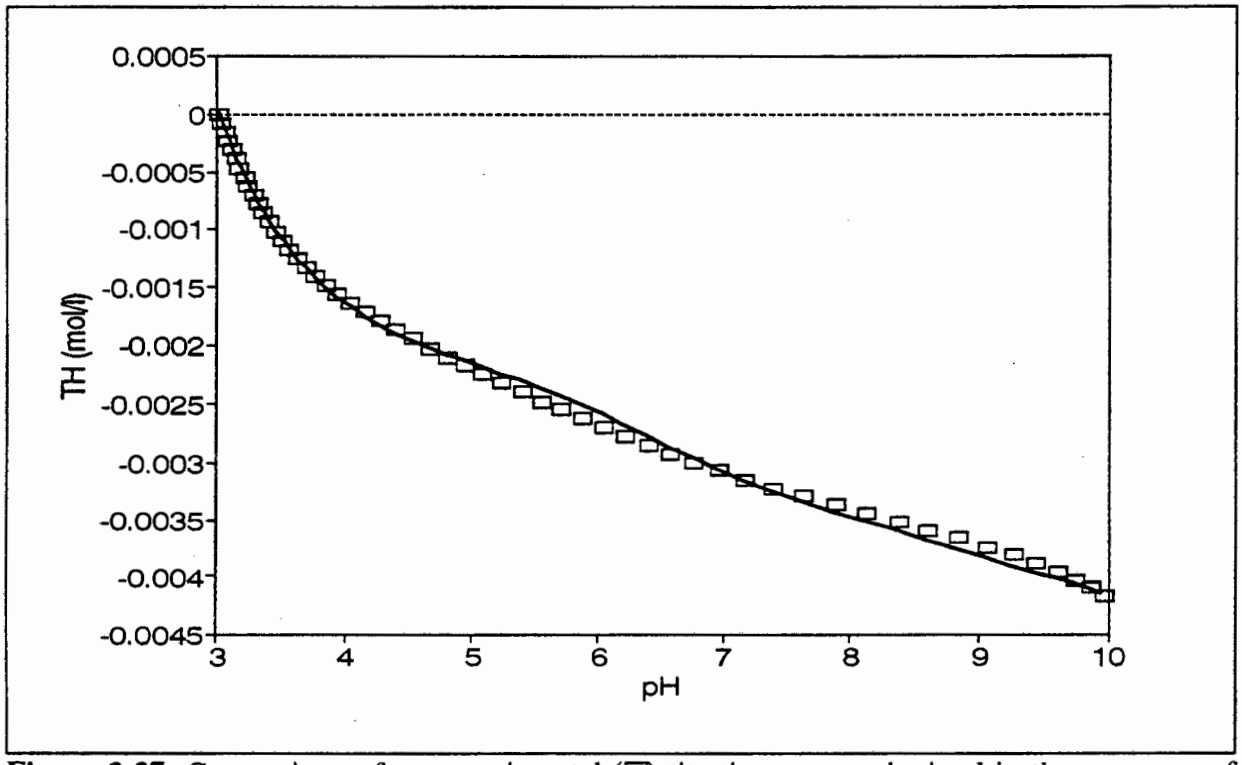

Figure 3.27 Comparison of an experimental (□) titration curve, obtained in the presence of cadmium, with a calculated (—) titration curve generated with Model 2.

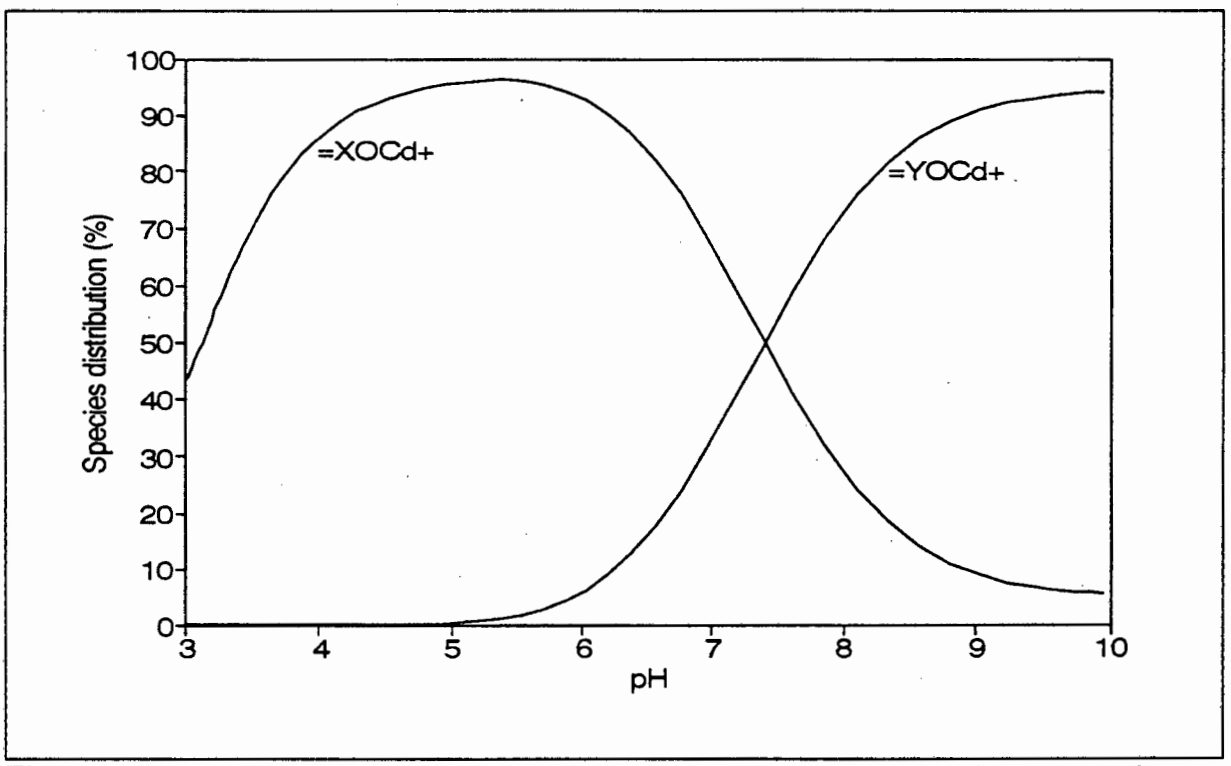

Figure 3.28 Surface complex distribution, as predicted by Model 2, expressed as a percentage of total cadmium vs pH.

3.3.1(e) Lead:

Manceau *et al.* (1992c) and Chisholm-Brause *et al.* (1990a) performed *in situ* investigations into lead adsorption by Birnessite and γ-Al_2O_3 respectively, using X-ray absorption spectroscopy. The results presented by Manceau *et al.* suggest that, under their experimental conditions, lead adsorbed as multi-nuclear surface complexes with a Pb oxy/hydroxy-like local structure and that these poly-nuclear clusters coordinate with Birnessite edges. Chisholm-Brause *et al.* conclude that in their study, at least some of the adsorbed lead was present as small multinuclear complexes. Based on this information, the first attempt at explaining lead adsorption data included a multinuclear lead hydroxide species, Pb_2OH^{+3}. The model

consisted of the following species:

$\equiv XOH \rightleftharpoons \equiv XO^- + H^+$	Log K_1 = -1.26
$\equiv YOH \rightleftharpoons \equiv YO^- + H^+$	Log K_2 = -5.99
$\equiv YOH + H^+ \rightleftharpoons \equiv YOH_2^+$	Log K_3 = 3.52
$\equiv XOH + Pb^{2+} \rightleftharpoons \equiv XOPb^+ + H^+$	**Log K_4 : determine**
$\equiv XOH + 2Pb^{2+} + H_2O \rightleftharpoons \equiv XOPb_2OH^{+2} + 2H^+$	**Log K_5 : determine**

This model did not converge. In each case, the value for Log K_4 decreased systematically, indicating a redundant species, or a species present at too low concentration to be meaningful. Discarding $\equiv XOPb^+$ resulted in convergence. Results for this model are shown in Table 3.21. The agreement between this model and potentiometric results are shown in Figure 3.29. Other models including this species were also evaluated but none of them provided a better fit. Convergence problems were a common occurrence.

Although this model is quite successful in describing the adsorption data, both from a statistical and a visual point of view, the fit obtained is not perfect. Therefore, adsorption data were also modelled using mononuclear surface complexes.

Results obtained using mononuclear surface complexes only are listed in Tables 3.22 to 3.26. Figures 3.30 to 3.34 compare modelling and experimental results. A model consisting of four surface species, similar to those proposed for copper, nickel and zinc failed to converge. The constant for the species $\equiv YOPbOH$ decreased systematically, which is indicative of a species being either redundant or present at insignificant concentration levels.

Table 3.21 Lead adsorption constants for the formation of a multinuclear surface complex.

Species	Titration 1	Titration 2	Titration 3	Best estimate
$\equiv XOPb_2OH^{+2}$	-1.57 ± 0.056	-1.31 ± 0.065	-1.59 ± 0.056	-1.49 ± 0.034
WSOS/DF	0.5	1.4	1.3	1.1
Data points	55	55	55	165
pH range	3.00 - 9.85	3.00 - 9.83	3.01 - 9.81	3.00 - 9.85

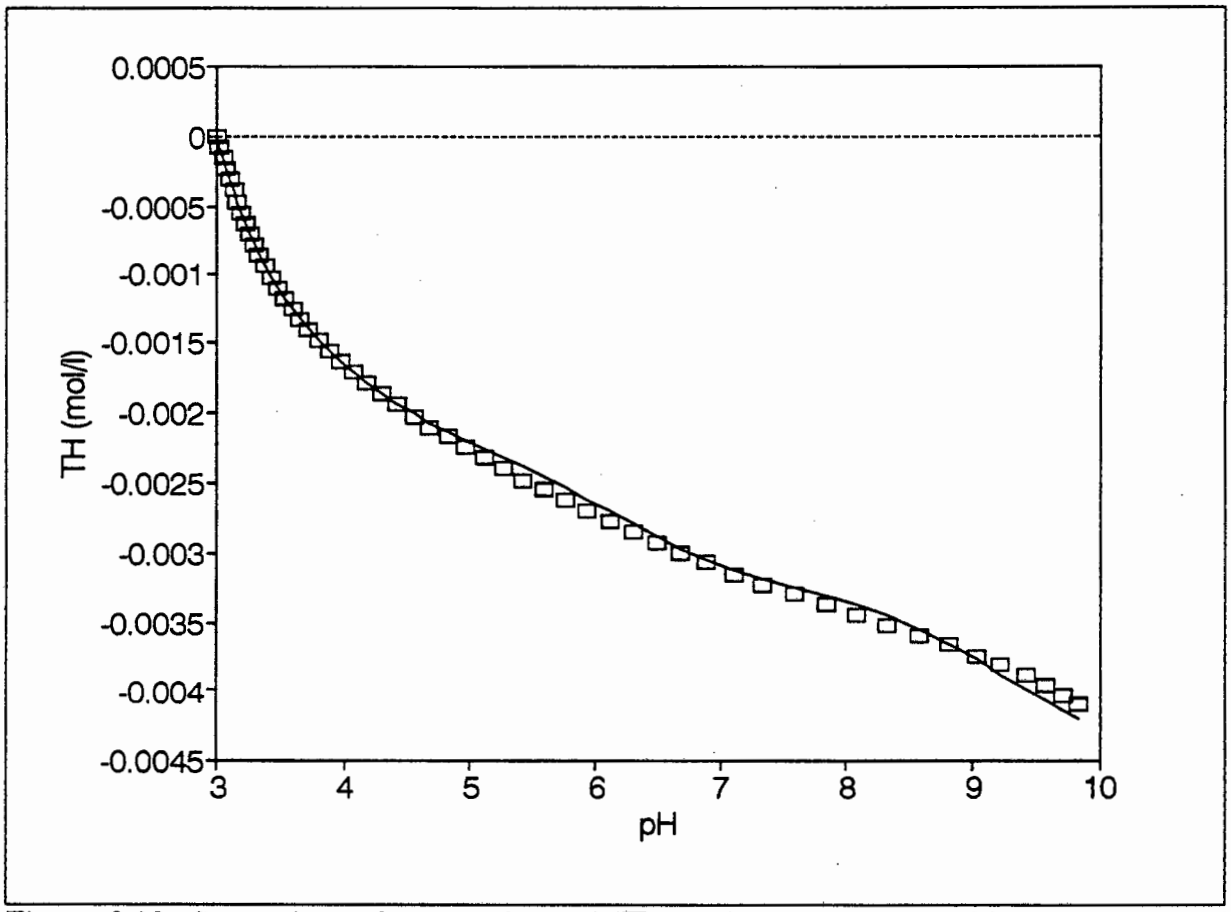

Figure 3.29 Comparison of an experimental (□) titration curve, obtained in the presence of lead, with a calculated (—) titration curve, assuming $\equiv XOPb_2OH^{+2}$ to form.

The model consisting of only one surface species, ≡XOPb$^+$, gave a fair representation of experimental results (Table 3.22 and Figure 3.30). It did, however, underestimate the base consumption of the system. Addition of a second species, ≡YOPb$^+$ improved the observed fit (Table 3.23 and Figure 3.31). However, quite a large discrepancy between model and experiment is observed in the region pH 6 to 7. Inclusion of ≡XOPbOH improved the fit slightly in the lower pH range (pH < 5) but the fit in the higher pH range did not improve (Table 3.24 & Figure 3.32). However, the Goodness of Fit parameter did show a decrease, indicating an overall improvement in fit.

Discarding ≡YOPb$^+$ did not have any effect on the Goodness of Fit parameter or the visual fit between model and experiment (cf. Tables 3.24 and 3.25; Figures 3.32 and 3.33). Thus, it may be deduced that ≡YOPb$^+$ is redundant for the explanation of adsorption data.

A model consisting of only ≡XOPbOH$^+$ was also evaluated. Results for this model are shown in Table 3.26 and Figure 3.34 plots the comparison between model and experiment. Based on the F-test, it may be stated that the ability of ≡XOPbOH to explain experimental results is not significantly different from the model consisting of ≡XOPb$^+$ and ≡XOPbOH. Thus, Ockham's razor dictates that ≡XOPbOH should be selected as the best explanation of experimental data using mononuclear surface species.

Comparison of the mononuclear model with the multinuclear surface complex model (cf. Tables 3.21 and 3.26; Figure 3.29 and 3.34) shows that the multinuclear model is more successful in describing adsorption data.

Table 3.22 Lead adsorption constants for the formation of ≡XOPb$^+$ as determined for three titrations.

Species	Titration 1	Titration 2	Titration 3	Best estimate
≡XOPb$^+$	-0.61 ± 0.056	-0.43 ± 0.065	-0.62 ± 0.056	-0.55 ± 0.034
WSOS/DF	5.4	8.1	8.3	7.2
Data points	55	55	55	165
pH range	3.00 - 9.85	3.00 - 9.83	3.01 - 9.81	3.00 - 9.85

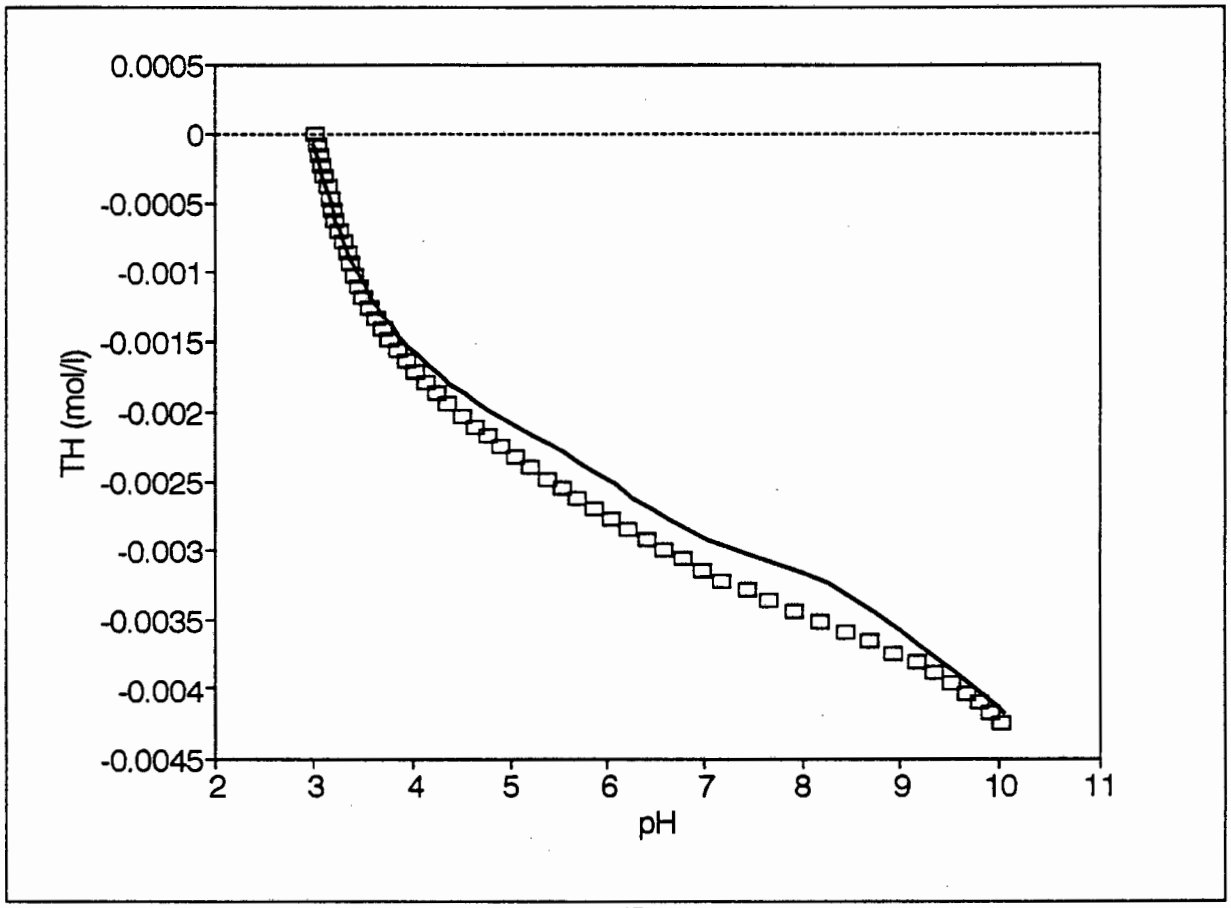

Figure 3.30 Comparison of an experimental (□) titration curve, obtained in the presence of lead, with a calculated (—) titration curve, assuming ≡XOPb$^+$ to form.

Table 3.23 Lead adsorption constants for the formation of ≡XOPb$^+$ and ≡YOPb$^+$ as determined for three titrations.

Species	Titration 1	Titration 2	Titration 3	Best estimates
≡XOPb$^+$	-0.62 ± 0.056	-0.49 ± 0.061	-0.66 ± 0.053	-0.59 ± 0.073
≡YOPb$^+$	-1.16 ± 0.10	-0.13 ± 0.089	-0.42 ± 0.085	-0.57 ± 0.43
WSOS/DF	2.5	3.6	3.3	3.2
Data points	55	55	55	165
pH range	3.00 - 9.85	3.00 - 9.83	3.01 - 9.81	3.00 - 9.85

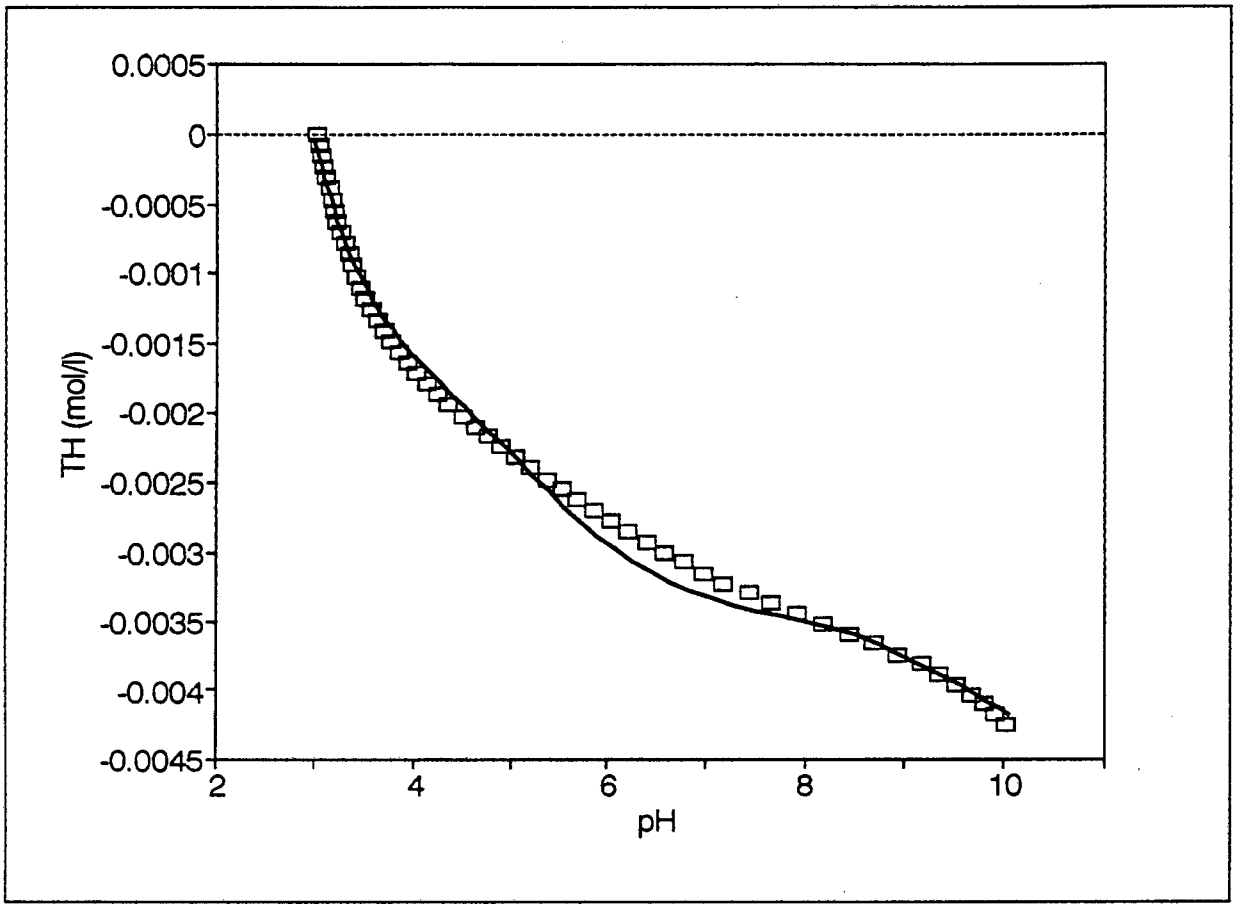

Figure 3.31 Comparison of an experimental (□) titration curve, obtained in the presence of lead, with a calculated (—) curve, assuming ≡XOPb$^+$ and ≡YOPb$^+$ to form.

Table 3.24 Lead adsorption constants for the formation of ≡XOPb$^+$, ≡YOPb$^+$ and ≡XOPbOH as determined for three titrations.

Species	Titration 1	Titration 2	Titration 3	Best estimates
≡XOPb$^+$	-0.87 ± 0.065	-1.10 ± 0.097	-1.22 ± 0.092	-1.04± 0.047
≡YOPb$^+$	-1.34 ± 0.21	-0.98 ± 0.22	-1.31 ± 0.27	-1.21 ± 0.14
≡XOPbOH	-3.09 ± 0.075	-2.71 ± 0.047	-2.86 ±0.047	-2.87 ± 0.032
WSOS/DF	1.9	1.8	1.4	1.8
Data points	55	55	55	165
pH range	3.00 - 9.85	3.00 - 9.83	3.01 - 9.81	3.00 - 9.85

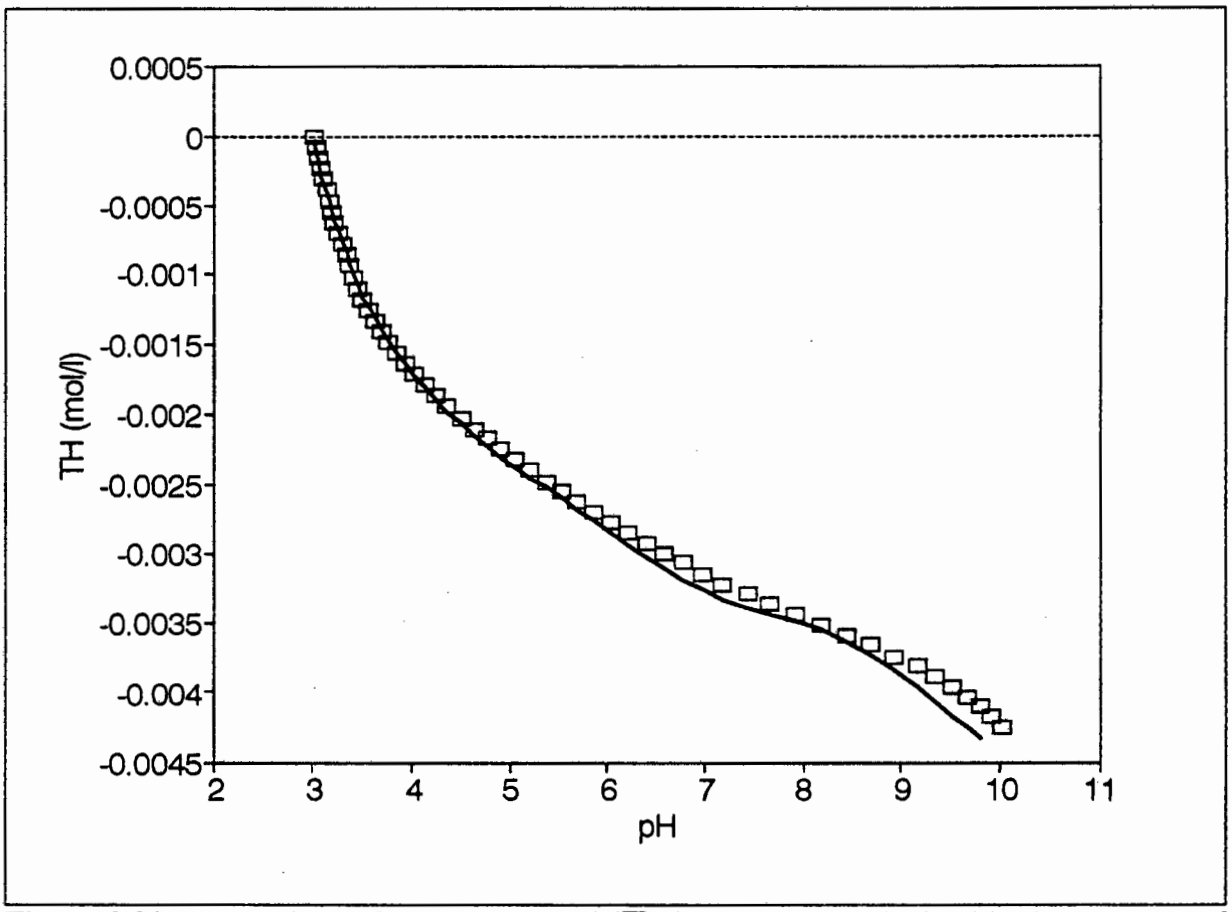

Figure 3.32 Comparison of an experimental (□) titration curve, obtained in the presence of lead, with a calculated (—) curve, assuming ≡XOPb$^+$, ≡YOPb$^+$ and ≡XOPbOH to form.

Table 3.25 Lead adsorption constants for the formation of ≡XOPb$^+$ and ≡XOPbOH as determined for three titrations.

Species	Titration 1	Titration 2	Titration 3	Best estimates
≡XOPb$^+$	-0.93 ± 0.067	-1.16 ± 0.10	-1.28 ± 0.097	-1.09 ± 0.049
≡XOPbOH	-3.01 ± 0.063	-2.68 ± 0.044	-2.84 ± 0.044	-2.38 ± 0.028
WSOS/DF	2.0	1.9	1.4	1.9
Data points	55	55	55	165
pH range	3.00 - 9.85	3.00 - 9.83	3.01 - 9.81	3.00 - 9.85

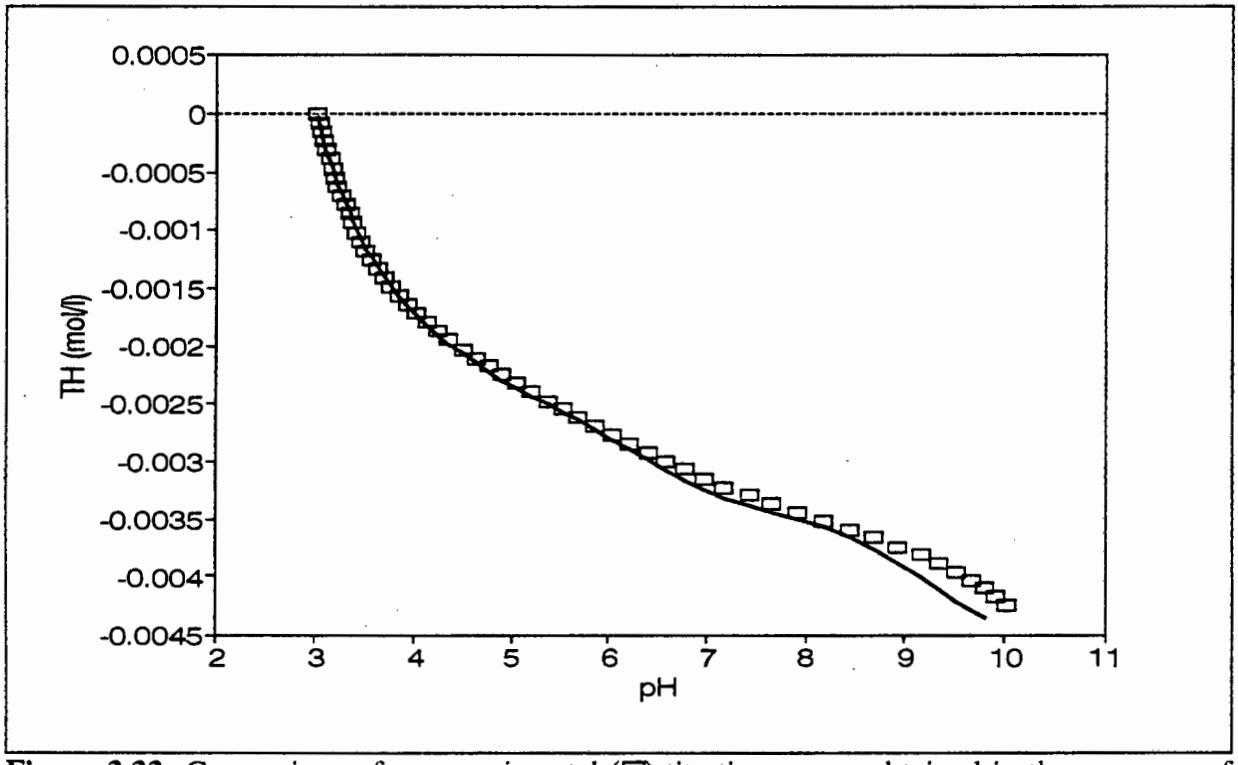

Figure 3.33 Comparison of an experimental (□) titration curve, obtained in the presence of lead, with a calculated (—) curve, assuming ≡XOPb$^+$ and ≡XOPbOH to form.

Table 3.26 Lead adsorption constant for the formation of ≡XOPbOH as determined for three titrations.

Species	Titration 1	Titration 2	Titration 3	Best estimates
≡XOPbOH	-2.72 ± 0.028	-2.60 ± 0.030	-2.72 ± 0.028	-2.68 ± 0.017
WSOS/DF	3.8	2.3	2.0	2.7
Data points	55	55	55	165
pH range	3.00 - 9.85	3.00 - 9.83	3.00 - 9.81	3.00 - 9.85

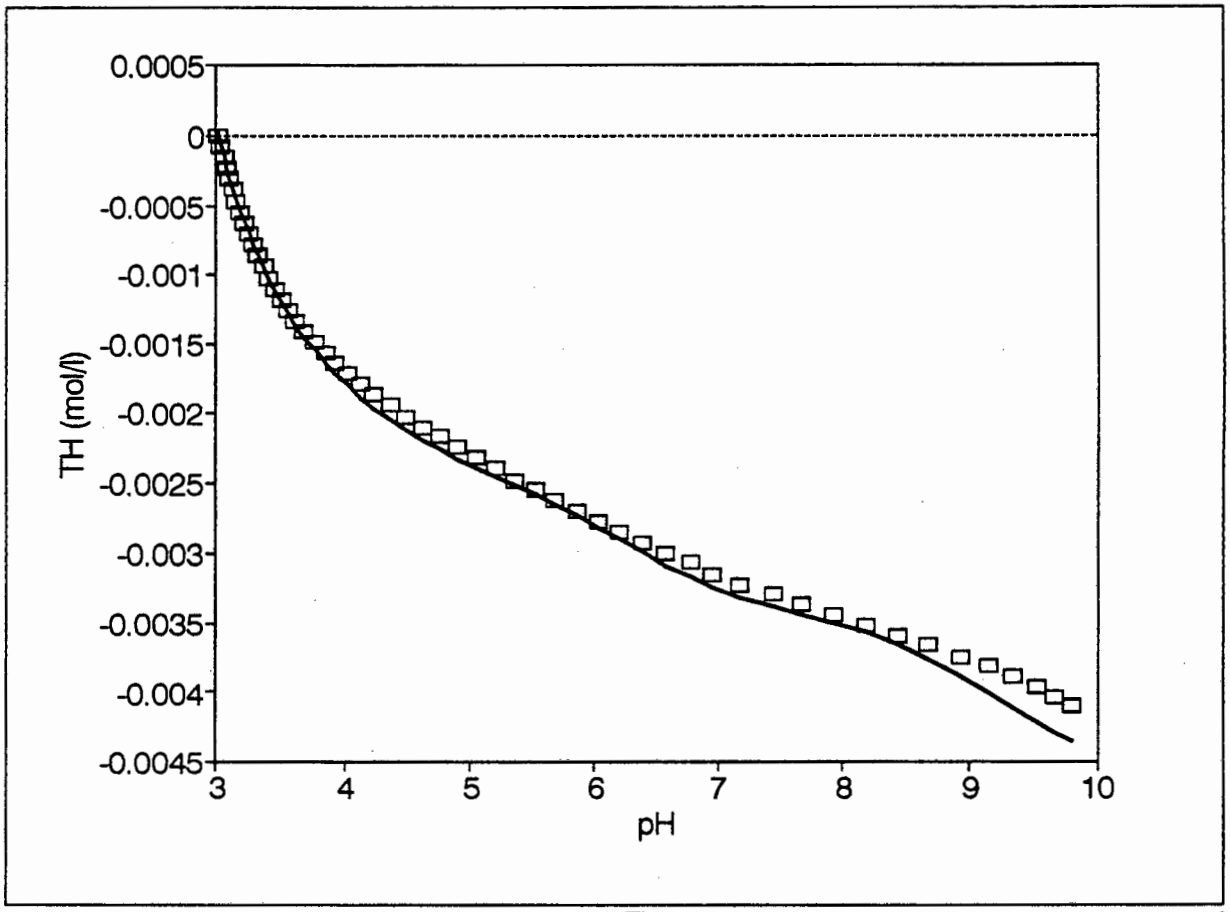

Figure 3.34 Comparison of an experimental (□) titration curve, obtained in the presence of lead, with a calculated (—) curve assuming ≡XOPbOH to form.

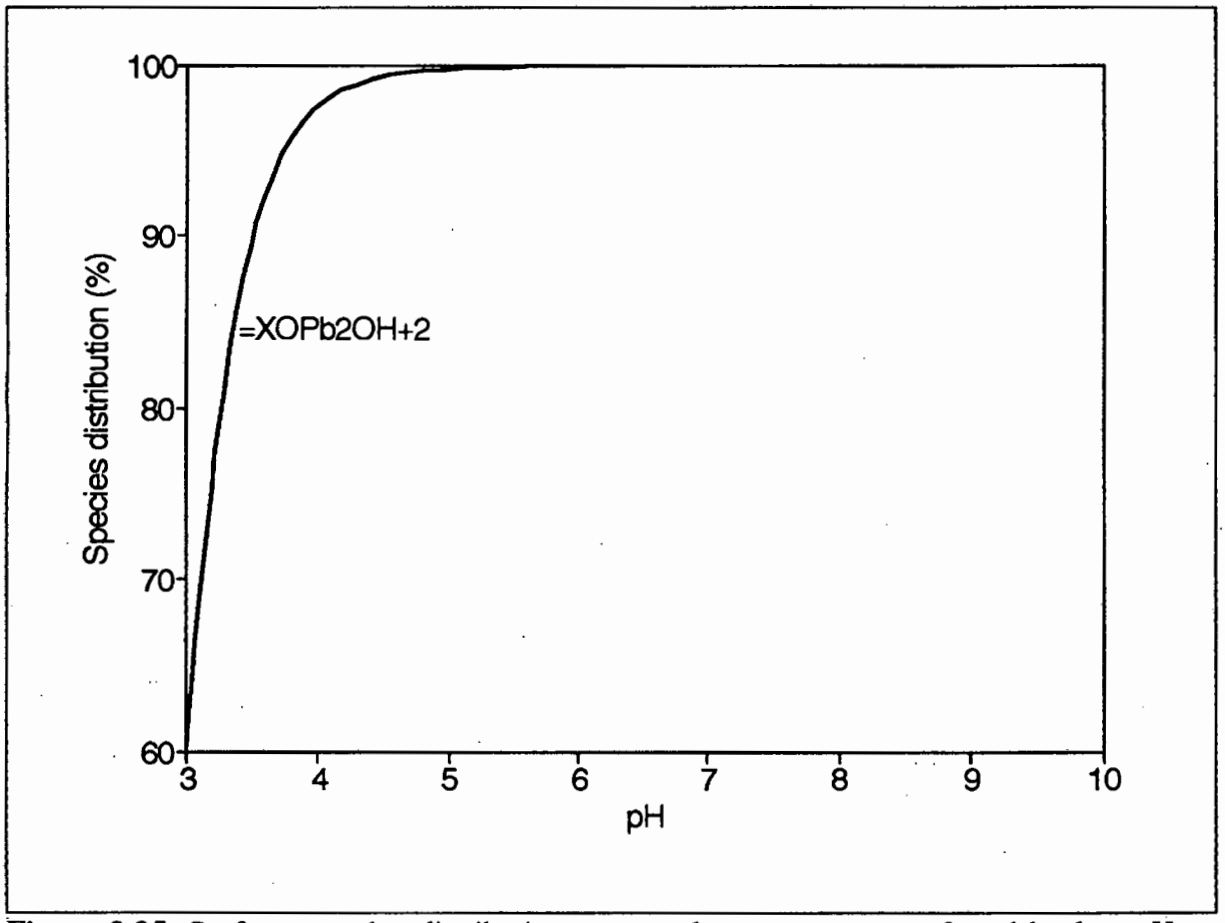

Figure 3.35 Surface complex distribution expressed as a percentage of total lead vs pH.

Based on the F-test, the difference in the Goodness of Fit parameter observed between the two models is significant at the 5% probability level for all titrations, as well as for the combined data set. Thus, it was decided to select $\equiv XOPb_2OH^{+2}$ as the model for lead adsorption. The surface speciation of this model is shown by Figure 3.35.

3.4 Discussion

Some of the surface species presented as models in the preceding paragraphs may be criticised on the grounds of a very low abundance in the solution phase at pH values where these are postulated to adsorb significantly. This is the case for all the ≡XOMOH species.

However, Le Châtelier's principle (Atkins, 1983) should be kept in mind when these results are interpreted. These hydroxy species are present in solution, albeit at quite low concentrations especially in the lower pH ranges. The solid surface acts as a sink for these species by adsorbing them and thereby removing them from solution. The system will respond to this disturbance of equilibrium by shifting the equilibrium in a direction which favours the species being consumed.

The EXAFS results obtained by Manceau *et al.* (1992c), which indicated the existence of polynuclear lead surface complexes, were obtained at pH 3. This provides proof for the existence of hydroxy surface complexes even at low pH values.

Other criticisms which may be levelled against the proposed surface species relate to their actual existence. This issue has two aspects to it: first, from a structural point of view, it may be asked whether surface complexes of the type proposed in this work do exist. The data collected in the present study do not give an answer to this question. However, as was discussed in the paragraph on modelling procedure (paragraph 3.3), the species postulated here are fundamental to the surface complexation approach. Also, the agreement between spectroscopic results and modelling results obtained for lead is encouraging and does provide a certain degree of support for the postulated species.

The second aspect of this issue relates to the non-linear optimization procedure used to interpret alkalimetric titration data. It may be asked whether the proposed species are real or simply artifacts of experimental error present in the data. From an optimization point of view, certain criteria exist which may be used as tests to decide whether a species is real or

simply an artifact arising from error in the experimental data set. These criteria are mainly applied by workers active in the field of solution chemistry. Baes and Mesmer (1976) require that an equilibrium constant be larger than or equal to three times it's standard deviation, σ_K, before accepting a species as real. In logarithmic terms, this is equal to $\sigma_{Log\,K} \leq 0.15$. This criterion was also employed by Dzombak and Morel (1990). Sillén (as referenced by Baes and Mesmer), requires a less strict criterion of an equilibrium constant being larger than or equal to $1.5\sigma_K$, which is equal to $\sigma_{Log\,K} \leq 0.29$. Most of the species postulated in this work satisfy the criterion of Baes and Mesmer, with the exception of $\equiv YOZn^+$, which satisfies the criterion of Sillén.

Other workers (e.g. Kramer, 1988) require species to be present at a certain fraction of total metal and ligand concentrations employed. Kramer required all species to be present at levels of at least 5% of total metal and total ligand. Here, all species postulated are present at levels of more than 5% of the total metal concentration employed. This criterion is not always satisfied when species abundance is expressed in terms of total binding site concentration. This is a direct result of the fact that a metal to total binding site ratio of approximately 1:10 was employed in this work.

As far as the adsorption literature is concerned, this is not an aspect which enjoys a lot of attention. Neither Catts and Langmuir (1986) nor Fu *et al.* (1991) discuss this aspect in their work. It is also not discussed in the FITEQL manual (Herbelin and Westall, 1994). It is therefore not possible to compare the criteria used here with others which have previously been used in adsorption studies.

The accuracy of the constants is difficult to assess. According to Martell and Motekaitis (1988), "absolute accuracy, even though it is difficult to obtain, always requires a carefully calibrated pH meter-electrode system, a low σ_{Fit}, the assurance that the stoichiometric variables are accurate, and the presence of a substantial proportion of each species in the equilibrium expression under the conditions of the experiment". In the present work, most of these criteria are satisfied. However, due to the fact that so little structural information regarding the surface is available (and therefore little information about binding site characteristics), the accuracy of stoichiometric variables is difficult to assess. Furthermore, the fact that equilibration problems were to some extent experienced also affects the accuracy of the calculated constants. Also, binding site concentrations were arrived at by fitting of protonation data and no independent technique was used to assess these concentrations. However, as was shown in paragraph 3.5.2, the optimization procedure was able to reproduce constants and binding site concentrations from a titration curve generated using a known set of constants and site concentrations.

It may be concluded that the results presented in paragraphs 3.3.1(a) to 3.3.1(e) are sound from a procedural point of view. A statement as to whether the proposed surface complexes really exist or not cannot be made on the basis of the current work. However, that was never the intention of the current study. In the next chapter, the proposed models are applied to data sets which have been published in the open literature. This will assess the ability of the proposed models to predict metal adsorption by manganese dioxide.

Chapter 4 Adsorption model validation

A test of the validity (or applicability) of any model is its ability to reproduce experimental observations. In the preceding chapter, it was shown that the postulated adsorption models for each of the metals studied were able to reproduce potentiometric results. In this chapter, the model is used to reproduce adsorption data published in the open literature. Validation will be viewed from two angles: (i) in a qualitative manner and (ii) in a quantitative manner. If the model is capable of predicting trends observed by other workers in experimental studies, or general observations in the field of surface chemistry, the model will be taken as valid in a qualitative manner. If, however, the model is also able to reproduce adsorption results obtained by independent workers quantitatively, the model will be taken as quantitatively validated. In this chapter, the validation procedure followed as well as results obtained, are discussed.

4.1 Validation procedure

The following model validation approach was followed. From the literature, several studies in metal adsorption by manganese dioxide were identified. These studies are described in section 4.2. An attempt was then made to reproduce these results using the adsorption model determined in the previous chapter. All simulations were carried out using MINTEQA2 (Allison *et al.*, 1991). Adsorption constants were corrected to the ionic strengths (or background electrolyte concentrations) listed in the respective publications. Activity coefficients were obtained from Dzombak and Morel (1990), who employed the Davies equation to calculate activity coefficients. Manual correction of adsorption constants was

necessary since MINTEQA2 does not correct adsorption constants for ionic strength. Appendix A contains a listing of adsorption constants at four ionic strengths.

MINTEQA2 also requires an estimate for the solid's surface area as input. Although some workers state a surface area value for the particular solid they worked with, surface area was fixed at $331 m^2.g^{-1}$, which was used in the adsorption constant determination exercise described in chapters 2 and 3. Simulation conditions were kept as close to experimental conditions as possible. In all cases, however, it was ensured that the aqueous phase concentration of the adsorbing metal at equilibrium spanned the range reported in the specific study being simulated.

Simulated and literature data sets were compared (i) on a visual basis (i.e. adsorption isotherms or pH dependent pH edges were compared) and (ii) in terms of adsorption capacities. Adsorption capacities were calculated by plotting both simulated and literature data according to the linearized Langmuir equation, equation 4.1, as given by Loganathan and Burau (1973),

$$c(x/m)^{-1} = (ab)^{-1} + ca^{-1} \quad \ldots\ldots\ldots\ldots\ldots\ldots \quad (4.1)$$

where c = metal concentration in solution at equilibrium ($mmol.dm^{-3}$), (x/m) = metal adsorbed ($mmol.g^{-1}$), a = maximum adsorption capacity ($mmol.g^{-1}$) and b = parameter related to the energy of sorption. Linear regression of $c(x/m)^{-1}$ vs c yielded a^{-1}, from which adsorption capacity was calculated.

Certain workers listed adsorption capacities obtained from non-linear regressions of the

Langmuir equation on their data. In such cases, their adsorption data were plotted according to equation 4.1 and adsorption capacity was obtained from the linear regression exercise.

The reader should please note that this exercise is by no means an attempt to prove or validate the linearized Langmuir equation, or for that matter, any other data manipulation approach applied in the literature. The aim is simply to show that the proposed adsorption model with it's adsorption constants is able to reproduce experimental adsorption studies published in the literature.

4.2 Description of adsorption studies available.

Loganathan and Burau (1973) studied the adsorption of cobalt, calcium, sodium and zinc by 0.1 $g.dm^{-3}$ δ-MnO_2 at pH 4, temperature of 24°C and an ionic strength of 0.001<u>M</u> $NaNO_3$. Metal sorption experiments were carried out in batch reactors. After the addition of metal, pH was adjusted to 4. Flasks were mechanically agitated for 24 hours. After this period, pH was again adjusted to 4 and agitated for a further 24 hours. Final pH is given as 4 ± 0.1. Aliquots of the suspension was removed and solid-solution separation was affected by centrifuging at 33 000*g* for 20 minutes. The temperature at which centrifuging took place is not given. Metal concentration in the supernatant was determined by Flame Atomic Absorption Spectrophotometry (FAAS), using an air-acetylene flame. In Figure 4 of their paper, they present eight experimental points obtained from duplicate experiments. Results are presented as (i) zinc adsorbed per unit mass solid ($mmol.g^{-1}$, denoted by x/m) vs equilibrium zinc concentration in the solution phase ($mmol.dm^{-3}$, denoted by c) and (ii) in Figure 6 of the paper, a linearized Langmuir plot, which plots c/(x/m) (units: $g.dm^{-3}$) vs c

(units: $mmol.dm^{-3}$). Only their results obtained for zinc is of interest here. It was observed that (i) below 10^{-4} $mol.dm^{-3}$ zinc at equilibrium in the aqueous phase, the data, plotted in the linearized Langmuir form, deviated from linearity and (ii) δ-MnO_2 has a Langmuir adsorption capacity of 1.02 $mmol.g^{-1}$ for zinc at pH 4.

Gadde and Laitinen (1974) studied the adsorption of lead, zinc and cadmium by hydrous manganese oxide. Conditions under which experiments were carried out are not clearly stated. All studies were performed at pH 6. Results of interest in their paper are (i) sorption capacities for the metals investigated and (ii) shapes of adsorption isotherms obtained. Adsorption isotherms and adsorption capacities are expressed in terms of mol metal adsorbed per mol MnO_2. It is, however, not clear what molar mass for MnO_2 these workers used. In reworking their data, a molar mass of $87g.mol^{-1}$ was used.

Gray and Malati (1979b) studied, amongst others, the sorption of nickel, zinc and cadmium by 0.17 $g.dm^{-3}$ δ-MnO_2, at pH 6 and an ionic strength of 0.01M KCl, using batch reactors. Zinc and cadmium adsorption were studied at temperatures of 279K, 293K, 308K and 311K while nickel adsorption was studied at 282K, 298K and 310K. Solid-solution separation was affected by filtering over a 0.45μm membrane filter. Supernatant metal concentration was measured using FAAS (Gray and Malati, 1979a). They fitted their results to the linear form of the Langmuir equation, from which adsorption capacities were determined. Adsorption capacities of 0.58 $mmol.g^{-1}$, 1.41 $mmol.g^{-1}$ and 1.38 $mmol.g^{-1}$ for nickel, cadmium and zinc at pH 6 were obtained.

Catts and Langmuir (1986) studied the adsorption of copper, zinc and lead by δ-MnO_2.

Experiments were carried out in batch reactors at 25°C and I = 0.01**M** $NaNO_3$. Solids concentration of 6.25mg.dm^{-3} and total metal concentrations of $1.0x10^{-5}$ mol.dm^{-3} were employed. Equilibration times of three days were allowed. Solid-solution separation was effected by centrifuging. Metal concentration in solution was determined using FAAS or Graphite Furnace-Atomic Absorption Spectroscopy (GF-AAS). Experimental results are presented as plots of $[M]_{soln}$ vs pH. All experiments were performed under atmospheric conditions. This indicates that simulations of their work should be equilibrated with atmospheric CO_2.

Stroes-Gascoyne (1983) and Stroes-Gascoyne *et al.* (1987) provide a wealth of information. The most interesting result (in the present context) deals with the adsorption of copper by δ-MnO_2 samples prepared according to the same preparation strategy used in this work. This provides information regarding the reproducibility of metal adsorption and therefore, some idea of what may be expected from the model postulated in this work. Experiments were carried out in batch reactors at 25°C, pH 6 and 0.01 **M** KNO_3 background electrolyte. The effect of aging on the adsorption capacity was also investigated. Of further interest is the adsorption capacities determined for solid phases prepared according to various preparation strategies. These values are reported as μmol Cu/μmol MnO_2. The values were converted to mmol Cu.g^{-1} MnO_2 by assuming a molar mass of ca. 87g.mol^{-1} for MnO_2.

Balikungeri and Haerdi (1988) applied differential pulse polarography (DPP) to study the adsorption of lead, copper, zinc and cadmium at pH 5.5, 6.0 and 6.5. The result of interest in this paper is the adsorption capacities measured at the three pH's. There are, however, a few problems with this paper. First, no information regarding the solid used in the study is

given, i.e. no characterization data or any preparation method. Second, it is not clear what the units of the given binding capacities for the respective metals are. If one assumes that it is $mol.dm^{-3}$, it is not evident what the quantities in $mol.g^{-1}$ should be since the solids concentrations used are not stated explicitly for all metals. In the case of Pb, a concentration of ca. $0.1 g.dm^{-3}$ was listed. Since they compare results obtained for the metals directly, it was assumed that the solids concentrations were similar in all experiments.

Zasoski and Burau (1988) studied the adsorption of zinc and cadmium by 0.1 $g.dm^{-3}$ δ-MnO_2 at pH 4, 6 and 8. They also investigated the effects of competition between zinc and cadmium on adsorption. Adsorption experiments were carried out in batch reactors at a background electrolyte concentration of 0.001 $mol.dm^{-3}$ $NaNO_3$ and a temperature of 25°C. Suspensions were mechanically agitated for three days. Experiments performed at pH 6 and 8 were performed under N_2 atmosphere to exclude CO_2. Solid-solution separation was affected by filtration over a 0.45μm cellulose acetate membrane filter. Metal concentration in the supernatant was determined using atomic absorption spectrophotometry (flame or graphite furnace). They present their results in tabular form. Results of interest are: (i) adsorption capacities calculated at pH 4 and 6 and (ii) competitive effects. The data listed at pH 8 are very limited (2 points for Cd, 3 points for Zn), so it was decided ignore these points.

Fu *et al.* (1991) studied adsorption of copper and cadmium by δ-MnO_2 at 25°C, I = 0.01**M** $NaNO_3$ using ion selective electrode potentiometry. Adsorption was studied at pH 5.5 (Cu and Cd), 7 and 8 (Cd). Data are presented as (i) % Metal adsorbed vs pH and (ii) metal adsorbed ($mmol.g^{-1}$) vs $[M^{2+}]_{eq}$ ($\mu mol.dm^{-3}$). Adsorption capacities for cadmium at pH 5.5,

7.0 and 8.0 were determined to be 0.434, 1.08 and 1.92 mmol.g^{-1} respectively. For copper, adsorption capacity at pH 5.5 was found to be 1.54 mmol.g^{-1}.

Data sets available for model validation are summarized in Table 4.1. The results of interest in each data set are listed under the "Remarks" heading.

Table 4.1 Metal adsorption data sets available for the validation of the adsorption models proposed in this work.

Metal	Data set	Remarks
Ni	Gray & Malati, 1979b	• pH 6 isotherm and adsorption capacity.
Cu	Catts & Langmuir, 1986	• pH dependent sorption.
	Stroes-Gascoyne *et al.*, 1987	• pH 6 isotherm; binding capacity at this pH for different preparations.
	Stroes-Gascoyne, 1983	• Binding capacities @ pH 5.5, 6.0 & 6.5.
	Balikungeri & Haerdi, 1988	• pH dependent sorption; pH 5.5 isotherm and binding capacity.
	Fu *et al.*, 1991	
Zn	Loganathan & Burau, 1973	• sorption isotherm @ pH 4; Langmuir plot; adsorption capacity.
	Gadde & Laitinen, 1974	• pH 6 isotherm & adsorption capacity.
	Gray & Malati, 1979b	• pH 6 isotherm & adsorption capacity.
	Catts & Langmuir, 1986	• pH dependent sorption.
	Zasoski & Burau, 1988	• adsorption data at pH 4, 6 & 8(limited); binding capacities at different pH's.
Cd	Gadde & Laitinen, 1974	• pH 6 isotherm and adsorption capacity.
	Gray & Malati, 1979b	• pH 6 isotherm and adsorption capacity.
	Zasoski & Burau, 1988	• adsorption data at pH 4, 6 & 8(limited); binding capacities at different pH's.
	Balikungeri & Haerdi, 1988	• Binding capacities @ pH 5.5, 6.0 & 6.5.
	Fu *et al.*, 1991.	• pH dependent sorption; isotherms at pH 5.5, 7.0 & 8; binding capacities.
Pb	Gadde & Laitinen, 1974	• pH 6 isotherm and adsorption capacity.
	Catts & Langmuir, 1986	• pH dependent sorption.
	Balikungeri & Haerdi, 1988	• Binding capacities @ pH 5.5, 6.0 & 6.5.

4.3 Model validation results

Before results for each metal are discussed, general trends/observations obtained from the literature will be compared with that predicted by the model.

The first general observation relates to adsorption orders of metals by δ-MnO_2. McKenzie (1989) states that in general, metal ions are adsorbed by manganese dioxide in the following order: Pb > Cu > Mn > Co > Zn > Ni. The adsorption order determined by Balikungeri and Haerdi (1988) is Pb > Cu > Cd > Zn. Zasoski and Burau (1988) found an adsorption order of Zn > Cd. Gray and Malati (1979b) found an adsorption order of Zn ≈ Cd > Ni. Gadde and Laitinen (1974) observed an absorption order of Pb > Zn > Cd. Fu *et al.* (1991) determined an adsorption order of Cu > Cd. It is clear that different workers found different adsorption sequences, especially with respect to Cd and Zn. These results may be summarized by stating that Pb and Cu are adsorbed strongest, there is confusion about the preference of the solid for Cd and Zn but the solid has a lower preference for these metals than Pb and Cu. The one data set available for Ni suggest that this metal is adsorbed only weakly by the solid.

Model results suggest that the adsorption sequence depends on pH and metal:binding site concentration ratio. Using a metal : binding site ratio of 1 : 30, the model predicts an adsorption sequence at pH 4 of Pb ≈ Cu > Ni ≈ Zn > Cd. At pH 6 and 8, 100% adsorption is observed and an adsorption sequence can not be determined. Simulating the situation with a ratio of 1 : 3, an adsorption sequence of Cu > Pb > Ni > Zn > Cd is predicted at pH 4. At pH 6 and 8, an adsorption sequence of Cu ≈ Pb ≈ Ni ≈ Zn > Cd is found. Modelling results

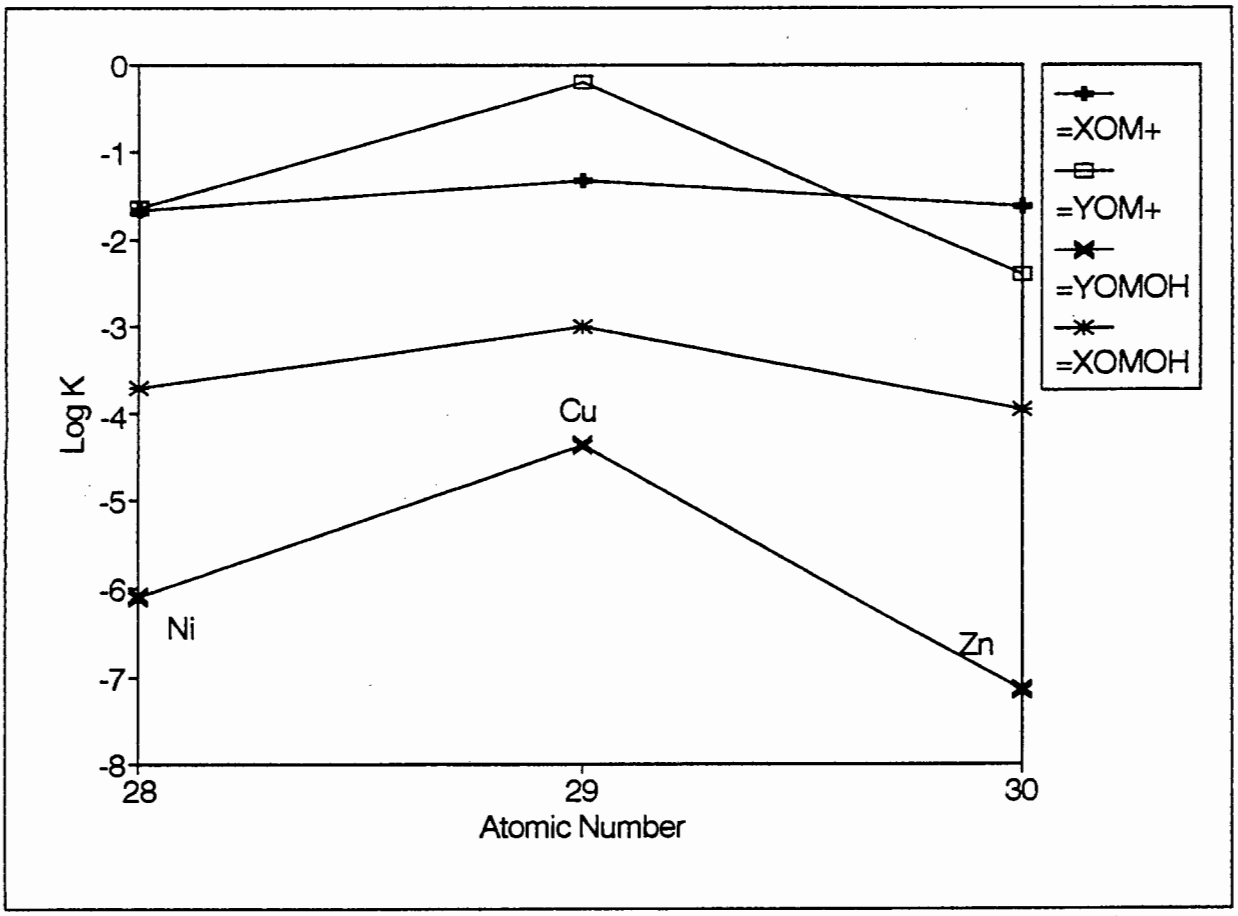

Figure 4.1 Adsorption constants plotted as a function of atomic number.

agree with the experimental observations that Pb and Cu are adsorbed preferentially over other metals. For Zn and Cd, the model results agree with those of Zasoski and Burau and Gadde and Laitinen. It does not agree with the sequence found by Balikungeri and Haerdi. The position of Ni, as predicted by the model, does not agree with the result of Gray and Malati for this metal. The result obtained by Gray and Malati is also contrary to what would be expected on the basis of the Irving-Williams stability series (Irving & Williams, 1948; 1953). According to this series, Ni and Zn would exhibit similar positions in the adsorption sequence. Behaviour in accordance with the Irving-Williams stability sequence is observed for the adsorption constants determined for Ni, Cu and Zn in the present work (Figure 4.1). Adsorption constants for Ni, Cu and Zn by iron oxides also conform to this stability sequence (Stumm, 1992).

The results discussed above may thus be summarized by stating that in broad terms, the modelling results correspond with observed trends. However, some of the observed adsorption sequences are doubtful if evaluated against well known chemical trends, such as the Irving-Williams stability sequence. The model further suggests that a statement such as that by McKenzie regarding a general adsorption order is not valid.

4.3.1 Copper

Figure 4.2 shows the ability of the model to predict pH dependent copper adsorption data collected by Catts and Langmuir.

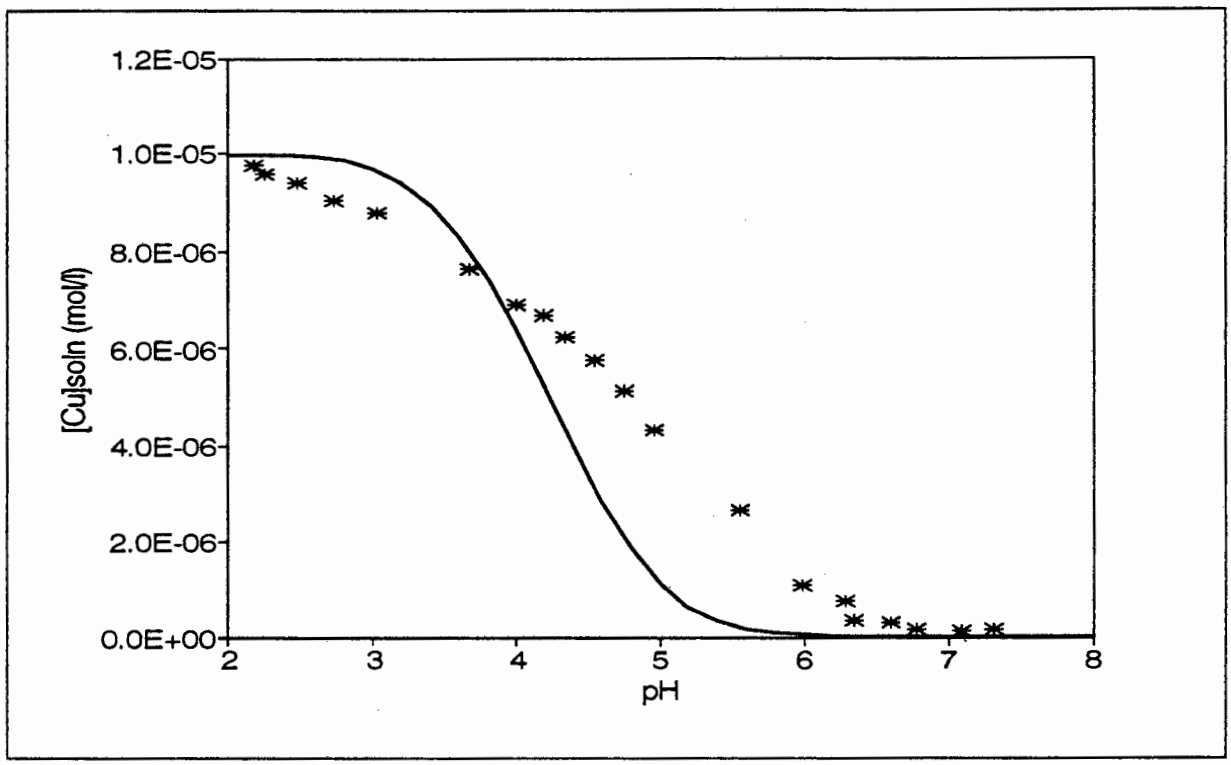

Figure 4.2 Comparison between simulated (–) and experimental (*) copper adsorption data (Data set: Catts & Langmuir, 1986).

The model is reasonably successful in predicting the experimental results. The modelled curve exhibits a strongly sigmoidal shape suggesting a sharp increase in adsorption in the pH range 4 to 5, as shown by the sharp decrease in aqueous phase equilibrium copper concentration. The experimental curve exhibits a diffuse sigmoidal shape, suggesting that adsorption increases gradually over the pH range investigated. The model overestimates adsorption from pH 4 onwards. A similar result is obtained when the model is compared with the pH dependent adsorption data of Fu (Figure 4.3).

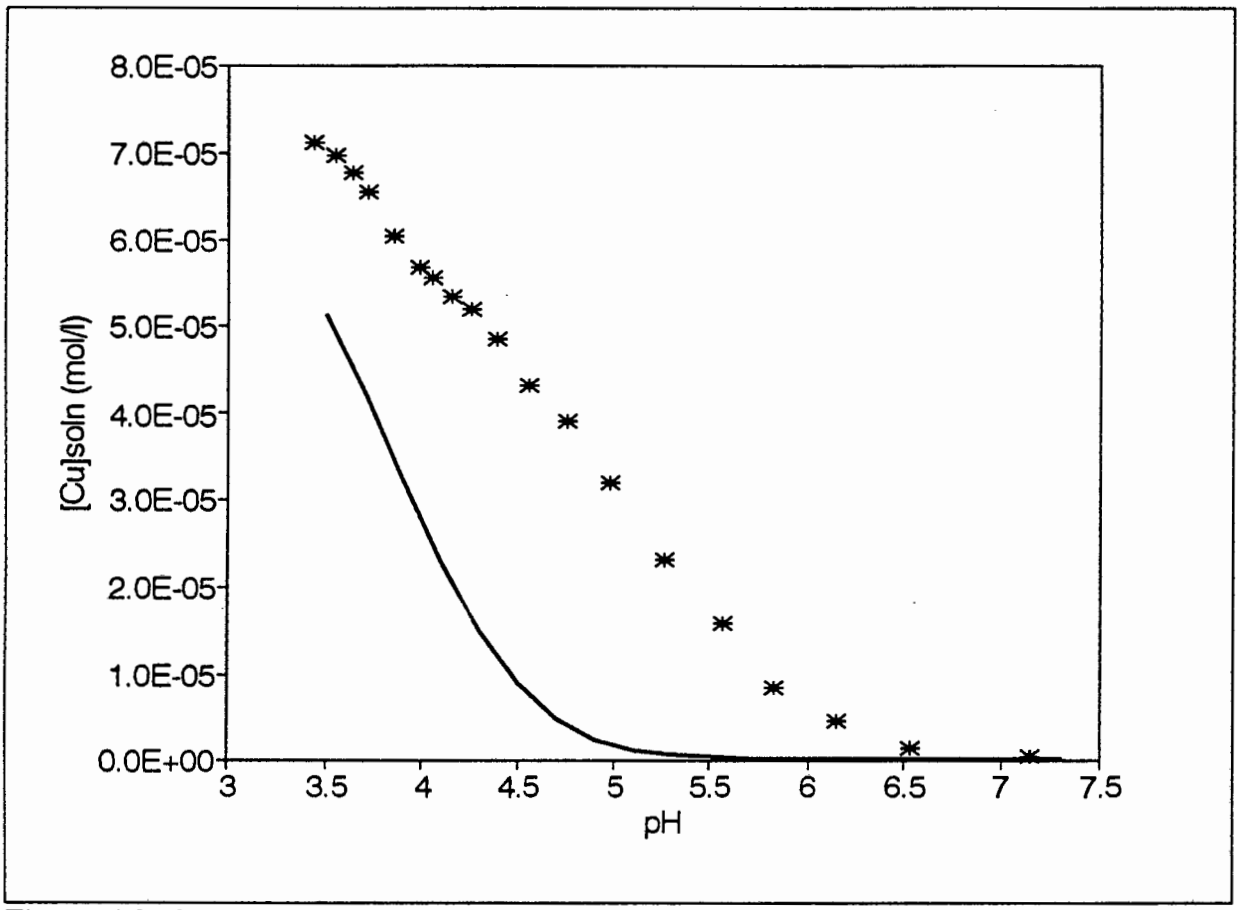

Figure 4.3 Comparison between simulated (–) and experimental (*) copper adsorption data. (Data set: Fu *et al.*, 1991).

A comparison between the model and a copper adsorption isotherm obtained at pH 5.5 by Fu *et al.* is shown in Figure 4.4. The model overestimates copper adsorption over the whole

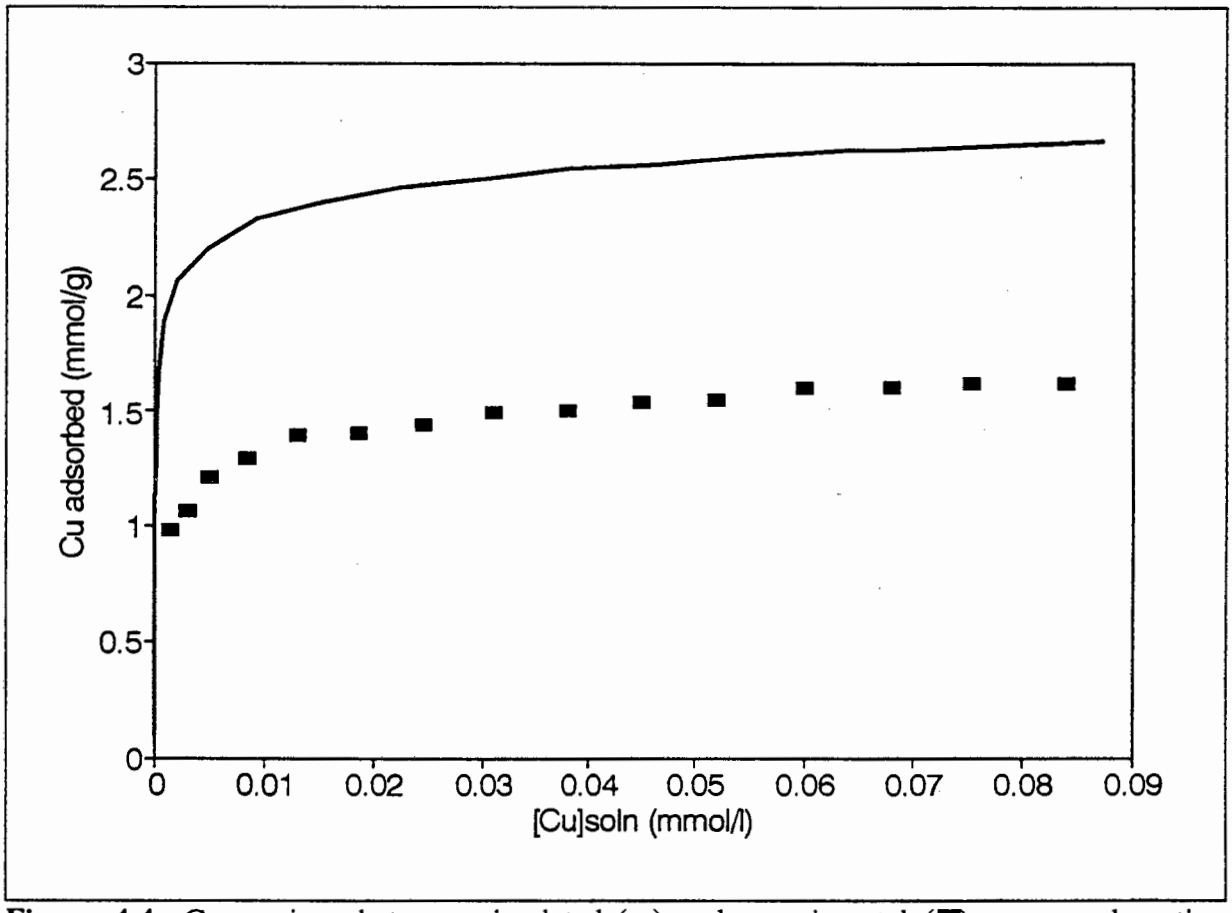

Figure 4.4 Comparison between simulated (—) and experimental (■) copper adsorption isotherm at pH 5.5 (Data set: Fu *et al.*, 1991).

equilibrium copper concentration investigated. A constant difference of approximately 1mmol.g^{-1} is observed throughout. There is, however, good qualitative agreement between the experimental and simulated data sets.

Figure 4.5 compares adsorption isotherms obtained by Stroes-Gascoyne (1983) at pH 6 with that predicted by the model. The experimental data were obtained using three δ-MnO_2 samples which were prepared according to the same preparation scheme (denoted by MNO2III, MNO2VI and MNO2XV in Figure 4.5). Furthermore, data obtained for copper adsorption by the same batch of solid (MNO2VI) are also shown in Figure 4.5. It is quite interesting to observe the amount of variability present in the experimental adsorption data.

The isotherm predicted by the model fits the experimental results rather well, and in all cases falls within the reported experimental values.

The simulated data set does, however, increase at a faster rate than the experimental data sets. In other words, at equilibrium solution copper concentration less than 5μmol.dm^{-3}, the model predicts higher amounts of copper adsorbed than observed from experimental results. However, in general, the model provides an excellent description of experimental results.

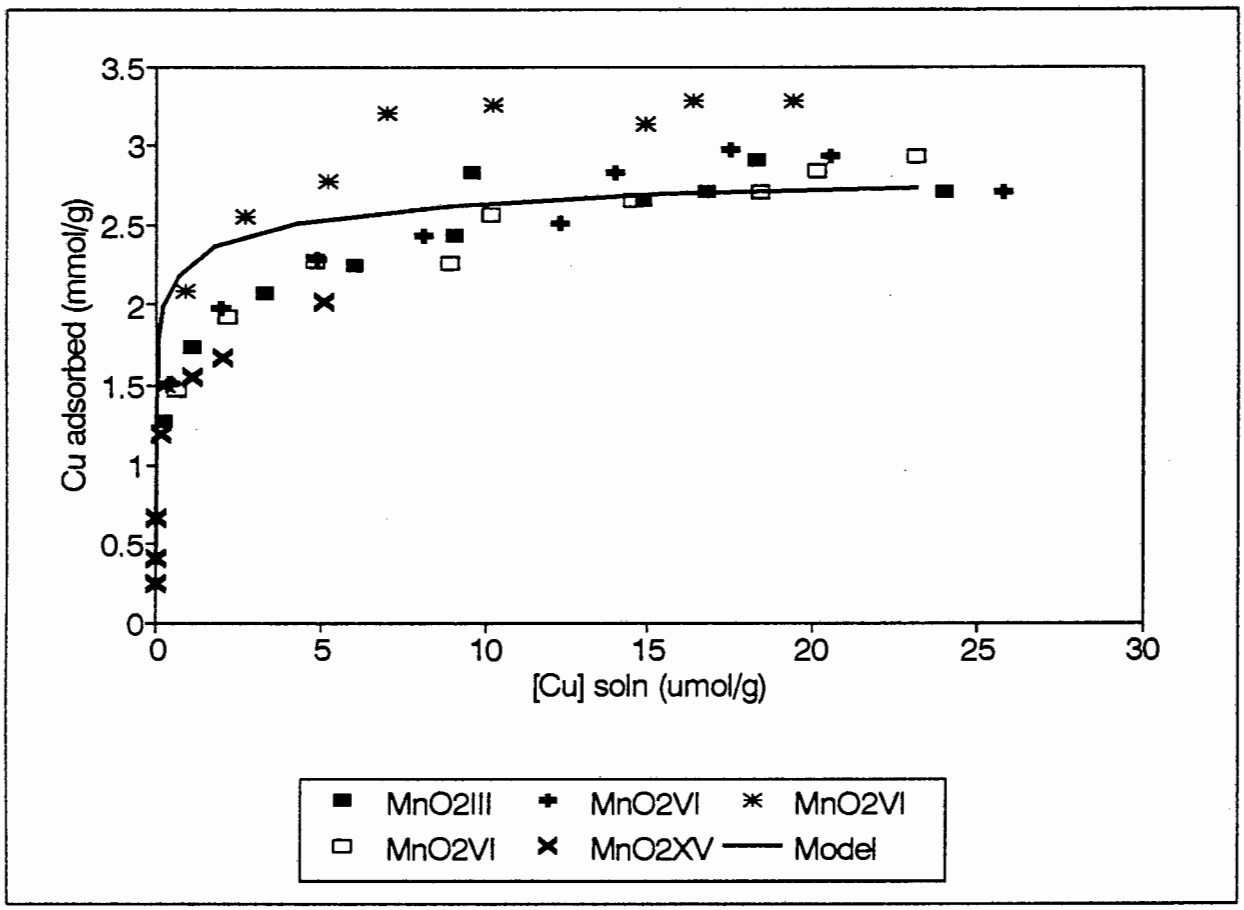

Figure 4.5 Comparison between a simulated and experimental copper adsorption isotherm at pH 6 (Data set: Stroes-Gascoyne, 1983).

This result is encouraging since the δ-MnO_2 sample used in this study was prepared according to the procedure used by Stroes-Gascoyne. Also, the results reported by Stroes-Gascoyne

show that even amongst samples prepared according to similar methods, a large amount of variability may be expected.

An interesting aspect of the results is that the model predicts very little difference in the isotherms obtained at pH 5.5 and pH 6. Unfortunately Stroes-Gascoyne did not perform any pH dependent sorption experiments. However, by considering the pH dependent adsorption curve determined by Fu *et al.* (Figure 4.3), one sees that the solution concentration of copper at pH 6 is ca. 5μmol.dm^{-3}. A solution concentration of 5μmol.dm^{-3} corresponds to ca. 2 to 2.7 mmol copper adsorbed per gram solid on the Stroes-Gascoyne isotherm (Figure 5.3), whereas, for the Fu data, a value of 1.5mmol.g^{-1} is calculated. From this it may be deduced that at pH 6, the solid used by Fu *et al.* sorbs significantly less copper than what was observed by Stroes-Gascoyne.

Based on experimental methods reported by Fu *et al.*, possible reasons for this discrepancy seem to preclude solid preparation and storage procedures. Fu *et al.* reports a solid preparation procedure similar to that employed by Stroes-Gascoyne (1983). They also report a solid storage procedure identical to that employed by Stroes-Gascoyne.

The fact that the model overestimated copper sorption compared to the Catts and Langmuir data set may be explained by the fact that they stored their MnO_2 sample dry. It is well known that drying of the solid may lead to surface dehydration and a concomitant change in surface properties (Parks, 1965).

In Table 4.2 experimentally determined copper adsorption capacities are compared with

adsorption capacities calculated from simulated results. Adsorption capacities were calculated from adsorption isotherms using equation 4.1, except in the case of Balikungeri and Haerdi, who's values were used directly. The experimental values listed for Stroes-Gascoyne were obtained from Stroes-Gascoyne (1983), where they were determined by linear regression on isotherms plotted according to the linear Langmuir equation.

Table 4.2 Summary of copper adsorption capacity results obtained from literature and simulated data sets.

pH	I	Adsorption capacity $mmol.g^{-1}$		Source
		Exp	Model	
5.5	0.01	1.54	2.64	Fu *et al.*, 1991
	0.1	2.40	2.39	Balikungeri & Haerdi, 1988
6.0	0.01	2.2-3.0	2.77	Stroes-Gascoyne, 1979,1987
	0.1	3.20	2.65	Balikungeri & Haerdi, 1988
6.5	0.1	3.00	2.80	Balikungeri & Haerdi, 1988

To summarize, the model corresponds well with the data sets of Stroes-Gascoyne and Balikungeri and Haerdi. The data set of Stroes-Gascoyne (1983, 1987) is extensive, reporting sorption results obtained over a range of conditions. The method of solid preparation in the present study is similar to the method used by Stroes-Gascoyne. However, for the Catts and Langmuir and the Fu *et al.* data sets, poor agreement between model and experiment was found. This does not point to the model being invalid though, since it is thought that the data set of Fu *et al.* underestimates copper adsorption at pH 6 when compared with the Stroes-Gascoyne data set. Furthermore, binding capacities calculated from the Fu data at pH 5.5 is significantly lower than that determined by Balikungeri and Haerdi at this pH.

As an aside, it is interesting to note that in both cases where good agreement between model and experiment was obtained, Differential Pulse Polarography had been used to determine equilibrium solution phase concentration of the metal.

4.3.2 Nickel

The only data set available for model validation is that of Gray and Malati (1979b). Figure 4.6 shows a comparison between the literature data set and the model. It is immediately clear that the model overestimates the adsorption of nickel, as determined by Gray and Malati, significantly. It is not possible to draw any firm conclusions from this result since only one data set is available.

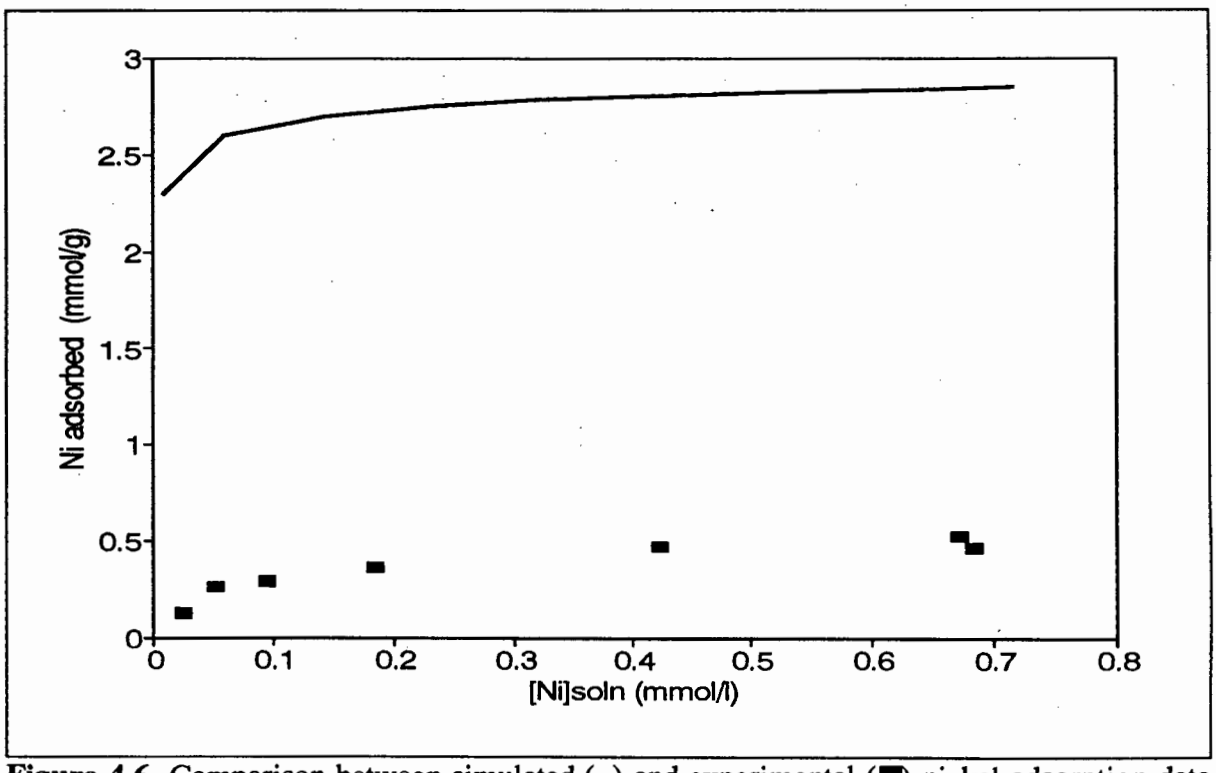

Figure 4.6 Comparison between simulated (—) and experimental (■) nickel adsorption data (Data set: Gray and Malati, 1979b).

4.3.3 Zinc

For zinc, data sets at pH 4, 6 and 8 are available. The pH 4 data sets originate from the laboratory of Burau. Conditions employed were similar, except that the Zasoski and Burau study employed lower metal concentrations than the Loganathan and Burau study. These data sets will thus be discussed together. Figure 4.7 compares both experimental data sets with model predictions.

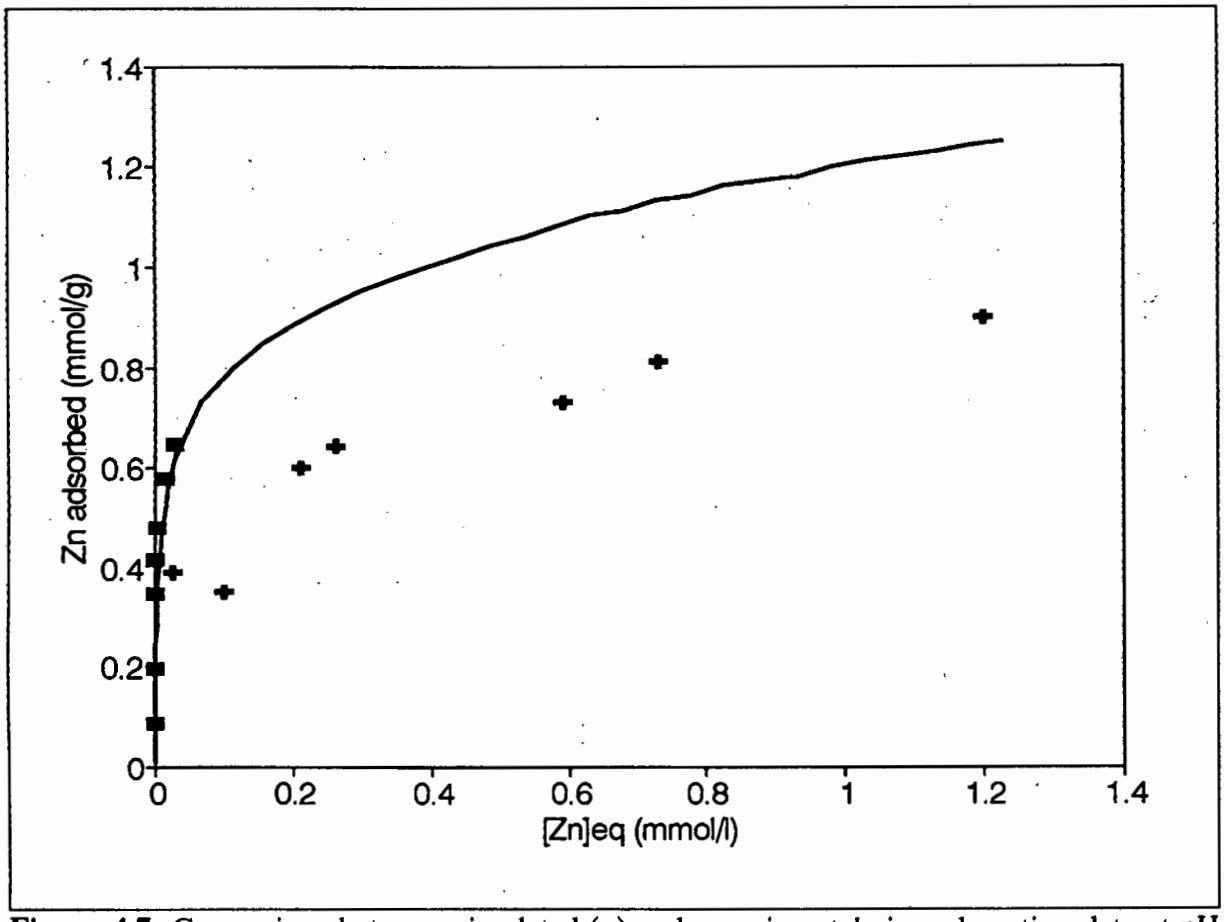

Figure 4.7 Comparison between simulated (—) and experimental zinc adsorption data at pH 4 (Data sets: Loganathan & Burau (+); Zasoski & Burau (■)).

Agreement between the model and the data set of Zasoski and Burau is good. In the case of the Loganathan & Burau data set, agreement is not good, with the model overestimating

adsorbed zinc. However, the agreement between the two experimental data sets is also not good. Although only a limited number of points overlap in terms of equilibrium zinc concentration, it is probably fair to say that the trend observed for the data of Zasoski and Burau suggests higher values for zinc adsorbed that observed by Loganathan and Burau. A possible explanation for the discrepancy observed between the two sets of experimental data may be found in the solid-solution separation techniques employed in the different studies. Loganathan and Burau centrifuged their sample at 33 000*g* for 20 minutes. Zasoski and Burau filtered their sample through a 0.45μm membrane filter. It is quite possible that the centrifuging technique of Loganathan and Burau was not sufficient to remove all colloidal particles from the solution phase. Zinc adsorbed to these colloidal particles would therefore inflate the solution phase concentration. Dzombak and Morel (1990), in their work on Hydrous Ferric Oxide sorption properties, discarded all studies in which a centrifuging time of less than 30 minutes was employed. These results may be summarized by stating that, at pH 4, good agreement is observed between modelled and experimental results. The discrepancy between the model and the Loganathan and Burau results is also observed between the Loganathan and Burau and Zasoski and Burau results.

The situation at pH 6 is shown in Figure 4.8. This figure shows a comparison between the experimental data sets of Gray and Malati (1979b) and Zasoski and Burau (1988) and the simulated data set. It is clear that the model provides a better approximation of the Zasoski and Burau data set than the Gray and Malati data set. However, in both cases the model overestimates zinc adsorption. The discrepancy between the model and the Zasoski and Burau data set is, however, less than the discrepancy between the two experimental data sets.

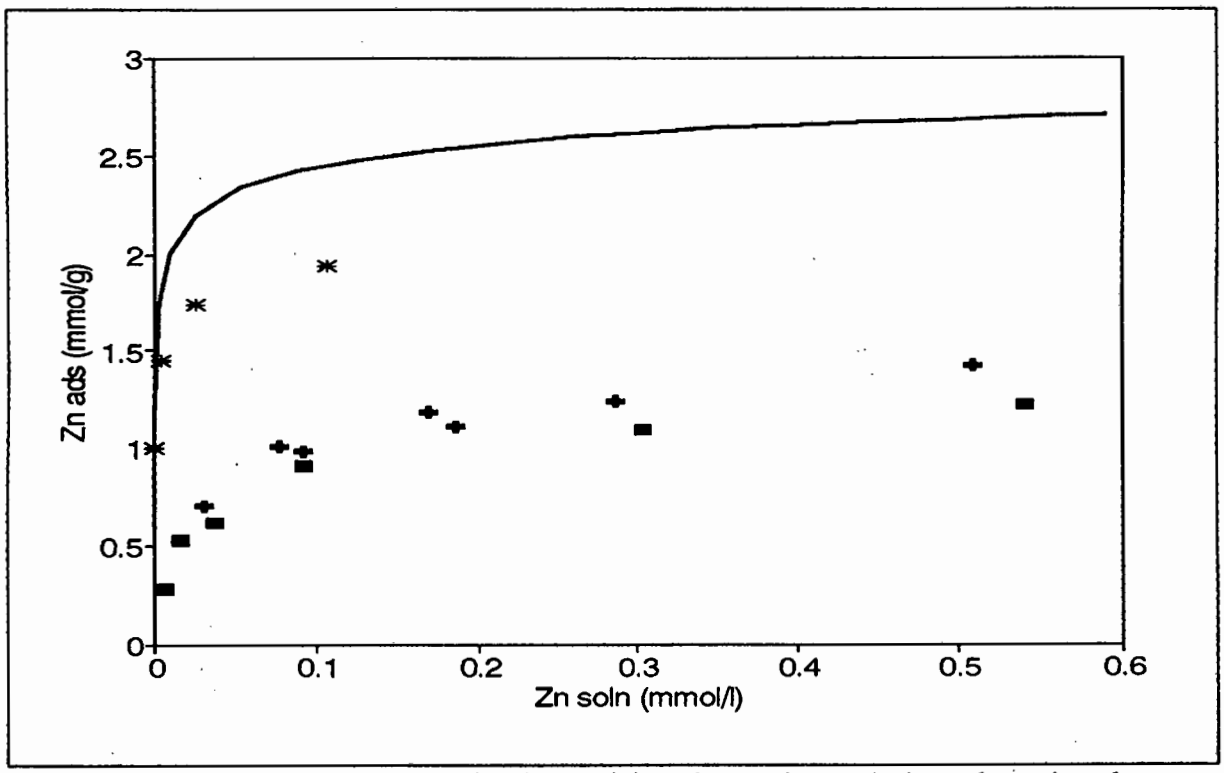

Figure 4.8 Comparison between simulated (—) and experimental zinc adsorption data sets at pH 6. (Data sets: * = Zasoski and Burau; + = Gray and Malati (308K); ■ = Gray and Malati (293K)).

Adsorption capacities calculated by eq. 4.1 from experimental and simulated adsorption results are compared in Table 4.3. At pH 4, using that portion of the simulated points which corresponds with the solution phase equilibrium concentration data of Zasoski and Burau, an adsorption capacity of ca. 0.7mmol.g^{-1} is calculated. This compares favourably with the value of 0.65mmol.g^{-1} obtained from the experimental data set. Using simulated points corresponding to the solution phase equilibrium concentration data of Loganathan and Burau, an adsorption capacity of 1.3mmol.g^{-1} is calculated. This is in reasonable agreement with the value of ca. 1.0mmol.g^{-1} obtained for the experimental data set.

At pH 6, adsorption capacities of 1.96mmol.g^{-1} and 1.51mmol.g^{-1} were found by Zasoski and Burau and Gray and Malati respectively. From the simulated data sets, values of 2.50mmol.g^{-1} and 2.70mmol.g^{-1} are calculated. The value predicted for the Zasoski and Burau

data set is lower than that predicted for the Gray and Malati data set, even though the model predicts more zinc to be adsorbed under the conditions employed by Zasoski and Burau. This follows from the fact that the slope of the linear Langmuir equation, which is used to estimate adsorption capacity, depends on the equilibrium concentration range employed in an adsorption experiment (or, in effect, on the metal:solid ratio). This results from the fact that the obtained Langmuir isotherms deviate from linearity. The range of adsorption capacities calculated from the simulated data sets at pH 6 correspond closely with that of ca. 2.8mmol/g found by Gadde and Laitinen (1974).

Table 4.3 Summary of zinc adsorption capacity results obtained from literature and simulated data sets.

pH	I	Adsorption capacity $mmol.g^{-1}$		Source
		Exp	Model	
4.0	0.001	1.00	1.30	Loganathan & Burau, 1974
	0.001	0.70	0.70	Zasoski & Burau, 1988
6.0	0.1	0.47	2.16	Balikungeri & Haerdi, 1988
	0.01	1.51	2.70	Gray & Malati, 1979b
	0.001	1.96	2.50	Zasoski & Burau, 1988
	?	2.80	2.2-2.7	Gadde & Laitinen, 1974
6.5	0.1	1.15	2.48	Balikungeri & Haerdi, 1988

Figure 4.9 compares the pH dependent adsorption experiment of Catts and Langmuir (1986) with a model simulation of their experiment. The model predicts experimental results well up to pH ca. 4. At higher pH, the model overestimates zinc adsorbed.

The results discussed in the preceding paragraphs may be tentatively summarized by stating

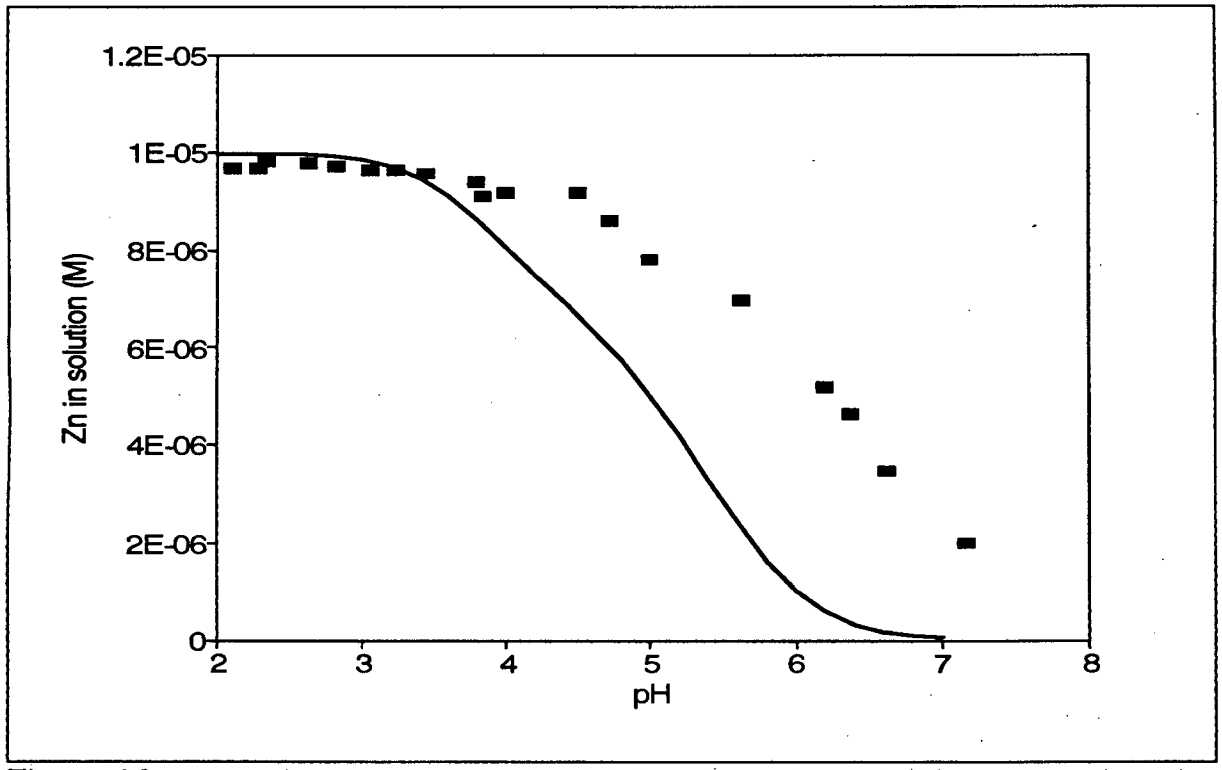

Figure 4.9 Comparison between simulated (—) and experimental (■) pH dependent zinc adsorption data set of Catts and Langmuir.

that the model is more successful in predicting zinc sorption at low pH than at high pH. However, not enough data sets are available to assess the variability which may be expected in experimental studies aimed at determining zinc adsorption by δ-MnO_2.

4.3.4 Cadmium

A reasonably extensive data set for cadmium is available. In Figure 4.10, simulated adsorption results are compared with the data set obtained by Zasoski and Burau at pH 4. The model underestimates cadmium sorption.

In Figure 4.11, the adsorption data of Fu *et al.* obtained at pH 5.5 is compared with that predicted by the model for cadmium adsorption under similar conditions. Here, the model

overestimates cadmium sorption significantly. There is, however, an anomaly between the results reported by Fu at pH 5.5 and those of Zasoski and Burau at pH 4. If the amount of cadmium adsorbed per gram of solid phase at a solution concentration of 0.015 - 0.020mmol.dm^{-3} is compared for the two data sets, it is found that Cd_{ads} (pH4) > Cd_{ads}(pH5.5) by approximately a factor of 2. The fact that the pH 4 study was carried out at an ionic strength of 0.001M while the pH 5.5 study was carried out at 0.01M may explain some of this discrepancy, but not all.

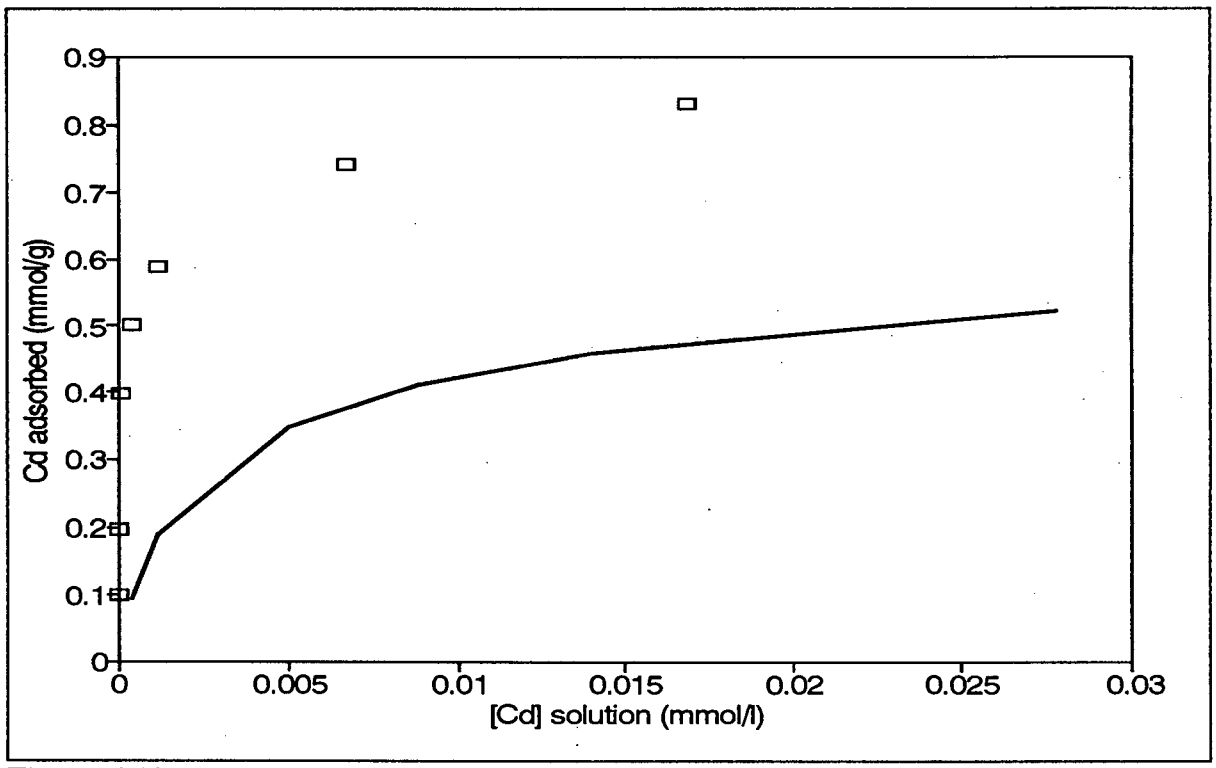

Figure 4.10 Comparison between simulated (—) and experimental (□) cadmium adsorption data at pH 4 (Data set: Zasoski & Burau).

At pH 6, two data sets are available. Figure 4.12 compares the data set of Gray and Malati (1979b) with a simulated data set while Figure 4.13 shows a comparison of the Zasoski & Burau data set with a simulated data set. The two experimental data sets cannot compared with each other directly since they were collected at different ionic strengths.

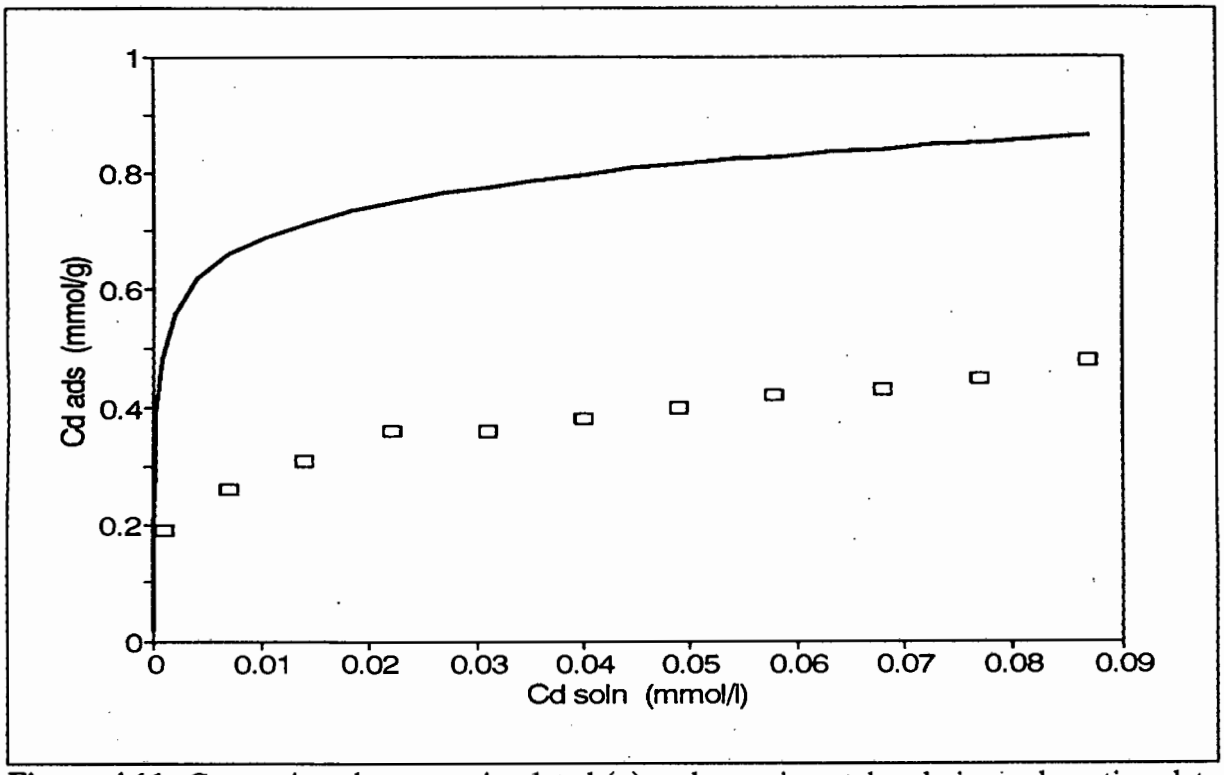

Figure 4.11 Comparison between simulated (—) and experimental cadmium adsorption data at pH 5.5 (Data set: Fu *et al.*, 1991).

The results shown in Figure 4.12 show excellent agreement between simulated and experimental data sets. Comparison of simulated adsorption data with that of Zasoski and Burau (Figure 4.13) indicates that the model underestimates cadmium adsorption. However, the discrepancy between model and experiment is quite small (ca. 0.2 $mmol.g^{-1}$).

The situation at pH 7 and 8 is illustrated in Figures 4.14 and 4.15. In Figure 4.14, the data set of Fu *et al.* at pH 7 is compared with a simulated data set. Good agreement is observed between the model and the experimental data set. The model overestimates the amount of cadmium adsorbed slightly. At pH 8, the situation is reversed, with the model underestimating adsorption results throughout the whole experiment. Adsorption capacities obtained from experimental and simulated results are shown in Table 4.4.

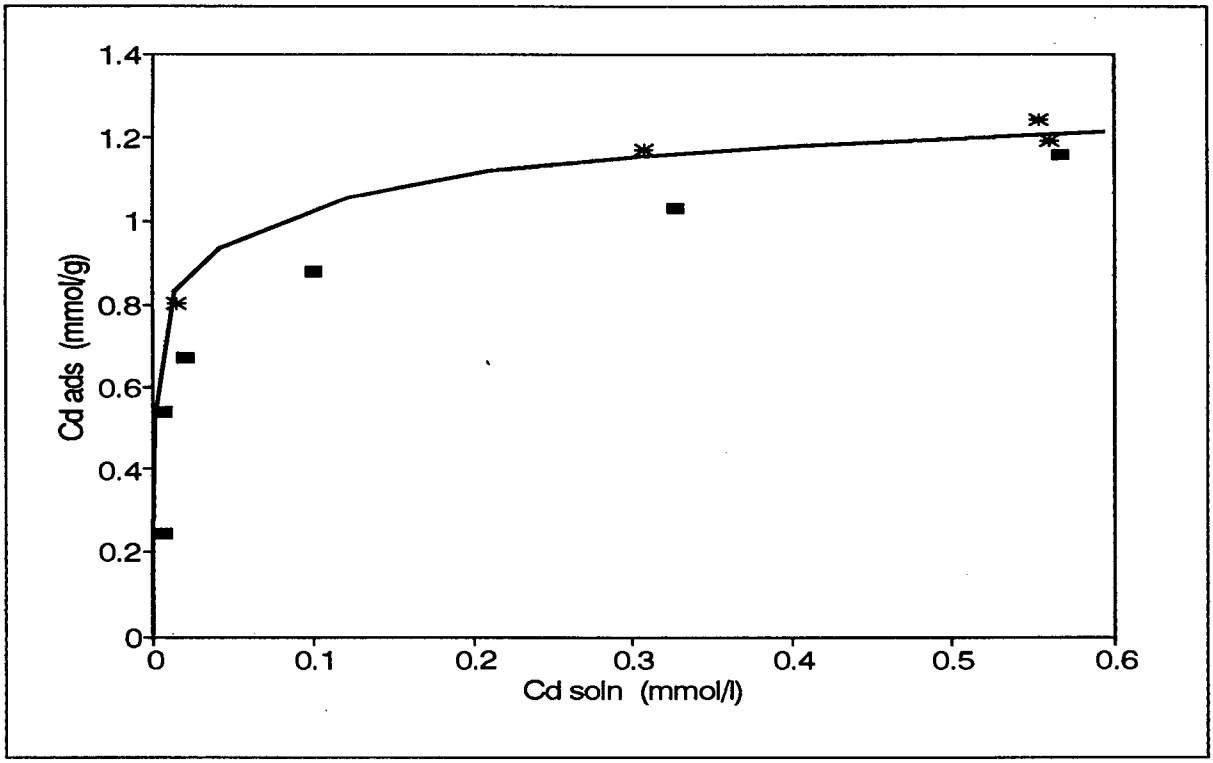

Figure 4.12 Comparison between simulated (–) and experimental cadmium adsorption data collected at pH 6 and T = 293K (■), 311K (*) (Data set: Gray and Malati, 1979b).

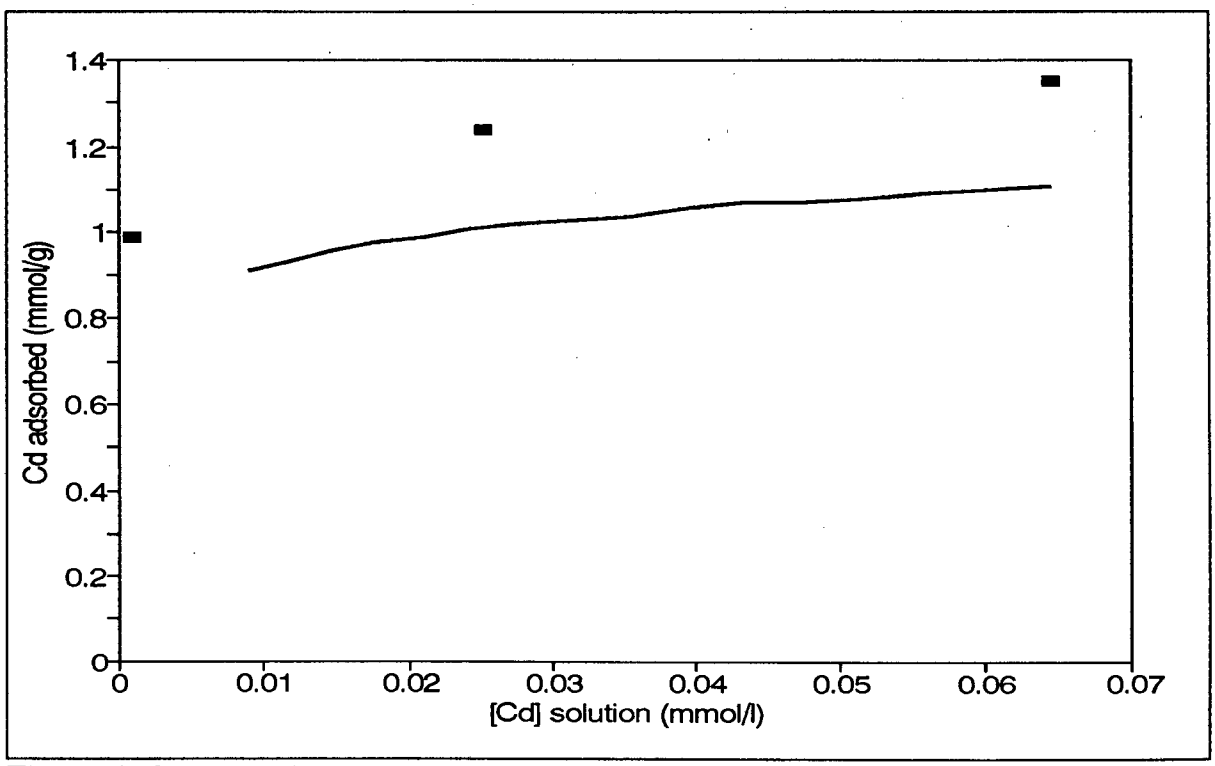

Figure 4.13 Comparison between simulated (–) and experimental (■) cadmium adsorption data at pH 6 (Data set: Zasoski & Burau, 1988).

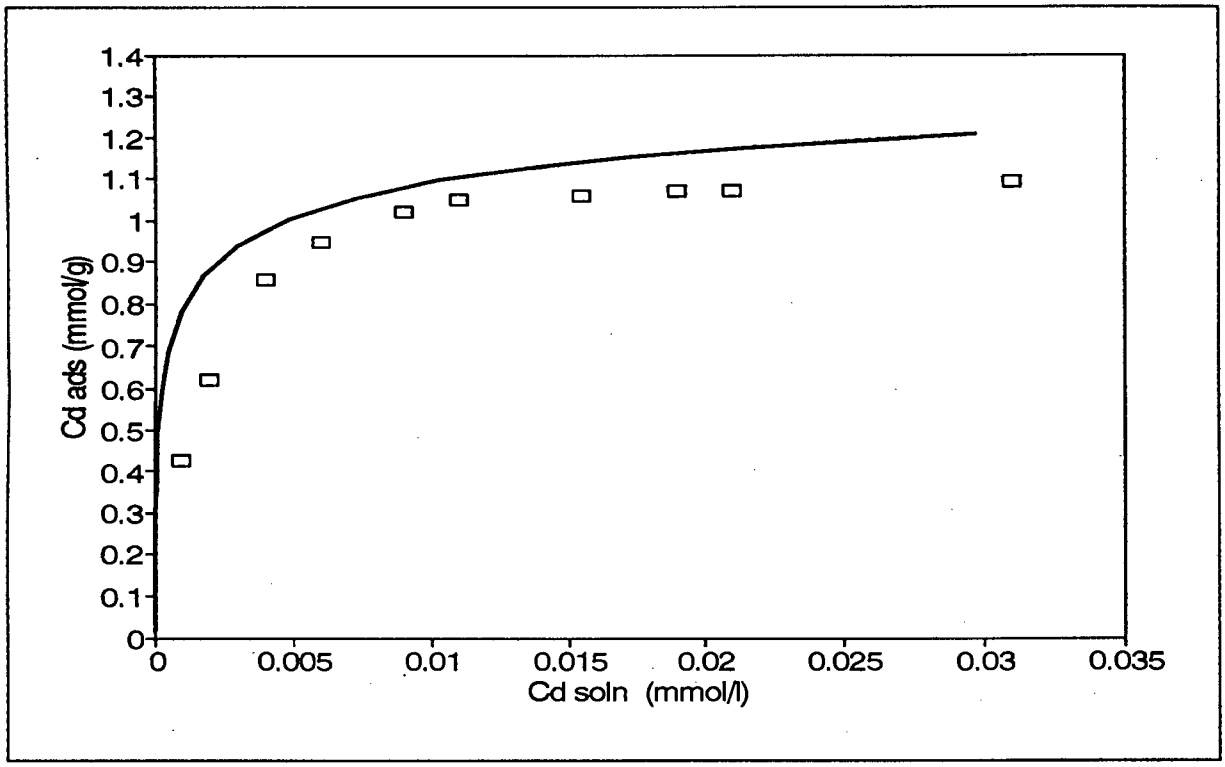

Figure 4.14 Comparison between simulated (—) and experimental cadmium adsorption data at pH 7 (Data set: Fu *et al.*, 1991).

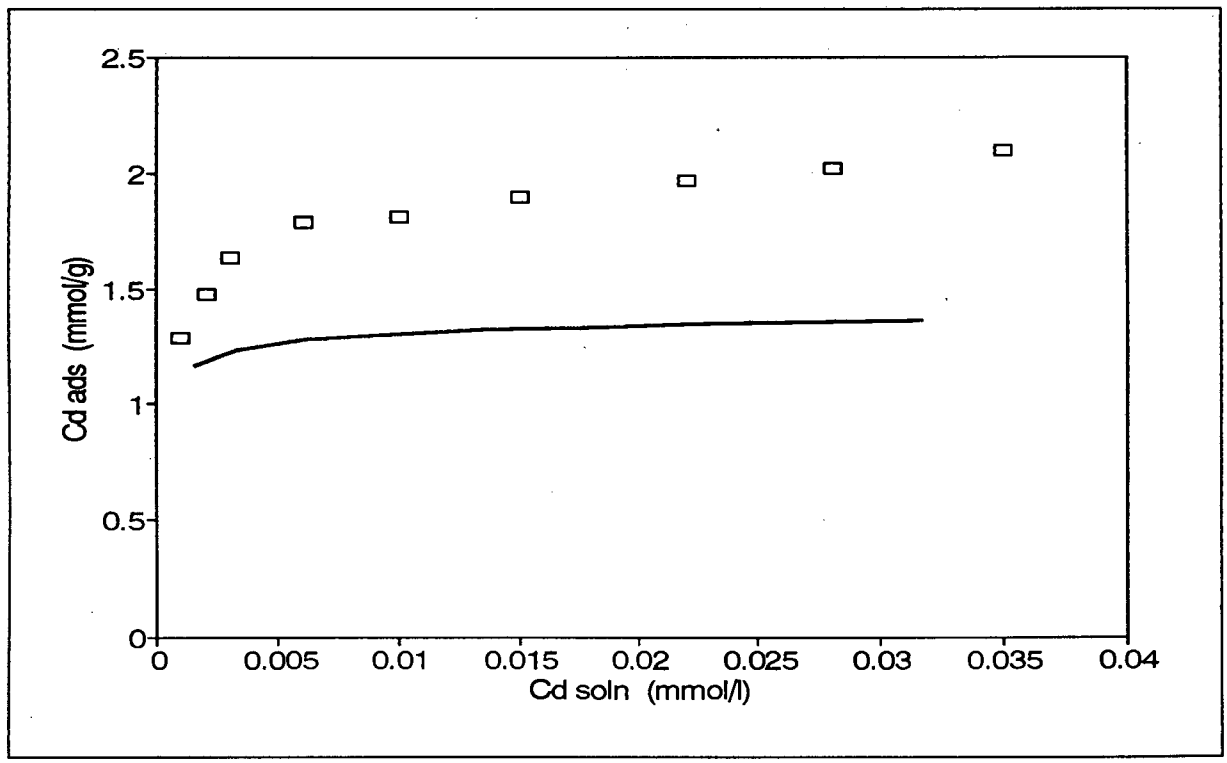

Figure 4.15 Comparison between simulated (—) and experimental (□) adsorption data for cadmium at pH 8 (Data set: Fu *et al.*, 1991).

In general, good agreement between adsorption capacities obtained from experimental observations with those obtained from simulated adsorption data, is observed. Exceptions are the Fu *et al.* data set at pH 5.5 and pH 8, where the model provides an over- and an underestimation of the respective adsorption capacities. The result obtained by Fu *et al.* at pH 5.5 seems low if it is compared with the result obtained by Zasoski and Burau at pH 4. Granted, the pH 4 value was obtained at an ionic strength of a factor of 10 lower than the ionic strength at which the pH 5.5 value was obtained, but it would be expected that the 1.5 pH unit increase will compensate for any depressing influence of the higher ionic strength at pH 5.5. Furthermore, results presented by Hayes and Leckie (1987) indicates that cation adsorption is rather insensitive to ionic strength changes.

In Figure 4.16, a pH dependent adsorption experiment reported by Fu *et al.* is compared with a simulated pH dependent data set. This is a poor result. The model has difficulty in predicting the shape of the adsorption curve in the low pH range. It does, however, predict the point of full adsorption quite well. This is surprising, seen against the background of the results obtained for the pH 8 isotherm of Fu *et al.*.

The results obtained for cadmium may be summarized by stating that the model appears more successful in simulating constant pH adsorption data than pH dependent data. This statement is, however, based on only one pH dependent data set.

Table 4.4 Summary of cadmium adsorption capacity results obtained from literature and simulated data sets.

pH	I	Adsorption capacity mmol.g^{-1}		Source
		Exp	Model	
4.0	0.001	0.83	0.60	Zasoski & Burau, 1988
5.5	0.01	0.43	0.85	Fu *et al.*, 1991
	0.1	0.62	0.65	Balikungeri & Haerdi, 1988
6.0	0.001	1.40	1.20	Zasoski & Burau, 1988
	0.01	1.21	1.17	Gray & Malati, 1979b
	0.1	0.93	0.81	Balikungeri & Haerdi, 1988
	?	1.95	0.8-1.2	Gadde & Laitinen, 1974
6.5	0.1	0.93	1.00	Balikungeri & Haerdi, 1988
7.0	0.01	1.20	1.15	Fu *et al.*, 1991
8.0	0.01	2.12	1.58	Fu *et al.*, 1991

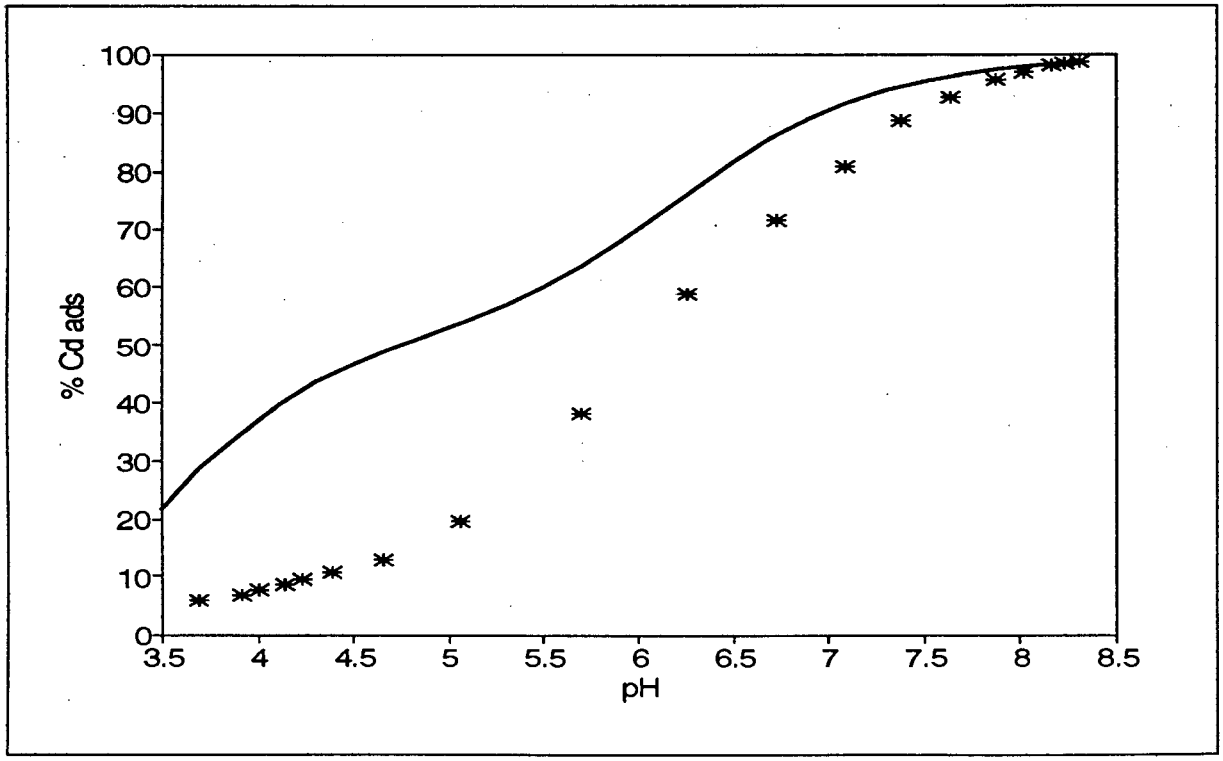

Figure 4.16 Comparison between simulated (—) and experimental (*) cadmium adsorption data (Data set: Fu *et al.*, 1991).

4.3.5 Lead

A rather limited number of lead adsorption data sets are available for model validation purposes. In Figure 4.17, simulated pH dependent adsorption data are compared with the experimental data of Catts and Langmuir.

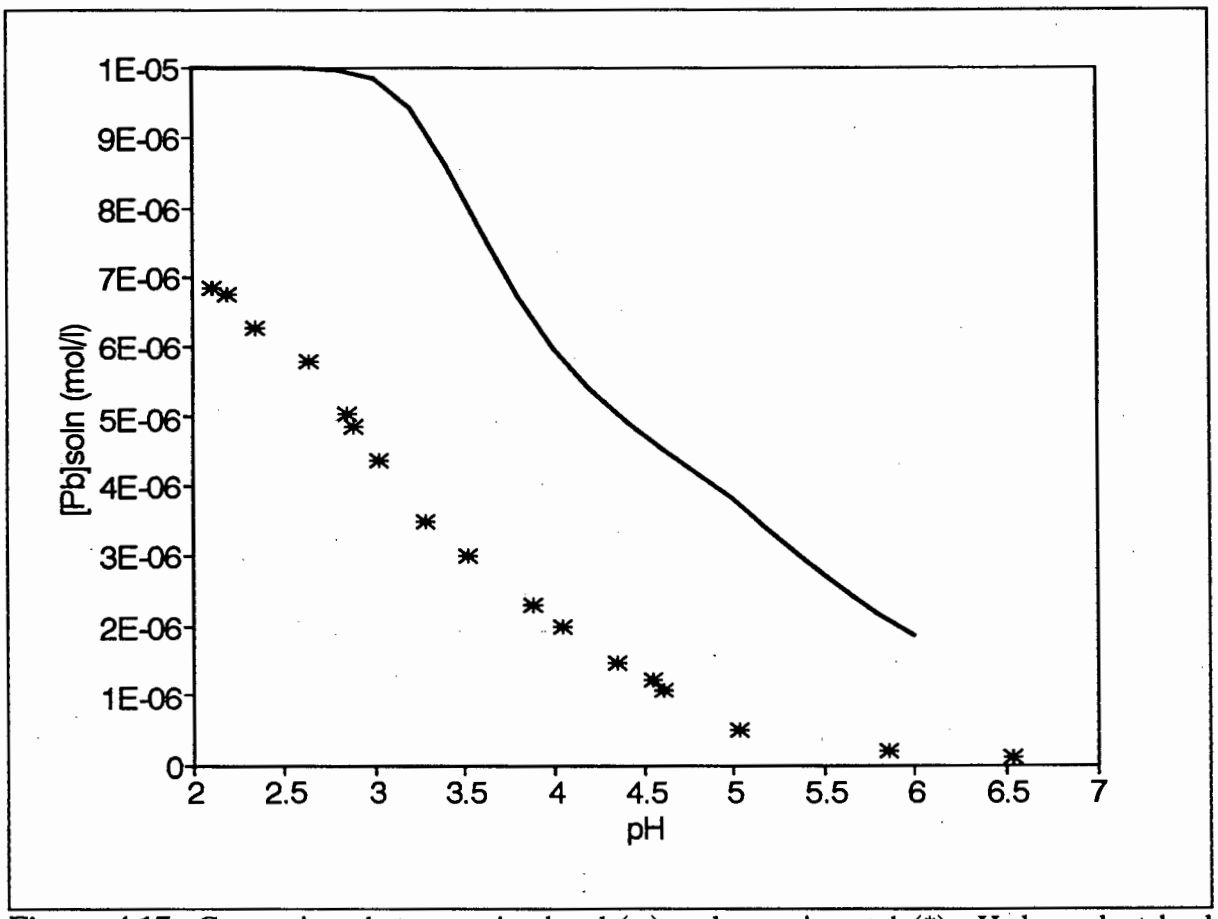

Figure 4.17 Comparison between simulated (—) and experimental (*) pH dependent lead adsorption data (Data set: Catts & Langmuir, 1986).

Agreement between model and experiment is poor. The model underestimates lead adsorption (i.e. overestimates lead in solution) by approximately a factor of 2 to 3. Neither of the models which were evaluated for lead in Chapter 3 is successful in describing the pH dependent data set of Catts and Langmuir (Figure 4.18).

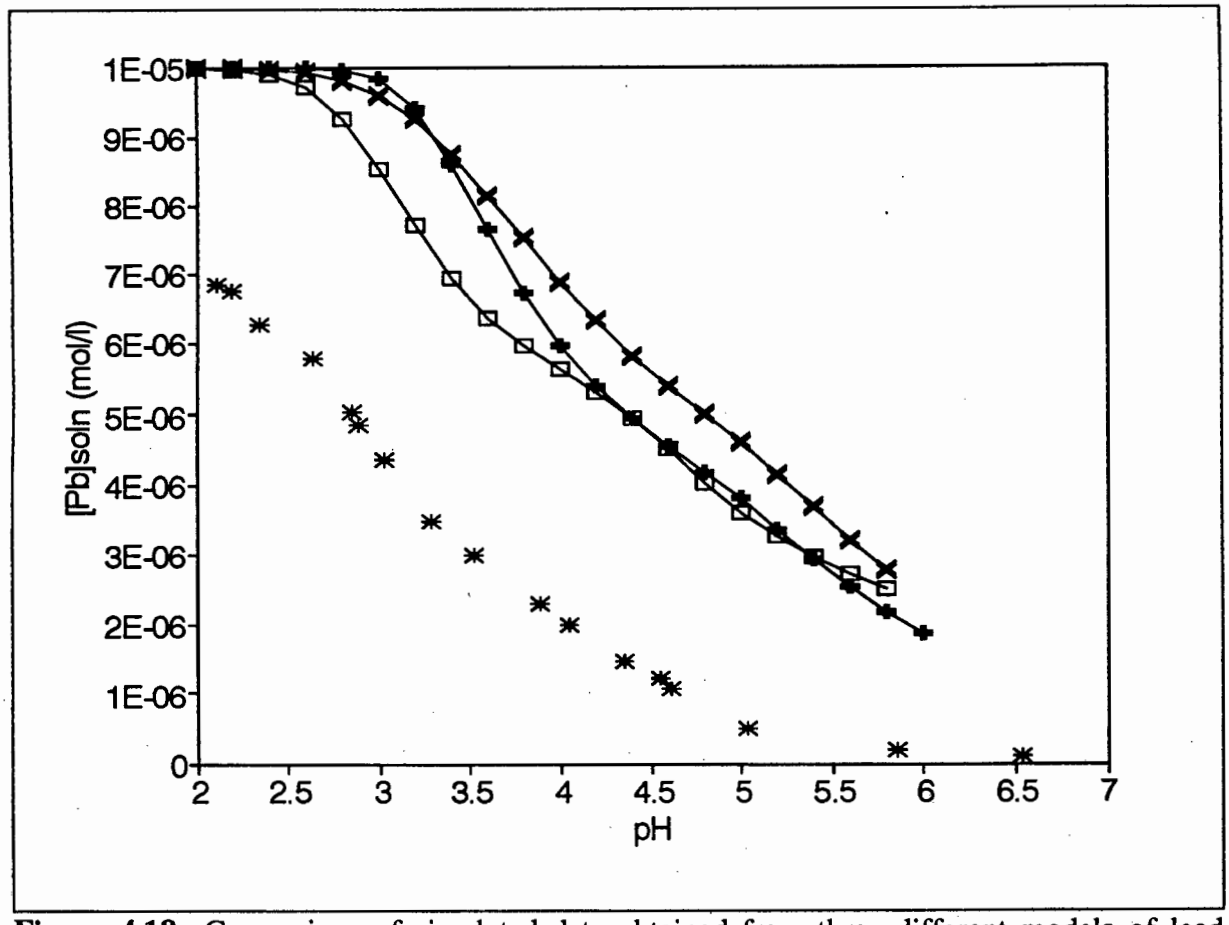

Figure 4.18 Comparison of simulated data obtained from three different models of lead adsorption with pH the dependent data of Catts and Langmuir (1986).

Gadde and Laitinen (1974) report a lead adsorption isotherm obtained at pH 6. They found that lead adsorption did not exhibit a plateau. Instead, adsorption continued to increase. From this, they calculated a lead adsorption capacity of 6.4 $mmol.g^{-1}$. This value, is however, thought to be unrealistic and most probably to include a lead precipitate. Equilibrium simulations of their experimental procedure do, however, not indicate the formation of a Pb precipitate. If the system is equilibrated with atmospheric CO_2, the suspension is found to be supersaturated with a number of lead carbonates. Gadde and Laitinen do not describe any precautionary steps to exclude CO_2 from their experiments. Thus, the possibility of precipitates contributing to their results cannot be excluded.

4.4 Discussion

The model validation procedure was met with mixed success. In certain cases excellent agreement between model and experiment was obtained while in others agreement was poor. A problem is, however, that in some cases good agreement was obtained with one set of data from a specific laboratory but then poor agreement was obtained with a second data set from the same laboratory. No trend manifests itself. Few data sets are available in which experiments were performed under similar conditions. It is therefore not possible to gauge how reproducible results obtained from different laboratories are. The results presented by Stroes-Gascoyne suggest that reproducible results may be difficult to obtain. This may be a result of the amorphous nature of manganese dioxide phases which may result in different surface arrangements for compounds exhibiting similar XRD patterns. Charlet and Manceau (1993) state that EXAFS studies have shown that for solids with similar XRD patterns, several distinct local structures may be present owing to the way the gel has formed. It is therefore impossible to make any definite statements regarding reasons for the discrepancies between model and experiment. It can however be stated that both experimental results and model structure contribute to this, but in indeterminable proportions.

The fact that the model is quite successful in describing adsorption isotherms in terms of trend suggests that the concept of multiple adsorption site classes is valid. It can probably be stated that the model, in a qualitative sense, provides an adequate description of independent adsorption data. The quantitative prowess of the model is somewhat less certain. However, the variability observed in experimental adsorption studies suggests that the model was in most cases within range of observed results. However, compared with the situation

before this study, a degree of progress has been made. This study has produced a consistent set of Diffuse Double Layer model adsorption constants for 5 metals viz. Ni, Cu, Zn, Cd and Pb. It is thus now possible, by using these data, together with the Dzombak and Morel data base for HFO, to include more than one adsorption phase in equilibrium models of systems in which adsorption processes feature prominently.

In the next chapter, the constants determined for metal adsorption by δ-MnO_2 will be applied in an equilibrium model aimed at predicting the partitioning of metals in soil solutions.

Chapter 5 Modelling considerations

In setting up an equilibrium model of any system, careful thought should be given regarding the questions which the modeller seeks to answer regarding the system. Usually, general models are set up to model a generic system, be it the ocean, fresh-water body or a soil system. From these models, certain generalizations may be made regarding the behaviour of constituents in the system.

In this work, a different philosophy was followed. The specific question which was addressed referred to the partitioning of the metals Ni, Cu, Zn, Cd and Pb over the solid-solution interface in a number of specific soil samples. Thus, the soil model was constructed keeping (a) specific processes affecting metal partitioning in soil systems and (b) the analytical data available, in mind.

5.1 Experimental data available

The equilibrium model was validated against soil data collected in the Netherlands (van den Hoop, 1995; Janssen *et al.*, 1995). The data sets are listed in Appendix D. The van den Hoop data set refers to unpolluted soils, with metal levels similar to natural background levels observed in Dutch soils. The Janssen data set was obtained from polluted soils. The sampled soils span a wide range of pH values, metal concentrations and solid and solution phase compositions. Extracted pore water was analyzed for major cations, anions, Dissolved Organic Carbon (DOC) and metals. Pore water pH was also determined.

The solid phase was analyzed for total metal content (concentrated HNO_3) and poorly crystalline Fe oxides (acid ammonium oxalate). Total solid phase concentrations were reported as mass of component per unit mass of soil, e.g. g $Cd.kg^{-1}$ oven dried soil. These values were converted to volume units ($mass.dm^{-3)}$ by dividing by the moisture content of the soil at field conditions. According to Lindsay (1979), this procedure gives the limiting concentration of components in the soil solution.

5.2 Estimation of unavailable and poorly determined data

Data that were not available are solid phase anion concentrations, redox potential measurements and, for the van den Hoop data set, total carbonate concentration in the pore waters. Organic material from both the solution and solid phases were also not extracted and characterized separately. Therefore, a number of assumptions had to be made to estimate the unavailable quantities.

5.2.1 Total anion concentrations

Instead of specifying total anion (SO_4^{2-}, PO_4^{3-}, NO_3^- and Cl^-) concentrations in the partitioning calculations, anion activities were fixed at values obtained from calculation performed with pore water data. In these calculations, the Fe(II)/Fe(III) and Mn(II)/Mn(III) redox couples were included. Calculations were performed so that the extremes of the redox conditions which may be expected in soils (Baas-Becking, 1960; Lindsay, 1979), were covered. It was found that the calculated equilibrium activities of these anions were insensitive to redox conditions. Dissolved organic matter was also excluded from these calculations. Therefore,

it may be expected that the acitivties calculated for SO_4^{2-}, PO_4^{3-}, NO_3^- and Cl^- are perhaps under-estimating the true levels. This follows from the fact that competition between DOM and these anions for cations is not accounted for, which will result in an over-estimation of complexes involving SO_4^{2-}, PO_4^{3-}, NO_3^- and Cl^-.

Carbonate concentration was obtained by equilibrating the soil solutions with $CO_2(g)$ at a fixed partial pressure. Following Lindsay (1979), CO_2 partial pressure was fixed at $10^{-2.5}$ atmospheres, which is one order of magnitude higher than the atmospheric partial pressure of CO_2. Lindsay justifies the use of a higher partial pressure by arguing that biological activity in soils will lead to an increased CO_2 partial pressure.

5.2.2 Soil pH

The pH concept in soil systems is not as well defined as in systems consisting only of a solution phase. Soil pH values were estimated using several approaches: (i) pore water pH, (ii) pH of a soil suspension in contact with a 0.01 M $CaCl_2$ solution, (iii) pH of a soil suspension in contact with 1 M KCl solution and (iv) pH of a soil suspension in contact with demineralized water. Each method yielded a different value for pH, as is illustrated in Tables 5.1 and 5.2. The question now is which value for pH is the appropriate one to use in the equilibrium calculations. Janssen *et al.* (1996) showed that all the pH values are highly correlated with each other. Differences amongst the readings are most probably the result of ionic strength effects, except for the values listed in the first row of Table 5.1. The high value of 6 obtained for $pH(H_2O)$ is most probably due to experimental error.

It was decided to use pore water pH in all simulations since it was felt that it probably gives a better approximation of the equilibrium state of the system than any of the other methods.

Table 5.1 Soil pH as measured by van den Hoop (1995).

Sample	pH (pore water)	pH (KCl)	pH (H_2O)
E930423A	4.75	4.6	6.0
E930423B	4.36	4.2	4.7
E930611C	7.72	7.1	7.8
E930624D	5.82	5.0	6.0
E930707G	4.56	5.1	6.5
E930715J	7.85	7.0	7.8
E930715K	6.50	5.2	6.7
E930715L	4.14	3.4	4.5
E930720M	5.39	4.5	5.5
E930720N	5.35	5.0	6.0

5.3 Thermodynamic data quality for inorganic solution species

The thermodynamic database used in this work is listed in Appendix B. It was not attempted to do a critical evaluation of the literature to assess the quality of the constants employed in the database. Several such compilations are available (NIST, 1989; JESS version 5.2 and 5.3, 1996, 1997 {see May and Murray, 1991a and 1991b for references to JESS}; MINTEQA2 version 3.1 {see Allison *et al.*, 1991}; Woolard, 1995). What was done here was to compare the constants for all reactions included in the MINTEQA2 database with those listed in JESS, NIST and Woolard. This is shown in Appendix B. Certain general remarks regarding the thermodynamic data may be made.

Table 5.2 Soil pH as measured by Janssen *et al.* (1996).

Sample	pH (pore water)	pH (H_2O)	pH (KCl)	pH ($CaCl_2$)
E941129S	7.91	7.8	7.0	7.0
E941102G	7.57	7.6	7.0	6.8
E941129T	7.5	7.9	7.0	7.0
E941104L	7.45	7.6	6.7	6.8
E941102D	7.43	7.4	6.8	7.2
E941128R	7.41	7.7	6.9	6.9
E941102E	7.2	7.2	6.5	6.5
E941128Q	7.14	7.0	6.4	6.7
E941128P	7.09	7.5	6.7	6.8
E941102F	6.79	6.6	6.0	6.5
E941125O	6.09	5.9	5.1	5.3
E941103J	5.97	5.5	4.9	5.0
E941027B	5.74	5.8	5.0	5.7
E941027C	5.15	5.8	4.5	5.4
E941104K	4.21	4.8	3.4	3.8
E941122M	4.02	4.5	3.5	3.8
E941122N	4.01	4.4	3.6	3.9
E941103H	3.78	4.4	3.2	3.5
E941018A	3.57	3.8	3.0	3.4
E941103I	3.40	3.9	2.8	3.0

5.3.1 Data for species including H, Na, K, Ca, Mg

Good agreement amongst the databases is observed for (a) species formed and (b) thermodynamic data. The protonation constants for the inorganic ligands CO_3^{2-}, SO_4^{2-} and PO_4^{3-} are well determined.

Data for magnesium species agree well amongst the different databases, the only exception

being $MgCl^+$. For this constant, the MINTEQA2 and NIST constants (0.5 and 0.6 respectively) correspond well, but JESS values (-0.46 to -1.1) differ significantly from the other values. It was decided to leave the MINTEQ value unchanged.

Calcium species and constants correspond well amongst the databases consulted. An exception is the value listed by JESS for the formation of $CaHPO_4$: it lists 2 values of 15.09, which correspond well with MINTEQ (15.09), NIST (15.04) and Woolard (15.01), and a value of 14.09. Both these values have equal weighting, so it is not possible to use this facility to decide which constant is the more reliable. The NIST constant was used.

For Na, the constant for $NaHPO_4^-$ listed in the MINTEQ database differed significantly from those listed by Woolard, NIST and JESS (12.64 vs 13.20 to 13.50). This constant was replaced by the NIST value of 13.23.

5.3.2 Iron, aluminium and manganese

Because Fe(III) was excluded from the model (see paragraph 5.4), its data will not be discussed. For Fe(II), good agreement for equilibrium constants was observed. $Fe(OH)_3^-$ is an exception, with a difference of 2 log units between the MINTEQ and NIST value of -28.99 and the JESS and Woolard value of -31.00. The MINTEQA2 value was left unchanged because of its agreement with the NIST value.

Of the aluminium species included in the MINTEQA2 database, formation constants for $Al(OH)_2^+$, $Al(OH)_3$, $Al(OH)_4^-$ and $Al(SO_4)^+$ differ significantly amongst the databases. This

means that for 5 out of the 6 inorganic aluminium species included in the database, data are quite uncertain. It was decided to use the constants as listed in MINTEQA2 since they were within the range of values reported in the other databases.

The constant for $Mn_2(OH)^{+3}$ is given as -10.56 (MINTEQ, Woolard), -10.60 to -10.10 (JESS) and -7.20 by NIST. Based on the good agreement between three of the databases, the MINTEQ value was left unchanged. This value also agrees well with that listed by Baes and Mesmer (1976).

5.3.3 Nickel, copper, zinc, lead and cadmium

Data for these metals may be summarized by noting that data for hydroxy and carbonate species have a high degree of uncertainty associated with them. As far as possible, constants from the NIST database were used.

5.3.4 Solubility products for potential precipitates

No general discussion on solubility data is presented. Data for solids which precipitated in specific simulations are discussed in Chapter 6.

5.4 Construction of the soil model: assumptions and simplifications

Assumptions and simplifications were made on two levels: first, processes accounted for in the chemical model of the soil system were trimmed down or simplified. Second, due to

experimental difficulties in characterizing soil systems, certain assumptions and operational definitions had to be employed. In the construction of the current model, the following assumptions and simplifications were made.

Certain chemical reactions were not included because consistent data for these reactions are not yet available. In particular, the adsorption of dissolved organic matter (DOM) by Hydrous Ferric Oxide and MnO_2 were disregarded. Also, the formation of ternary complexes involving an adsorption phase, and dissolved organic matter and a metal, is disregarded. The effect of DOM adsorption on oxide surface properties has been discussed by a number of workers (Tipping, 1981a,b; Tipping and Cooke, 1982; Vermöhlen *et al.*, 1996). Their results indicate that adsorption of DOM occurs mostly in the lower pH ranges and the nett effect of DOM adsorption is a reversal of particle surface charge.

Organic ligands adsorbed to a surface may affect metal adsorption in two ways: first, if all the ligand's donor groups are utilized in ligand-surface binding, adsorption of the ligand will decrease metal adsorption. If, however, one or more of the ligand's functional groups remain free, these compounds can facilitate metal sorption by acting as a bridge between the surface site and the metal ion (Coughlin and Stone, 1995). The inclusion of this process in an equilibrium model is fraught with difficulty. The first problem is related to sorption constants describing the sorption of organics by mineral phases. A second problem is related to sorption constants describing sorption of metals by the organic material adsorbed to the mineral phase. Also, the extent to which the mineral surface is covered by organic material will affect metal sorption. Because of this large amount of uncertainty, it was decided to exclude these processes from the model.

Adsorption by clay minerals was disregarded. The reason for this is two-fold: first, clay minerals present in the soil samples considered were not characterized and second, MINTEQA2 does not allow the simultaneous use of different sorption models in the same equilibrium problem (Allison, 1991). Adsorption data for clays are usually reported as ion exchange constants (Evans, 1989).

Redox processes were also excluded from the model since no redox potential measurements were available. This is not seen as a problematic assumption for the following reasons. Preliminary model runs on the pore water systems in which redox potential was varied over the range commonly found in soil systems (Baas-Becking, 1960; Lindsay, 1979), indicated that the major effect of redox potential is the formation of metal ferrites. Metal ferrites are mixed oxides containing nickel, copper or zinc and Fe_2O_3, with the general formula of MFe_2O_3. The formation of these solids depends on Fe(III) concentration, which is again dependent on redox potential. These solids were predicted to be highly supersaturated at very low redox potentials in a number of samples. Since the soils were surface soils which were not water-logged, it is reasonable to assume an oxidizing soil environment. Thus, the formation of these solids can reasonably be expected to occur in the soils. However, the existence of $CuFe_2O_4$, $NiFe_2O_4$ and $ZnFe_2O_4$ is by no means free of controversy.

Evidence for their existence in soils is scarce. Sadiq and Enfield (1984a, 1984b) equilibrated soil suspensions for periods ranging from 1 to 50 days. Soil suspensions were analysed for Ni, Fe, Al, PO_4^{-3}, Si and Cl^-. Redox potential and pH were also determined. Based on these data, they plotted Log $\{[Ni^{2+}]^3[Fe^{3+}]^2\}$ vs suspension pH. This was compared with a similar plot predicted from $NiFe_2O_4$ solubility data. Their results show good agreement between

observed and calculated curves, which they use as evidence for the existence of $NiFe_2O_4$ in their soils.

On the other hand, Bruemmer *et al.* (1983) illustrated that for zinc, observed zinc concentrations in solution did not follow those predicted by $ZnFe_2O_4$. They concluded from their results that zinc concentration in the soil aqueous phase is not controlled by $ZnFe_2O_4$, but rather by an adsorption process. A major objection levelled against their existence in soil solutions is that conditions required for their formation are quite different from ambient soil conditions. According to McBride (1994), these structures violate the radius ratio rule, which suggests that extreme conditions are necessary for their formation.

Examination of the more recent literature on the formation of $CuFe_2O_4$ supports these objections. Xu and Wang (1993) considered the interaction between CuO and Fe_2O_3 and CuO and $Fe(NO_3)_3$. Their results indicated that under ambient conditions and mechanical stirring no reaction took place. Only once the temperature was elevated to 1073 K for 2 hours did they detect the formation of $CuFe_2O_3$. Also, a patent registered by Li (1993) forms $CuFe_2O_4$ by mixing a ferric compound with a metal sludge and then heating the mixture at 500 to 1400 °C for 1 to 10 hours.

Apart from the controversy about the existence of these solids in soils, the thermodynamic data describing their formation are quite uncertain. This is borne out by the fact that (a) the constant for $CuFe_2O_4$ varies from 5.9 (JESS, MINTEQA2) to 10.13 (Lindsay, 1979), (b) data for $NiFe_2O_4$ is only listed by Sadiq and Enfield (1984a) and (c) data for $ZnFe_2O_4$ is listed only by Lindsay (1979).

The evidence presented suggests that the formation of these solids in soil systems are highly unlikely. Therefore, they were disregarded in all subsequent simulations.

Redox potential is also important for the formation and dissolution of ferric adsorption phases in soils. Here, however, the ammonium oxalate extractions provided experimental evidence for the existence of ferric solids in contact with the pore water phase. Also, MINTEQ does not allow the adsorption phase concentration to change during the course of a simulation. In other words, if adsorption processes are to be modelled, a situation of constant solid phase composition must be assumed. Thus, in the current application the formation/dissolution reactions can be disregarded. In all simulations, pore water iron was assumed to be present in the Fe(II) state.

Manganese redox reactions were disregarded on the basis of (i) kinetic considerations (McBride, 1994) and (ii) the fact that MnO_2 was assumed to be present in the solid phase in all simulations. Pore water manganese was assumed to be all in the Mn(II) form. The Cu(I)/Cu(II) redox couple was also excluded since Cu(I) is not stable in aqueous solution (Cotton and Wilkinson, 1980).

The cation binding characteristics of Natural Organic Matter (NOM) was estimated using a modelling approach. The exact functional group arrangements on NOM responsible for cation binding, together with the abundance of these arrangements, are ill-defined. This necessitates an additional modelling step to obtain estimates of these. This is discussed in paragraph 5.5.

Soil adsorption phases were assumed to approximate, in behaviour and identity, well-defined solids prepared and studied under laboratory conditions. Soil solid phases are operationally defined in terms of an extraction procedure. Characteristics of pure solid phases measured under controlled laboratory conditions, such as β's, surface areas and binding capacities are taken as approximations for these properties of the soil solid phase. Although this extrapolation may be criticized, recent work by Tessier *et al.* (1996) has shown that there is some merit in the use of laboratory determined parameters in the modelling of natural systems. Furthermore, the adsorption of anions and cations at the soil solid phase were assumed to occur according to the surface complexation model together with the Diffuse Double Layer model of the solid/solution interface. Determination of the relevant parameters describing the adsorption phases is described in paragraph 5.6.

Apart from the assumptions regarding the soil chemical processes, we are forced to make certain assumption regarding the physical properties of the soil as well. Physical properties of soils are of major importance in controlling movement and composition of the soil solution (Greenland and Hayes, 1981). Implicitly, it is assumed that the soil is a homogeneous system of particles surrounded by the soil solution, or pore water. In reality however, the soil is a highly non-homogeneous system consisting of an unequal distribution of particles, particle sizes and pore sizes.

5.5 Inclusion of Dissolved Organic Matter

The experimental data available on dissolved organic compounds present in the pore waters were Dissolved Organic Carbon (DOC) concentrations. Van den Hoop (1995) and Janssen

et al. (1995) did not perform any extraction and characterization studies, such as C, H and N analysis, IR, NMR and MS. Thus no information regarding the molecular structure and possible functional group arrangements of the Dissolved Organic Matter (DOM) in which the DOC is present, was available. The inclusion of these compounds therefore necessitated several assumptions. These are:

(i) all DOC is present as humic and fulvic type materials

(ii) only R-COOH, R-OH, Ø-COOH, Ø-OH are available to form binding sites

(iii) average values for elemental composition and functional group content is representative of the DOM in the present samples.

The major assumption was that average values for elemental composition and functional group content published in the literature was a good estimate for the DOM in the systems to be modelled in this work. Evidence from fractionation studies on a wide variety of humic substances supports this assumption. Therefore, values reported in the literature were used as estimates for the required input (Buffle, 1988; Krajnc *et al.*, 1995; Cleven, 1984; de Wit, 1988; Mountney and Williams, 1992; Alloway, 1995). These values are listed in Table 5.3. The set of values used throughout all simulations are listed in Table 5.5. The compounds chosen as models for binding sites are listed in Table 5.6. Although the RANDOM model allows for the inclusion of nitrogen containing binding sites, only sites containing oxygen as donor were included in the present study. RANDOM requires the user to specify a binding site counting order. This is needed to ensure that certain functional group arrangements are not counted twice. This was decided on by performing calculations at $3 \leq pH \leq 9$ using all the oxygen donor ligands at equal concentrations with only one metal present. Ligands were

present in excess. All ligands binding less than 1% metal at each pH value were disregarded. The eight remaining ligands were then ranked in terms of their ability to bind metals. This procedure is similar to that employed by Mountney and Williams (1992). The following site counting order was established:

MAL, ACAC, CAT, SUCC, 2HMP, PHTH, HBT, PROP

In the soil simulations, concentrations for each of the binding sites listed in Table 5.5 were multiplied by the HM concentration for the particular sample, listed in Table 5.6. Humic material concentration was calculated by assuming that the soil humic material consists of 45% carbon (see Table 5.3).

Table 5.3 Data used in humic material binding site concentration determination.

Elemental composition	
%C:	45
%Aromatic C:	53
Functional group content (mmol/g)	
COOH:	8.2
R-OH:	6.0
Ar-OH:	3.0
R=O:	1.3
Ar=O:	1.3
$R\text{-}OCH_3$:	0.8

Table 5.4 Ligands considered for inclusion as DOM model binding sites.

Site name	Abbreviation
Phthalic acid	PHTH
Salicylic acid	SAL
Catechol	CAT
Benzoic acid	BENZ
Phenol	PHEN
Malic acid	MAL
2,3-dihydroxy-2-methylbutanoic acid	DHMB
2-Hydroxy-2-methylpropionic acid	2HMP
Succinic acid	SUCC
Diethylmalonic acid	DEM
3-Hydroxybutanoic acid	3HBT
Propionic acid	PROP
Acetylacetone	ACAC

Table 5.5 Binding site concentrations calculated by RANDOM

Binding site	[Site] (mmol/g HM)
MAL	0.8385
ACAC	0.0290
CAT	0.3385
SUCC	0.3715
2HMP	0.6560
PHTH	0.1235
3HBT	0.6400
PROP	0.5361

Table 5.6 Humic material (HM) concentration calculated for pore water samples from DOC concentration by assuming 45% carbon content.

Sample ID	DOC mg/l	HM (45% C) mg/l
E930423A	15.16	33.69
E930423B	36.01	80.02
E930611C	28.80	64.00
E930624D	47.17	104.82
E930707G	65.42	145.38
E930715J	80.88	179.73
E930715K	39.85	88.78
E930715L	53.35	118.56
E930720M	53.35	118.56
E930720N	53.29	118.42
E941018A	51.72	114.93
E941027B	75.00	166.67
E941027C	88.44	196.53
E941102D	113.64	252.53
E941102E	67.56	150.13
E941102F	88.08	195.73
E941102G	75.84	168.53
E941103H	87.60	194.67
E941103I	146.40	325.33
E941103J	58.20	129.33
E941104K	148.80	330.67
E941104L	147.6	328.00
E941122M	55.92	124.27
E941122N	53.64	119.20
E941125O	34.32	76.27
E941128P	21.24	47.20
E941128Q	54.00	120.00
E941128R	20.40	45.33
E941129S	26.40	58.67
E941129T	34.68	77.07

5.6 Inclusion of adsorption processes

The implementation of the surface complexation/diffuse double layer adsorption model requires certain data viz. (a) model adsorption reactions, (b) adsorption constants for the reactions in (a), (c) adsorption phase characteristics such as surface area, amounts of strong and weak binding sites and (d) the amount of adsorption phase present in the soil system.

For HFO, the data required under points (a) - (c) were used as recommended by Dzombak and Morel (1990). These are listed in Tables 5.7 and 5.9 for the respective data sets. The amount of poorly crystalline ferric oxides in the soil solid phase was estimated from acid ammonium oxalate extractions of the soils. Schwertmann and Taylor (1989) discuss the determination of iron oxides in soils. Extraction with acid ammonium oxalate provides an estimate of the poorly crystalline iron oxides.

The more crystalline phases such as Goethite, Hematite and Lepidocrocite are not solubilized unless some source of Fe^{2+} is present. The acid ammonium oxalate extraction may thus provide an overestimation of the amount of poorly crystalline, highly reactive iron oxides. However, numerous factors, such as surface structure and species sorbed onto the surface, may inhibit or enhance the dissolution of ferric oxides (Biber *et al.*, 1994). Equating the ammonium oxalate extractable iron to HFO is, however, purely operational. The effect of this may be that (i) the pH range in which the soil solid phase actively adsorbs cations is not reflected in the model (i.e. the soil solid phase may also be quite active at low pH whereas the model solid is only active at pH≥6), (ii) binding site density estimations are wrong and (iii) adsorption constants which relate to amorphous hydrous ferric oxide are not applicable.

Table 5.7 HFO data used in modelling the van de Hoop data set. HFO content estimated by ammonium oxalate extractions of soils.

Sample	#Moisture content %wght	Fe g/kg air dried soil	*Fe g/L soil solution	Fe mol/L soil solution	[1][Type 1] (mol/l)	[2][Type 2] (mol/l)
E930423A	32	24.301	75.939	1.360	6.80e-03	2.72e-01
E930423B	74	11.964	16.167	0.289	1.45e-03	5.79e-02
E930611C	19	6.543	34.435	0.617	3.08e-03	1.23e-01
E930624D	49	15.712	32.065	0.574	2.87e-03	1.15e-01
E930707G	19	8.327	43.825	0.785	3.92e-03	1.57e-01
E930715J	14	2.441	17.433	0.312	1.56e-03	6.24e-02
E930715K	22	10.582	48.100	0.861	4.31e-03	1.72e-01
E930715L	33	6.022	18.249	0.327	1.63e-03	6.54e-02
E930720M	9	1.524	16.936	0.303	1.52e-03	6.07e-02
E930720N	7	4.240	60.565	1.084	5.42e-03	2.17e-01

\# field conditions
* calculated through: (g Fe/kg air dried soil)/(field soil moisture content)
1 0.005 mol sites per mol Fe
2 0.2 mol sites per mol Fe
Surface area: 600 $m^2.g^{-1}$

Table 5.8 MnO_2 data used in modelling the van den Hoop data set. MnO_2 content equated to total manganese content of solid phase estimated from concentrated HNO_3 destruction of solid phase.

Sample	#Moisture content (wght %)	Mn g/kg air dried soil	*Mn g/L soil solution	Mn mol/L soil solution	[1][Type 1] (mol/l)	[2][Type 2] (mol/l)
E930423A	32	0.714	2.23	4.059e-02	7.71e-03	2.72e-03
E930423B	74	0.131	0.177	5.260e-03	9.99e-04	3.52e-04
E930611C	19	0.648	3.41	6.206e-02	1.18e-02	4.16e-03
E930624D	49	0.145	0.296	5.388e-03	1.02e-03	3.61e-04
E930707G	19	0.775	4.08	7.426e-02	1.41e-02	4.98e-03
E930715J	14	0.315	2.25	4.095e-02	7.78e-03	2.74e-03
E930715K	22	2.837	12.90	2.348e-01	4.46e-02	1.57e-02
E930715L	33	0.539	1.63	2.967e-02	5.64e-03	1.99e-03
E930720M	9	0.167	1.86	3.386e-02	6.43e-03	2.27e-03
E930720N	7	0.662	9.46	1.722e-01	3.27e-02	1.15e-02

\# field conditions
* calculated through: (g Mn/kg air dried soil)/(field soil moisture content)
1 0.19 mol sites per mol Mn
2 0.067 mol sites per mol Mn
Surface area: 331 $m^2.g^{-1}$

Table 5.9 HFO data used in modelling the Janssen data set. HFO content estimated by ammonium oxalate extractions of soils.

Sample	#Moisture content (wght %)	Fe g/kg air dried soil	*Fe g/L soil soln	Fe mol/L soil soln	[1][Type 1] mol/L	[2][Type 2] mol/L
E941018A	12.3	1.48	12.03	0.216	1.08e-03	4.31e-02
E941027B	73.5	8.85	12.04	0.216	1.08e-03	4.32e-02
E941027C	55.3	11.09	20.05	0.359	1.80e-03	7.19e-02
E941102D	29	3.58	12.35	0.221	1.11e-03	4.43e-02
E941102E	25.7	4.73	18.38	0.330	1.65e-03	6.59e-02
E941102F	32.5	3.86	11.86	0.213	1.06e-03	4.25e-02
E941102G	37.1	16.04	43.23	0.775	3.87e-03	1.55e-01
E941103H	10.4	0.20	1.884	0.034	1.69e-04	6.75e-03
E941103I	12.9	0.36	2.759	0.049	2.47e-04	9.89e-03
E941103J	43	15.02	34.93	0.626	3.13e-03	1.25e-01
E941104K	8.2	0.27	3.243	0.058	2.91e-04	1.16e-02
E941104L	29.6	3.50	11.82	0.212	1.06e-03	4.24e-02
E941122M	11.9	1.65	13.84	0.248	1.24e-03	4.96e-02
E941122N	5.8	1.18	20.41	0.366	1.83e-03	7.32e-02
E941125O	31.5	15.44	49.00	0.878	4.39e-03	1.76e-01
E941128P	66.3	12.95	19.53	0.350	1.75e-03	7.00e-02
E941128Q	55.8	7.71	13.81	0.247	1.24e-03	4.95e-02
E941128R	57.6	9.39	16.30	0.292	1.46e-03	5.84e-02
E941129S	32.9	6.26	19.03	0.341	1.70e-03	6.82e-02
E941129T	39.7	4.99	12.55	0.225	1.13e-03	4.50e-02

\# field conditions
* calculated through: (g Fe/kg air dried soil)/(field soil moisture content)
1 0.005 mol sites per mol Fe
2 0.2 mol sites per mol Fe
Surface area: 600 $m^2.g^{-1}$

Table 5.10 MnO_2 data used in modelling the Janssen data set. MnO_2 content equated to total manganese content of solid phase estimated from concentrated HNO_3 destruction of solid phase.

Sample	#Moisture content (wght %)	Mn g/kg air dried soil	*Mn g/l soil soln	Mn mol/L soil soln	[1][Type 1] mol/L	[2][Type 2] mol/L
E941018A	12.3	0.07444	0.605	1.10e-02	2.09e-03	7.39e-04
E941027B	73.5	0.2259	0.307	5.60e-03	1.06e-03	3.75e-04
E941027C	55.3	0.4434	0.802	1.46e-02	2.78e-03	9.79e-04
E941102D	29	0.3270	1.128	2.05e-02	3.90e-03	1.38e-03
E941102E	25.7	0.4861	1.892	3.45e-02	6.55e-03	2.31e-03
E941102F	32.5	0.5946	1.830	3.33e-02	6.33e-03	2.23e-03
E941102G	37.1	0.9445	2.546	4.64e-02	8.81e-03	3.11e-03
E941103H	10.4	0.006149	0.059	1.08e-03	2.05e-04	7.22e-05
E941103I	12.9	0.009113	0.071	1.29e-03	2.44e-04	8.62e-05
E941103J	43	0.1291	0.300	5.47e-03	1.04e-03	3.66e-04
E941104K	8.2	0.0223	0.273	4.98e-03	9.45e-04	3.33e-04
E941104L	29.6	0.4024	1.360	2.48e-02	4.71e-03	1.66e-03
E941122M	11.9	0.0772	0.650	1.18e-02	2.25e-03	7.93e-04
E941122N	5.8	0.04172	0.719	1.31e-02	2.49e-03	8.78e-04
E941125O	31.5	0.4146	1.316	2.40e-02	4.56e-03	1.61e-03
E941128P	66.3	0.7324	1.105	2.01e-02	3.82e-03	1.35e-03
E941128Q	55.8	0.2351	0.421	7.68e-03	1.46e-03	5.14e-04
E941128R	57.6	0.3737	0.649	1.18e-02	2.25e-03	7.92e-04
E941129S	32.9	0.5479	1.665	3.03e-02	5.76e-03	2.03e-03
E941129T	39.7	0.6894	1.737	3.16e-02	6.01e-03	2.12e-03

\# field conditions
* calculated through: (g Mn/kg air dried soil)/(field soil moisture content)
1 0.19 mol sites per mol Mn
2 0.067 mol sites per mol Mn
Surface area: 331 $m^2.g^{-1}$

For MnO_2, the parameters determined in Chapters 2 and 3 in this work were used to fulfil the data requirements listed under points (a) - (c). The MnO_2 content of the soil solid phase was not measured. The only data available were total manganese, as determined from a concentrated nitric acid extraction of the solid phase. Thus, the potential effect of MnO_2 on metal partitioning was modelled by assuming that all manganese in the solid phase is present as MnO_2 (McBride, 1994). This scenario will represent the maximum effect that may be expected due to metal adsorption by MnO_2. Tables 5.8 and 5.10 contain a summary of binding site concentrations used to represent MnO_2 in the models for the various soil samples.

5.7 Summary of soil model

The processes included in the equilibrium model, together with thermodynamic data sources, are summarized in Table 5.11.

Table 5.11 Summary of the soil chemical equilibrium model.

Process	Participating components	Equilibrium data source
Complexation	Major cations, anions, Fe(II), Mn(II), Cu, Zn, Cd, Pb, Ni, Dissolved Organic Matter (DOM)	Woollard, 1995. JESS NIST,. 1993. Allison *et al.*, 1991.
Redox	Excluded	
Precipitation	As for complexation, *excluding* DOM	Allison *et al.*, 1991.
Adsorption	As for complexation, *excluding* Fe(II), Mn(II), Al, CO_3^{2-}, Cl^-, NO_3^-, DOM. Hydrous Ferric Oxide (HFO) and Manganese dioxide as adsorption phases.	Dzombak and Morel, 1990. This work, Chapters 2 & 3.

In the next chapter, the equilibrium model described in the preceding sections will be used to predict pore water concentrations in a number of Dutch soils.

Chapter 6 Metal partitioning in soils

The main objective of this work was the measurement of adsorption data which would allow the inclusion of more than one adsorption phase in equilibrium models of soil and sedimentary systems. The focus was, in particular, on manganese dioxide. Therefore, the modelling results presented here are those which illustrate the influence of MnO_2 on predicted metal partitioning.

The first set of simulation results relate to the situation before the work described in Chapters 2, 3 and 4 was carried out. In these simulations, adsorption of metals by HFO, using the Dzombak and Morel (1990) data, and precipitate formation were the only mechanisms specified which allowed the incorporation of metals into the soil solid phase. These simulations are referred to as **HFO-PPT** in the subsequent text. The second modelling scenario includes MnO_2 as an additional sorption phase. This is referred to as **HFO-MNO_2-PPT**.

Agreement between predicted and observed metal partitioning were assessed (a) visually and (b) by calculating the mean deviation for each model over all samples. In the visual comparisons, observed and calculated pore water concentrations of each metal were plotted as a function of soil sample pH. The mean deviation was calculated according to

$$\frac{\sum |Observed - Calculated|}{n}$$

where n is the number of soil samples considered. It was also used to assess whether a specific model provided a better description of experimental results compared to another.

6.1 The HFO-PPT model.

Results obtained with this model are presented in Figures 6.1 to 6.5. Mean deviations for each metal are presented in Table 6.1. The results may be summarized by noting that in general, agreement between model and experiment improves with increasing pH. The model thus exhibits a pH dependency. This is not observed for the observed pore water concentrations, which are reasonably constant over the complete pH range covered by the soil samples. The pH dependence of model results are confirmed by the mean deviations listed in Table 6.1.

Table 6.1 Mean deviations calculated for the HFO-PPT model.

pH range	Ni	Cu	Zn	Cd	Pb
3.4-4.4	3.22	2.42	2.44	2.81	1.54
4.4-6.1	3.19	0.88	2.69	3.02	1.02
>6.1	2.11	0.87	0.76	1.33	0.32
Overall	2.74	1.28	1.82	2.26	0.85

As far as specific metals are concerned, the model is most successful in predicting pore water concentrations for lead and copper. For lead (Figure 6.5), the maximum discrepancy between model and experiment is 3.5 log units for samples with pH less than 4.4. Above this pH, the agreement was always to within 1.5 log units. The overall mean deviation between observed and calculated pore water concentrations is 0.85 log units.

In the case of copper (Figure 6.2), predicted pore water concentrations are up to 3 orders of magnitude higher than observed concentrations in samples with pH less than 4.3. For samples falling in the range pH 4.3 to pH 5.5, predicted concentrations are higher than observed

concentrations by 1 to 2 orders of magnitude. For samples with pH greater than 5.5, predicted pore water concentrations were consistently lower than observed concentrations. The difference between observed and calculated ranged from approximately 0.1 to 1.5 log units. The overall mean deviation between observed and calculated pore water concentrations is 1.28 log units.

For nickel (Figure 6.1), pore water concentrations are over-estimated for all samples by more than 1 log unit. The overall mean deviation between calculated and observed concentrations is 2.74 log units. Cadmium (Figure 6.4) and zinc (Figure 6.3) pore water concentrations are overestimated in most of the samples. Some agreement between model and experiment is observed in samples with pH higher than 6, with the best agreement being observed above pH 7. Even so, the model overestimates cadmium pore water concentrations in this pH range by 0.5 to 2.5 log units. An overall mean deviation of 2.26 log units was obtained.

For zinc, the situation is slightly better, with the model overestimating pore water concentrations by 0.5 to 1 log units. A mean deviation of 1.82 log units is observed for zinc.

Thus, it may be stated that the agreement between observed and calculated pore water concentrations is not good, especially for samples with pH values less than 6. In these samples, the model predicted pore water concentrations virtually equal to the total metal concentration.

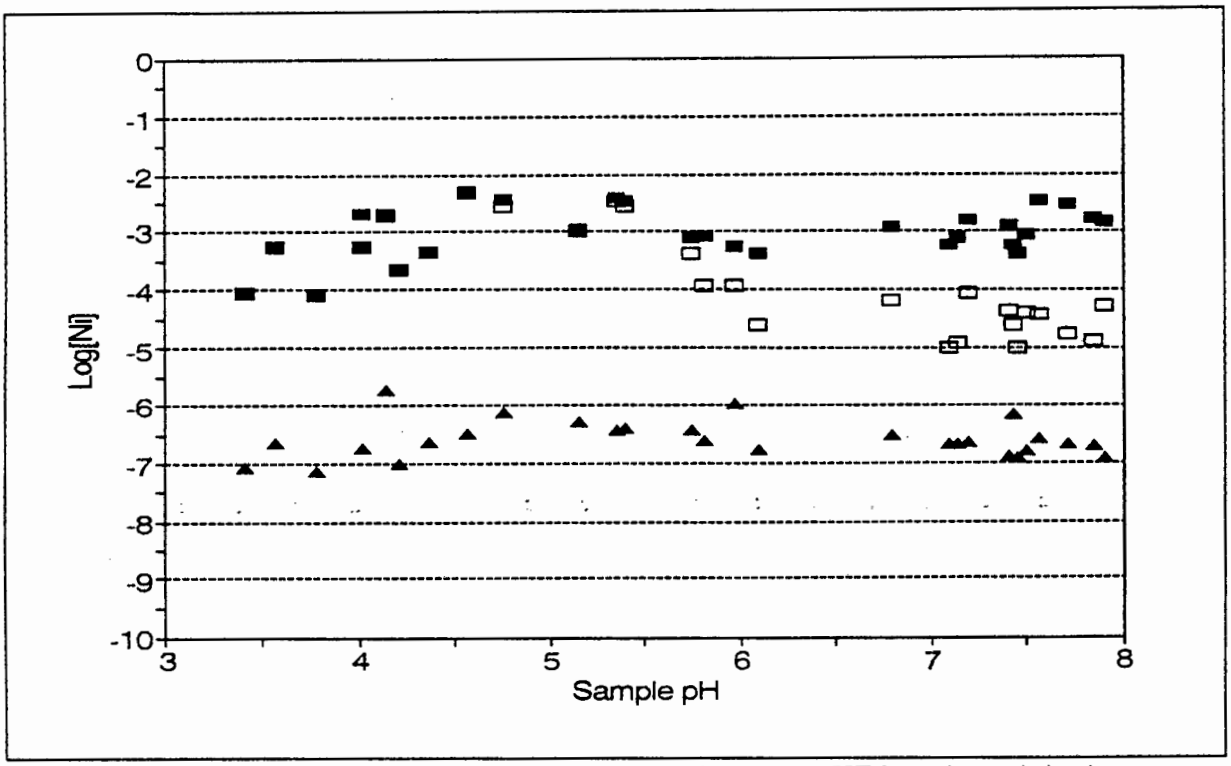

Figure 6.1 Nickel partitioning predicted by model including HFO and precipitation. (■ - $[Ni]_{Tot}$, ▲ - $[Ni_{pw}]_{obs}$, □ - $[Ni_{pw}]_{clc}$).

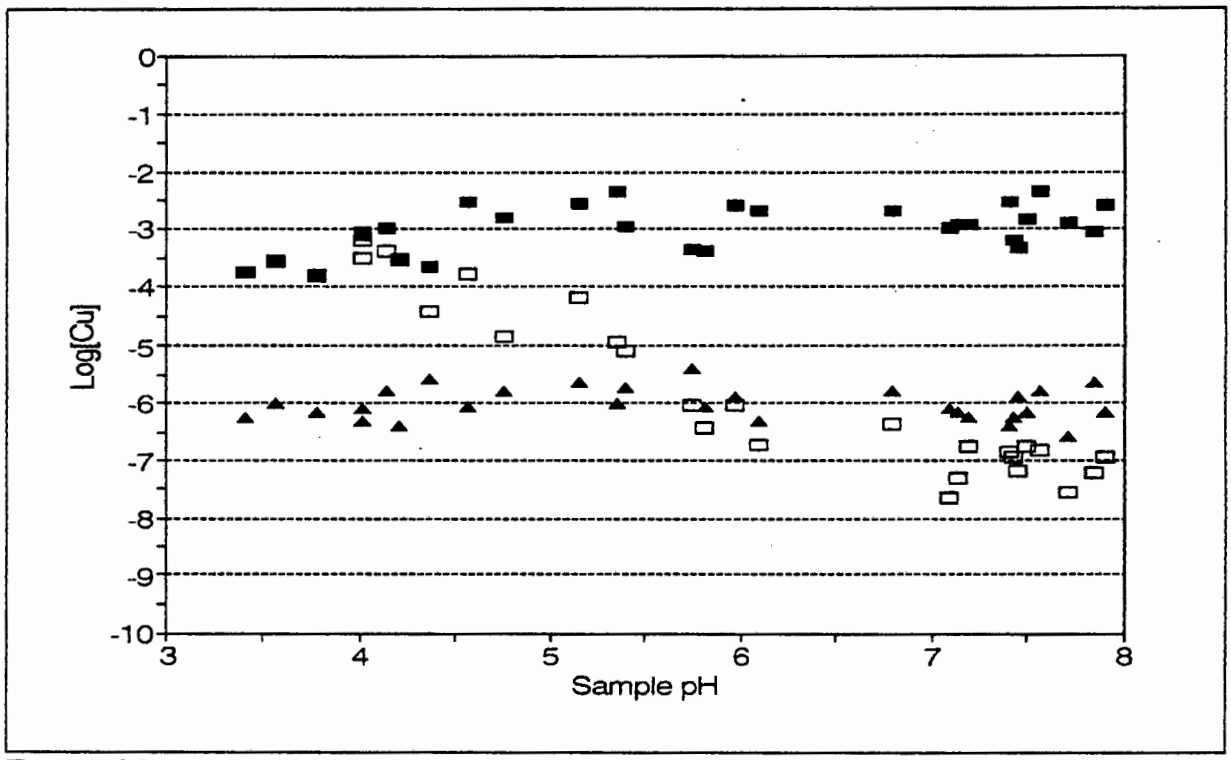

Figure 6.2 Copper partitioning predicted by model including HFO and precipitation. (- $[Cu]_{Tot}$, ▲ - $[Cu_{pw}]_{obs}$, □ - $[Cu_{pw}]_{clc}$).

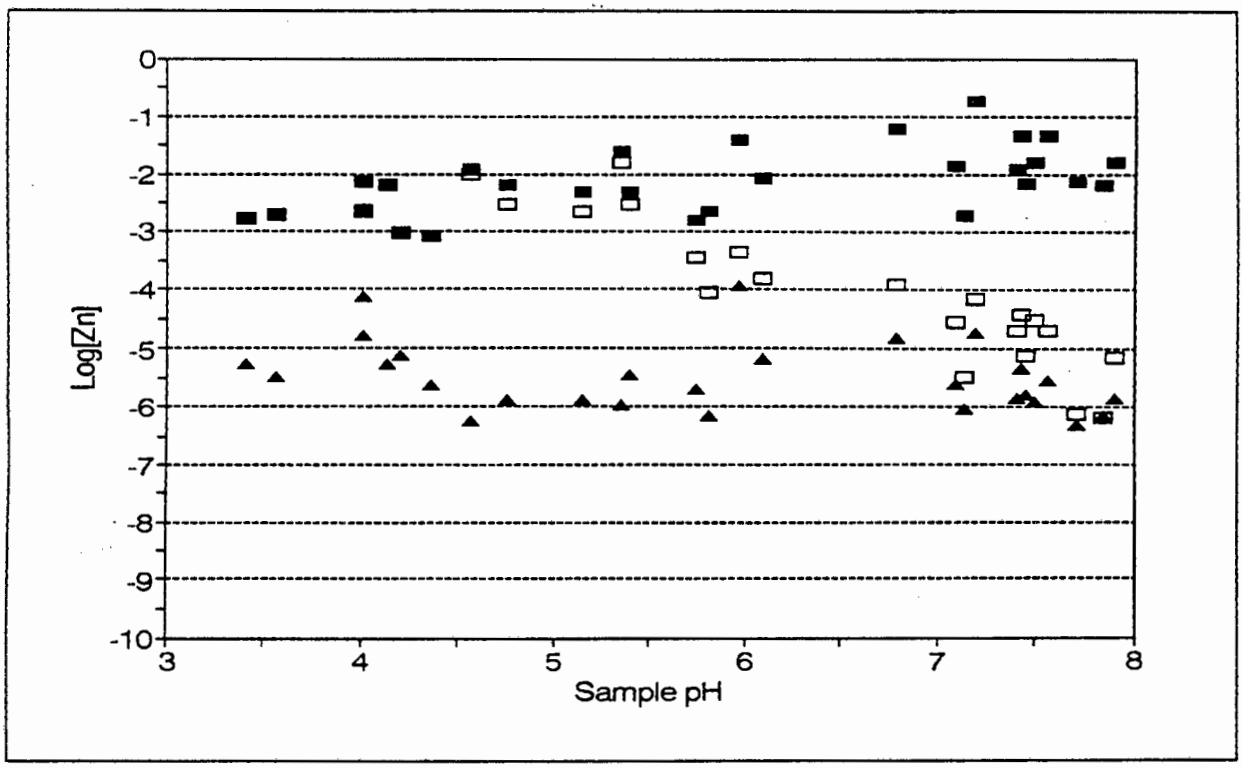

Figure 6.3 Zinc partitioning predicted by model including HFO and precipitation. (- $[Zn]_{Tot}$, ▲ - $[Zn_{pw}]_{obs}$, □ - $[Zn_{pw}]_{clc}$).

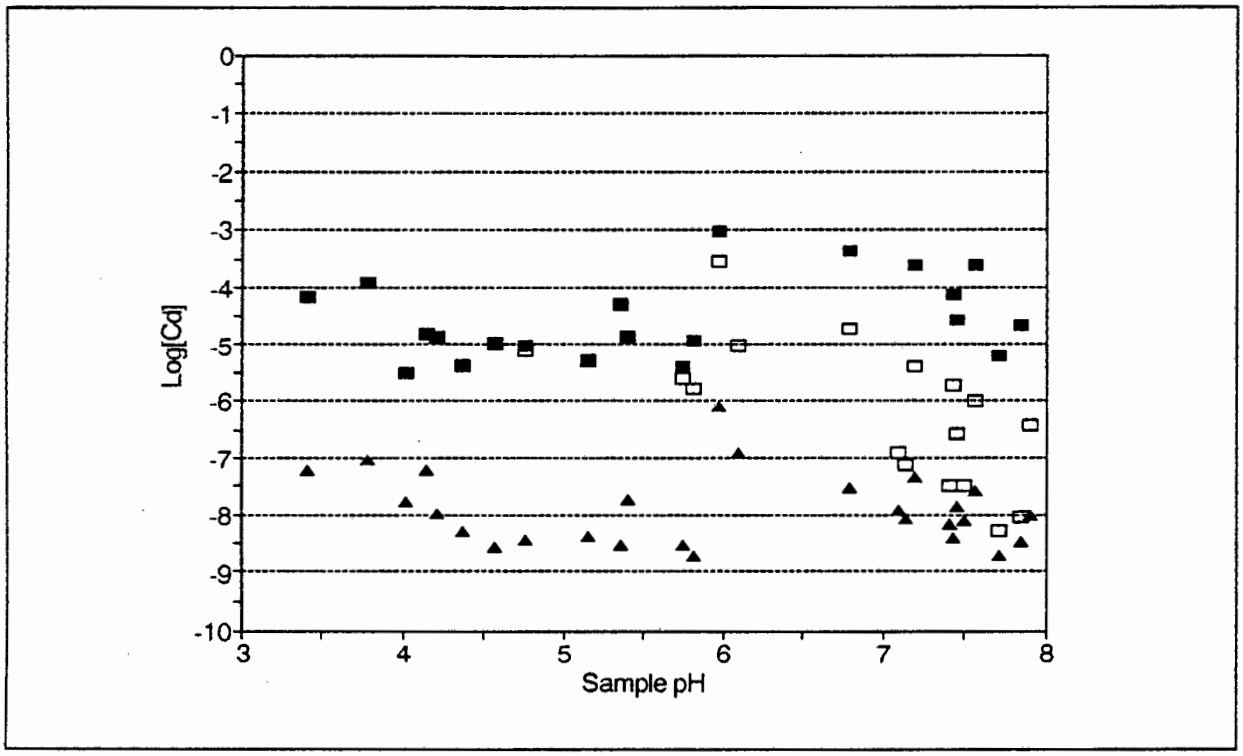

Figure 6.4 Cadmium partitioning predicted by model including HFO and precipitation. (- $[Cd]_{Tot}$, ▲ - $[Cd_{pw}]_{obs}$, □ - $[Cd_{pw}]_{clc}$).

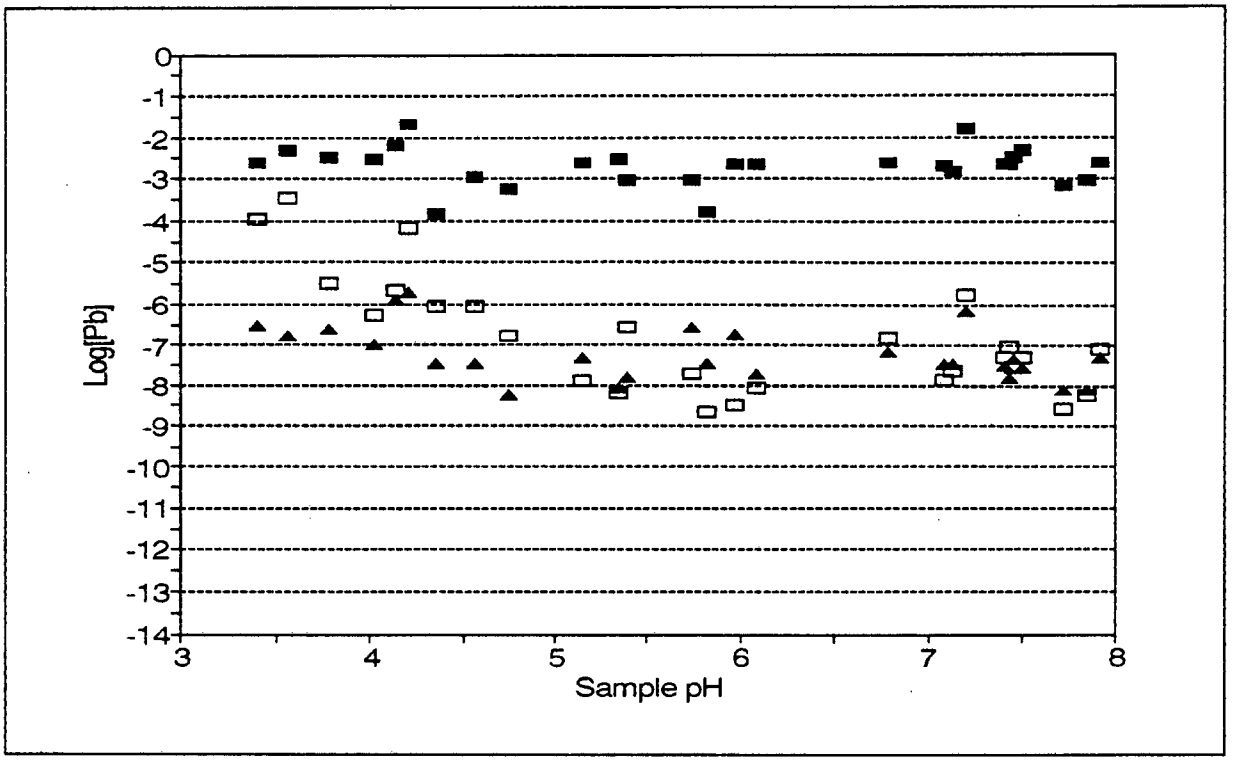

Figure 6.5 Lead partitioning predicted by model including HFO and precipitation. (■ - $[Pb]_{Tot}$, ▲ - $[Pb_{pw}]_{obs}$, □ - $[Pb_{pw}]_{clc}$).

6.2 The HFO-MnO_2-PPT model.

Results for this model are presented in Figures 6.6 to 6.10. The mean deviations observed for each metal are summarized in Table 6.2.

Table 6.2 Mean deviations calculated for the HFO-MnO_2-PPT model.

pH range	Ni	Cu	Zn	Cd	Pb
3.4-4.4	3.11	1.95	2.37	2.78	1.19
4.4-6.1	2.69	0.77	2.48	2.89	1.03
>6.1	1.36	1.03	0.75	1.30	0.99
Overall	2.23	1.20	1.74	2.16	1.05

It is immediately obvious that the inclusion of MnO_2 as a second adsorption phase did not result in a sudden exact agreement between observed and predicted pore water concentrations. However, in general an improvement in the predictions was observed.

As for the previous model, lead pore water concentrations are predicted best by the model (cf Figure 6.10). A mean deviation of 1.05 log units is observed for this metal. Thus, inclusion of MnO_2 led to a decrease in the agreement between model and experiment. If, however, the pH range 3.4 to 4.4 is considered, inclusion of MnO_2 improved the mean deviation from 1.54 for HFO-PPT to 1.19 for HFO-MnO_2-PPT. For samples with pH greater than 6.5, however, inclusion of MnO_2 led to a decrease in the agreement between observed and calculated pore water concentrations. In this pH range, the mean deviation changed from 0.32 for HFO-PPT to 0.99 for HFO-MnO_2-PPT.

Considering copper (Figure 6.7), the inclusion of MnO_2 led to an overall drop in the mean deviation of 0.08 log units. In the pH range 3.4 to 4.4, the improvement between calculated and observed is greatest, with a change in the mean deviation from 2.42 to 1.95 log units. However, in samples with pH greater than 6, the inclusion of MnO_2 led to a decrease in the agreement between observed and predicted pore water concentrations. A similar trend as before is observed, with the model overestimating pore water concentrations for samples in the pH range 3.4 to 5.5 and underestimating pore water concentration for samples with pH greater than 5.5.

The ability of the model to predict pore water concentrations for cadmium is presented in Figure 6.9. An overall mean deviation of 2.16 log units is obtained. This is, however, a slight improvement over the HFO-PPT model, which had a mean deviation of 2.26 log units.

Results for zinc are presented in Figure 6.9. The overall picture is similar to that observed for the HFO-PPT model. However, the inclusion of MnO_2 did result in a slight improvement in the calculated pore water concentrations. A mean deviation of 1.74 log units, compared with the 1.82 log units for the HFO-PPT model, is observed.

Calculated nickel pore water concentrations (Figure 6.6) was impacted most by the inclusion of MnO_2. The model predicted some partitioning into the solid phase to occur even in samples with low pH. This was not observed in the HFO-PPT model. Above pH 6, pore water concentrations are now predicted to range from approximately $3.2x10^{-5}$ mol.dm^{-3} to approximately $6x10^{-7}$ mol.dm^{-3}. This represents approximately a 1 order of magnitude decrease in the calculated pore water concentrations in these samples. The improvement is reflected in the mean deviation of 2.23 log units, compared with 2.74 log units for the previous model.

6.3 Importance of precipitation

In order to asses the role played by precipitation processes in the modelling results, simulations were carried out including only adsorption processes. In these simulations, both HFO and MnO_2 were included as adsorption phases. The mean deviations for each metal calculated with this model are compared with those of the other models in Table 6.3. The exclusion of precipitation processes led to an increase in the mean deviation for all metals, indicating a decrease in the agreement between calculated and experimental results.

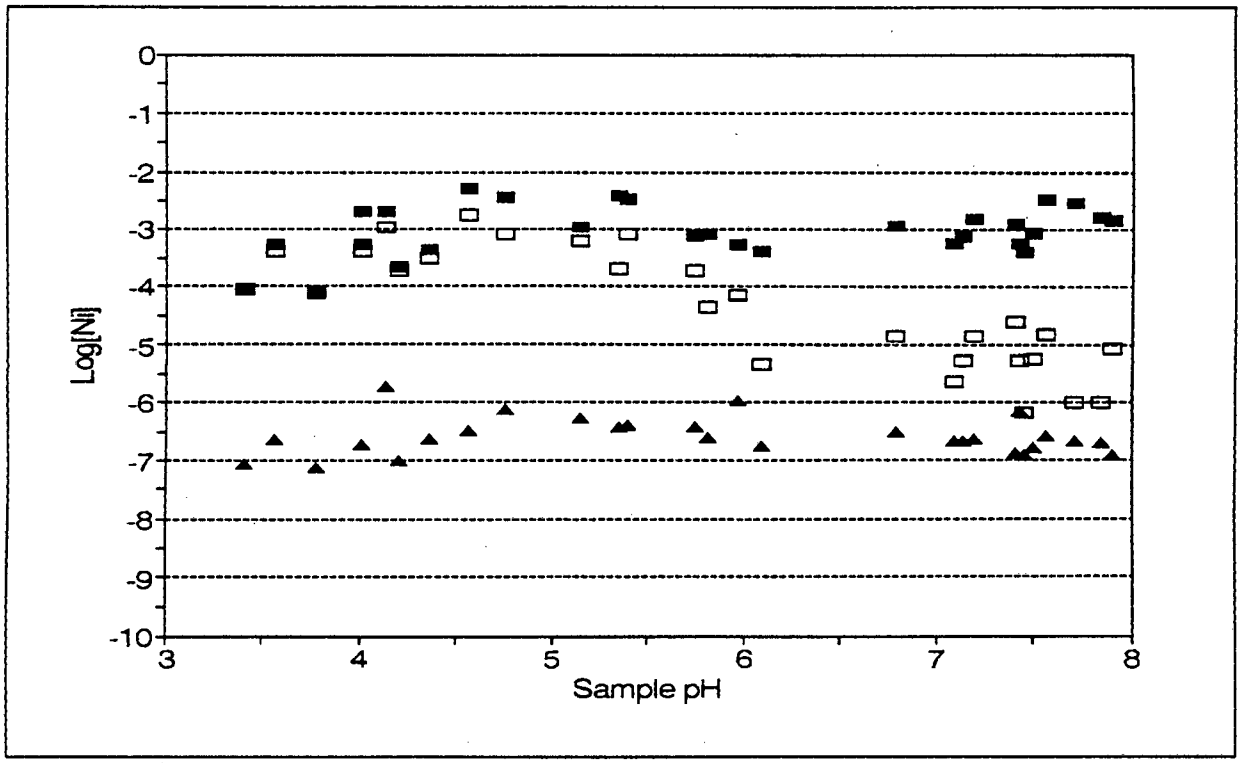

Figure 6.6 Nickel partitioning predicted by model including HFO, MnO_2 and precipitation. (■ - $[Ni]_{Tot}$, ▲ - $[Ni_{pw}]_{obs}$, □ - $[Ni_{pw}]_{clc}$).

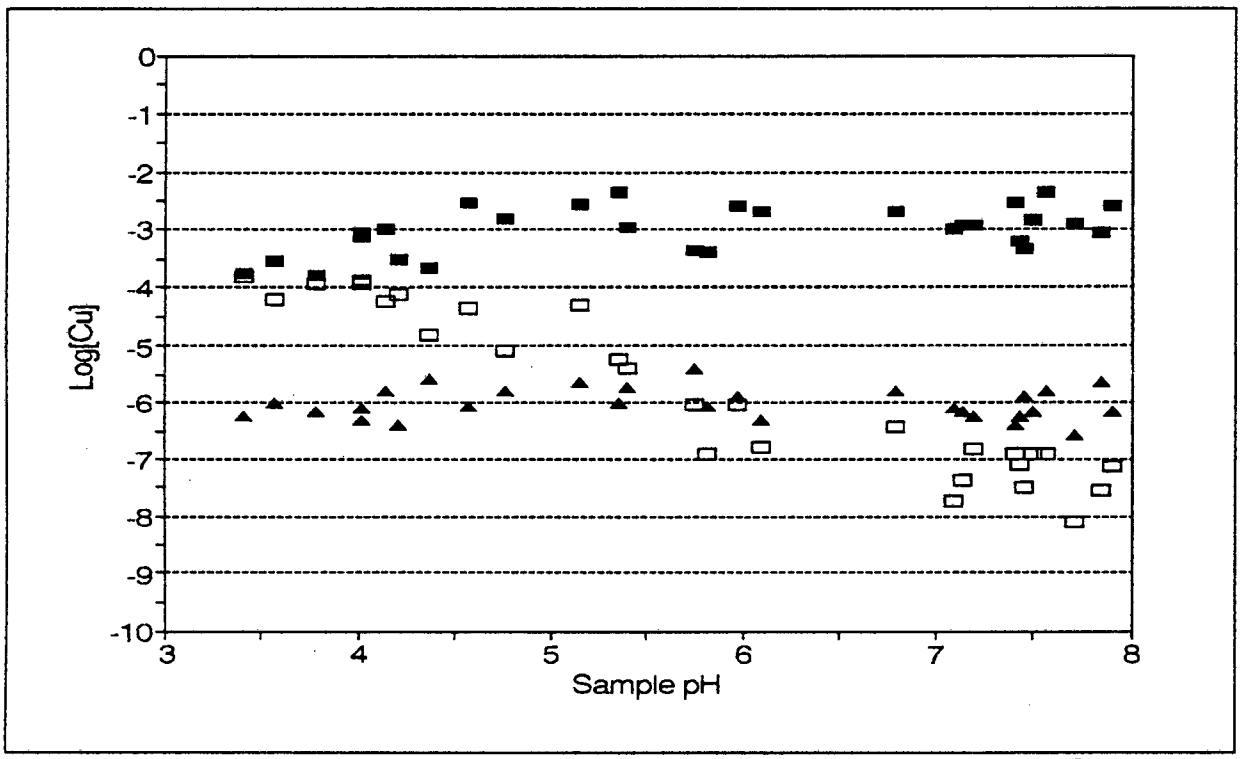

Figure 6.7 Copper partitioning predicted by model including HFO, MnO_2 and precipitation. (■ - $[Cu]_{Tot}$, ▲- $[Cu_{pw}]_{obs}$, □-$[Cu_{pw}]_{clc}$).

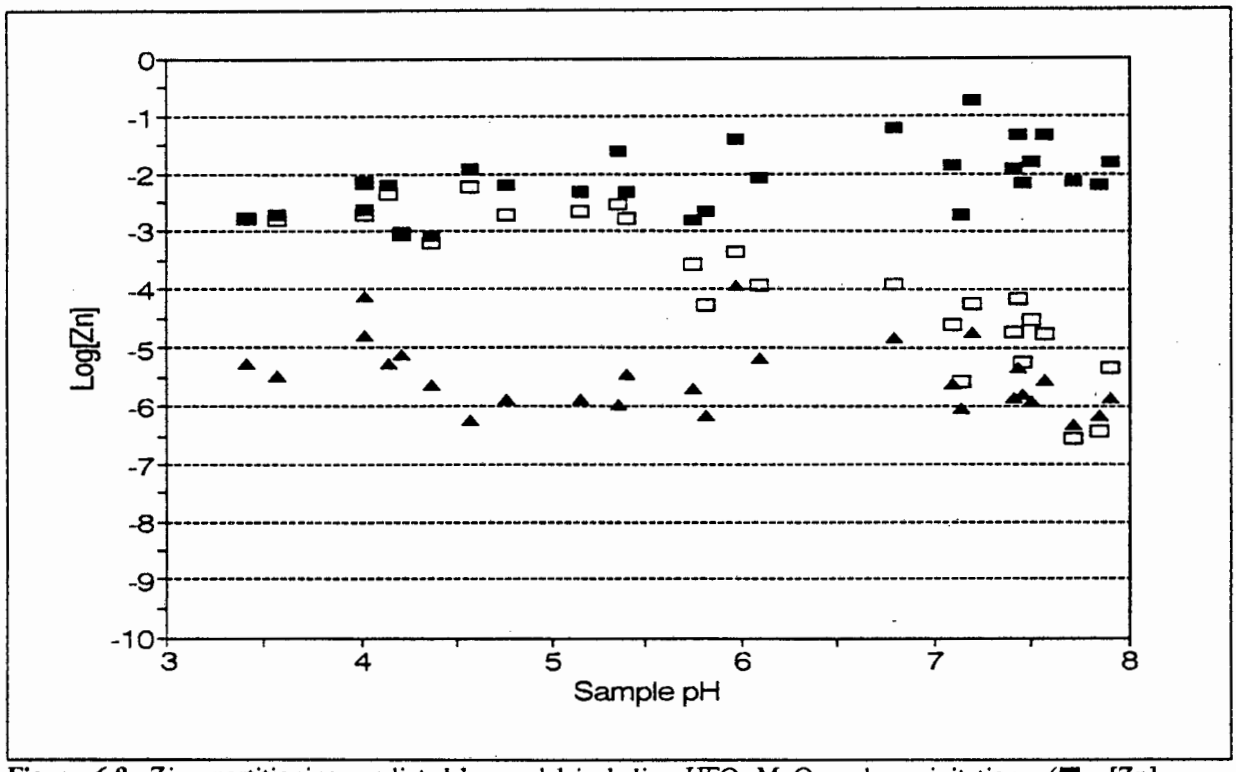

Figure 6.8 Zinc partitioning predicted by model including HFO, MnO_2 and precipitation. (■ - $[Zn]_{Tot}$, ▲ - $[Zn_{pw}]_{obs}$, □ - $[Zn_{pw}]_{clc}$).

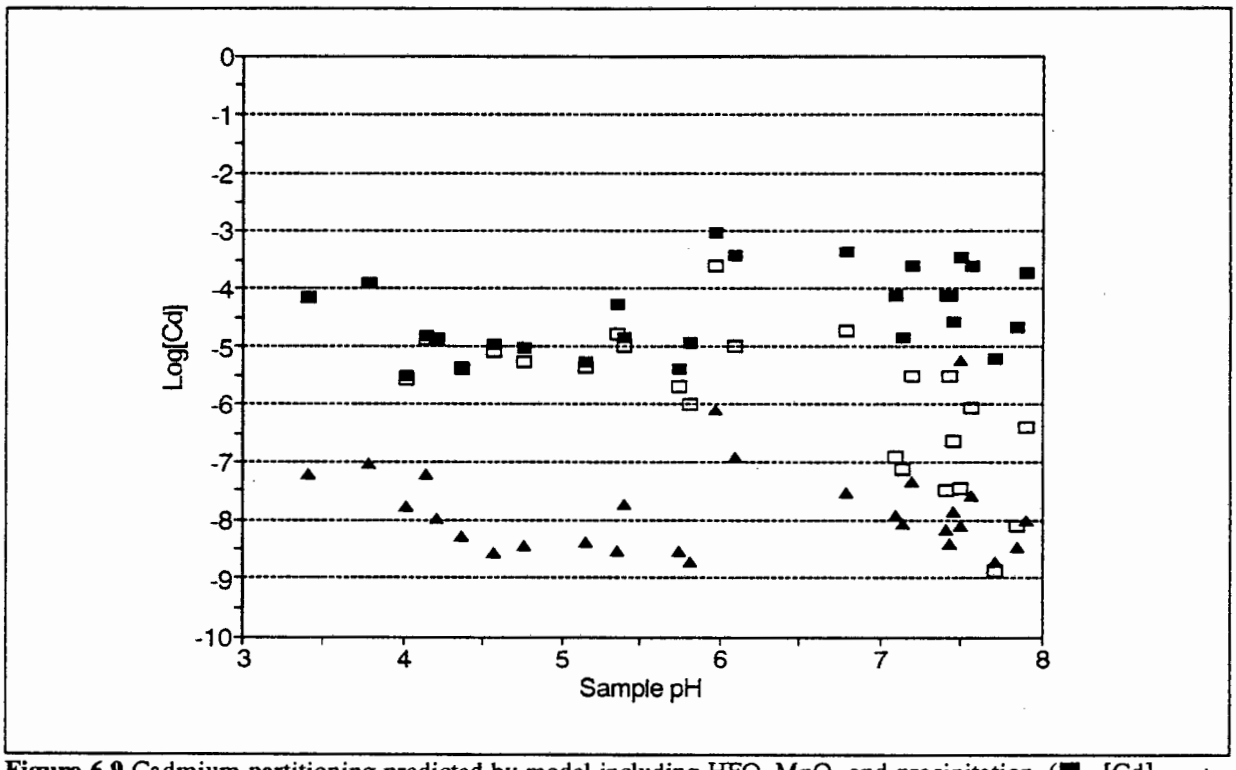

Figure 6.9 Cadmium partitioning predicted by model including HFO, MnO_2 and precipitation. (■ - $[Cd]_{Tot}$, ▲ - $[Cd_{pw}]_{obs}$, □-$[Cd_{pw}]_{clc}$).

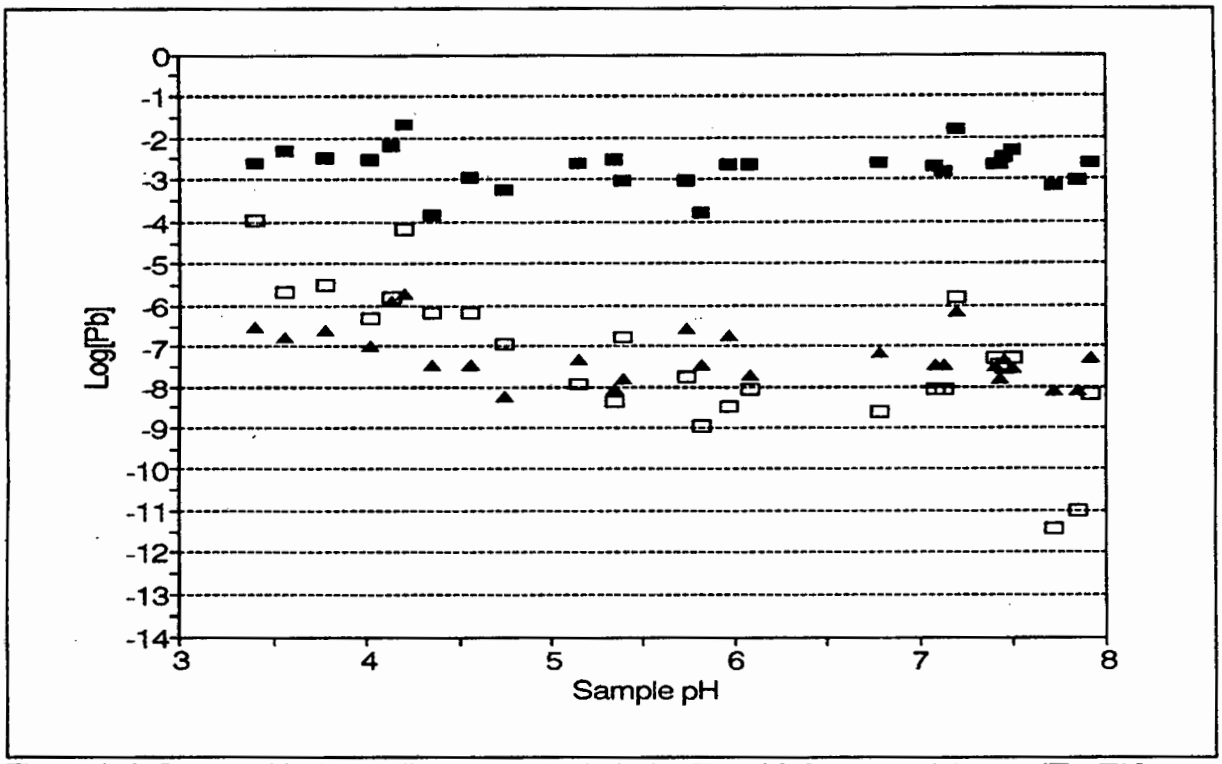

Figure 6.10 Lead partitioning predicted by model including HFO, MnO_2 and precipitation. (■ - $[Pb]_{Tot}$, ▲ - $[Pb_{pw}]_{obs}$, □ - $[Pb_{pw}]_{calc}$).

The improvement in the mean deviation observed for all the metals with precipitation processes included does not, however, arise directly from the formation of precipitates.

Table 6.3 Comparison of the mean deviations obtained for the three models used to predict metal partitioning.

Metal	ADS	HFO-MnO_2-PPT	HFO-PPT
Ni	2.48	2.23	2.74
Cu	1.32	1.20	1.28
Zn	2.10	1.74	1.82
Cd	2.60	2.16	2.26
Pb	1.85	1.05	0.85

Precipitates (carbonates and phosphates) were only formed for zinc, lead and cadmium. The effect of this is to decrease competition for adsorption sites from these metals with copper and nickel, resulting in larger quantities of nickel and copper to be adsorbed. The relative distribution of these metals over the solution, adsorbed and precipitated phases are presented in Figures 6.11 to 6.13. In these figures, samples are indicated using the last alphabetical character present in sample codes, listed in Appendix D.

A number of general observations can be made. First, a difference in trends exhibited by the data sets is immediately obvious. The Janssen data set, depicted by upper case, has a significant number of soils in which precipitation is a contributing factor in controlling metal partitioning. This is not observed in the van den Hoop results, depicted by lower case, with the exception of lead. The van den Hoop data set corresponds to unpolluted soils, whereas the Janssen data set corresponds to polluted soils. This suggests that in unpolluted soils, where metals are present at background levels, adsorption processes dominate metal fate, whereas precipitation plays a significant role in polluted soils. A similar observation was made by Ma and Rao (1997). Using sequential extraction procedures, they found that cadmium distribution over the various soil fractions in their extractions was a function of total cadmium concentration.

6.4 Discussion.

The inclusion of MnO_2 as an additional adsorption phase active in the lower pH ranges led to an improvement in the correspondence between calculated and observed pore water concentrations for samples with low pH. The improvement was most notable for nickel, followed by cadmium, copper and zinc.

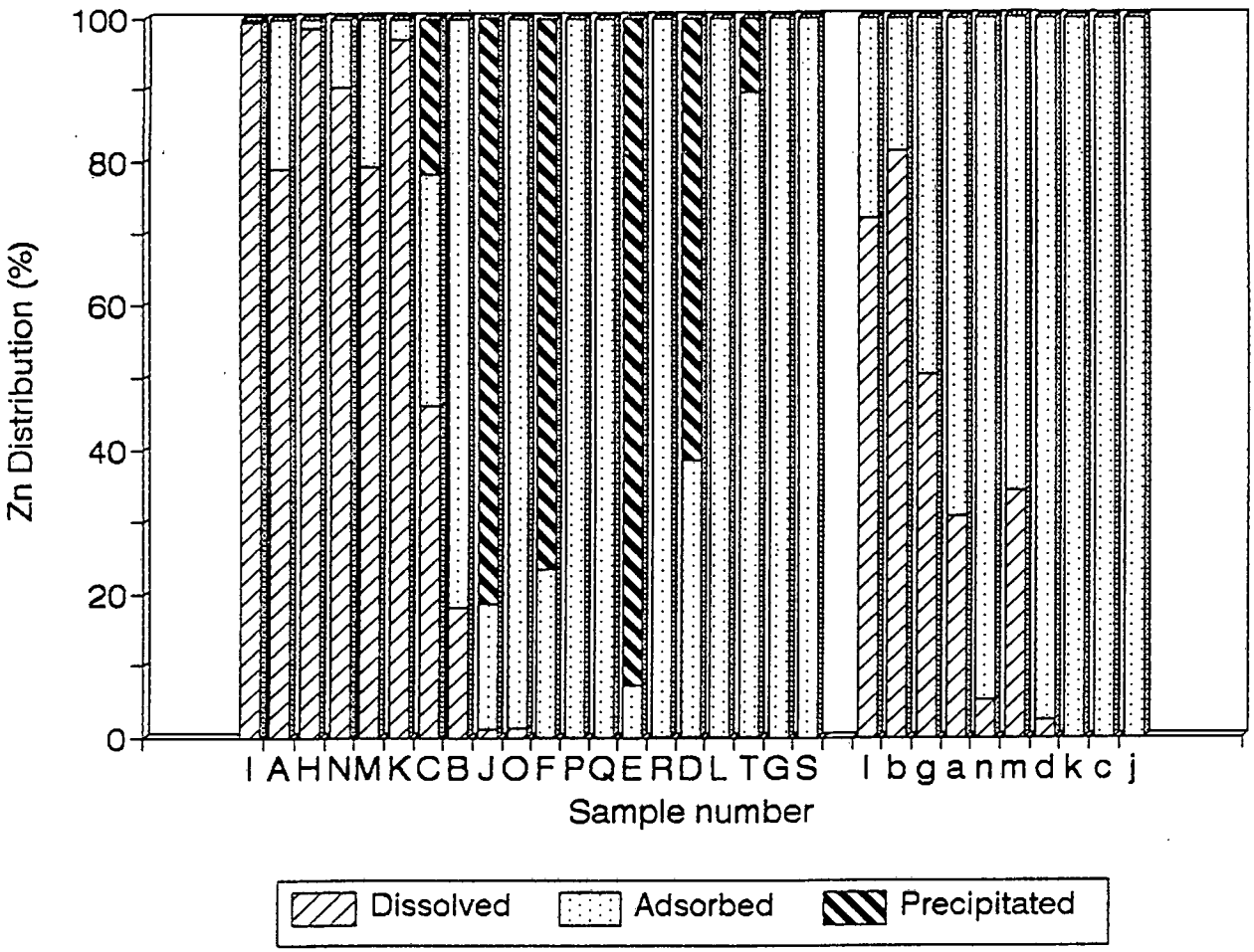

Figure 6.11 Distribution of zinc as dissolved, adsorbed and precipitated species predicted by the model including HFO, δ-MnO_2 and precipitation.

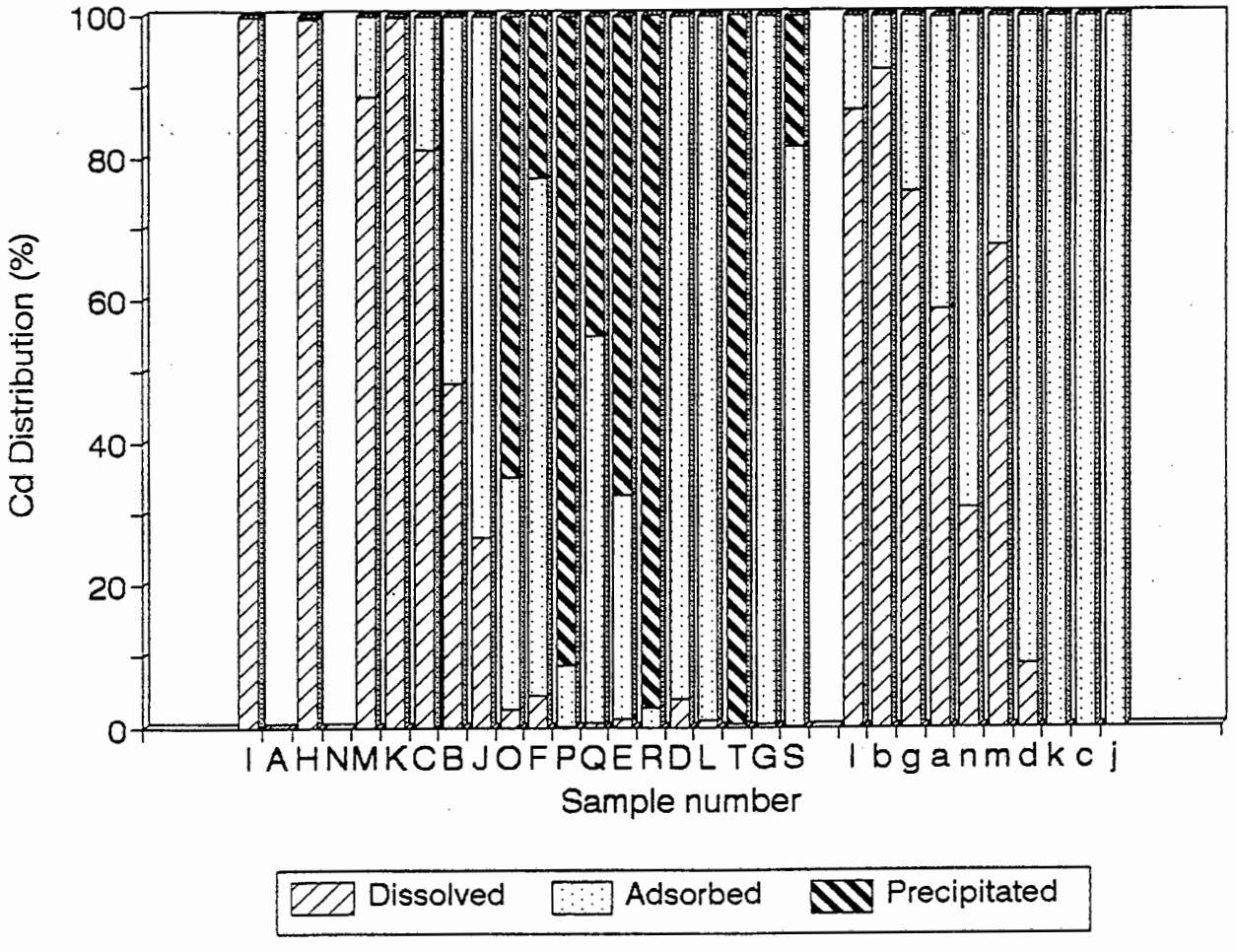

Figure 6.12 Distribution of cadmium as dissolved, adsorbed and precipitated species predicted by the model including HFO, δ-MnO_2 and precipitation.

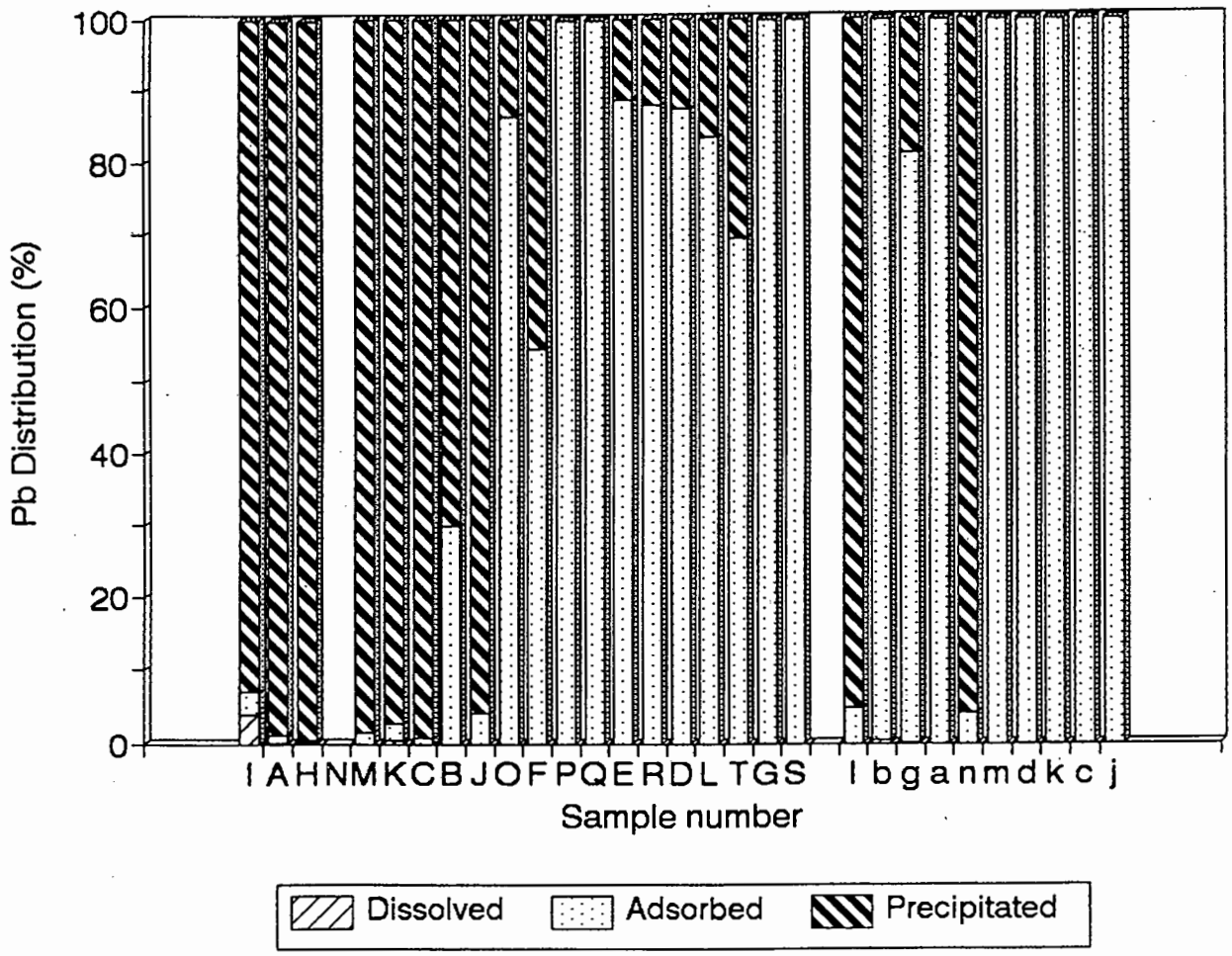

Figure 6.13 Distribution of lead as dissolved, adsorbed and precipitated species predicted by the model including HFO, δ-MnO_2 and precipitation.

The improvement noted for nickel should, however, immediately be seen against the uncertainty in the adsorption parameters for this metal by MnO_2. In the validation exercise reported in Chapter 4, it was found that the current set of adsorption parameters led to an overestimation of nickel adsorbed by MnO_2.

For lead, inclusion of MnO_2 led to a decrease in the agreement between predicted and observed pore water concentrations compared to the HFO-PPT model. This is mainly due to the fact that lead adsorption is overestimated in samples with pH greater than 7. This is interesting since in validating the MnO_2 adsorption parameters for lead, it was found that lead adsorbed was underestimated. It should, however, be kept in mind that the MnO_2 concentration in the soil simulations was set equal to total manganese in the solid phase, which may therefore have resulted in a high estimate of manganese adsorption sites. This, off-course, will impact results for all other metals as well.

Reasons for the discrepancy between calculated and observed pore water concentrations are manifold. The fact that the model overestimates pore water concentrations in the lower pH ranges may be a result of the exclusion of organic matter and clay minerals. In these low pH ranges, organic matter may sorb metal more strongly or they may be sorbed onto the surfaces of soil minerals, causing a change in the sorption properties of the solid phase. At high pH, the organics may desorb (Tipping, 1981; Schlautman and Morgan, 1994; Spark *et al.*, 1997) from the soil minerals so the phases included in the model provide a better approximation of the soil solid phase. Tessier *et al.* (1996) report results which are consistent with this view.

The under-estimation of pore water concentrations at high pH observed for copper and lead may be the result of either or both of the following factors: (i) the assumption that the

adsorption properties of the soil solid phase is the sum of the adsorption properties of HFO and MnO_2 and (ii) the role of solution phase ligands at high pH in solubilizing copper and lead is underestimated.

Anderson and Benjamin (1990a, 1990b) investigated the surface and bulk characteristics of binary aluminium - and iron oxide suspensions. Their results indicated that the properties of binary oxide suspensions can be different from their component parts, even in a physical mixture. It was found that the adsorption of zinc by the binary oxide system was similar to that observed for the component solids. However, in the case of cadmium, it was found that, compared to the pure iron oxide, cadmium adsorption was inhibited in the binary oxide system. Compared with the aluminium oxide system, cadmium adsorption was enhanced. Meng and Letterman (1993) concluded from their investigation of cadmium and calcium adsorption by two mixed oxide systems [$Al(OH)_3/SiO_2$] and [$Fe(OH)_3/SiO_2$] that the adsorption properties of mixed oxide systems are determined by interactions between components and the relative amounts of the components present in the system. They found that in cases where a sufficient amount of either $Fe(OH)_3$ or $Al(OH)_3$ was present to cover the SiO_2 surface completely, calcium and cadmium adsorption were similar to that observed for the pure $Fe(OH)_3$ and $Al(OH)_3$ phases. These results may be summarized by stating that the adsorption behaviour of a multi-component solid phase is not always well approximated by the adsorption behaviour of its constituents.

The role played by solution phase ligands is to compete with the solid phase for metal ions and in doing so, lead to desorption and a concomitant increase in solution phase concentration. It may be that the current model is underestimating the role of DOM at high pH. Woolard (1995) and Pretorius (1990) found that for the complexation of copper by

Suwannee River fulvic acid, RANDOM over-estimated free copper (and therefore underestimated complexed copper) over a wide range of copper concentrations. However, in this work, nothing can be stated with certainty regarding the appropriateness of the set of RANDOM ligands and concentrations used as an approximation of DOM complexation properties. This is a direct result of the fact that no information regarding DOM characteristics was available.

Another aspect which may be responsible for the discrepancy between predicted and observed pore water concentrations is the pore water separation technique employed. Bufflap and Allen (1995) investigated centrifugation, squeezing, vacuum filtration and dialysis as means for collecting pore water. Their results indicate that centrifugation and dialysis provided the best estimates of expected pore water cadmium concentration in an artificial sediment. Both methods, however, underestimated pore water cadmium concentrations. For centrifugation, the difference between expected and observed pore water concentrations was 0.21 log units (expected Log [Cd]: -6.87; observed Log [Cd]: -7.08). The pore water data in the current work were obtained for pore waters extracted with centrifugation. If this degree of underestimation is taken as being typical of the method of pore water collection, the agreement between model and experiment may be taken as being within experimental error for a number of samples in the high pH region. In the low pH region, however, it does not influence the observed agreement. Their is, however, not enough evidence to state unequivocally that the discrepancy observed by Bufflap and Allen is typical for the centrifugation method.

The role of precipitation suggested by the model is an interesting result since this is generally disregarded in the calculation of partitioning coefficients of metals in soils (Bruemmer *et al.*,

1983; Shea, 1988; van den Hoop, 1995; Janssen *et al.*, 1996; Lee *et al.*, 1996). It will, however, immediately be conceded that the model employed is not complete with respect to adsorption phases included since natural organics and clay minerals are not included. This has been shown by a number of workers to be an important sorption phase (Lee *et al.*, 1996; Tiller and Bruemmer, 1984). Inclusion of these adsorption phases in the model may be sufficient to suppress the formation of precipitates. Apart from this, there are also a number of uncertainties regarding to the formation of precipitates which should be discussed.

Marani *et al.* (1995) came to the conclusion that equilibrium modelling is not able to predict lead solids formed in their study on the precipitation of lead in the presence of carbonate and sulphate. They found that satisfactory agreement between solubility predictions and filterable lead concentrations were only obtained with a critical selection of the solid phases considered in the equilibrium model. They used XRD analysis to identify solid phases which formed in their experimental system and allowed only these phases to precipitate in the equilibrium simulations. According to Marani *et al.* (1995), discrepancies between experimental and modelling results may be attributed to (i) non-equilibrium conditions, (ii) soluble and solid species considered and (iii) equilibrium constants used.

Non-equilibrium conditions refer to the fact that the thermodynamically most stable solid phase is not always the phase observed in experiments. This observation may be explained by invoking Ostwald's Step Rule (Morse and Casey, 1988):

If a reaction can result in several products, it is not the stablest state with the least amount of free energy that is initially obtained, but the least stable one, lying nearest to the original state in free energy.

The implication of this observation is that, even though the formation of a solid is thermodynamically favoured, the formation of the solid might be kinetically inhibited (Morse and Casey, 1988). The effect of this is that it may be very difficult, if not impossible, to anticipate beforehand which solid will form under actual system conditions.

Points (ii) and (iii) mentioned by Marani *et al.* deals with the quality of the database employed in the equilibrium calculations as well as the assumption that solid phases formed in soil solutions has the same solubility characteristics as the pure phases to which the thermodynamic data refers. The quality of the data will be discussed in the next paragraph. The second aspect, viz. the similarity between soil solid phases and pure solid phases has been discussed by McBride (1994) and has to do with the formation of solid solutions. The theory of solid solutions predicts that the solubility of an ion can be lowered in a mixed ionic compound relative to the solubility of the pure compound. Thus, the solid phases being formed in soils may have different solubility characteristics from the pure laboratory solids being used as models.

Lead precipitated as chloropyromorphite, $[Pb_5(PO_4)_3Cl]$, cadmium as otavite, $CdCO_3(s)$ while zinc precipitated as $ZnCO_3.H_2O$ and $Zn_3(PO_4)_2.4H_2O$. Thermodynamic data for $[Pb_5(PO_4)_3Cl]$ agrees well amongst the different databases consulted (Log K = 84.43). Thermodynamic data for $ZnCO_3.H_2O$ range from Log K = 10.3 (MINTEQA2) to 10.7 (JESS). Lindsay (1979) and NIST (1989) do not list equilibrium data for $ZnCO_3.H_2O$. For $Zn_3(PO_4)_2.4H_2O$, values range from 32.0 (MINTEQA2) to 35.4 (NIST). JESS lists a value of 35.3. In the soil simulations, the NIST value was used. The equilibrium constant for the formation of otavite according to

$$Cd^{+2} + CO_3^{2-} \rightleftharpoons CdCO_3(s) \quad \ldots\ldots\ldots\ldots\ldots\ldots \quad (A)$$

varies from 11.20 to 13.81, with a value of 13.7 selected in the MINTEQA2 database (Allison *et al.*, 1991). The value contained in the JESS database is 11.7 while the NIST database lists a value of 12.00, which corresponds closely to the value of 11.98 obtained from Lindsay (1979). Rock *et al.* (1994) measured ΔG_f for the reaction $CdCO_3(s) + 2H^+ \rightleftharpoons Cd^{+2} + CO_2(g) + H_2O$ as -671.1 $kJ.mol^{-1}$, which translates to a value of 11.48 for reaction (A). Based on the reported error of 1.01$kJ.mol^{-1}$ in ΔG_f, values ranging from 11.3 to 11.7 is calculated for the Log K of reaction (A). On the basis of this uncertainty, it was decided to use the NIST value (Log K = 12.0) for the formation of otavite according to reaction (A). From the preceding it may be concluded that the thermodynamic data used in the simulations are well determined.

Independent evidence which supports the formation of the precipitates predicted by the model, exists. Davis *et al.* (1993) used Electron Microprobe Analysis to investigate lead phases in soils and waste rock in Butte, Montana. Their results indicated that lead is most frequently present as lead phosphates, such as chloropyromorphite [$Pb_5(PO_4)_3Cl$], corkite [$PbFe_3(PO_4)SO_4(OH)_6$], drugmannite [$Pb_2Fe(PO_4)_2(OH).H_2O$], hinsdallite [$PbAl_3(PO_4)SO_4(OH)_6$ and plumbogummite [$Pb_2Al_3(PO_4)_2(OH)_5.H_2O$]. However, these phosphates were found not to be end members because substitution of Ca and Mn in the crystal lattice gave rise to complex solid-solution systems. Ma *et al.* (1993) studied the *in situ* immobilization of Pb in contaminated soils using hydroxyapatite, [$Ca_{10}(PO_4)_6(OH)_2$]. Their results indicate that Pb is immobilized as hydroxypyromorphite, [$Pb_{10}(PO_4)_6(OH)_2$].

Berti and Cunningham (1997) investigated several soil amendments to inactivate lead in contaminated soils. The amendments employed were portland cement, iron rich materials, KH_2PO_4, humate and natural humus. Of these, addition of KH_2PO_4 proved to be the most successful in immobilizing lead, suggesting the formation of lead phosphate solids.

Kabata-Pendias and Pendias (1985) and Alloway (1995), in their reviews on the behaviour of metals in soils, cite evidence for the occurrence of $CdCO_3(s)$ in soils of pH greater than 7.5. Hickey and Kittrick (1984) and Ma and Rao (1997) used sequential extraction to study the partitioning of cadmium in polluted soils. Their results indicate that a significant amount of total cadmium was associated with the so-called exchangeable fraction, followed by the carbonate fraction. Hickey and Kittrick also found that the amount of cadmium associated with the carbonate fraction increased as soil pH increased. Harrison *et al.* (1981) also used sequential extractions to study the distribution of lead, cadmium, copper and zinc in street dusts and soils. The soils investigated had pH values in the range 6.9 to 8.4. They found that for lead, cadmium and zinc, the carbonate phase was important.

6.5 Conclusion

The results from the modelling exercise may be summarized as follows: using only HFO as a model for the soil solid phase, partitioning of copper and lead was predicted well for samples with pH greater than 4 while for zinc good agreement was observed for samples with pH greater than 6. Poor agreement was observed throughout for cadmium and nickel. Inclusion of MnO_2 as an additional adsorption phase led to an improvement in the agreement between observed and calculated pore water concentrations for four out of the five metals investigated. The improvement was most marked in samples with pH values below 6. Apart from adsorption processes, the formation of precipitates may also be an important mechanism for the partitioning of lead, cadmium and zinc, particularly in polluted soils. There are, however, a number of uncertainties associated with the actual solid phases which will form because of kinetic factors. Therefore, the thermodynamically predicted phase may not always be the phase to form in reality. Furthermore, the model employed is not complete in that the

sorption properties of organic matter associated with the solid phase and those of clay minerals, were not included. Inclusion of these phases may be sufficient to suppress the formation of precipitates.

It is not possible, with the experimental data at our disposal, to isolate unequivocally any specific cause for the discrepancy between observed and predicted pore water metal concentrations. Based on literature evidence, the exclusion of adsorption of natural organic material onto metal (hydr)oxide surfaces, and the adsorption of metals by these organically coated particles, may be largely responsible for the discrepancy observed for low pH samples. For samples of pH greater than 6.5, the underestimation of copper and lead levels in pore waters may be caused by underestimating the complexation capacity of dissolved organic matter present in the pore waters.

Chapter 7 Conclusion

The main objectives of this work were the determination of constants for the adsorption of protons, nickel, copper, zinc, lead and cadmium by δ-MnO_2 and the inclusion of this adsorption phase in an equilibrium model with the aim of predicting the partitioning of the metals of interest over the solid/solution interface in a number of field soils.

Good reproducibility was achieved for replicate potentiometric titrations. The variability observed in the respective titrations is comparable to that reported by other workers who have investigated the surface properties of manganese dioxide. Titrations performed in the presence of metal ion exhibited similar reproducibility to that observed in the protonation study. Examination of titration time profiles indicated that the variability observed in titration data does not result from a systematic, reproducible process since no underlying pattern was evident. No evidence of surface changes due to aging, which would result in variability in titration results, was found. This points to a random or poorly reproducible process being operative.

A new insight provided by the current study is the necessity of a heterogeneous surface model to describe alkalimetric titration data. This is contrary to results reported by other workers investigating manganese dioxide protonation. It was found that the homogeneous surface assumption did not provide a satisfactory description of experimental data. The relative abundance of the more acidic site over the less acidic site has probably led previous workers to overlook the existence of the latter. The existence of surface sites of different chemical reactivities is supported by data available for other solids as well as some structural

information on manganese dioxide. Support for the approach adopted to obtain adsorption constants and binding site concentrations were provided by the successful determination of surface complexation parameters for (i) HFO and (ii) a synthetic data set, generated using a set of hypothetical, known parameters.

The adsorption data obtained for nickel, copper and zinc were described successfully by the heterogeneous surface model assuming the adsorption of M^{2+} and the monohydroxy species, MOH^{+}. Adsorption constants for these species obey the Irving-Williams stability sequence. Cadmium adsorption data could be explained without the adsorption of the hydroxy species being invoked. This may be explained by noting that cadmium does not hydrolyse to the same extent as nickel, copper or zinc. Lead adsorption data were best described by invoking the adsorption of a polynuclear lead species, Pb_2OH^{3+}, to form the surface species $\equiv XOPb_2OH^{2+}$. The formation of this species is supported by EXAFS results.

The surface complexation model was validated against adsorption studies reported in the open literature. The validation of the model was met with mixed success. In general, the surface parameters were able to reproduce literature results in terms of trends observed (i.e. qualitatively), but not always in a quantitative manner. However, comparison of experimental results from different laboratories, or results from the same laboratory but using different batches of the solid, suggests that a large degree of variability in adsorption results are to be expected.

The results obtained from the validation exercise, together with the observation that constants determined for nickel, copper and zinc follow the Irving-Williams series, show that the

objective of measuring constants for the adsorption of nickel, copper, zinc, cadmium and lead by δ-MnO_2 has been fulfilled. The model parameters were not able to reproduce experimental results obtained by independent workers exactly, but then, experimental results suggest that it may be difficult to obtain reproducible results in the first instance. It is thus not possible to decide whether observed discrepancies are a result of model deficiencies or a result of differences in surface properties between the manganese solid employed in this study and those employed by other workers.

In the construction of the soil model, it became clear that several assumptions were necessary, due to (a) incomplete analytical data, (b) the operational nature of the soil solid phase characterization and (c) lack of thermodynamic data for certain important processes, such as the adsorption of organic material by the oxide fraction of the soil solid phase. Also, the inclusion of metal complexation by dissolved organic matter is problematic, necessitating further assumptions. Thermodynamic data for important solution phase reactions were found to be, in general, of variable quality.

Results obtained for the prediction of metal partitioning in soils indicate that, compared to results obtained with HFO as the only sorption phase, the inclusion of manganese dioxide did lead to a slight improvement in the agreement between calculated and observed pore water concentrations. The improvement was most marked in the lower pH ranges. The model also suggested that precipitation is an important process for the partitioning of zinc, cadmium and lead, especially in polluted soils. This, however, should be seen against the background of the numerous uncertainties present in the precipitation process.

The modelling results suggest that there are other processes responsible for the partitioning of metals, particularly in soils of low pH, not accounted for in the model. An immediate candidate for this is metal sorption by particulate organic matter.

In summary, it may be stated that the objectives of the research have been fulfilled in that an equilibrium model of soil systems which includes adsorption parameters for two soil solid phases, has been constructed. There are, however, a number of uncertainties present which warrant further research. These are (i) the uniqueness of the surface parameters determined for manganese dioxide, (ii) the existence of the surface species postulated in these chapters, (iii) the processes which were excluded from the soil equilibrium model, in particular the effects of organic material and (iv) the role played by the formation of precipitates suggested by the model. The uniqueness of adsorption constants should be investigated by studies using different batches of solid under a variety of conditions, such as solid:metal ratios. The existence of the surface species postulated should be pursued using sophisticated spectroscopic techniques, such as EXAFS. The role played by precipitation in metal partitioning should be investigated through the mineralogical characterization of soil systems.

Appendix A δ-MnO_2 adsorption constants at different ionic strengths.

Species	I = 0.1	I = 0.01	I = 0.001	I = 0.00
≡XO^-	-1.27	-1.33	-1.36	-1.38
≡YO^-	-5.99	-6.05	-6.08	-6.10
≡YOH_2^+	3.52	3.58	3.61	3.63
≡$XONi^+$	-1.65	-1.45	-1.36	-1.32
≡$YONi^+$	-1.63	-1.43	-1.34	-1.30
≡XONiOH	-3.70	-3.56	-3.50	-3.48
≡YONiOH	-6.08	-5.94	-5.88	-5.86
≡$XOCu^+$	-1.31	-1.11	-1.02	-0.98
≡$YOCu^+$	-0.20	0.00	0.09	0.13
≡XOCuOH	-3.01	-2.87	-2.81	-2.79
≡YOCuOH	-4.37	-4.23	-4.17	-4.15
≡$XOZn^+$	-1.62	-1.42	-1.33	-1.29
≡$YOZn^+$	-2.39	-2.19	-2.10	-2.06
≡XOZnOH	-3.95	-3.81	-3.75	-3.73
≡YOZnOH	-7.16	-7.02	-6.96	-6.94
≡$XOCd^+$	-1.60	-1.40	-1.31	-1.27
≡$YOCd^+$	-4.32	-4.12	-4.03	-3.99
≡$XOPb_2OH^{+2}$	-1.49	-1.09	-0.91	-0.83

Appendix B Thermodynamic data used in this work compared with other compilations available. Constants are listed at I = 0.0, T = 25°C.

MINTEQ ID	Species	This work	Woolard	NIST	JESS
3300020	OH-	-14.00	-14.00	-14.00	-14.00
3301400	HCO3 -	10.33	10.33	10.33	10.30
3301401	H2CO3 AQ	16.68	16.68	16.68	(16.68;16.70)
3307320	HSO4 -	1.99	1.99	1.99	****
3305800	HPO4 -2	12.35	12.35	12.38	12.35
3305801	H2PO4 -	19.55	19.55	19.58	19.55
3305802	H3PO4	21.70	21.70	21.73	21.84
4603300	MgOH +	-11.20	-11.79	-11.20	-11.40
4601400	MgCO3 AQ	2.92	2.92	2.92	2.92
4601401	MgHCO3 +	11.34	11.41	11.34	(11.20;11.34)
4601403	Mg2CO3 +2	3.68	3.68	*****	*****
4607320	MgSO4 AQ	2.25	2.23	2.23	2.23
4605800	MgPO4 -	6.59	5.86	*****	4.83
4605801	MgH2PO4 +	21.07	20.68	21.23	20.69
4605802	MgHPO4 AQ	15.22	15.16	15.15	(15.10;15.26)
4603304	Mg4(OH)4+4	-39.71	-39.71	*****	-39.66
4601801	MgCl+	0.60	*****	0.60	(-0.46;-0.10)
1503300	CaOH +	-12.70	-12.70	-12.70	-12.80
1501400	CaHCO3 +	11.60	11.58	11.60	(11.43;11.60)
1501401	CaCO3 AQ	3.20	3.15	3.20	3.15
1507320	CaSO4 AQ	2.30	2.30	2.30	(2.30;2.43)
1505800	CaHPO4 AQ	15.04	15.01	15.04	(14.09;15.09)
1505801	CaPO4 -	6.46	6.46	*****	6.46
1505802	CaH2PO4 +	20.96	20.55	21.10	(20.60;20.95)
1504921	CaNO3+	0.50	0.70	0.50	0.60
1504920	Ca(NO3)2	0.60	0.60	*****	0.50
1501403	CaMgCO3+2	4.18	*****	*****	*****
5001400	NaCO3 -	1.27	1.27	1.27	(0.45;1.27)
5001401	NaHCO3 AQ	10.08	10.08	10.08	(10.08;10.51)
5007320	NaSO4 -	0.70	1.03	0.72	(0.65;0.82)
5005801	NaPO4-2	1.83	1.83	1.83	1.83
5005800	NaHPO4 -	13.23	13.20	13.23	(13.00;13.50)
5005802	NaH2PO4	21.64	21.48	*****	21.48
5004920	NaNO3	-0.55	-0.55	-0.55	-0.55
5003300	NaOH	-14.10	-14.18	-14.10	-14.18

MINTEQ ID	Species	This work	Woolard	NIST	JESS
4107320	KSO4 -	0.85	0.85	0.85	0.80
4105801	KPO4-2	1.73	1.73	*****	1.73
4105800	KHPO4 -	12.64	13.00	*****	(12.64;13.40)
4105801	KH2PO4	19.50	*****	*****	*****
4101400	KCO3-	1.27	1.27	*****	1.27
4101401	KHCO3	10.08	10.08	*****	10.08
4104920	KNO3	-0.19	-0.19	-0.19	-0.20
4103300	KOH	-14.46	-14.46	*****	-14.46
4101801	KCl	-0.50	*****	-0.50	(-0.70;0.001)
303300	AlOH +2	-4.99	-4.99	-4.99	-4.99
303301	Al(OH)2 +	-10.10	-10.10	-10.20	-9.30
303302	Al(OH)4 -	-23.00	-23.00	-22.70	-22.90
307320	AlSO4 +	3.02	3.90	3.89	(3.01;3.89)
307321	Al(SO4)2 -	4.92	*****	******	4.90
303303	Al(OH)3 AQ	-16.00	-16.30	-16.50	(-15.90;-15.00)
2803300	FeOH+	-9.40	-9.50	-9.40	-9.50
2803302	Fe(OH)2 AQ	-20.49	-20.60	-20.50	-20.60
2803301	Fe(OH)3 -1	-28.99	-31.00	-28.99	-31.00
2803301	Fe(OH)4 -1	-45.99	-46.00	-45.99	-46.00
2801401	FeHCO3 +	11.43	11.43	11.43	11.43
2807320	FeSO4 AQ	2.25	2.20	2.39	2.20
2805800	FeH2PO4 +	22.25	22.25	22.28	22.25
2805801	FeHPO4 AQ	15.95	15.95	15.98	15.95
4701800	MnCl +	0.61	0.35	*****	0.61
4701801	MnCl2 AQ	0.04	*****	*****	0.04
4701802	MnCl3 -	0.30	*****	*****	0.31
4704921	MnNO3+	0.20	0.20	0.20	0.16
4704920	Mn(NO3)2AQ	0.60	0.60	0.60	0.50
4703300	MnOH +	-10.59	-10.59	-10.60	(-10.59;-10.20)
4703302	Mn(OH)2	-22.20	-22.20	*****	*****
4703301	Mn(OH)3 -1	-34.80	-34.80	*****	(-34.80;-34.18)
4703303	Mn(OH)4 -2	-48.30	*****	-48.30	-48.30
4703304	Mn2(OH)+3	-10.56	-10.56	-7.20	(-10.60;-10.10)
4703305	Mn2(OH)3 +	-23.90	-23.90	-23.90	(-24.90;-23.90)
4707320	MnSO4 AQ	2.26	2.26	2.26	2.26
4701401	MnCO3	4.32	4.32	*****	6.50
4701400	MnHCO3 +	11.60	11.60	11.63	(11.20;11.60)
4705800	MnPO4-	7.20	*****	*****	*****
4705801	MnHPO4	15.29	15.29	*****	(16.09;16.30)
4705802	MnH2PO4	20.90	*****	*****	*****

MINTEQ ID	Species	This work	Woolard	NIST	JESS
2311402	CuHCO3 +	12.13	12.13	12.13	12.13
2311400	CuCO3 AQ	6.73	6.80	6.77	6.80
2311401	Cu(CO3)2-2	10.20	10.80	10.20	10.20
2311403	CuOHCO3-	-2.41	-2.41	*****	*****
2311800	CuCl +	0.20	0.35	0.20	0.02
2311801	CuCl2 AQ	0.16	0.48	*****	-0.7
2311802	CuCl3 -	-2.29	*****	*****	-2
2311803	CuCl4 -2	-4.59	*****	*****	-5
2313300	CuOH +	-7.50	-7.50	-7.50	*****
2313301	Cu(OH)2 AQ	-16.20	-16.22	-16.19	*****
2313302	Cu(OH)3 -	-26.90	-28.00	*****	*****
2313303	Cu(OH)4 -2	-39.60	-39.60	*****	*****
2313304	Cu2(OH)2+2	-10.36	-10.75	-10.59	-10.75
2314920	CuNO3+	0.50	0.50	0.50	0.50
2314921	Cu(NO3)2	-0.43	-0.43	-0.40	-0.40
2315800	$CuPO_4^-$	9.80	*****	*****	*****
2315801	CuHPO4	16.39	16.39	*****	16.39
2315802	Cu(H2PO4)+	21.25	21.25	*****	21.25
2317320	CuSO4 AQ	2.31	2.34	2.34	2.40
9501800	ZnCl +	0.43	0.05	0.46	0.40
9501801	ZnCl2 AQ	0.60	0.60	0.60	0.60
9501802	ZnCl3 -	0.50	0.50	*****	0.50
9501803	ZnCl4 -2	0.20	0.20	*****	0.88
9503300	ZnOH +	-9.00	-9.00	-9.00	-9.00
9503301	Zn(OH)2 AQ	-17.79	-18.90	-17.79	-18.90
9503302	Zn(OH)3 -	-28.10	-28.40	-28.10	*****
9503303	Zn(OH)4 -2	-40.50	-38.02	-40.49	*****
9503304	Zn2(OH) +3	-9.00	-9.00	*****	-9.00
9501804	ZnOHCl AQ	-7.48	*****	*****	*****
9507320	ZnSO4 AQ	2.34	2.34	2.34	(2.11;2.40)
9507321	Zn(SO4)2-2	3.28	3.60	*****	3.60
9501400	ZnHCO3 +	11.74	11.97	11.74	11.97
9501401	ZnCO3 AQ	5.10	4.75	5.10	5.00
9501402	Zn(CO3)2-2	9.63	*****	*****	*****
9504920	ZnNO3 +	0.40	0.40	*****	*****
9504921	Zn(NO3)2	-0.30	0.65	-0.30	-0.30
9505801	Zn(HPO4)	15.59	15.59	*****	15.59
9505802	Zn(H2PO4)+	21.15	21.15	*****	21.15
1601800	CdCl +	1.98	1.98	1.97	1.97
1601801	CdCl2 AQ	2.60	2.59	2.60	2.60
1601802	CdCl3 -	2.40	2.40	2.40	2.40

MINTEQ ID	Species	This work	Woolard	NIST	JESS
1601803	CdCl4 2-	1.70	1.70	*****	1.70
1603300	CdOH +	-10.08	-10.08	-10.10	-10.08
1603301	Cd(OH)2 AQ	-20.35	-20.35	-20.29	*****
1603302	Cd(OH)3 -	-33.30	-32.06	*****	*****
1603303	Cd(OH)4 -2	-47.35	-47.35	-47.29	*****
1603304	Cd2OH +3	-9.39	-9.39	-9.40	-9.39
1603305	Cd4(OH)4+4	-32.85	-32.85	-32.79	*****
1601804	CdOHCl AQ	-7.40	*****	*****	*****
1604920	CdNO3 +	0.50	0.50	0.50	0.50
1604921	Cd(NO3)2	0.20	0.20	0.20	0.20
1607320	CdSO4 AQ	2.46	2.46	2.46	2.50
1607321	Cd(SO4)2-2	3.50	3.65	*****	3.50
1605801	$CdPO_4^-$	6.50	*****	*****	*****
1605802	Cd(HPO4)	16.73	16.73	*****	*****
1605803	Cd(H2PO4)+	20.93	20.93	******	*****
1601400	CdHCO3 +	12.40	*****	*****	12.40
1601401	CdCO3 AQ	5.40	4.33	*****	4.30
1601402	Cd(CO3)2-2	4.60	*****	*****	4.60
1601403	Cd(CO3)3-4	6.22	*****	*****	6.22
6001800	PbCl +	1.60	1.51	1.55	0.84
6001801	PbCl2 AQ	2.20	2.16	2.20	1.10
6001802	PbCl3 -	1.80	2.00	1.80	1.22
6001803	PbCl4 -2	1.38	1.10	*****	1.10
6003300	PbOH +	-7.60	-7.65	-7.60	-7.65
6003301	Pb(OH)2 AQ	-17.10	-17.10	-17.09	-17.10
6003302	Pb(OH)3 -	-28.10	-28.10	-28.09	*****
6003305	Pb(OH)4 -2	-39.70	*****	*****	*****
6003303	Pb2OH +3	-6.36	-6.36	-6.40	*****
6003304	Pb3(OH)4+2	-23.88	-23.40	-23.89	*****
6003305	Pb4(OH)4+4	-20.00	-20.84	-19.99	*****
6003306	Pb6(OH)8+4	-43.60	-43.43	-43.43	-43.58
6004920	PbNO3 +	1.17	1.17	1.17	1.10
6004921	Pb(NO3)2	1.40	1.40	1.40	1.40
6007320	PbSO4 AQ	2.69	2.70	2.69	2.75
6007321	Pb(SO4)2-2	3.47	4.74	*****	3.47
6001401	PbCO3 AQ	7.24	7.00	*****	7.00
6001400	Pb(CO3)2-2	10.64	10.50	*****	10.40
6001402	PbHCO3 +	13.20	*****	*****	*****
6001403	PbOHCO3 -	-3.30	-3.30	*****	-3.30
6005801	$PbPO_4^-$	9.10	*****	*****	*****
6005802	PbHPO4	15.48	15.45	15.48	15.45
6005803	Pb(H2PO4)+	21.05	21.05	21.08	21.05

MINTEQ ID	Species	This work	Woolard	NIST	JESS
5401800	NiCl +	0.40	0.55	*****	0.55
5401801	NiCl2 AQ	0.96	*****	*****	0.96
5403300	NiOH +	-9.90	-9.86	-9.90	-9.86
5403301	Ni(OH)2 AQ	-19.00	-19.00	-19.00	*****
5403302	Ni(OH)3 -	-30.00	-30.00	-29.99	*****
5403303	Ni(OH)4-2	-44.00	*****	*****	*****
5403304	Ni2(OH)+3	-10.70	-10.70	*****	*****
5403305	Ni4(OH)4+4	-27.74	-27.74	-27.69	-27.74
5404920	NiNO3+	0.40	0.50	0.40	0.40
5404921	Ni(NO3)2	0.00	0.00	*****	0.00
5405801	NiHPO4 AQ	15.29	15.29	*****	15.29
5405800	NiH2PO4+	20.43	20.43	*****	20.43
5401401	NiCO3 AQ	6.87	4.91	*****	4.91
5401402	Ni(CO3)2-2	10.11	*****	*****	*****
5401400	NiHCO3 +	12.47	12.29	*****	12.83
5407320	NiSO4 AQ	2.29	2.34	2.34	2.30
5407321	Ni(SO4)2-2	1.02	3.47	*****	3.47
5405802	$NiPO_4^-$	8.40	*****	*****	*****

**** data for species not listed in this data base

Appendix C Metal stock solution concentrations

All reagents used were Merck pro analysi

2.037×10^{-3} mol.dm^{-3} $Ni(NO_3)_2.6H_2O$

2.088×10^{-3} mol.dm^{-3} $Cu(NO_3)_2.2H_2O$

2.070×10^{-3} mol.dm^{-3} $Zn(NO_3)_2.4H_2O$

2.549×10^{-3} mol.dm^{-3} $Cd(NO_3)_2.4H_2O$

2.020×10^{-3} mol.dm^{-3} $Pb(NO_3)_2$

Appendix D Analytical results for soil samples simulated.

Table D.1 Anion concentrations and pH measured in pore waters by van den Hoop (1995).

Sample	pH	DOC mol/l	PO_4^{3-} mol/l	Cl^- mol/l	NO_3^- mol/l	SO_4^{2-} mol/l
E930423A	4.75	1.26e-03	2.60e-07	1.11e-03	4.58e-03	3.20e-04
E930423B	4.36	3.00e-03	7.60e-07	7.58e-04	7.51e-04	1.11e-02
E930611C	7.72	2.40e-03	1.90e-07	6.17e-04	2.14e-03	1.62e-03
E930624D	5.82	3.93e-03	4.30e-07	1.62e-03	2.05e-04	1.18e-03
E930707G	4.56	5.45e-03	1.20e-06	1.52e-03	2.33e-04	7.46e-04
E930715J	7.85	6.73e-03	1.17e-05	3.84e-03	4.61e-04	1.50e-03
E930715K	6.50	3.33e-03	1.50e-07	3.73e-04	3.33e-04	6.51e-04
E930715L	4.14	4.44e-03	8.47e-06	5.44e-04	6.57e-03	4.46e-04
E930720M	5.39	4.44e-03	2.40e-07	2.39e-03	4.83e-03	2.61e-03
E930720N	5.35	4.44e-03	1.24e-04	9.52e-04	2.08e-04	3.56e-04

Table D.2 Cation concentrations in pore waters collected by van den Hoop (1995).

Sample	K mol/l	Na mol/l	Ca mol/l	Mg mol/l
E930423A	2.305e-05	1.266e-03	2.124e-03	5.711e-04
E930423B	7.121e-05	8.243e-04	9.687e-03	1.853e-03
E930611C	1.983e-04	4.724e-04	3.570e-03	3.098e-04
E930624D	1.101e-05	1.445e-03	1.511e-03	2.370e-04
E930707G	2.997e-05	1.288e-03	1.018e-03	2.728e-04
E930715J	3.099e-05	1.368e-03	4.156e-03	7.019e-04
E930715K	9.990e-06	4.132e-04	8.890e-04	1.588e-04
E930715L	5.428e-04	7.956e-04	2.671e-03	8.077e-04
E930720M	6.301e-05	2.050e-03	4.238e-03	1.308e-03
E930720N	1.281e-04	6.211e-04	8.281e-04	1.921e-04

Table D.3 Metal concentrations in pore waters collected by van den Hoop (1995).

Sample	Fe mol/l	Mn mol/l	Cd mol/l	Cu mol/l	Ni mol/l	Pb mol/l	Zn mol/l
E930423A	1.16e-05	6.65e-07	3.74e-09	1.67e-06	7.63e-07	5.99e-09	1.30e-06
E930423B	4.66e-06	4.72e-05	5.34e-09	2.83e-06	2.31e-07	3.50e-08	2.30e-06
E930611C	3.04e-06	1.49e-08	1.87e-09	2.65e-07	2.09e-07	8.01e-09	5.00e-07
E930624D	1.10e-04	1.56e-06	1.96e-09	8.75e-07	2.52e-07	3.60e-08	7.00e-07
E930707G	4.48e-06	1.14e-06	2.85e-09	8.35e-07	3.25e-07	1.80e-08	6.00e-07
E930715J	5.37e-06	1.24e-07	3.47e-09	2.34e-06	2.04e-07	8.01e-09	7.00e-07
E930715K	3.76e-06	5.05e-07	3.38e-09	1.02e-06	2.17e-07	5.99e-09	1.00e-06
E930715L	9.49e-06	8.67e-05	6.18e-08	1.63e-06	1.91e-06	1.27e-06	5.10e-06
E930720M	1.24e-05	7.59e-06	1.91e-08	1.96e-06	5.15e-07	1.60e-08	3.60e-06
E930720N	6.27e-06	3.75e-07	3.03e-09	1.03e-06	3.82e-07	8.98e-09	1.10e-06

Table D.4 Solid phase metal concentrations determined by concentrated HNO_3 destruction of soil samples (van den Hoop, 1995).

Sample	Cd mol/l	Cu mol/l	Ni mol/l	Pb mol/l	Zn mol/l
E930423A	9.45e-06	1.53e-03	3.52e-03	5.81e-04	6.24e-03
E930423B	4.21e-06	2.12e-04	4.42e-04	1.48e-04	8.59e-04
E930611C	6.09e-06	1.26e-03	2.89e-03	7.15e-04	7.20e-03
E930624D	1.14e-05	4.08e-04	8.38e-04	1.66e-04	2.34e-03
E930707G	1.08e-05	2.88e-03	5.00e-03	1.12e-03	1.17e-02
E930715J	2.16e-05	9.32e-04	1.67e-03	9.12e-03	6.42e-03
E930715K	1.86e-05	1.70e-03	4.13e-03	7.04e-04	8.45e-03
E930715L	1.56e-05	1.06e-03	2.02e-03	6.49e-03	6.32e-03
E930720M	1.48e-05	1.14e-03	3.28e-03	8.84e-04	4.86e-03
E930720N	5.59e-05	4.52e-03	4.01e-03	2.85e-03	2.49e-02

Table D.5 Anion concentrations in pore waters collected by Janssen *et al.* (1996).

	pH	DOC mol/l	CO_3^{2-}-TOT mol/l	Cl^- mol/l	NO_3^- mol/l	PO_4^{-3} mol/l	SO_4^{-2} mol/l
E941018A	3.57	4.31e-03	5.45e-04	2.87e-04	8.79e-04	1.24e-05	8.15e-05
E941027B	5.74	6.25e-03	3.66e-04	9.04e-04	1.26e-03	1.80e-06	1.24e-03
E941027C	5.15	7.37e-03	4.48e-04	8.69e-04	1.00e-06	4.53e-05	4.36e-04
E941102D	7.43	9.47e-03	5.07e-03	7.73e-04	2.95e-05	3.10e-06	1.45e-02
E941102E	7.2	5.63e-03	1.57e-03	6.85e-05	7.17e-05	1.41e-05	2.88e-04
E941102F	6.79	7.34e-03	7.16e-04	1.56e-04	3.89e-04	2.97e-06	3.89e-04
E941102G	7.57	6.32e-03	6.35e-03	1.12e-03	4.02e-05	3.39e-06	4.34e-03
E941103H	3.78	7.30e-03	6.70e-05	1.85e-04	2.26e-05	3.12e-06	1.22e-04
E941103I	3.4	1.22e-02	1.06e-04	2.31e-04	6.76e-05	7.30e-06	2.64e-04
E941103J	5.97	4.85e-03	3.70e-04	5.39e-04	1.55e-04	1.38e-05	1.44e-03
E941104K	4.21	1.24e-02	3.08e-04	0.00	0.00	2.13e-05	0.00
E941104L	7.45	1.23e-02	7.01e-03	3.18e-03	2.14e-04	1.30e-05	1.01e-03
E941122M	4.02	4.66e-03	2.40e-05	2.08e-04	9.30e-04	1.97e-05	8.53e-05
E941122N	4.01	4.47e-03	1.90e-05	5.67e-04	9.80e-04	5.50e-07	9.82e-05
E941125O	6.09	2.86e-03	6.65e-04	1.97e-03	2.09e-04	8.90e-07	2.43e-03
E941128P	7.09	1.77e-03	5.64e-03	4.71e-03	4.30e-06	6.83e-06	1.15e-03
E941128Q	7.14	4.50e-03	1.29e-03	7.99e-04	7.03e-04	1.52e-05	1.11e-03
E941128R	7.41	1.70e-03	4.46e-03	3.90e-03	1.00e-05	8.00e-07	1.81e-03
E941129S	7.91	2.20e-03	4.36e-03	1.62e-03	2.12e-04	4.78e-06	9.87e-04
E941129T	7.5	2.89e-03	3.97e-03	2.22e-03	7.48e-04	7.81e-06	1.17e-03

Table D.6 Cation concentrations in pore waters collected by Janssen *et al.* (1996).

Sample	K mol/l	Na mol/l	Ca mol/l	Mg mol/l
E941129S	6.07e-04	1.33e-03	2.91e-03	4.10e-04
E941102G	1.54e-04	1.09e-03	6.92e-03	7.04e-04
E941129T	1.07e-03	1.78e-03	2.81e-03	5.61e-04
E941104L	1.34e-03	3.63e-03	2.95e-03	1.08e-03
E941102D	8.71e-04	3.59e-03	1.31e-02	2.56e-03
E941128R	8.20e-05	3.90e-03	3.53e-03	5.83e-04
E941102E	7.70e-05	2.29e-04	8.54e-04	1.58e-04
E941128Q	9.82e-04	5.04e-04	1.52e-03	2.81e-04
E941128P	9.90e-05	4.61e-03	3.29e-03	4.96e-04
E941102F	3.90e-05	2.41e-04	9.18e-04	1.62e-04
E941125O	5.95e-04	1.79e-03	1.95e-03	5.98e-04
E941103J	1.57e-04	9.95e-04	9.80e-04	2.08e-04
E941027B	3.70e-04	7.21e-04	1.79e-03	2.92e-04
E941027C	2.01e-04	4.10e-04	6.90e-04	2.80e-04
E941104K	2.46e-04	8.31e-04	1.87e-04	2.03e-04
E941122M	2.18e-04	2.49e-04	2.93e-04	1.11e-04
E941122N	9.58e-04	3.81e-04	2.45e-04	1.59e-04
E941103H	6.10e-05	1.43e-04	3.60e-05	1.20e-05
E941018A	1.48e-04	1.68e-04	1.39e-04	5.80e-05
E941103I	5.80e-05	2.81e-04	5.93e-05	2.40e-05

Table D.7 Metal concentrations measured in pore waters collected by Janssen *et al.* (1996).

Sample	Mn mol/l	Fe mol/l	Al mol/l	Cd mol/l	Cu mol/l	Ni mol/l	Pb mol/l	Zn mol/l
E941129S	4.20e-07	1.68e-05	2.76e-05	1.01e-08	7.00e-07	1.19e-07	5.17e-08	1.40e-06
E941102G	2.20e-07	3.70e-06	6.00e-06	2.68e-08	1.60e-06	2.56e-07	2.12e-08	2.90e-06
E941129T	6.00e-07	1.05e-05	1.76e-05	7.92e-09	7.00e-07	1.59e-07	2.92e-08	1.20e-06
E941104L	3.90e-07	4.40e-06	5.80e-06	1.36e-08	1.30e-06	1.19e-07	4.61e-08	1.60e-06
E941102D	8.00e-06	1.80e-06	3.40e-06	4.00e-09	6.00e-07	7.24e-07	1.59e-08	4.80e-06
E941128R	3.18e-06	7.90e-06	1.54e-05	7.12e-09	4.00e-07	1.32e-07	2.98e-08	1.40e-06
E941102E	8.60e-07	4.33e-05	3.55e-05	4.73e-08	6.00e-07	2.32e-07	7.71e-07	1.95e-05
E941128Q	3.80e-07	2.84e-05	5.72e-05	8.63e-09	7.00e-07	2.07e-07	3.31e-08	9.00e-07
E941128P	1.27e-05	1.06e-05	4.90e-06	1.17e-08	8.00e-07	2.19e-07	3.62e-08	2.50e-06
E941102F	5.80e-07	1.90e-05	3.11e-05	2.87e-08	1.60e-06	3.05e-07	6.60e-08	1.54e-05
E941125O	5.15e-06	8.70e-06	5.20e-06	1.28e-07	5.00e-07	1.75e-07	1.95e-08	6.50e-06
E941103J	6.50e-07	5.48e-05	1.68e-05	8.23e-07	1.30e-06	1.08e-06	1.78e-07	1.17e-04
E941027B	8.00e-07	5.83e-05	3.33e-05	3.02e-09	4.00e-06	3.64e-07	2.66e-07	2.00e-06
E941027C	1.13e-06	4.32e-05	1.47e-04	4.27e-09	2.40e-06	5.26e-07	4.44e-08	1.30e-06
E941104K	3.46e-06	2.25e-05	4.47e-05	1.06e-08	4.00e-07	1.00e-07	1.89e-06	2.40e-06
E941122M	1.28e-05	2.47e-05	7.01e-05	1.75e-08	8.00e-07	1.79e-07	1.00e-07	7.40e-06
E941122N	1.56e-05	9.18e-05	2.04e-04	0.00	5.00e-07	0.00	0.00	7.69e-05
E941103H	1.80e-07	1.02e-05	4.85e-05	9.31e-08	7.00e-07	7.58e-08	2.53e-07	1.61e-05
E941018A	1.08e-05	7.30e-06	5.05e-05	1.46e-08	1.00e-06	2.37e-07	1.71e-07	3.30e-06
E941103I	5.00e-07	2.29e-05	7.48e-05	5.86e-08	6.00e-07	8.98e-08	2.98e-07	5.40e-06

Table D.8 Soil solid phase metal concentrations determined by concentrated HNO_3 destruction of soil samples (Janssen *et al.*, 1996).

Sample	Cd mol/l	Cu mol/l	Ni mol/l	Pb mol/l	Zn mol/l
E941018A	N.D	2.78e-04	5.57e-04	4.71e-03	1.95e-03
E941027B	4.12e-06	4.63e-04	7.62e-04	8.86e-04	1.52e-03
E941027C	5.47e-06	2.86e-03	1.12e-03	2.62e-03	4.95e-03
E941102D	7.92e-05	6.55e-04	5.97e-04	2.28e-03	4.56e-02
E941102E	2.49e-04	1.21e-03	1.63e-03	1.56e-02	1.82e-01
E941102F	4.33e-04	2.15e-03	1.17e-03	2.46e-03	5.96e-02
E941102G	2.48e-04	4.31e-03	2.10e-03	3.34e-03	4.71e-02
E941103H	1.27e-04	1.62e-04	8.19e-05	3.16e-03	3.46e-03
E941103I	7.17e-05	1.77e-04	8.98e-05	2.66e-03	1.71e-03
E941103J	9.67e-04	2.51e-03	5.62e-04	2.33e-03	3.98e-02
E941104K	1.30e-05	3.24e-04	2.24e-04	2.09e-02	9.76e-04
E941104L	2.71e-05	4.68e-04	4.28e-04	3.49e-03	6.82e-03
E941122M	2.99e-06	8.95e-04	5.61e-04	2.97e-03	2.35e-03
E941122N	6.14e-06	7.52e-04	2.03e-03	8.10e-03	7.59e-03
E941125O	3.88e-04	2.03e-03	4.04e-04	2.24e-03	8.51e-03
E941128P	8.05e-05	9.95e-04	6.03e-04	2.01e-03	1.37e-02
E941128Q	1.40e-05	1.18e-03	7.69e-04	1.57e-03	1.97e-03
E941128R	7.57e-05	2.92e-03	1.28e-03	2.29e-03	1.21e-02
E941129S	1.93e-04	2.61e-03	1.46e-03	2.61e-03	2.82e-02
E941129T	3.57e-04	1.51e-03	9.07e-04	4.89e-03	1.62e-02

Appendix E Determination of surface protonation constants for Hydrous Ferric Oxide (HFO).

In this section, results obtained from acidimetric titrations of hydrous ferric oxide are discussed. The surface protonation properties of HFO were studied in order to familiarize myself with the potentiometric and modelling procedures used in surface complexation constant determination studies.

E-1 Preparation of HFO

Preparation of HFO took place in a titration vessel under purified N_2 atmosphere (see paragraph 2.1.5 for N_2 purification steps). The gas was pre-wetted by bubling through a 0.3 **M** $NaNO_3$ solution. 40.4 g $Fe(NO_3)_3.9H_2O$ (Merck pro analysi) was weighed into a 1000cm^3 volumetric flask. To this, 7.65 g $NaNO_3$ (Merck GR) was added. Using boiled out deionized glass distilled water, the solution was made up to the mark. This resulted in a 0.1 **M** $Fe(NO_3)$ solution with an ionic strength of 0.69 **M**. 20.00 cm^3 of this solution was added to a N_2 flushed, thermostatted glass titration vessel using a Metrohm Dosimat 665 automatic burette. After the attainment of temperature equilibration (25°C), 6.00 cm^3 1 **M** NaOH was slowly added to the solution using a Metrohm dosimat 665 burette. The solution was constantly stirred using a Teflon coated stirrer bar and a magnetic stirrer. HFO started precipitating immediately upon addition of NaOH. The precipitate was aged for 4 hours under constant stirring and inert atmosphere.

E-2 Acidimetric titrations

After 4 hours, an additional amount of 0.20 cm^3 NaOH was added to the suspension. The suspension was titrated with 0.1004 M HNO_3 with an ionic strength of 0.3 M $NaNO_3$. Titrations were carried out using a computer controlled Metrohm ABU 80 automatic burette. EMF was monitored using a glass electrode and calomel reference electrode (both Metrohm). The electrode assembly was calibrated following the procedure described in paragraph 2.1.3. Acid additions were made once EMF drift was less than 0.2 mV/300 seconds.

E-3 Experimental results

Figure E.1 shows pH vs TH results for three titrations. pH values were calculated from EMF readings using the Nernst equation and electrode parameters (E_{Cell}, s) determined during electrode calibration (see paragraph 2.1.3 for procedure). Good reproducibility was obtained. The curves are quite featureless, with a slight levelling off at high and low pH.

E-4 Adsorption constant determination

Surface protonation constants were determined using FITEQL (Westall & Herbelin, 1994). Default FITEQL error estimates were used throughout (see also paragraph 2.4).

Following Dzombak and Morel (1991), titration data were modelled assuming a homogeneous surface (i.e., all sites ≡XOH are equivalent) and the following surface species:

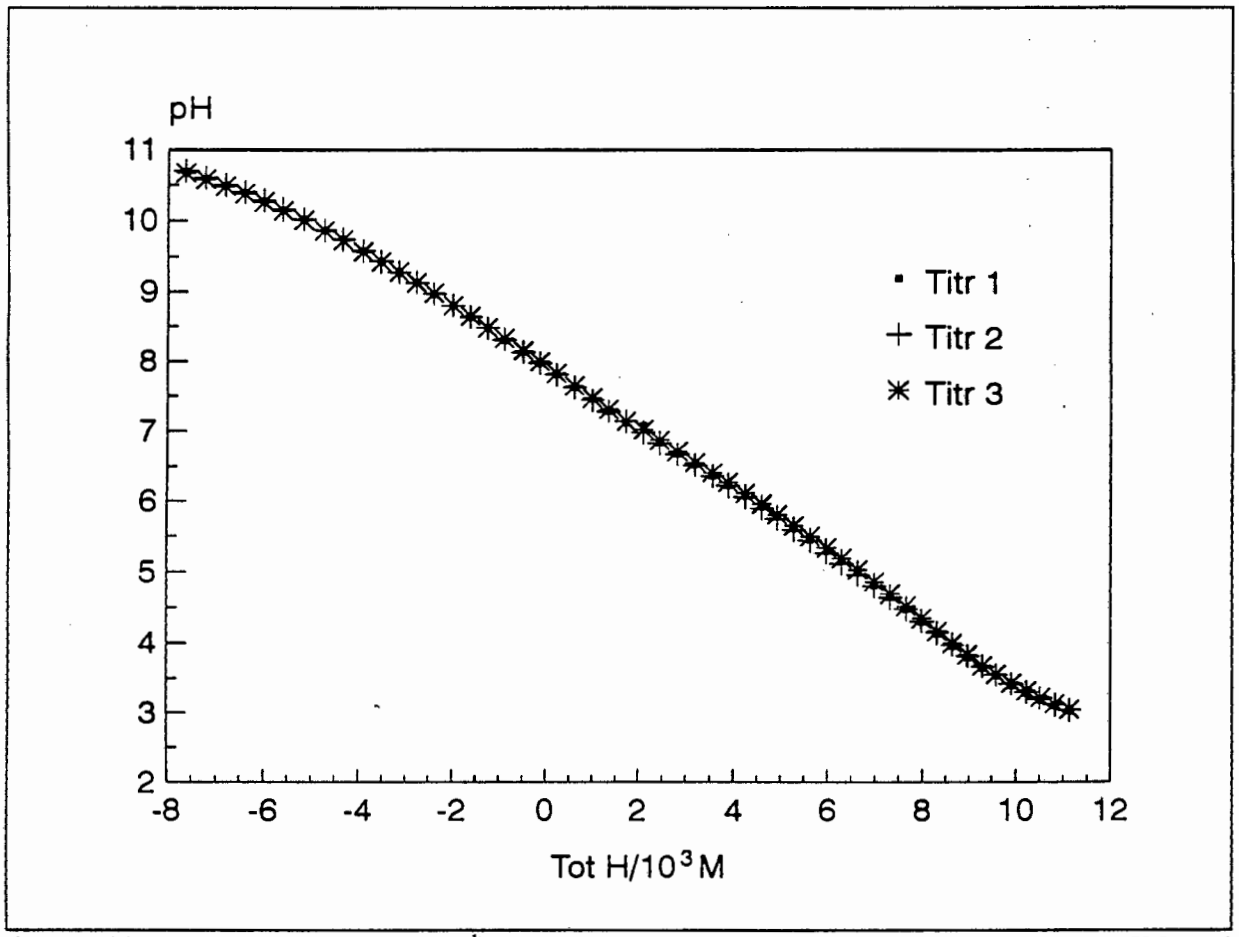

Figure E-1 pH vs Total H (mol.l^{-1}) data for three HFO titrations recorded at T = 25°C and I = 0.3.

$$\equiv XOH + H^+ \rightleftharpoons \equiv XOH_2^+ \qquad \text{Log } K_1$$

$$\equiv XOH \rightleftharpoons \equiv XO^- + H^+ \qquad \text{Log } K_2$$

The parameters which were optimized are Log K_1, Log K_2 and total site concentration [≡XOH]. The HFO surface area was assumed to be 600 $m^2.g^{-1}$, which is equivalent to the value used by Dzombak and Morel. Actual N_2-BET surface area was determined to be 327 $m^2.g^{-1}$. This corresponds well with values listed in Table 5.1 of Dzombak and Morel.

Figure E-2 compares experimental and calculated TH values over a pH range of 3 to 10.7. A total of 53 data points were used in this calculation. A summary of the results obtained from this calculation is given in Table E.1. The goodness of fit is given by the value

WSOS/DF, which is the sum of squares divided by the degrees of freedom. A value for this parameter between 0.1 and 20 indicates a reasonably good fit, whereas a value greatly in excess of 20 indicates an inapropriate model (Herbelin and Westall, 1994).

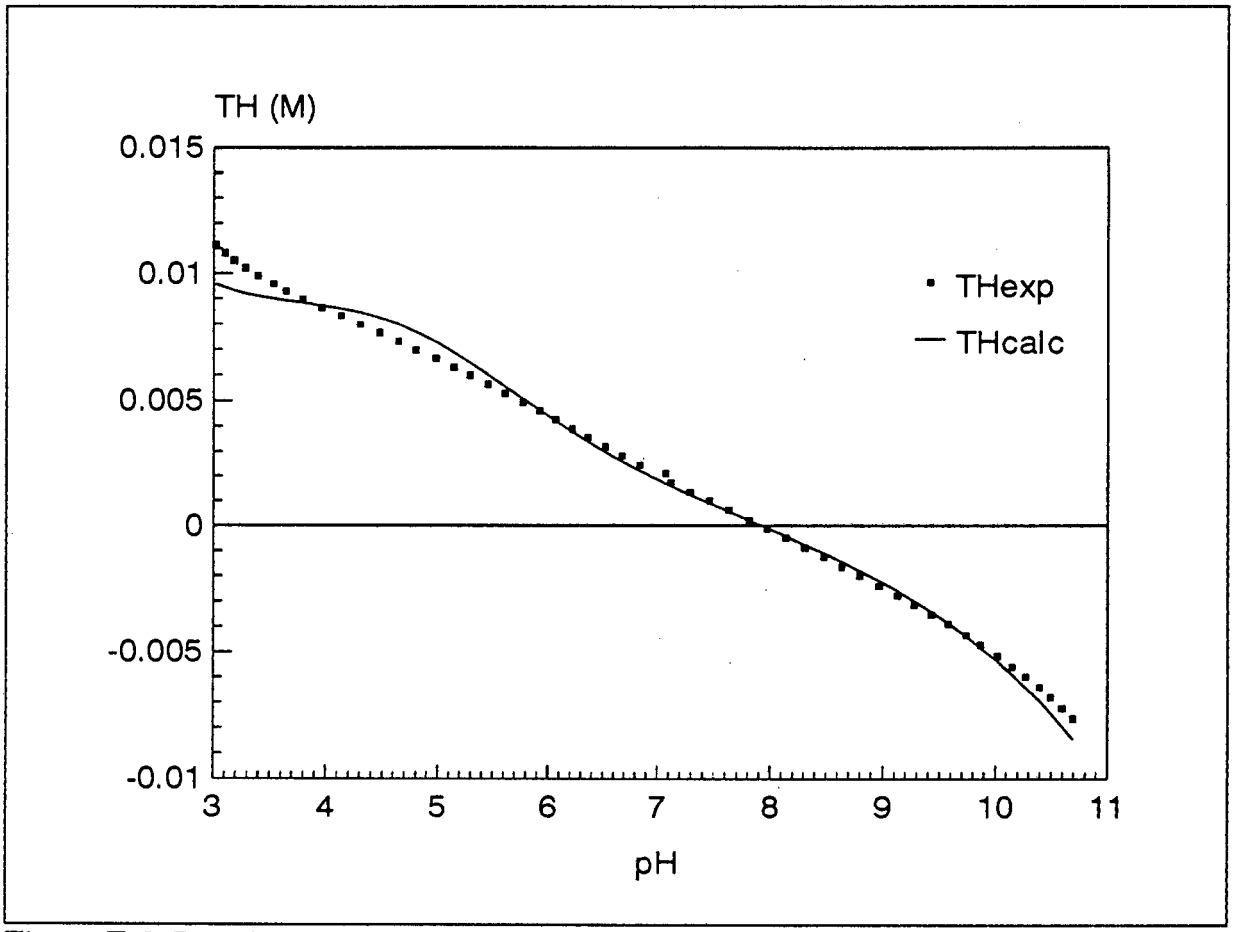

Figure E-2 Experimental and calculated (FITEQL) Total H vs pH curves using data recorded at T = 25°C, I = 0.3 and pH 3 to 10.7.

Table E.1 Summary of hydrous ferric oxide protonation results obtained using 53 data points.

Parameter	Titration 1		Titration 2		Titration 3	
	Ionic strength (M)		Ionic strength (M)		Ionic strength (M)	
	0.3	0.0	0.3	0.0	0.3	0.0
Log K_1	6.95	7.08	6.92	7.05	6.97	7.10
Log K_2	-8.87	-9.00	-8.88	-9.01	-8.87	-9.00
Site concentration (M)	1.05×10^{-2}		1.08×10^{-2}		1.08×10^{-2}	
SOS/DF	25.0		24.9		23.6	
pH range	3.02-10.7		3.03-10.7		3.03-10.7	

Goodness of Fit parameters determined for the respective titrations are just outside the range regarded as indicating an acceptable fit. Inspection of Figure E.2 shows that the fit at low pH is not very good. A possible reason may be that, at low pH, dissolution of HFO takes place. Because of this, aqueous phase Fe(III) concentration may become significant, leading to reactions not accounted for in the FITEQL model used to obtain the calculated values shown in Figure E-2.

In order to investigate this, the experimental system was simulated, using MINTEQA2 (Allison, 1991). Simulations were carried out over a pH range of 2 to 7 and a different iron solid was allowed to precipitate in each simulation. Equilibrium constants used in these simulations were those supplied in the MINTEQA2 database. The constants were compared with those listed in NIST and JESS. Good agreement amongst the various databases were found.

Simulation results are shown in Figure E-3. The iron solids which were allowed to precipitate

are Ferrihydrite (curve a), Lepidocrocite (curve b), Maghemite (curve c), Goethite (curve d) and Hematite (curve c).

It is clear from Figure E.3 that Fe^{3+} concentrations ranging from 10^{-2} **M** to 10^{-10} **M** may be expected at pH 3, depending on the iron solid allowed to precipitate. Figure E-3 thus suggests that data collected below pH 4 should be disregarded because of possible dissolution of the solid being studied.

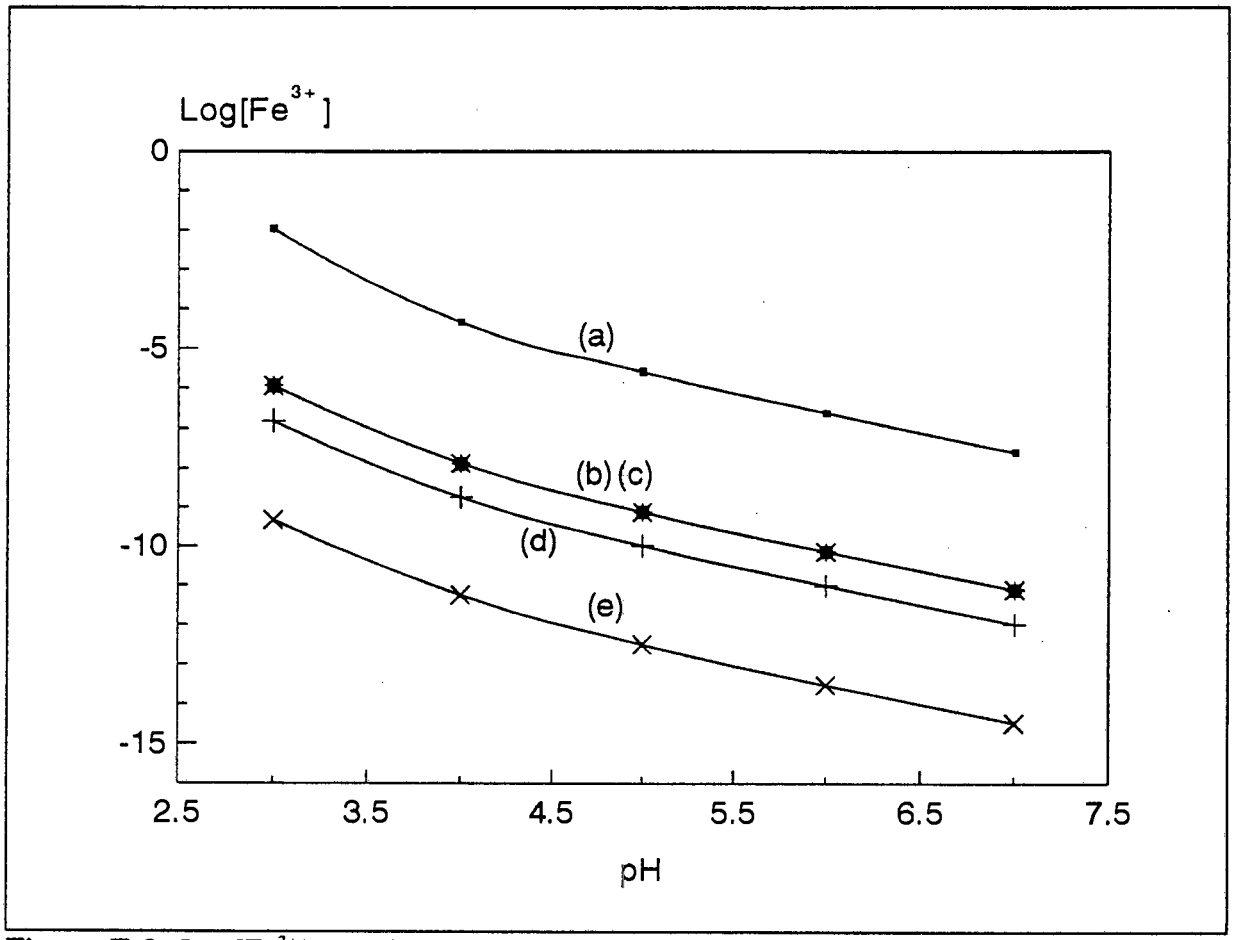

Figure E-3 Log[Fe^{3+}] as a function of pH and mineral allowed to form as calculated using MINTEQA2.

A typical result obtained using a smaller data set is shown in Figure E.4. Figure E.4 compares experimental and calculated TH vs pH curves over a pH range of approximately

4.5 to 10.7. A summary of the optimized parameters obtained from using smaller data sets is shown in Table E.2.

Rewriting the adsorption reactions as acid dissociation constants, we obtain best estimates by calculating average Log K's:

$$\equiv XOH_2^+ \rightleftharpoons \equiv XOH + H^+ \qquad \text{Log } K_1 = -7.33 \pm 0.02$$

$$\equiv XOH \rightleftharpoons \equiv XO^- + H^+ \qquad \text{Log } K_2 = -8.80 \pm 0.004$$

This compares well with the values of -7.29 and -8.93 obtained by Dzombak and Morel for the corresponding reactions. From the relationship

$$PZC = 0.5(pK^{int}_1 + pK^{int}_2)$$

we obtain PZC = 8.07, which is in close agreement with values listed by Dzombak and Morel.

Average binding site concentration calculated from the data in Tabel E.2 is 8.75×10^{-3} mol.dm^{-3}. This is equivalent to 0.108 mol sites/mol HFO, assuming 89g HFO per mol Fe. This value is lower than the 0.2 mol sites/mol HFO used by Dzombak and Morel, but it is within the range observed by others (Table 5.3 in Dzombak and Morel).

It may thus be concluded that the agreement between protonation constants determined in this work and those determined by Dzombak and Morel is good. This provides support for the experimental technique employed in this work.

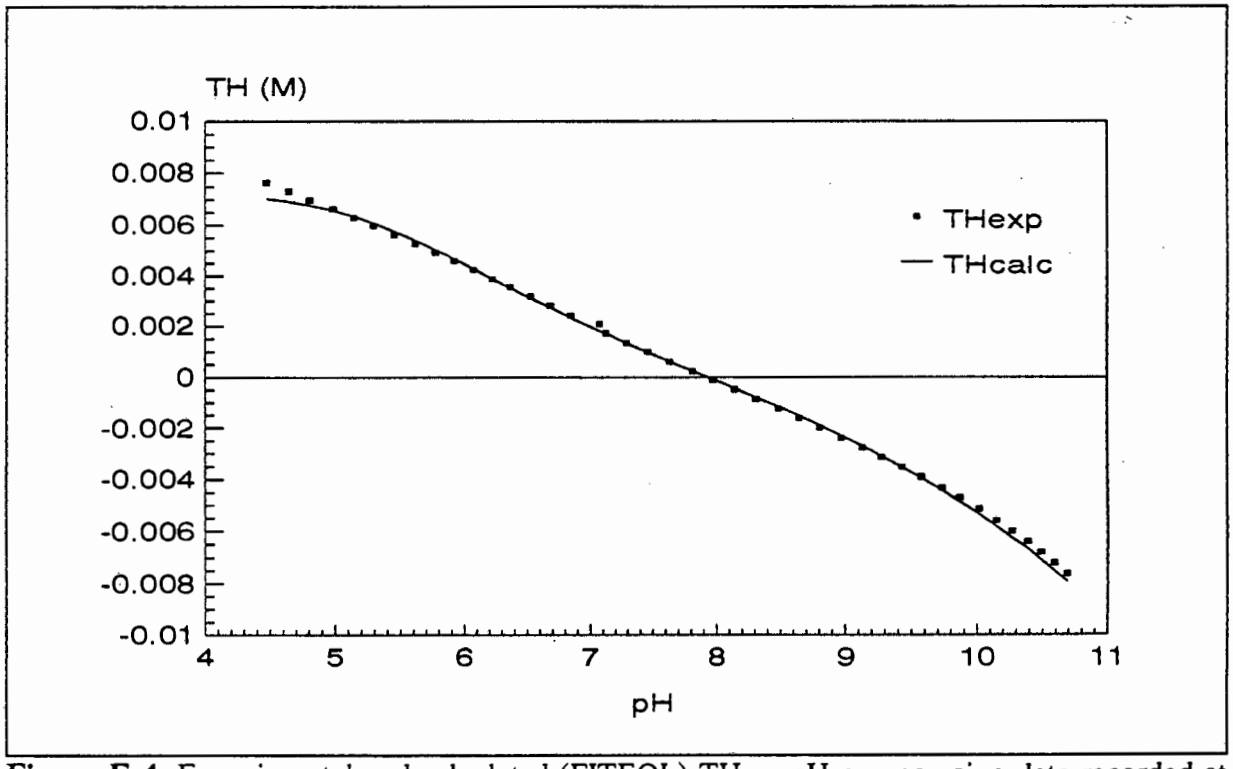

Figure E-4 Experimental and calculated (FITEQL) TH vs pH curves using data recorded at T = 25°C, I = 0.3 over a pH range of 4.47 to 10.7.

Table E.2 Summary of hydrous ferric oxide protonation results obtained using 42 data points.

Parameter	Titration 1		Titration 2		Titration 3	
	Ionic strength (M)		Ionic strength (M)		Ionic strength (M)	
	0.3	0.0	0.3	0.0	0.3	0.0
Log K_1	7.20	7.33	7.18	7.31	7.22	7.35
Log K_2	-8.67	-8.80	-8.67	-8.80	-8.66	-8.79
Site concentration (M)	8.74×10^{-3}		8.73×10^{-3}		8.79×10^{-3}	
SOS/DF	4.4		4.2		3.5	
pH range	4.47-10.7		4.47-10.7		4.50-10.7	

References

Adams WJ, Kimberle RA, Barnett JW (1992). Sediment quality criteria and aquatic life assessment. Environmental Science and Technology, **26**, 1864 - 1875.

Allen HE (1996). Specialist report to RIVM, the Netherlands.

Allison JD, Brown DS, Novo-Gradac KJ (1991). MINTEQA2/PRODEFA2, a geochemical assessment model for environmental systems: version 3.0 user's manual. EPA/600/3-91/021, Environmental Research Laboratory, U.S. Environmental Protection Agency, Athens, Georgia.

Alloway BJ (1995). Cadmium. *In* Heavy Metals in Soils, 2nd Edition. Edited by BJ Alloway, Blackie Academic and Professional, London.

Alloway BJ (1995). Introduction. *In* Heavy Metals in Soils, 2nd Edition. Edited by BJ Alloway, Blackie Academic and Professional, London.

Anderson PR, Benjamin MM (1990a). Surface and bulk characteristics of binary oxide suspensions. Environmental Science and Technology, **24**, 692 - 698.

Anderson PR, Benjamin MM (1990b). Modelling adsorption in aluminium - iron binary oxide suspensions. Environmental Science and Technology, **24**, 1586 - 1592.

Atkins PW (1983). Physical Chemistry, 2nd Edition, Oxford University Press, Oxford.

Baas-Becking LGM, Kaplan IR, Moore D (1960). Limits of the natural environment in terms of pH and oxidation-reduction potentials. The Journal of Geology, **68**, 243 - 284.

Baes CF, Mesmer RF (1976). The Hydrolysis of Cations. John Wiley & Sons, New York.

Balikungeri A, Haerdi W (1988). Complexing abilities of hydrous manganese oxide surfaces and their role in the speciation of heavy metals. International Journal of Environmental Analytical Chemistry, **34**, 215 - 225.

Balistriery LS, Murray JW (1982). The surface chemistry of δ-MnO_2 in major ion sea water. Geochimica et Cosmochimica Acta, **46**, 1041 - 1052.

Barrow NJ (1993). Effects of surface heterogeneity on ion adsorption by metal oxides and by soils. Langmuir, **9**, 2606 - 2611.

Bates RG (1964). Determination of pH. Theory and practice. John Wiley and Sons, New York.

Baxter DC, Frech W (1995). Speciation of lead in environmental and biological samples., Pure and Applied Chemistry, **67**, 615 - 648.

Beck MY, Nagypal I (1990). Chemistry of Chemical Equilibria. John Wiley and Sons, New York.

Benedetti MF, Milne CJ, Kinniburgh DG, van Riemsdijk WH, Koopal LK (1995). Metal ion binding to humic substances: Application of the non-ideal competitive adsorption model. Environmental Science and Technology, **29**, 446 - 457.

Benjamin MM, Leckie JO (1981). Multiple site adsorption of Cd, Cu and Pb on amorphous iron oxyhydroxide. Journal of Colloid and Interface Science, **79**, 209 - 221.

Berti WR, Cunningham SD (1997). In-place inactivation of Pb in Pb-contaminated soils. Environmental Science and Technology, **31**, 1359 - 1364.

Bérubé YG, de Bruyn PL (1968). Adsorption at the rutile-solution interface. I. Thermodynamic and experimental study. Journal of Colloid and Interface Science, **27**, 305 - 318.

Bérubé YG, Onada YG, de Bruyn PL (1967). Proton adsorption at the ferric oxide/aqueous solution interface. II. Analysis of kinetic data. Surface Science, **8**, 448 - 461.

Biber MV, dos Santos Afonso M, Stumm W (1994). The coordination chemistry of weathering: IV. Inhibition of the dissolution of oxide minerals. Geochimica et Cosmochimica Acta, **58**, 1999 - 2010.

Bolt GH, van Riemsdijk WH (1987). Surface chemical processes in soil. *In* Aquatic Surface Chemistry: Chemical Processes at the Particle - Water Interface. Edited by W Stumm, John Wiley & Sons, New York.

Bruemmer G, Tiller KG, Herms U, Clayton PM (1983). Adsorption-desorption and/or precipitation-dissolution processes of zinc in soils. Geoderma, **31**, 337 - 354.

Bufflap SE, Allen HE (1995). Comparison of pore water sampling techniques for trace metals. Water Research, **29**, 2051 - 2054.

Buffle J (1988). Complexation reactions in aquatic systems: an analytical approach. Ellis Horwood, Chichester.

Catts JG, Langmuir D (1986). Adsorption of Cu, Pb and Zn by δ-MnO_2: Applicability of the site binding-surface complexation model. Applied Geochemistry, **1**, 255 - 264.

Charlet L, Manceau A (1993). Structure, formation and reactivity of hydrous oxide particles: insights from X-ray absorption spectroscopy. *In* Environmental Particles Volume 2. Edited by J Buffle and HP van Leeuwen, Lewis Publishers, Boca Raton.

Chisholm-Brause CJ, Hayes KF, Roe AL, Brown GE, Parks GA and Leckie JO (1990a). Spectroscopic investigation of Pb(II) complexes at the γ-Al_2O_3/water interface. Geochimica et Cosmochimica Acta, **54**, 1897 - 1909.

Chisholm-Brause CJ, O'Day PA, Brown GE(jr), Parks GA (1990b). Evidence for multinuclear metal-ion complexes at solid/water interfaces from X-ray absorption spectroscopy. Nature, **348**, 528 - 530.

Cleven RFMJ (1984). Heavy metal/polyacid interaction. An electrochemical study of the binding of Cd(II), Pb(II) and Zn(II) to polycarboxylic and humic acids. PhD Thesis, Wageningen Agricultural University, the Netherlands.

Contescu C, Jagiello J, Schwarz JA (1993). Heterogeneity of proton binding sites at the oxide/solution interface. Langmuir, **9**, 1754 - 1765.

Contescu C, Contescu A, Schwartz JA (1994). Thermodynamics of proton binding at the alumina/aqueous solution interface. A phenomenological approach. Journal of Physical Chemistry, **98**, 4327 - 4335.

Cotton FA, Wilkinson G (1980). Advanced Inorganic Chemistry. A Comprehensive Text. John Wiley and Sons, New York.

Coughlin BR, Stone AT (1995). Nonreversible adsorption of divalent metal ions (Mn^{II}, Co^{II}, Ni^{II}, Cu^{II} and Pb^{II}) onto goethite: effects of acidification, Fe^{II} addition and picolinic acid. Environmental Science and Technology, **29**, 2445 - 2455.

CRC Handbook of Chemistry and Physics, 65th Edition, CRC Press, Boca Raton, Florida.

Davis A, Drexier JW, Ruby MV, Nicholson A (1993). Micromineralogy of mine wastes in relation to lead bioavailability, Butte, Montana. Environmental Science and Technology, **27**, 1415 - 1425.

Davis JA, James RO, Leckie JO (1978). Surface ionization and complexation at the oxide/water interface. I. Computation of electrical double layer properties in simple electrolytes. Journal of Colloid and Interface Science, **63**, 480 - 499.

de Wit JCM (1988). Proton and metal binding to humic substances. PhD Thesis, Wageningen Agricultural University, the Netherlands.

Dobbs JC, Susetyo W, Knight FE, Castles MA, Carreira LA (1989). Characterization of metal binding sites in fulvic acids by lanthanide ion probe spectroscopy. Analytical Chemistry, **61**, 483 - 488.

Dobbs JC, Susetyo W, Knight FE, Castles MA, Carreira LA (1989). Competitive binding of protons and metal ions in humic substances by lanthanide ion probe spectroscopy. Analytical Chemistry, **61**, 1519 - 1524.

Dzombak DA, Hayes KF (1992). Comment on "Recalculation, evaluation and prediction of surface complexation constants for metal adsorption on iron and manganese dioxides. Environmental Science and Technology, **26**, 1251 - 1253.

Dzombak DA, Morel FMM (1990). Surface complexation modelling: Hydrous ferric oxide. John Wiley and Sons, New York.

Evans LJ (1989). Chemistry of metal retention in soils. Environmental Science and Technology, **23**, 1046 - 1056.

Fu G, Allen HE, Cowan CE (1991). Adsorption of cadmium and copper by Manganese oxide. Soil Science, **152**, 72 - 81.

Gadde RR, Laitinen HA (1974). Studies of heavy metal adsorption by hydrous iron and manganese oxides. Analytical Chemistry, **46**, 2022 - 2026.

Gans P (1976). Numerical methods for data-fitting problems. Coordination Chemistry Reviews, **19**, 99 - 124.

Garčia-Miragaya J (1984). Levels, chemical fractionation and solubility of lead in roadside soils of Caracas, Venezuela. Soil Science, **138**, 147 - 152.

Gray MJ, Malati MA (1979a). Adsorption from aqueous solution by δ-Manganese dioxide I. Adsorption of the alkaline-earth cations. J. Chem. Tech. Biotechnol., **29**, 127 -134.

Gray MJ, Malati MA (1979b). Adsorption from aqueous solution by δ-Manganese dioxide II. Adsorption of some heavy metal cations. J. Chem. Tech. Biotechnol., **29**, 135 -144.

Greenland DJ, Hayes MHB (1981). Soil processes. *In* The Chemistry of Soil Processes. Edited by DJ Greenland and MHB Hayes, John Wiley and Sons, New York.

Hamilton WC (1965). Significance tests on the crystallographic R factor, Acta Crystallographica, **18**, 502 - 510.

Harrison RM, Laxen DPH, Wilson SJ (1981). Chemical associations of lead, copper and zinc in street dusts and roadside soils. Environmental Science and Technology, **15**, 1378 - 1383.

Hayes KF, Leckie JO (1987). Modelling ionic strength effects on cation adsorption at hydrous oxide/solution interfaces. Journal of Colloid and Interface Science, **115**, 564 - 572.

Herbelin A, Westall JC (1994). FITEQL: A computer program for determination of chemical equilibrium constants from experimental data, version 3.1., Report 94-01, Oregon State University, Corvallis.

Hickey MG, Kittrick JA (1984). Chemical partitioning of cadmium, copper, nickel and zinc in soils and sediments containing high levels of heavy metals. Journal of Environmental Quality, **13**, 372 - 376.

Hiemenz PC (1986). Priciples of colloid and surface chemistry, 2nd Edition, Marcel Dekker Inc, New York.

Hiemstra T, van Riemsdijk WH, Bolt GH (1989). Multisite proton adsorption modelling at the solid/solution interface of (hydr)oxides: A new approach. 1. Model description and evaluation of intrinsic reaction constants. Journal of Colloid and Interface Science, **133**, 91 - 104.

Holm PE, Andersen S, Christensen TH (1995). Speciation of dissolved cadmium: Interpretation of dialysis, ion exchange and computer (GEOCHEM) methods. Water Research, **29**, 803 - 809.

Irving H, Williams RJP (1948). Order of stability of metal complexes. Nature, 162, 746 - 747.

Irving H, Williams RJP (1953). The stability of transition metal complexes. Journal of the Chemical Society, 3192 - 3210.

Janssen RPT, Pretorius PJ, Peijnenburg WJGM, van den Hoop MAGT (1996). Determination of field based partition coefficients for heavy metals in Dutch soils and the relationship of these coefficients with soil characteristics. RIVM report 719101023, Bilthoven, the Netherlands.

Jenny H, Nielsen TR, Coleman NT, Williams DE (1950). Concerning the measurement of pH, ion activities and membrane potentials in colloidal systems. Science, **112**, 164 - 167.

JESS - see May and Murray, 1991a,b.

Jones LHP, Jarvis SC (1981). The fate of heavy metals. *In* The Chemistry of Soil Processes. Edited by DJ Greenland and MHB Hayes, John Wiley and Sons, New York.

Jones C, Williams DR (1987). Surface water pH measurements - Theory and practice. The Science of the Total Environment, **64**, 211 - 230.

Kabata-Pendias A, Pendias H (1985). Trace elements in soils and plants, CRC Press, Boca Raton, Florida.

Krajnc M, Stupar J, Milecev S (1995). Characterization of copper and chromium complexes with fulvic acids isolated from soils in Slovenia. Science of the Total Environment, **159**, 23 -

Kramer U (1988). Complexation of divalent copper , zinc and calcium ions by phosphate esters in aqueous solution. PhD Thesis, University of Cape Town, South Africa.

Lamy I, Djafer M, Terce M (1991). Influence of oxalic acid on the adsorption of cadmium at the goethite surface. Water, Air and Soil Pollution, **57-58**, 457 - 465.

Lee SZ, Allen HE, Huang CP, Sparks CP, Sanders PF, Peijnenburg WJGM (1996). Predicting soil-water partition coefficients for cadmium. Environmental Science and Technology, **12**, 3418 - 3424.

Li CL (1993). US Patent 5221 323 (Only abstract available).

Linder PW, Torrington RG, Williams DR (1984). Analysis using Glass Electrodes. Open University Press, Milton Keynes.

Lindsay WL (1979). Chemical Equilibria in Soils. John Wiley and Sons, New York.

Loganathan P, Burau RG (1973). Sorption of heavy metal ions by a hydrous manganese dioxide. Geochimica et Cosmochimica Acta, **37**, 1277 - 1293.

Lyklema J (1991). Electrified interfaces in aqueous dispersions of solids. Pure and Applied Chemistry, **63**, 895 - 906.

Ma LQ, Rao GN (1997). Chemical fractionation of cadmium, copper, nickel and zn in contaminated soils. Journal of Environmental Quality, **26**, 259 - 264.

Ma QY, Traina SJ, Logan TJ, Ryan JA (1993). *In situ* lead immobilization by apatite. Environmental Science and Technology, **27**, 1803 - 1810.

Manceau A, Gorshkov AI, Drits VA (1992a). Structural chemistry of Mn, Fe, Co and Ni in manganese hydrous oxides: Part I. Information from XANES spectroscopy. American Mineralogist, **77**, 1133 - 1143.

Manceau A, Gorshkov AI, Drits VA (1992b). Structural chemistry of Mn, Fe, Co and Ni in manganese hydrous oxides: Part II. Information from EXAFS spectroscopy and electron and X-ray diffraction. American Mineralogist, **77**, 1144 - 1157.

Manceau A, Charlet L, Boisset MC, Didier B, Spadini L (1992c). Sorption and speciation of heavy metals on hydrous Fe and Mn oxides. From microscopic to macroscopic. Applied Clay Science, **7**, 201 - 223.

Marani D, Macchi G, Pagano M (1995). Lead precipitation in the presence of sulphate and carbonate: Testing of thermodynamic predictions. Water Research, **29**, 1085 - 1092.

Marinsky JA, Reddy MM, Ephraim JH, Mathuthu AS (1995). Computational scheme for the prediction of metal ion binding by a soil fulvic acid. Analytica Chimica Acta, **302**, 309 - 322.

Martell AE, Motekaitis RJ (1988). Determination and Use of Stability Constants. VCH Publishers, Weinheim, Germany.

Martell AE, Motekaitis RJ, Smith RM (1988). Structure-stability relationships of metal complexes and metal speciation in environmental aqueous solutions. Environmental Toxicology and Chemistry, **7**, 417 - 434.

May PM, Murray K (1991a). JESS, a joint expert speciation system. I. Raison d'être. Talanta, **38**, 1409 - 1417.

May PM, Murray K (1991b). JESS, a joint expert speciation system. II. The thermodynamic database. Talanta, **38**, 1419 - 1426.

May PM, Williams DR, Linder PW, Torrington RG (1982). The use of glass electrodes for the determination of formation constants - I. A definitive method for calibration. Talanta, **29**, 249 - 256.

May PM, Murray K, Williams DR (1985). The use of glass electrodes for the determination of formation constants II. Simulation of titration data. Talanta, **32**, 483 - 489.

May PM, Murray K, Williams DR (1988). The use of glass electrodes for the determination of formation constants III. Optimization of titration data: the ESTA library of computer programs. Talanta, **35**, 825 - 830.

McBride MB (1989). Reactions controlling heavy metal solubility in soils. *In* Advances in Soil Science, **10**. Edited by BA Stewart, Springer Verlag, New York.

McBride MB (1994). Environmental Chemistry of Soils. Oxford University Press, New York.

McKenzie RM (1989). Manganese oxides and hydroxides. *In* Minerals in Soil Environments: SSSA Book series 1. Edited by J.B. Dixon and S.B. Weed, Soil Science Society of America, Madison.

Meng X, Letterman RD (1993). Effect of component oxide interaction on the adsorption properties of mixed oxides. Environmental Science and Technology, **27**, 970 - 975.

Mesuere K, Fish W (1992). Chromate and oxalate adsorption on Goethite. 1. Calibration of surface complexation models. Environmental Science and Technology, **26**, 2357 - 2364.

METROHM Monographs, Electrodes in Potentiometry.

Morgan JJ, Stumm W (1964). Colloid-chemical properties of manganese dioxide. Journal of Colloid and Interface Science, **19**, 347 - 359.

Morse JW, Casey WH (1988). Ostwald processes and mineral paragenesis in sediments. American Journal of Science, **288**, 537 - 560.

Mountney AW, Williams DR (1992). Computer simulation of metal ion - humic and fulvic acid interactions. Journal of Soil Science, **43**, 679 - 688.

Murray JW (1974). The surface chemistry of hydrous manganese dioxide. Journal of Colloid and Interface Science, **46**, 357 - 371.

Murray K, Linder PW (1983). Fulvic acids: structure and metal binding. I. A random molecular model. Journal of Soil Science, **34**, 511 - 523.

Murray K, Linder PW (1984). Fulvic acids: structure and metal binding. II. Predominant metal binding sites. Journal of Soil Science, **35**, 217 - 222.

Nilsson N, Lövgren L, Sjöberg S (1992). Phosphate complexation at the surface of goethite. Chemical Speciation and Bioavailability, **4**, 121 - 130.

NIST Critical Stability Constants of Metal Complexes Database version 1.0 (1993). NIST Standard Reference Database 46, US Dept of Commerce, Gaithersburg, MD.

Nowack B, Sigg L (1996). Adsorption of EDTA and metal-EDTA complexes onto goethite. Journal of Colloid and Interface Science, **177**, 106 - 121.

Onada GY, de Bruyn PL (1966). Proton adsorption at the ferric oxide-aqueous solution interface. 1. Kinetic study of adsorption. Surface Science, **4**, 48 - 63.

Onuki T (1990). Adsorption of radioactive cobalt by a mixture of manganese dioxide and montmorillonite. Journal of Nuclear Science and Technology, **27**, 1068 - 1071.

Pankow JF, Morgan JJ (1981a). Kinetics of the aquatic environment. Environmental Science and Technology, **15**, 1155 - 1164.

Pankow JF, Morgan JJ (1981b). Kinetics of the aquatic environment. Environmental Science and Technology, **15**, 1306 - 1313.

Parks GA (1965). The isoelectric points of solid oxides, solid hydroxides and aqueous hydroxo complex systems. Chemical Reviews, **65**, 177 - 198.

Perdue EM, Reuter JH, Parrish RS (1984). A statistical model of proton binding by humus. Geochimica et Cosmochimica Acta, **48**, 1257 - 1263.

Pickering WF (1995). General strategies for speciation. *In* Chemical Speciation in the Environment. Edited by AM Ure and CM Davids, Blackie Academic and Professional, London.

Pretorius PJ (1990). A computer simulation of the protonation and metal complexation properties of fulvic acids. MSc thesis, University of Cape Town, South Africa.

Pretorius PJ, Janssen RPT, Peijnenburg WJGM and van den Hoop MAGT (1996). Chemical equilibrium modelling of metal partitioning in soils. RIVM report no. 719101024, Bilthoven, the Netherlands.

Ritchie GSP, Sposito G (1995). Speciation in soils. *In* Chemical speciation in the environment. Edited by AM Ure and CM Davidson, Blackie Academic & Professional.

Rock PA, Casey WH, McBeath MK, Walling EM (1994). A new method for determining Gibbs energies of formation of metal-carbonate solid solutions: 1. The $Ca_xCd_{1-x}CO_3(s)$ system at 298K and 1 bar. Geochimica et Cosmochimica Acta, **58**, 4281 - 4291.

Rönngren L, Sjöberg S, Sun Z, Forsling W (1994). Surface reactions in aqueous metal sulfide systems. 5. The complexation of sulfide ions at the ZnS-H_2O and PbS-H_2O interfaces. Journal of Colloid and Interface Science, **162**, 227 - 235.

Rustad JA, Felmy AR, Hay BP (1996). Molecular statics calculations of proton binding to goethite surfaces: A new approach to estimation of stability constants for multisite surface complexation models. Geochimica et Cosmochimica Acta, **60**, 1563 - 1567.

Sadiq M, Enfield CG (1984a). Solid phase formation and solution chemistry of nickel in soils: 1. Theoretical. Soil Science, **138**, 262 - 270.

Sadiq M, Enfield CG (1984b). Solid phase formation and solution chemistry of nickel in soils: 2. Experimental. Soil Science, **138**, 335 - 340.

Schindler PW (1991). A solution chemists view of surface chemistry. Pure and Applied Chemistry, **63**, 1697 - 1704.

Schindler PW, Stumm W (1987). The surface chemistry of oxides, hydroxides and oxide minerals. *In* Aquatic Surface Chemistry: Chemical Processes at the Particle-Water Interface. Edited by W Stumm, John Wiley and Sons, New York.

Schlautman MA, Morgan JJ (1994). Adsorption of aquatic humic substances on colloidal-size aluminum oxide particles: Influence of solution chemistry. Geochimica et Cosmochimica Acta, **58**, 4293 - 4303.

Schwertmann U, Taylor RM (1989). Iron Oxides. *In* Minerals in Soil Environments, 2nd Edition, SSSA Book series 1. Edited by JB Dixon and SB Weed, Soil Science Society of America, Madison.

Shea D (1988). Developing national sediment quality criteria. Environmental Science and Technology, **22**, 1256 - 1261.

Sing KSW (1985). Reporting physisorption data for gas/solid systems. Pure and Applied Chemistry, **57**, 603 - 619.

Smith RW, Jenne EA (1991). Recalculation, evaluation and prediction of surface complexation constants for iron and manganese oxides. Environmental Science and Technology, **25**, 525 - 531.

Soon YK, Bates TE (1982). Chemical pools of cadmium, nickel and zinc in polluted soils and some preliminary indications of their availability to plants. Journal of Soil Science, **33**, 477 - 488.

Spark KM, Wells JD, Johnson BB (1997). Sorption of heavy metals by mineral-humic acid substrates. Australian Journal of Soil Research, **35**, 113 - 122.

Sposito G (1989). The Chemistry of Soils. Oxford University Press, Oxford.

Stroes-Gascoyne S (1983). Adsorption behaviour of δ-manganese dioxide in relation to its use as a resin in trace metal speciation studies. PhD Thesis, McMaster University, Canada.

Stroes-Gascoyne S, Kramer JR, Snodgrass WJ (1987). Preparation, characterization and aging of δ-MnO_2, for use in trace metal speciation studies. Applied Geochemistry, **2**, 217 -226.

Stumm W (1992). Chemistry of the Solid-Water Interface, John Wiley and Sons, New York.

Susetyo W, Dobbs JC, Carreira LA, Azzaraga LV, Grimm DM (1990). Development of a statistical model for metal-humic interactions. Analytical Chemistry, **62**, 1215 - 1221.

Tessier A, Campbell PGC, Bisson M (1979). Sequential extraction procedure for the speciation of particulate trace metals. Analytical Chemistry, **51**, 844 - 851.

Tessier A, Fortin D, Belzile N, de Vitre RR, Leppard GG (1996). Metal sorption to diagenetic iron and manganese oxyhydroxides and associated organic matter: narrowing the gap between field and laboratory measurements. Geochimica et Cosmochimica Acta, **60**, 387 - 404.

Tiller KG, Bruemmer G (1984). The relative affinities of Cd, Ni and Zn for different soil clay fractions and goethite. Geoderma, **34**, 17 - 35.

Tipping E (1981a). The adsorption of aquatic humic substances by iron oxides. Geochimica et Cosmochimica Acta, **45**, 191 - 199.

Tipping E (1981b). Adsorption by goethite (α-FeOOH) of humic substances from three different lakes. Chemical Geology, **33**, 81 - 89.

Tipping E (1994). WHAM - A chemical equilibrium model and computer code for waters, sediments and soils incorporating a discrete site/electrostatic model of ion-binding by humic substances. Computers and Geosciences, **20**, 973 - 1023.

Tipping E, Cooke D (1982). The effects of adsorbed humic substances on the surface charge of goethite (α-FeOOH) in freshwaters. Geochimica et Cosmochimica Acta, **46**, 75 - 80.

Ure AM, Davidson CM (1995). Introduction to speciation. *In* Chemical Speciation in the Environment. Edited by AM Ure and CM Davidson, Blackie Academic & Professional, London.

Vacca A, Sabatini A and Gristina MA (1972). Two problems involved in solving complex formation equilibria: The selection of species and the calculation of stability constants, Coordination Chemistry Reviews, **8**, 45 - 53.

van den Hoop MAGT (1995). Metal speciation in Dutch soils: Field based partition coefficients for heavy metals at background levels. Dutch Institute of Public Health and the Environment report no. 719101013, Bilthoven, the Netherlands.

Van der Kooij LA, van de Meent D, van Leeuwen C, WA Bruggeman (1991). Deriving quality criteria for water and sediment from the results of aquatic toxicity tests and product standards: Application of the equilibrium partitioning method. Water Research, **25**, 697 - 705.

van Geen A, Robertson AP, Leckie JO (1994). Complexation of carbonate species at the goethite surface: Implications for adsorption of metal ions in natural waters. Geochimica et Cosmochimica Acta, **58**, 2073 - 2086.

van Stralen NM, Bergema WF (1995). Ecological risks of increased bioavailability of metals under acidification. Pedobiologica, **39**, 1 - 9.

Vermöhlen K, Lewandowski H, Klumpp E, Narres H-D (1996). Modification of oxide surfaces with organic polyelectrolytes. 14th European Chemistry at Interfaces Conference, October 1996, Antwerp, Belgium.

Vogel IA (1981). Vogel's Textbook of Quantitative Inorganic Analysis, 4th Edition, Longmans, Essex.

Vogel IA (1989). Vogel's Textbook of Practical Organic Chemistry, 5th edition. Edited by BS Furniss, AJ Hannaford, PWG Smith and AR Tatchell. Longman Scientific and Technical, Harlow.

Westall JC (1987). Adsorption mechanisms in aquatic surface chemistry. *In* Aquatic Surface Chemistry. Edited by W Stumm, Wiley Interscience, New York.

Westall JC (1993). Modelling chemical speciation: past accomplishments and future directions. Paper presented at "Metal speciation and contamination of aquatic sediments", June 8 - 11, 1993, Clarion Resort Buccaneer, Jekyll Island, Georgia.

Westall JC, Hohl H (1980). A comparison of electrostatic models for the oxide/solution interface. Advances in Colloid and Interface Science, **12**, 265 - 294.

Woollard CD (1994). A computer simulation of trace metal speciation in seawater. PhD Thesis, University of Cape Town, South Africa.

Xu J, Wang W (1993). Interaction of cupric oxide-ferric oxide systems. Cuiha Xuebao, **13**, 420-424 (paper in Chinese, only English abstract available).

Zhang M, Alva AK, Li YC, Calvert DV (1997). Chemical association of Cu, Zn, Mn and Pb in selected sandy citrus soils. Soil Science, **126**, 181 - 188.

Zasoski RJ, Burau RG (1988). Sorption and sorptive interaction of cadmium and zinc on hydrous manganese oxide. Journal of the American Soil Science Society, **52**, 81 - 87.